Flying-V Landing Gear

A Physics-Based Design Exploration

P.G. van den Berg

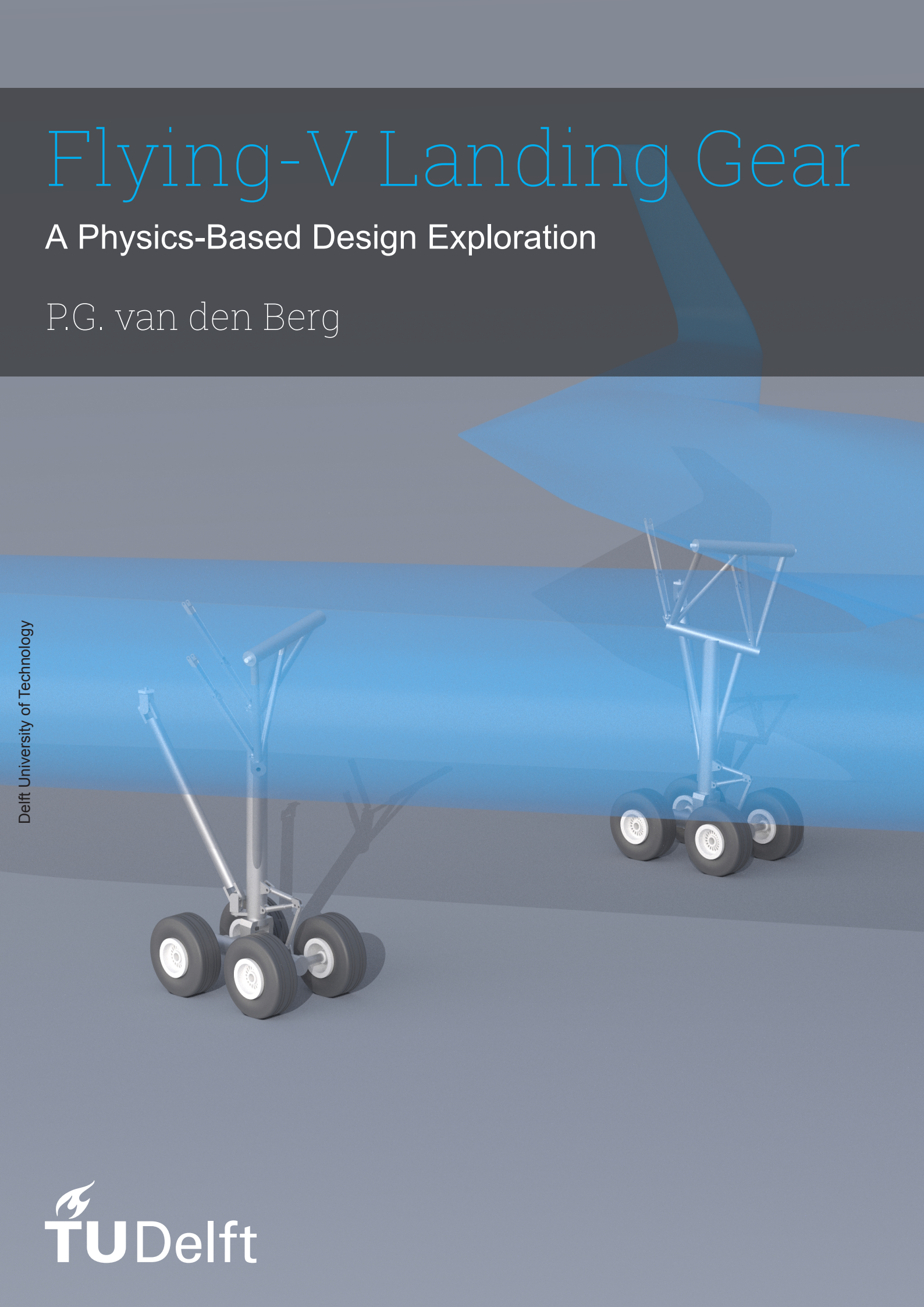

Delft University of Technology

TU Delft

Flying-V Landing Gear

A Physics-Based Design Exploration

by

P.G. van den Berg

to obtain the degree of Master of Science
at the Delft University of Technology,
to be defended publicly on November 11, 2024

Student number: 4553950
Project duration: April 15, 2023 – November 11, 2024
Thesis committee:

Dr.ir. R. Vos	TU Delft, supervisor
Dr.ir. M. Pini	TU Delft
Dr. J. Sodja	TU Delft
Ir. P. Vergouwen	GKN Fokker Landing Gear, external advisor

An electronic version of this thesis is available at `http://repository.tudelft.nl/`.

TU Delft Delft University of Technology

Abstract

The Flying-V is a novel aircraft concept that has improved fuel efficiency through its distinctive V-shaped structure containing the pressurised cabin, fuel tanks and cargo hold. This configuration presents several key design challenges, one of them being the design of the landing gear. Previous studies indicate that the Flying-V landing gear significantly contributes to the total mass of the aircraft and its placement influences overall aircraft design, both of which impact the viability of the concept. Landing gear designs have been proposed, but are based on outdated requirements, and have notable shortcomings when it comes to feasibility, reliability of mass estimates, aircraft integration and family design commonality. This research aims to explore landing gear designs to identify the best solution for the Flying-V family.

A novel conceptual landing gear design framework is developed, incorporating a gear positioning and sizing optimisation algorithm and physics-based structural sizing. The gear positioning and sizing algorithm allows for efficient exploration of various design features, and can quickly adapt to changing aircraft requirements, making it particularly suitable for the conceptual design phase and the development of family design derivatives. The algorithm is validated using five different reference aircraft with distinct specifications and landing gear configurations, and demonstrated its ability to accurately predict gear positions and lengths. The use of physics-based structural sizing reduces the reliance on statistics-based mass estimation methods, which are known to yield inaccurate results for large and unconventional aircraft. Reference aircraft gear mass data is used to derive a finite-element mass correction equation, improving the accuracy of the mass estimation.

Several Flying-V landing gear concepts are evaluated, each designed with different features, or optimised for a different set of aircraft requirements representing any of the Flying-V family members. For the FV-1000, this resulted in a final design that has a double folding strut, a four-wheel articulated bogie and a strut shortening mechanism, offering a feasible solution with optimal mass and stowage properties. The gear weighs 13.6 tonnes, which is 5.1% of the aircraft maximum take-off mass (MTOM). A derivative design for the FV-900 features the same structural components, but without an articulation mechanism and includes dedicated rolling stock sizing, resulting in a gear weight of 13.3 tonnes, or 5.7% of MTOM. The FV-800 landing gear design follows the same concept as for the FV-1000, but with dedicated structural and rolling stock sizing, significantly reducing mass compared to using the FV-1000-sized common gear. The FV-800 is more constrained by fuel tank capacity and range, which justifies deviating from the commonality principle. The dedicated FV-800 gear weighs 9.2 tonnes which is 5.0% of the MTOM.

Preface

Dear reader,

This Master's thesis marks the completion of my studies in Aerospace Engineering at Delft University of Technology. It represents not only the culmination of my academic journey but also the end of one of the most exciting and transformative periods of my life. Although I initially began my studies in Mechanical Engineering in 2016 (I simply could not chose my favourite mode of transport), my passion for aviation ultimately led me to transition to the Flight Performance and Propulsion Master's program. Doing this while studying from home due to the COVID-19 pandemic has been particularly challenging.

For my graduation project, I had the incredible opportunity to work on the Flying-V, focusing on the fascinating subject of landing gear design, which even resulted in patent applications. Balancing the demands of this thesis with a job at NACO and maintaining a social life was was no easy task, but it was immensely rewarding in every way.

I would like to extend my heartfelt thanks to my friends and family for their constant support throughout this journey. I am also deeply thankful to my colleagues at NACO for their understanding and flexibility in allowing me to pursue this thesis independently. Special thanks go to Patrick van Ginneken for his invaluable help with the patent process and to Peet Vergouwen, who, though not an official supervisor, provided tremendous insights and industry expertise. His guidance, along with the insightful trips to the Fokker Landing Gear facilities in Helmond and later Papendrecht, greatly enriched my understanding and fascination. I would like to sincerely thank my main supervisor, Roelof Vos, for his guidance and support throughout this project. His expertise and thoughtful feedback were invaluable in shaping this thesis, and I greatly appreciate his contributions to its success.

Lastly, and most importantly, I want to thank my beloved girlfriend, Femke, who has supported me through thick and thin, offering endless encouragement and patience throughout this journey.

P.G. van den Berg
Delft, October 2024

Contents

Nomenclature

Abbreviations

Abbreviation	Definition
ACR	Aircraft Classification Rating
BL	Baseline
CAD	Computer-Aided Design
CCP	Clearance Critical Point
CG	Centre of Gravity
CMG	Cockpit to Main Gear Distance
CRES	Corrosion-Resistant Steel
CS	Certification Specification
EASA	European Aviation Safety Agency
FAA	Federal Aviation Administration
FEA/FEM	Finite Element Analysis/Method
FV	Flying-V
GMCP	Ground Manoeuvring Critical Point
GSE	Ground Support Equipment
ICAO	International Civil Aviation Organisation
IDF	Individual Design Feasible
MAC	Mean Aerodynamic Chord
MDO	Multidisciplinary Design Optimisation
MDF	Multi Discipline Feasible
MDS	Main Gear Design Space
MLG	Main Landing Gear
MGW	Outer Main Gear Width
MLM	Maximum Landing Mass
MTOM	Maximum Take-Off Mass
MRM	Maximum Ramp Mass
NDS	Nose Gear Design Space
NLG	Nose Landing Gear
OEM	Operational Empty Mass
PCR	Pavement Classification Rating
SA	Shock Absorber
SQP	Sequential Quadratic Programming
SO	Single Optimisation
TDG	Taxiway Design Group
XDSM	Extended Design Structure Matrix

Symbols

Symbol	Definition	Unit
A	Cross-section area	m^2
a	Acceleration	m/s^2
b	Tube section width, SA breakout load fraction	m, -
c	Chord length, Constraint	m, -
d	Diameter	m
E	Energy, Young's modulus	J, Pa
F	Force (or load)	N
f	Objective function, Mass correction factor	-
g	Gravitational acceleration	m/s^2

Symbol	Definition	Unit
H	Height	m
I	Second area moment	m^4
K	Buckling effective length factor	-
k	Machinability factor	-
L	Lift	N
l	Length	m
M	Bending moment	Nm
m	Mass	kg
N	Number of wheels/tyres, Normal load	-, N
P	Pressure	Pa
r	Radius	m
r	Generic vector	-
S	Wing surface area	m^2
s	Clearance distance, SA compression fraction	m, -
T	Torque	Nm
t	Wall thickness	m
V	Velocity, Volume, Shear load	m/s, m^3, N
v	Folding axis unit vector	-
W	Weight	N
w	Width, weight factor	m, -
X, Y, Z	Inertial frame coordinates	m
x	Tyre/axle/shock absorber travel, Gear positioning parameter, Design vector	m, -, -
y	Gear positioning parameter	m
x, y, z	Body frame coordinates	m
α	Generic angle, angle of attack	$^\circ$
β	Load fraction	-
γ	Heat capacity ratio	-
δ		
η	Shock absorber or tyre efficiency	-
θ	Generic angle around y-axis, Aircraft pitch attitude, Tipback angle	$^\circ$
Λ	Planform sweep angle	-
λ	SA reaction factor, Steering angle, Planform (panel) taper ratio	-
σ	Axial stress, Von Mises stress	Pa
τ	Shear stress	Pa
ϕ	Generic angle around x-axis, Aircraft roll attitude	$^\circ$
ψ	Generic angle around z-axis, Aircraft yaw attitude, Turnover angle	$^\circ$

Subscripts

Subscript	Definition
0,1,2,n	SA compression states, CCP/GMCP numbering
A/B	Vector or scalar from point A to point B (generic)
abs	Absorbed
ac	Aircraft
aftCG	Refers to aft CG
art	Related to articulated bogie
axle	Refers to a wheel axle
bogie	Refers to bogie
brakes	Refers to brakes
CG	Centre of gravity
cl	Relative to aircraft centreline
corrected	Refers to corrected mass
critical	Refers to a critical load or stress
des	Design
DS	Design space
ext	Extended
extSA	Extended shock absorber

Subscript	Definition
FEM	Refers to finite element method
folding axis	Refers to folding axis
fpb	Relative to front pressure bulkhead
fuselage	Refers to aircraft fuselage
fwdCG	Refers to forward CG
gcp	Ground contact point
gear	Refers to a specific gear strut
grown	Refers to grown tyre dimensions
hs	Hockey stick
ineffective	Refers to ineffective SA piston length
kin	Kinetic
lat	Lateral
loaded	Refers to a loaded tyre radius
MAC	Mean aerodynamic chord
margin	Refers to dearticulation or clearance margin
max	Maximum
min	Minimum
Mises	Denotes von Mises stress
mlg	Refers to main landing gear
nlg	Refers to nose landing gear
piston	Refers to SA piston
pivot	Refers to rotation pivot
pot	Potential
rad	Radial
range	Refers to probable CG range
rated	Refers to tyre load rating
ref	Reference
ret	Retracted
rim	Refers to wheel rim
rot	Refers to rotated condition
rs	Relative to rear spar
SA	Refers to shock absorber
shortening	Refers to strut shortening
ss	Shock strut
stat	Static
statSA	Static shock absorber
steering	Refers to nose gear steering
T	Track
tc	Turn centre
tno	Turnover
to	Tipover
tpb	Tipback
turn	Refers to turn width
tyre	Refers to tyre
uloaded	Refers to a unloaded tyre radius
us	Upper strut
wheel	Refers to wheel
wheelbase	Refers to wheelbase
wt	Wing tip
y	Yield
x,y,z	Parallel to or rotation around x, y, z axis

List of Figures

List of Tables

1

Introduction

The aviation industry, which accounts for approximately 4% of current global warming [1], is facing growing pressure to lower its carbon footprint. The International Civil Aviation Organization (ICAO) aims for net-zero aviation emissions by 2050. However, with air travel demand growing at 3.6% per year [2], and conventional aircraft architectures approaching their fuel efficiency limits [3], this is an ambitious target. This has triggered research into disruptive technologies and unconventional aircraft architectures, including the Flying-V. The Flying-V is a novel aircraft concept, integrating both wings and fuselage into a single V-shaped body. After it was introduced by Benad [4], the Flying-V has been developed into an aircraft family that roughly has a 25% higher lift-to-drag ratio compared to the NASA common research model [3] and a 17% lower mass compared to the A350 [5]. These improvements have a significant impact on fuel consumption, with the largest member of the Flying-V family, the FV-1000, achieving a 20% reduction in fuel consumption compared to the A350-1000 on a similar mission with similar payload [6]. An artist impression of the Flying-V is shown in Figure 1.1.

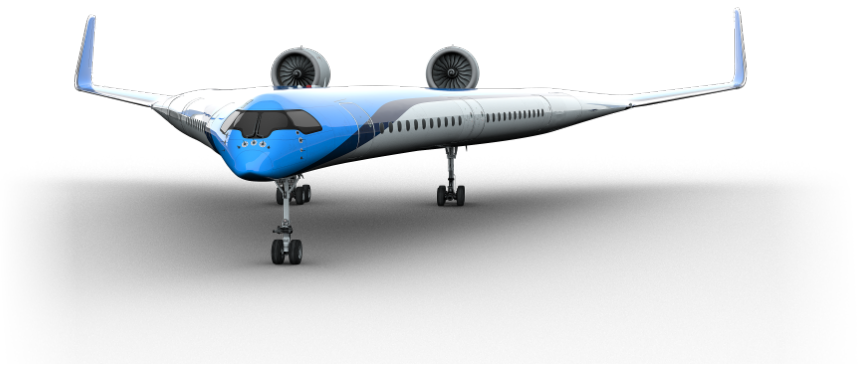

Figure 1.1: Flying-V artist impression [7]

To fully understand the performance advantages of the Flying-V over conventional aircraft and evaluate its overall feasibility, a comprehensive study of its landing gear system is required. For traditional aircraft, the weight of the landing gear is substantial, accounting for 3.5-5% of the maximum take-off mass [8]. For the Flying-V, it is expected that the weight contribution of the landing gear is even greater due to the long landing gear legs necessary for take-off and landing [9]. Furthermore, it can be concluded that the positioning of the landing gear has a large impact on the design of the Flying-V family, such as the location of the common fuselage section [10]. The limited space available presents additional challenges for stowing the landing gear without compromising aerodynamic performance and fuel tank volume.

Landing gear designs have been proposed by Bourget [9] and Rehbein [11], however, both designs have shortcomings. Bourget's design features complex kinematics and unverified feasibility. Moreover, the mass estimate is derived using a method that is known to yield inaccurate results for unconventional and large transport aircraft. On the other hand, Rehbein's design offers simplified kinematics

and a more representative quasi-analytical mass estimate, but its folded gear position is deemed unfavourable in terms of aerodynamics, integration, and family design commonality. Both designs are based on outdated aircraft properties and requirements.

More fundamentally, both Bourget and Rehbein have focused on the development and assessment of a single gear concept based on a static set of requirements. However, during the conceptual design phase, aircraft properties and requirements are rapidly evolving and involve trade-offs to achieve the best possible compromise. This is especially true for the Flying-V, being new and unconventional, naturally having a lot of unknowns and uncertainties, with aircraft properties and requirements getting frequent updates. A landing gear design concept exploration is needed that allows for exploring the effect of family design commonality and top-level landing gear design considerations in terms of feasibility, integration and mass in an early design stage. This supports further aircraft and landing gear research, as well as design trade-offs, ultimately leading to a better overall design.

1.1. Research Objective

The main objective of is this research is:

> *To set up a Flying-V landing gear design exploration, comparing various landing gear concepts to identify the most suitable landing gear for the Flying-V, using a dynamic, physics-based conceptual design and mass estimation method.*

Resulting in the following research question:

> *What is the best landing gear for the Flying-V family?*

Which can be split in the following sub-questions:

1. *What criteria determine the optimal landing gear design for the Flying-V family?*
2. *How do Flying-V landing gear design considerations affect landing gear feasibility and performance?*
3. *What is the penalty of imposing derivative landing gear designs for the Flying-V family?*

1.2. Thesis Outline

The research questions are addressed in the following chapters. Chapter 2 presents the research background, including an overview of landing gear fundamentals and previous Flying-V research relevant to the design of the landing gear. Moreover, the chapter outlines the state-of-the-art when it comes to conceptual landing gear design and landing gear mass estimation. Lastly, also an overview of landing gear design requirements is provided. Chapter 3 presents the design exploration setup, as well as the conceptual design and gear analysis methodologies. Verification, validation and calibration of the proposed methodologies is discussed in Chapter 4. In Chapter 5, the methods are applied to the Flying-V, resulting in a wide range of landing gear concepts contributing to the design exploration. Gear analysis results are discussed in Chapter 6. Chapter 7 reflects on the research questions, concludes the research, and provides recommendations for future research.

2

Background

This chapter presents background information relevant to this study. Fundamental landing gear knowledge is outlined, followed by a description of the Flying-V state-of-the-art, specifically that of preceding Flying-V landing gear studies and associated work. After that, conceptual landing gear design methods, requirements and mass estimation methods are discussed.

2.1. Introduction to the Landing Gear

Before delving into the specific details of the Flying-V and its landing gear design, it is important to first become familiar with the fundamentals of landing gear systems in general. This section provides insight into basic landing gear terminology, as well as key functions, components, and configurations commonly found on large transport aircraft. In addition, landing gear kinematics and mechanisms are discussed.

2.1.1. Landing Gear Functions and Components

The landing gear is one of the most complex and diverse systems on an aircraft due to its extensive range of functions and requirements, as well as the diverse array of distinct components it comprises [12]. The landing gear needs to provide a stable platform for ground manoeuvres, but on the contrary, it needs to maintain the right degree of instability for takeoff rotation. The landing gear plays a pivotal role in ensuring that all aircraft components such as engines, wingtips and fuselage remain clear of the ground during take-off and landing. It absorbs landing impact energy and ground manoeuvring shocks to mitigate airframe stress, and facilitates braking after landing and while taxiing. Typically, the landing gear is made to retract during flight, minimising aerodynamic drag to enhance fuel efficiency.

The main landing gear of a large transport aircraft typically consists of a shock strut that provides primary support to the aircraft during landing and taxiing. The strut is connected to the trunnion and support braces, which attach the landing gear to the airframe and support the gear in all relevant loading directions. Typically, locking mechanisms need to be provided to ensure that the strut can be locked into its retracted or folded position. The integrated shock absorber helps to absorb shocks and vibrations, reducing stress on the airframe and providing a smooth ride for passengers. The shock absorber piston is connected to an axle with wheels and tyres, which allow for ground manoeuvring and ensure that ground forces are properly transferred to the landing gear structure. If loads need to be distributed over a larger number of wheels, multiple axles may be integrated into a bogie assembly. When a bogie is implemented, it is typically required to have a torque link between the shock absorber piston and outer cylinder to maintain wheel alignment during ground manoeuvring. Main landing gear have brake assemblies responsible for applying braking force to the wheels, with brake rods transferring braking torque from the wheels to the main strut. An overview of these key components can be found in Figure 2.1.

2.1.2. Landing Gear Configurations

Landing gear configurations are categorised based on their specific strut layout and typology, each tailored to suit different aircraft requirements. In terms of strut configurations, three primary layouts stand out: the conventional (or taildragger), bicycle, and tricycle layouts. The conventional and bicycle

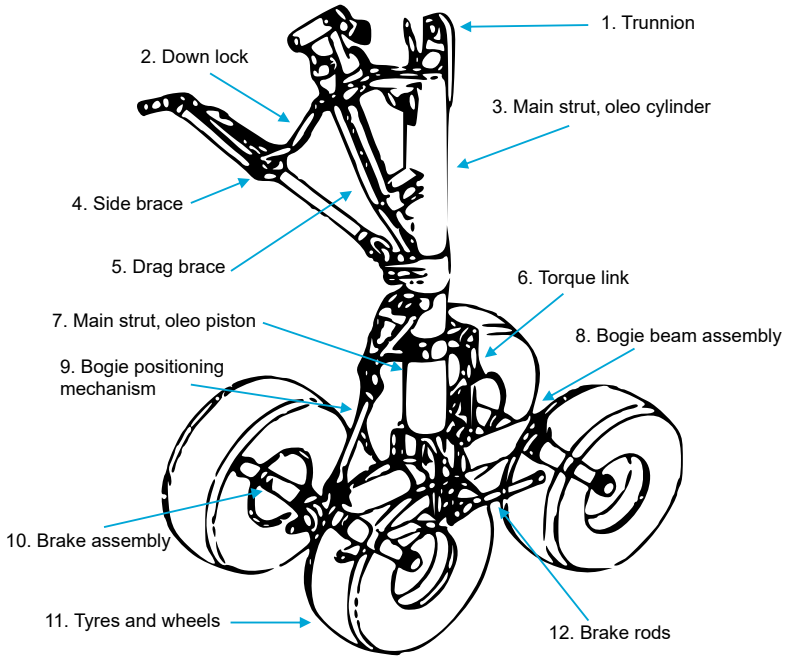

Figure 2.1: Overview of landing gear components, figure adapted from Rajamani et al. [13]

layouts employ a single support on the centreline behind the centre of gravity and one or more supports in front of the centre of gravity. In contrast, the tricycle layout is characterised by at least two main supports situated behind the aft centre of gravity limit and a single nose support on the centreline. The tricycle layout is the standard for modern large transport aircraft design, as it provides superior stability and offers the convenience of a horizontal ground attitude, facilitating efficient loading and boarding and superior visibility for pilots [12]. Specifically for the Flying-V, it is essentially the only layout that fits the V-shaped fuselage. Examples of the tricycle layout are illustrated in Figure 2.2a and 2.2c.

Landing gear typologies can be broadly classified into two primary categories: cantilevered (or telescopic) gear and articulated gear. The articulated gear features a distinctive hinged lever mechanism that connects the wheel axle to the primary fitting, allowing for a compact shock absorber design. The cantilevered gear, on the other hand, is characterised by its direct mounting of the wheel axle to the shock absorber. Because of its simplicity, it is generally preferred for nose and main landing gears [14]. Examples of cantilevered typologies are illustrated in Figure 2.2b and 2.2c.

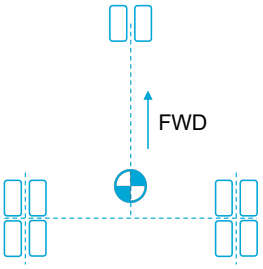

(a) Tricycle gear layout.

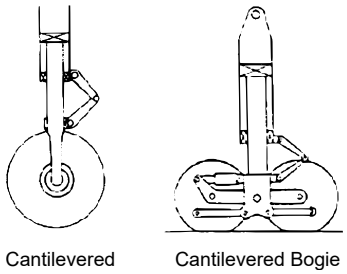

(b) Cantilevered (telescopic) gear typologies.

(c) A350-900 with a cantilevered nose gear and bogie cantilevered main gears in tricycle configuration. [15]

Figure 2.2: Overview of the standard landing gear configuration of large transport aircraft.

2.1.3. Landing Gear Mechanisms

Landing gear systems of large transport aircraft comprise mechanisms that ensure that the landing gear can be retracted to reduce aerodynamic drag [12]. Key to evaluating landing gear feasibility is

an assessment of kinematics and retraction path [8]. An overview of relevant retraction and extension mechanisms are outlined in this section. Additionally, special landing gear features related to compact landing gear stowage is discussed.

Retraction and Extension Kinematics

Fundamentally, two top-level kinematics mechanisms may be defined: sliding mechanisms and hinged mechanisms. Although sliding mechanisms have been reliably used on large transport aircraft, virtually all contemporary aircraft have hinged landing gears as they offer superior robustness [12]. Conway [16] defined a range of fundamental hinged kinematics, as illustrated in Figure 2.3. Hinged mechanisms are characterised by having one or more folding braces (Figure 2.3a), or a folding strut (Figure 2.3b and 2.3c, the latter often referred to as drop link arrangements. Please note that these mechanisms can be modified to make the gear retract in any direction.

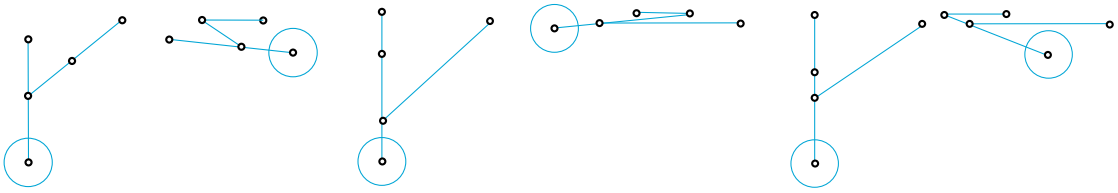

(a) Pivoting main strut with a folding brace.

(b) Folding main strut, pivoting brace, variation 1.

(c) Folding main strut, pivoting brace, variation 2.

Figure 2.3: Principal landing gear hinged kinematics [16].

Braces, or stays, typically support the structure to withstand side and drag loads applied to the landing gear. Locking mechanisms must be provided to secure the landing gear in its extended and retracted position [17]. Planar brace and locking mechanisms are generally preferred, as they offer the simplest and lightest solution [12]. They are typically used to support landing gears that retract forward, such as the nose gear, as wall as sideways retracting gears, if permitted by space and structural constraints. Figure 2.4a illustrates the planar retraction mechanism of the A320 nose gear. In situations where there is insufficient space or structure to incorporate a planar brace, which is often the case with most large transport aircraft, a rolling-folding brace may be utilised. Unlike planar braces, rolling-folding mechanisms fold and rotate simultaneously during retraction. The dual rolling-folding brace mechanism of the Boeing 767 main gear is illustrated in Figure 2.4b. In certain instances, a telescopic brace may be used instead of a folding brace. Telescopic braces offer superior locking capabilities with higher resistance to vibrations, and are frequently used when beneficial in terms of stowage [12] and mitigating the need for an additional actuator. A telescopic brace has been employed on the Concorde, as demonstrated in Figure 2.4c.

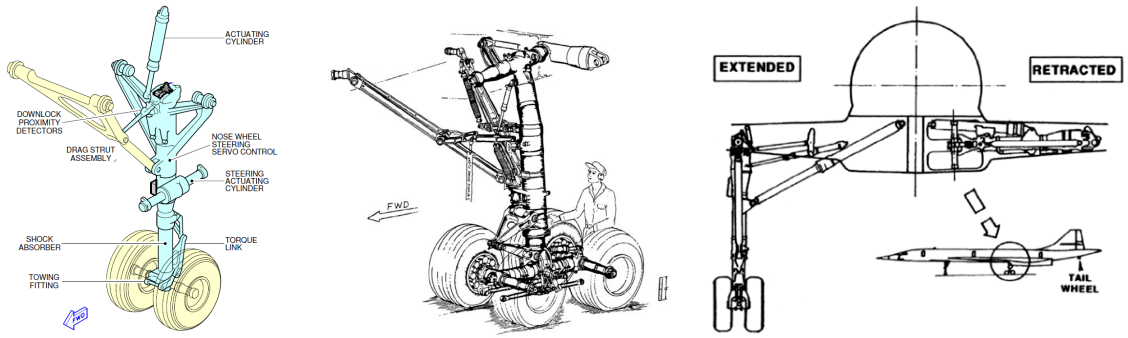

(a) A320 planar nose gear brace, adapted from Airbus [18].

(b) Boeing 767 dual rolling-folding brace, adapted from Schmidt [12].

(c) Concorde telescopic main gear brace, adapted from [12].

Figure 2.4: Overview of common landing gear retraction mechanisms.

Special Features

The potential benefits of implementing special features to reduce the stowage footprint of the Flying-V landing gear have been highlighted in prior research [9]. Bogie articulation has been presented as a

means to effectively reduce the required main strut length. When the bogie is articulated the bogie pivots along with shock absorber extension, which causes the aft wheel axle to extend further than the extension of the shock absorber alone, effectively creating more gear length. As an additional benefit, tyre spin-up loads are distributed more efficiently, as not all wheels touch the ground simultaneously. Figures 2.5a and 2.5b show the articulation mechanisms of the A330/A340 and Boeing 777 respectively.

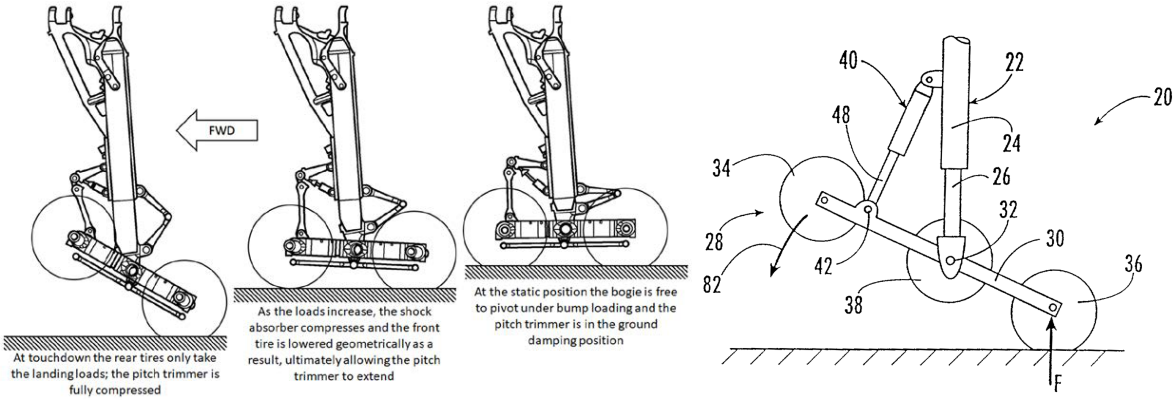

(a) A330/A340 articulation mechanism, adapted from Schmidt [12]. **(b)** Boeing 777 bogie beam locking mechanism [19].

Figure 2.5: Bogie articulation mechanism.

Apart from bogie articulation, also a strut shortening mechanism has been proposed as a way to reduce the stowage footprint [9]. Strut shortening mechanisms pull up the shock absorber assembly within the main strut cylinder, effectively negating the extension of the shock absorber due to decompression. Such mechanisms have been successfully integrated in the landing gear of the Concorde and Airbus A330/A340 family. An example of a strut shortening mechanism is illustrated in Figure 2.6.

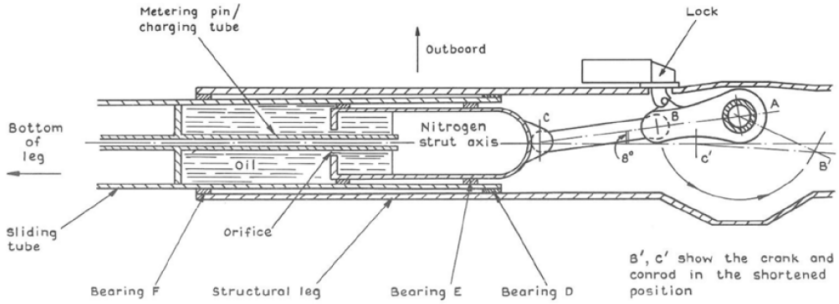

Figure 2.6: Concorde main landing gear shortening mechanism, adapted from Schmidt [12].

Looking at the fundamental kinematic schemes in Figure 2.3, the stowage footprint can also be reduced by adding an additional hinge axis to form a drop link arrangement. Although it adds complexity, this could be the only viable solution for the Flying-V [9]. A drop link arrangement is found on most Gulfstream aircraft, the Fokker 50, the de Havilland Canada Dash 8 and the Convair B-58 Hustler, the latter being illustrated in Figure 2.7.

Looking at Figure 2.7, one can see that the B-58 bogie is folded parallel to the main strut in the folded position, allowing for more compact stowage. In order to be able to achieve that, the connection of the bogie beam needs to be offset from the shock absorber piston. A so-called 'hockey stick' arrangement has been employed on the B-58 to offset the shock strut from the bogie midpoint. This, however, exposes the strut to large bending moments. An alternative solution is illustrated in Figure 2.8, where the bogie pivot is located above the bogie beam. For both solutions, it is crucial to ensure that the angle between the tyre contact patch's centre and the bogie pivot's centre is less than $45°$, according to Schmidt [12]. If this condition is not met, spin-up loads cause the bogie to tilt downward upon touchdown, resulting in excessive loads on the leading wheels.

Whenever a specific orientation of the bogie in stowed position is required, the strut folding axis can

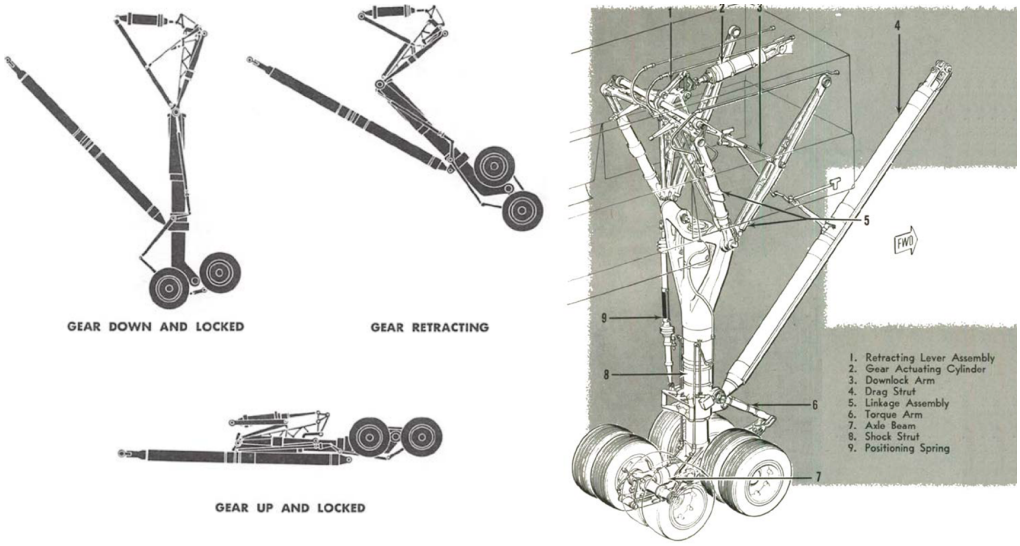

Figure 2.7: Convair B-58 Hustler drop-link main landing gear, adapted from Schmidt [12].

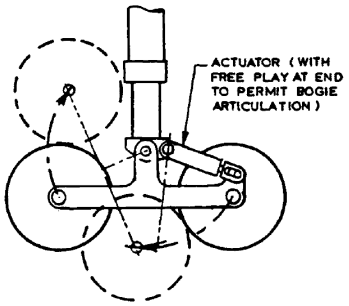

Figure 2.8: Bogie with pivot above bogie beam, adapted from Currey [20].

be skewed [12]. A mild skew is typically employed on the main gear pintle axle of most large transport aircraft. Aggressive skew angles are often employed on fuselage-mounted gears, such as that of the Panavia Tornado, as displayed in Figure 2.9.

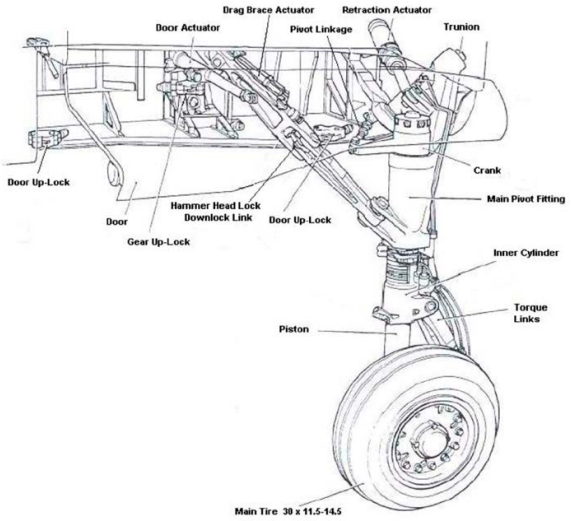

Figure 2.9: Panavia Tornado, main gear with skewed folding axis, adapted from Schmidt [12].

2.2. The Flying-V and its Landing Gear

This section provides an overview of relevant research related to the Flying-V and its landing gear design. It encompasses a review of the evolution of the Flying-V design, emphasising the need for a landing gear design and mass estimation. The section concludes with a review of the development of the landing gear design itself.

2.2.1. Flying-V Design Evolution

The Flying-V is introduced by Benad [4] as a novel aircraft concept, arranging two fuselage barrels in a V-shaped high sweep angle wing. Since then, many studies have contributed to the current Flying-V concept. Where initial research mainly looked at structural and aerodynamic feasibility, research focus has gradually focused more towards design refinement, including family design, flight performance optimisation and component level design considerations.

A family of Flying-V aircraft has been introduced by Oosterom [10], presenting the FV-800, FV-900, and FV-1000 from smallest to largest. The aircraft were developed through a multidisciplinary design optimisation aimed at minimising fuel consumption while maximising family commonality. The FV-1000 floor plan is illustrated in Figure 2.10. The family concept presents fuselage plugs that can be inserted or removed aft and in front of a common fuselage section to adjust the size of the inner wing, effectively changing the size of the aircraft. The shared section is of particular interest as it accommodates landing gear and engine, as well as landing gear stowage. The location of the common fuselage section is a direct result of the location of the landing gear. The size of the stowed landing gear must be minimised as much as it compromises the available fuel tank volume.

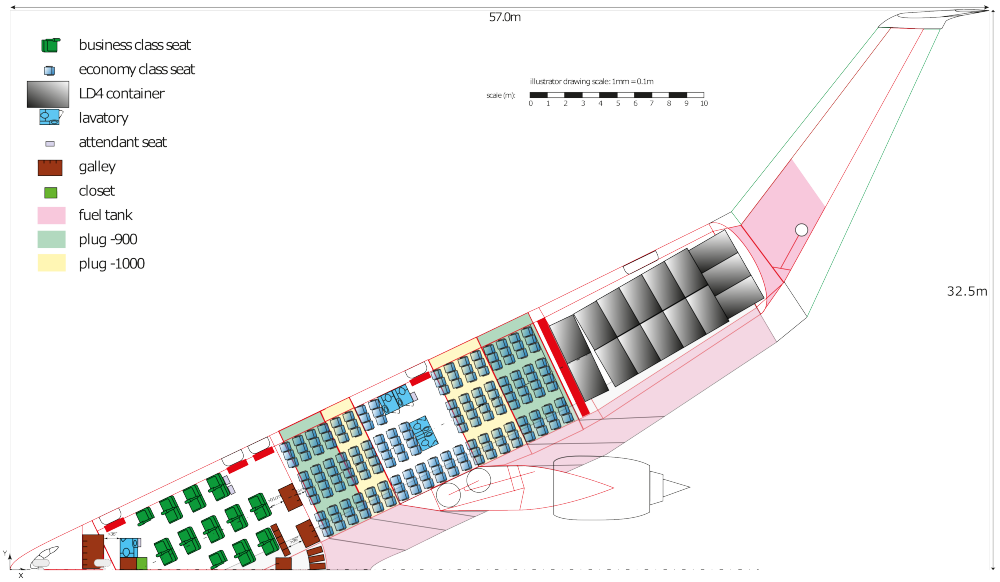

Figure 2.10: FV-1000 floor plan, visualising the plugs to form a FV-800 or FV-900 variant [10]. Image was modified from R. Vos.

Further research on the Flying-V family has been conducted by van der Toorn [21], looking into stability and control characteristics, as well as mass properties. The mass properties in particular are of great interest for the landing gear design. Van der Toorn presents a feasible centre of gravity range for all Flying-V family members. The feasible range of the FV-900 is shown in Figure 2.11a. Additionally, a loading diagram for the FV-900 is presented, as shown in Figure 2.11b. Interestingly, the loading diagram suggests a strong relation between the centre of gravity location and aircraft mass, which, upon inspection of Figure 2.10, can be explained by a large portion of the fuel tank volume being located aft of the centre of gravity. Practically, this implies that the forward centre of gravity cannot be reached for high fuel loads, which could be beneficial for nose gear structural requirements.

Research conducted by de Zoeten [22] compared the landing and take-off performance of the Flying-V with the Airbus A350. The study revealed that the Flying-V requires a shorter take-off distance and a

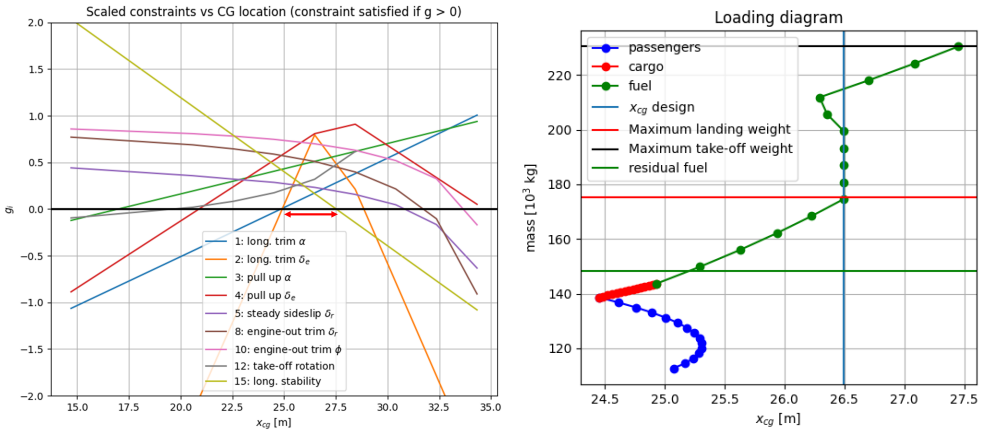

(a) Feasible centre of gravity range for the FV-900, indicated by red arrow.

(b) Loading diagram of the FV-900 (including fuel balancing).

Figure 2.11: FV-900 mass properties [21].

similar landing distance compared to the A350. However, it needs a significantly larger pitch attitude for both take-off and landing, which must be accommodated by the landing gear. Given the objective of achieving similar landing and take-off performance compared to the A350, the take-off speed can be increased to decrease take-off pitch attitude, as there is room to increase take-off distance. However, this cannot be done for landing as increasing landing speed would increase landing distance, which is already similar to that of the A350. It has been suggested to utilise spoilers to generate downforce, increasing the vertical load on the main gear, increasing braking performance and consequently, reducing landing distance [22, 23]. It should be noted that generating downforce and increasing braking loads imposes increased loads on the landing gear as well, which needs to be accounted for. As an additional measure to increase landing performance, the use of split flaps has been proposed [24]. The resulting reduction in landing pitch attitude reduces the time required for de-rotation, such that the Flying-V can start braking more rapidly after touchdown, reducing landing distance. Additionally, a reduced pitch attitude alleviates ground clearance requirements, allowing for a shorter gear.

Oosterom and Vos [25] recognised that the proposed engine mounting position for the Flying-V presents an opportunity for the structural integration of the engine mounting structure with the gear attachment and stowage bay. Subsequently Voeten [26] proposed three different engine mounting structure concepts, which are illustrated in Figure 2.12. All concepts allow for the engine to be lowered from its mounting structure for maintenance or replacement without the need to remove the landing gear, which is logically considered to be a primary requirement. The box-structure of concept 3 was selected for further refinement as the integration of the landing gear bay inside the mounting structure was considered advantageous. The concept does, however, come with a much longer load path compared to concept 1, imposing larger bending moments and consequently, a possible increase in structural weight. Next to that, the concept imposes significant constraints on the landing gear design in terms of both attachment and stowage.

2.2.2. Landing Gear Design Evolution

Initial research on the Flying-V landing gear has been conducted by Bourget [9]. It was found that traditional landing gear design practice is largely based on experience, and because of the unconventional character of the Flying-V, this experience may not always be applicable. Therefore, Bourget proposed a holistic gear design method, which considers ground stability and manoeuvring criteria, gear mass, rotation ability, fairing drag, cabin floor height, and the effect of implementing wing dihedral on low-speed aerodynamics and gear height. This design, as depicted in Figure 2.13, was based on the best available Flying-V characteristics and requirements at that time, and demonstrates satisfactory ground stability, rotation capability, and ground handling abilities. However, the landing gear system features long legs and complex kinematics, including a double folding main strut and a bogie that requires an additional rotation around the shock strut for stowage. The mechanical feasibility of such a system

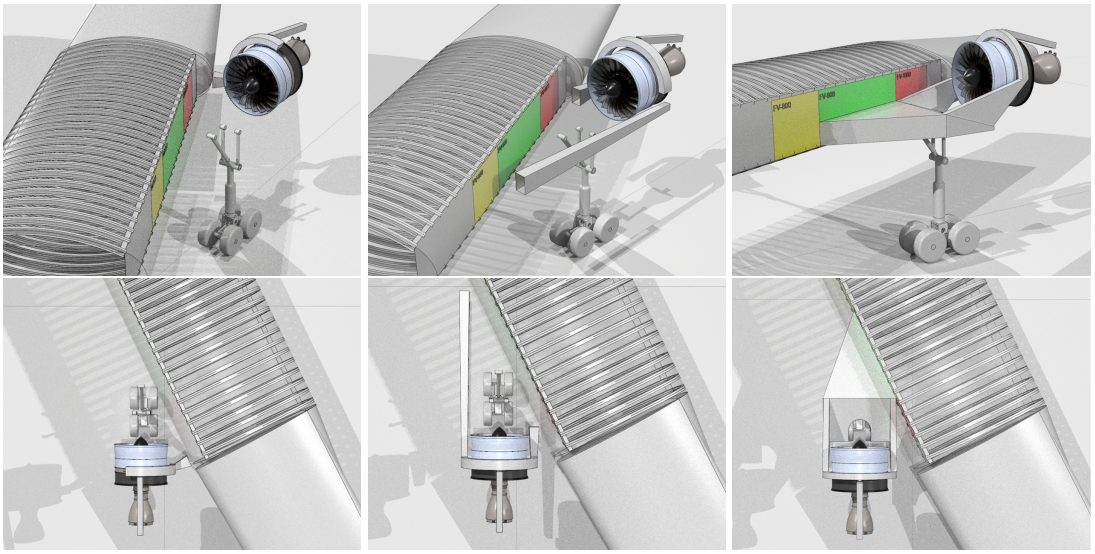

(a) Concept 1 **(b)** Concept 2 **(c)** Concept 3

Figure 2.12: Flying-V engine mounting structure concepts [26]

remains unverified. Additionally, outriggers are required to prevent the wing tips from touching the ground when maximum pitch and roll angle are applied simultaneously, adding complexity and mass. To reduce the length requirement, bogie articulation is proposed, further increasing complexity. Landing gear mass is estimated using an empirical method, known to yield inaccurate results for large and especially unconventional aircraft [12]. Results are shown in Table 2.1.

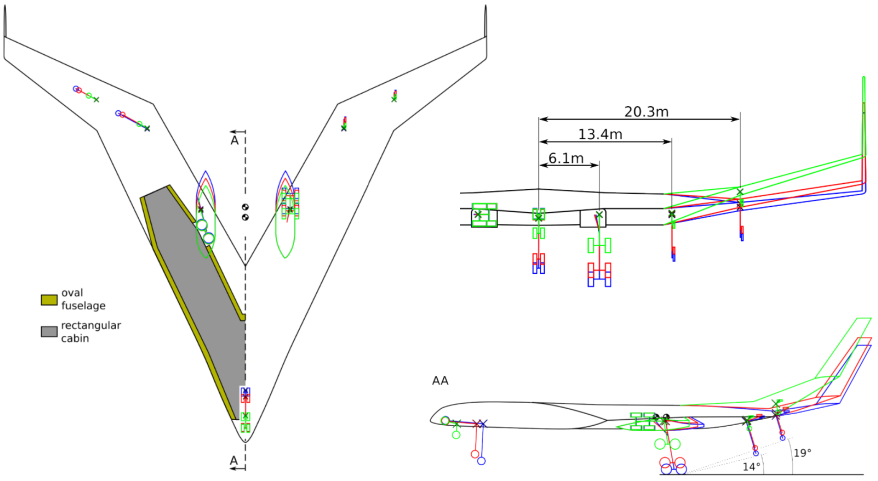

(a) Top, front and side view of the landing gear, showing folded and extended gear positions.

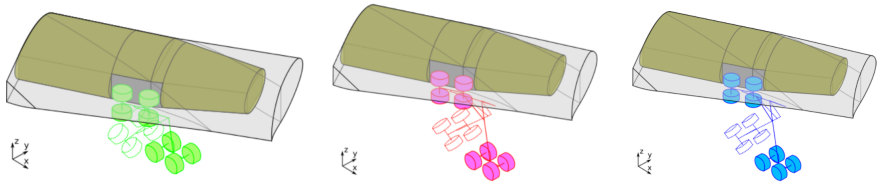

(b) Double folding gear retraction mechanism.

Figure 2.13: Flying-V landing gear for default dihedral (blue), Floor 5.5m dihedral (red) and max dihedral (green), as proposed by Bourget [9].

Table 2.1: Flying-V landing gear mass results from Bourget [9].

Item	Unit	Bourget (floor 5.5)
Main gear	kg (% MTOM)	5.4×10^3 (2.08%)
Nose gear	kg (% MTOM)	1.47×10^3 (0.57%)
Total	kg (% MTOM)	12.3×10^3 (4.73%)

2.3. Conceptual Landing Gear Design Methods

The current Flying-V design state calls for an assessment of landing gear feasibility and mass based on the latest requirements following from the family design [25] and updated centre of gravity locations [27]. To facilitate this, it becomes imperative to design a 'conceptual landing gear'.

Historically, landing gear design has been largely based on experience [8, 28], with the design processes for the landing gear and the aircraft being treated separately [12, 29]. During the conceptual phase of aircraft design, the landing gear requirements are established. These requirements are then used to choose a suitable gear based on semi-empirical relationships and historical landing gear designs, without any aircraft design feedback loop. This process, which is described in high detail in the landing gear design manuals of Conway [16], Currey [20] and Schmidt [12], is not suitable for designing landing gear for novel, unconventional aircraft concepts, such as the Flying-V. While traditional methods usually yield feasible gear designs when designed for aircraft similar to the current state-of-the-art, this cannot be guaranteed when relevant experience is scarce [30]. Next to that, the lack of an aircraft design feedback loop often leads to a compromised overall system integration and optimality of both the aircraft and landing gear [28], which cannot be solved in later design stages. Lastly, the exploratory nature of unconventional aircraft design may generate frequent updates to landing gear requirements, resulting in labour-intensive, time-consuming, and expensive updates to the landing gear design if performed in a traditional way [20].

To address these issues, physics-based design methods have been employed [8, 14, 31, 32]. Instead of relying on experience, physics-based methods use aircraft characteristics and requirements to calculate the position and size of the landing gear directly. If used in an automated design environment, this allows for quick design iterations and optimisation. Predefined load cases can be used to size the structural components and optimise wall thickness for minimum structural mass [8, 14]. Some methods incorporate the aircraft into the design loop for enhanced integration and a more optimised overall design [29, 30, 33]. It has been demonstrated that interdisciplinary physics-based landing gear design methods can be particularly beneficial when designing landing gear for unconventional aircraft, e.g., when no experience is available [30]. State-of-the-art physics-based landing gear design methods employ optimisation algorithms to minimise the mass of the primary structure by varying wall thickness and joint locations [34], or minimise the mass of the rolling stock by adjusting the bogie configuration and dimensions [35].

2.4. Landing Gear Design Requirements

Regardless of whether the landing gear is designed using a traditional, or physics-based design method, its design is influenced by a multitude of aircraft properties and requirements. It can easily be substantiated that in order to have a stable platform, the landing gear needs to be positioned such that the aircraft centre of gravity is always between the nose and main gear. However, the position of the landing gear also affects the amount of landing gear length required to ensure ground clearance during landing and take-off. In addition, the position needs to facilitate efficient integration with the airframe in terms of attachment and stowage. This section aims to provide an overview of landing gear requirements and aircraft properties relevant to conceptual landing gear design.

2.4.1. Stability

The design of the landing gear must ensure that it can adequately support the aircraft under all intended operating conditions, while also allowing for sufficient instability for the aircraft to rotate for take-off and smoothly derotate after landing. Figure 2.14 illustrates landing gear ground reaction loads. The aircraft is said to be longitudinally stable if either all nose and main gear reaction loads are negative, or if main

gear reaction loads are negative and aircraft pitch is controlled by inertia and control surfaces. This needs to be ensured for all possible centre of gravity locations and aircraft attitudes. Please note that the z-axis is defined positive in downward direction.

In general, the main landing gear is placed as far forward as possible to minimise control surface force required for take-off rotation and to avoid abrupt derotation after touch-down [12]. This is particularly important for the Flying-V, which due to its tail-less V-shaped design has a shorter control surface moment arm compared to conventional aircraft, compromising its ability to control pitch, in particular at low speed [9, 36, 37]. Conversely, the landing gear needs to be positioned far enough aft to prevent the aircraft from becoming unstable at maximum pitch-up attitude, known as rotated tipover, or when braking after push-back, known as push-back tipover [20]. The tipback angle θ_{tpb}, as illustrated in Figure 2.14 and defined in Equation 2.1, represents the position of the main landing gear pivot relative to the centre of gravity, and is a helpful metric when evaluating longitudinal stability. Schmidt [12] recommends that the tipback angle should be less than $25°$, but greater than the maximum aircraft tail-down angle to prevent rotated tipover. To avoid push-back tipover, Currey [20] recommends a tipback angle greater than $15°$.

$$\theta_{\text{tpb}} = \tan^{-1}\left(\frac{l_{x,\text{mlg/CG}}}{l_{z,\text{mlg/CG}}}\right) \tag{2.1}$$

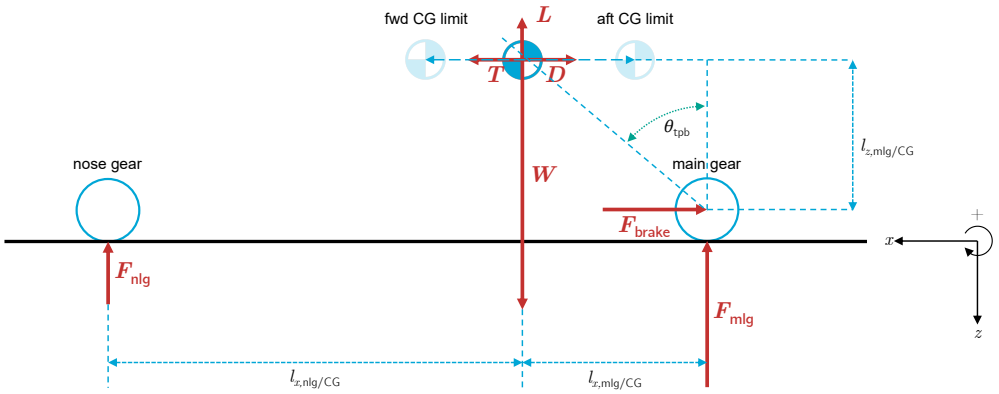

Figure 2.14: Longitudinal stability: landing gear reaction loads

In addition to longitudinal stability, the landing gear must provide lateral stability such that the aircraft does not roll over during a cross-wind landing or while taxiing. For tricycle landing gear, lateral stability is evaluated using the lateral turnover angle ψ_{tno}, as illustrated in Figure 2.15 and formulated by Equations 2.2, 2.3, 2.4 and 2.5. The turnover angle must be evaluated for the most forward centre of gravity location and static shock absorber and tyre deflections. The aircraft is considered laterally stable if the lateral turnover angle is less than $63°$, as this ensures that the tyres will slide before turnover happens [12, 20]. In practice however, aircraft typically have lateral turnover angles in the range $30°$ to $50°$ to increase the operational envelope.

$$\alpha_{\text{tno}} = \tan^{-1}\left(\frac{l_{\text{T,mlg}} - l_{\text{T,nlg}}}{l_{x,\text{nlg/CG}} + l_{x,\text{mlg/CG}}}\right) \tag{2.2}$$

$$l_x = \frac{l_{\text{T,nlg}}}{\tan\alpha_{\text{tno}}} \tag{2.3}$$

$$l_{y,\text{CG/tno}} = (l_{x,\text{nlg/CG}} + l_x)\sin\alpha_{\text{tno}} \tag{2.4}$$

$$\psi_{\text{tno}} = \tan^{-1}\left(\frac{l_{z,\text{gcp/CG}}}{l_{y,\text{CG/tno}}}\right) \tag{2.5}$$

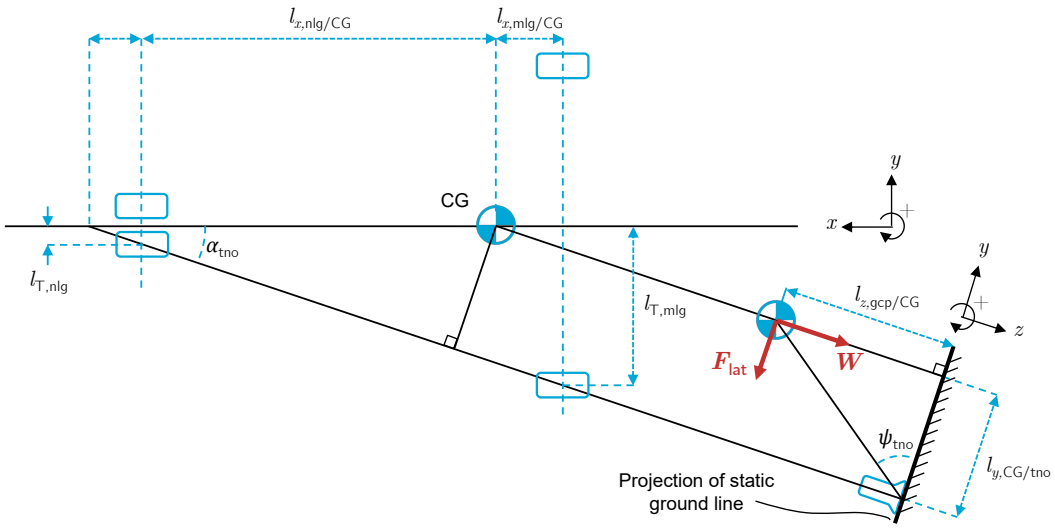

Figure 2.15: Turnover requirement for tricycle arrangement lateral stability. Inspired by Schmidt [12].

2.4.2. Strength

As for virtually all aircraft components, the design of a landing gear is a trade-off between mass, cost, reliability and performance [12]. In the first place, the landing gear must be strong enough to withstand all anticipated static and dynamic loads throughout its service life. Yet, it is equally imperative that the gear is as lightweight and cost-effective as possible. In this section, landing gear load cases, common failure modes and material properties are discussed.

Load Cases

Landing gears are subjected to a wide variety of loads, including ground loads, aerodynamic loads, inertial loads, and loads that may arise in case of equipment failure. Traditionally, the structural sizing of landing gears is based on ground load cases prescribed by regulations [12]. Ground load cases, as defined by the Certification Specification for Large Aeroplanes (CS-25) from EASA or its FAA equivalent, have been effectively incorporated into physics-based landing gear design models in earlier research [8, 14, 26, 29, 31–33, 38]. An overview of load cases that were considered critical in these studies is outlined in Table 2.2. A detailed description of these load cases can be found in Appendix A.

Table 2.2: Overview of CS-25 landing gear ground load cases used for structural analysis in this research

Item	Description	Type
CS 25.479	Level landing conditions	Landing
CS 25.481	Tail-down landing conditions	Landing
CS 25.483	One-gear landing conditions	Landing
CS 25.485	Side load conditions	Landing
CS 25.491	Taxi, take-off and landing roll	Ground handling
CS 25.493	Braked roll conditions	Ground handling
CS 25.495	Turning	Ground handling
CS 25.503	Pivoting	Ground handling
CS 25.507	Reversed braking	Ground handling

General ground load conditions are prescribed by certification specification 25.471. It states that maximum loads for each landing gear component must be calculated considering the least favourable centre of gravity location. In case of multiple wheel landing gear units, the distribution in wheel loads may not be equal due to factors such as aircraft attitude, tyre deviations, surface unevenness, and bogie articulation. CS 25.511 mandates that any variations in these loads must be taken into account.

General landing load conditions and general ground handling load conditions are outlined by CS 25.473

and CS 25.489 respectively. CS 25.473 specifies maximum descent velocities and aircraft mass that need to be considered when evaluating landing load cases. During landing, aircraft lift may be assumed equal to aircraft weight, implying that the landing gear only absorbs vertical kinetic energy upon touchdown. Ground handling conditions specify that ground handling load cases need to be evaluated with the aeroplane at design ramp mass, with zero wing lift, and with shock absorbers and tyres in their static position. Load analysis needs to consider dynamic phenomena, such as shock absorber and tyre characteristics, spin-up and spring back loads, rigid body responses, and structural dynamic response of the airframe. However, during initial sizing, dynamic phenomena may be accounted for using conservative quasi-static approximations [8, 12, 17].

Failure Modes

Loads prescribed by CS-25 load cases are limit loads, which is the maximum load to be expected in service. The landing gear structure must be sized to support limit loads without any permanent deformation. CS 25.303 prescribes that a 1.5 safety factor must be applied to any externally applied limit load to obtain the ultimate load [17]. The landing gear structure must be sized to support ultimate loads for at least three seconds without failure. Translating this to material stress limits, this means that limit loads may not result in stress higher than the material yield strength, and ultimate loads may not result in stress higher than the material ultimate strength [12].

When a structure experiences a combination of axial, bending, shear, and torsional loads, the onset of material yielding can be forecasted using the maximum distortion energy criterion, also known as the von Mises yield criterion [39]. The criterion states that yielding of a ductile material, e.g., a metal, starts when the equivalent von Mises stress σ_{Mises} is higher than the material yield strength σ_{y}. The equivalent von Mises stress can be calculated using Equation 2.6, where σ_{zz} is the normal stress due to combined axial and bending loads, and τ_{zs} is the shear stress due to combined transverse shear and torque loads. The von Mises yield criterion has been employed to determine the required wall thickness of landing gear structures in prior studies, using limit loads as sizing loads [8, 29, 32]. Typically, a 1.5 safety factor is used to ensure that actual stress resulting from limit loads and ultimate loads, stay well below the material yield stress and ultimate stress limits, respectively [40].

$$\sigma_{\text{Mises}} = \sqrt{\sigma_{zz}^2 + 3\tau_{zs}} \tag{2.6}$$

In long and slender structural components subjected to compressive loading, such as the drag and side stays, failure is generally caused by buckling instead of compression yielding [8, 12]. When the compressive load in the material reaches a certain critical buckling load, the member may suddenly become unstable, leading to the member losing its load-carrying capacity. The critical buckling load F_{critical} in a two force member, e.g., a truss member, can be estimated using Euler's critical load equation, as formulated by Equation 2.7 [8, 39]. Here, E is the Young's modulus, I is the second area moment, and l is the beam length. K is the dimensionless effective length factor, which is 1 for a pin-ended member, and 0.5 for a member with fixed ends.

$$F_{\text{critical}} = \frac{\pi^2 EI}{(Kl)^2} \tag{2.7}$$

CS 25.571 prescribes that landing gear components need to be designed following the safe-life design principle, meaning that the structural members must be free of fatigue cracks during their design life [12]. Typical design lives for landing gear structures are 50,000 cycles for short-haul aircraft and 25,000 cycles for long-haul aircraft. The maximum permissible cyclic stress is generally significantly lower than the yield stress limits of the material and depends on the number of cycles the material may be exposed to before failure.

Landing Gear Materials

Selecting the right landing gear material is a crucial part of landing gear design. Landing gear materials need to have a high strength-to-weight ratio (specific strength), be resistant to corrosion, fit within the designated space, and be suitable for the intended type of loading. The material must have adequate

stiffness to prevent unwanted dynamic behaviour or elastic deformation. Furthermore, material toughness and fatigue resistance must be sufficiently high to ensure the structure does not fail throughout its intended design life. Other factors to consider include the availability of the material, its manufacturability, maintenance requirements, and cost [12].

Table 2.3 summarises the properties of materials commonly used in landing gear structures. Landing gear structures of large transport aircraft are typically made of steel, corrosion-resistant steel (CRES), and titanium alloys [12]. Steel is most frequently used because it generally offers the best combination of strength-to-weight ratio, strength-to-volume ratio, fatigue properties, and cost. 300M steel in particular is very suitable for components where buckling is the critical failure mode due to its high Young's Modulus. For components that require high corrosion resistance, corrosion resistant steel and titanium may be a suitable alternative, albeit at a higher cost. Aluminium is not often used for landing gear structures as its low strength requires large member cross-sections to resist the structural loads.

While composites may seem to offer superior properties, their application in landing gear structures is not widespread, with only a few examples of certified structural landing gear components found in practice [12]. To support the large and typically multi-directional loads that the landing gear is subjected to, and to compensate for the strongly anisotropic material properties, composite components require a large number of laminations. However, when subjected to high-impact point loads, for instance due to foreign objects, composite structures are prone to delamination, causing failure. Because the landing gear is typically placed in an high-impact environment, it is challenging to incorporate composite components into landing gear [12]. Nevertheless, when a component is primarily loaded in one direction, the anisotropic strength of the composite material can be effectively utilised. For instance, composites have successfully integrated in the Boeing 787 main landing gear as side and drag brace, where the loads are primarily unidirectional [12].

Table 2.3: Typical properties of various landing gear structural materials [12]

Material	Ultimate strength (MPa)	Yield strength (MPa)	Young's Modulus (GPa)	Density (g/cm^3)	Specific ultimate strength	Specific modulus
Steel 300M	1931	1586	200	7.83	247	25.5
CRES Ferrium S53	1931	1468	199	7.98	242	24.9
Al 7050-T74	483	407	70	2.82	171	24.8
Ti 10-2-3	1193	1103	110	4.65	256	23.7
Carbon (HM)/epoxy[1,2]	930	-	213	1.6	581	133
Carbon (HS)/epoxy[1,2]	1620	-	148	1.5	1080	98.7
E-glass/epoxy[1,2]	1310	-	41	1.9	689	21.6
Ti-MMC (6-5/35% SiC)[1,3]	1650	-	196	3.0	550	65

[1] Properties shown for composites are for unidirectional reinforcement arrangement.
[2] Polymer matrix composite.
[3] Metal matrix composite.

2.4.3. Ground Interaction

The landing gear must be designed such that the aircraft has sufficient ground clearance for take-off and landing, and impact loads do not cause excessively large loads on the primary aircraft structure. Landing gear requirements related to landing and take-off ground clearance and shock absorption are discussed in this section.

Ground Clearance

It must be ensured that apart from the landing gear, the aircraft remains clear of the ground for all possible combinations of yaw, pitch and roll in the intended operating envelope. With the shock absorber extended, the aircraft needs to be able to attain its maximum pitch attitude required for take-off or landing without tailstrike. Typically, this angle is between 12 and 17 degrees [12]. If necessary, additional ground clearance can be achieved by extending the length of the gear, although this comes with an increase in mass. Alternatively, the gear can be positioned further aft, but this comes at the expense of

rotation ability. In cases where there is no structure available to attach the gear further aft, the ground contact points may be offset from the main fitting attachment by implementing a strut rake angle. Typically, this rake angle is limited to $7°$. However, larger rake angles up to $10°$ have been successfully employed, albeit in conjunction with large bearing overlap, large bearing friction and higher mass [12].

In addition to enabling the aircraft to achieve its maximum pitch attitude, the landing gear must permit the aircraft to roll about its longitudinal axis without wing tips or engine nacelles touching the ground. Typically, at least $8°$ roll must be permitted to allow for corrections during cross-wind landings, but often more is desired to open up the operational envelope [12, 41].

Shock Absorption

The landing gear needs to be designed to ensure that peak reaction loads that arise during landing and ground operations are efficiently transferred to the landing gear and aircraft structure. Shock absorbers and tyres provide spring suspension and damping, alleviating peak loads directly applied to the main structure. The required vertical shock absorber travel for appropriate landing impact energy absorption can be calculated using the conservation of energy principle, as shown by Equation 2.8 [12].

$$E_{\text{abs}} = E_{\text{kin}} + E_{\text{pot}} \tag{2.8}$$

Here, E_{kin} is the vertical kinetic energy, and is given by Equation 2.9 with aircraft mass m and vertical velocity V, which are defined by the descent conditions prescribed by certification specifications CS25.473 and CS25.723, as outlined in Table 2.4 [17].

$$E_{\text{kin}} = \frac{1}{2} m V^2 \tag{2.9}$$

Table 2.4: Descent conditions for large transport aircraft [17].

Condition	Descent velocity	Mass	Reference
Limit descent velocity	3.05 m/s	MLM	CS 25.473
Limit descent velocity	1.83 m/s	MTOM	CS 25.473
Reserve energy test	3.70 m/s	MTOM	CS 25.723

E_{pot} is the potential energy, given by Equation 2.10. For large transport aircraft, the lift fraction L in Equation 2.10 may be assumed to be equal to 1, such that $E_{\text{pot}} = 0$ [12, 17].

$$E_{\text{pot}} = (1 - L) m g (x_{\text{axle}} + x_{\text{tyre}}) \tag{2.10}$$

Lastly, E_{abs} is the energy absorbed, or work done by the shock absorber and tyre, given by Equation 2.11, with vertical reaction factor λ, aircraft mass m, acceleration due to gravity g, shock absorber and tyre efficiency η_{axle} and η_{tyre}, and vertical axle travel and tyre deflection x_{axle} and x_{tyre}. The reaction factor describes the ratio between the peak landing load and aircraft weight, and defines the maximum load subjected to the aircraft structure. The maximum vertical load on a single gear strut is given by Equation 2.12 [12], where m_{gear} is the aircraft mass carried by the respective strut. For large transport aircraft, the reaction factor is typically between 1.1 and 1.3 [12]. For sizing calculations, tyre and shock absorber efficiency may be assumed 47% and 80% respectively [12].

$$E_{\text{abs}} = \lambda m g (\eta_{\text{axle}} x_{\text{axle}} + \eta_{\text{tyre}} x_{\text{tyre}}) \tag{2.11}$$

$$F_{\text{gear,max}} = \lambda g m_{\text{gear}} \tag{2.12}$$

Substituting Equations 2.9 and 2.11 into Equation 2.8 and isolating axle travel x_{axle}, Equation 2.13 is obtained.

$$x_{\text{axle}} = \frac{1}{\eta_{\text{axle}}} \left(\frac{V^2}{2g\lambda} - \eta_{\text{tyre}} x_{\text{tyre}} \right) \tag{2.13}$$

Tyre deflection x_{tyre} can be estimated using Equation 2.14 [12], where r_{loaded} and r_{unloaded} are the loaded and unloaded tyre radii, $F_{\text{gear,rated}}$ is the rated tyre load, and N_{tyres} equals the number of tyres associated with the strut.

$$x_{\text{tyre}} = 0.9(r_{\text{unloaded}} - r_{\text{loaded}}) \frac{F_{\text{gear,max}}}{F_{\text{rated,tyre}} N_{\text{tyres}}} \tag{2.14}$$

Please note that vertical axle travel calculated using Equation 2.13 is rarely equal to the actual shock absorber stroke, because the strut is rarely perpendicular to the runway when landing due to the aircraft attitude and strut rake angle [12]. The largest actual shock absorber stroke can be calculated using Equation 2.15, where α is the largest angle between the shock strut and landing surface likely to occur within the landing envelope.

$$x_{\text{SA}} = \frac{x_{\text{axle}}}{\cos \alpha} \tag{2.15}$$

In order to ensure that there is sufficient axle travel available during ground operations, it is recommended to limit the static compression of the shock absorber to 80%-85% of the total available stroke [12]. For oleo-pneumatic shock absorbers, which are predominantly used in virtually all large transport aircraft landing gear, this can be verified by evaluating the spring curve described by Equation 2.16. Here P and V describe the gas pressures and volumes, and γ the heat capacity ratio. The value for γ depends on the shock absorber type. For shock absorbers where gas and oil are separated, the value is typically around 1.4 as a result of heat generated during the compression. For shock absorbers where oil is sprayed in the gas chambers directly, the gas is cooled by the oil, resulting in a heat capacity ratio around 1.

$$\frac{P_0}{P_1} = \left(\frac{V_1}{V_0} \right)^{\gamma} \tag{2.16}$$

To calculate the static shock absorber stroke, the desired breakout load, static load and maximum load on the landing gear are required, as well as the desired static pressure and the total shock absorber stroke between the fully extended and fully compressed position. The breakout load is the minimum load required to compress the shock absorber. The breakout load must be high enough to ensure that the shock absorber fully extends after take-off, but be low enough to ensure that the aircraft can operate smoothly. Typically, the breakout load is in the range of 7% to 17% of the static load on the gear at maximum landing mass [12].

The required shock absorber piston area and diameter can be calculated using the static load on the gear at maximum ramp mass and the maximum static shock absorber pressure, which is typically between 1500 and 2500 psi [12]. The total volume swept by the piston is calculated using the maximum shock absorber stroke and piston surface area, as shown by Equation 2.17. Because the shock absorber is generally allowed to bottom out during a reserve energy test, the maximum stroke is instead defined by the stroke required for the 3.05 m/s limit descent velocity condition. An additional 10% margin may be added to accommodate low temperature operations and future aircraft growth [12].

$$V_0 - V_2 = x_{\text{SA,max}} A_{\text{piston}} \tag{2.17}$$

The maximum pressure P_2 in the shock absorber is a result of the 1.7g bump load described by load case CS 25.491 (Table 2.2 and Table A.1) at maximum ramp mass, as shown in Equation 2.18. Here, β is the fraction of the aircraft mass supported by the respective gear strut.

$$P_2 = \frac{1.7\beta g \text{MRM}}{A_{\text{piston}}} \tag{2.18}$$

The fully extended shock absorber volume V_0 can be calculated by substituting Equations 2.17 and 2.18 in Equation 2.16. For γ = 1, this results in Equation 2.19.

$$V_0 = \frac{x_{\text{SA,max}} A_{\text{piston}} P_2}{P_2 - P_0} \tag{2.19}$$

The compressed gas volume in the static position is given Equation 2.20.

$$V_1 = V_0 - x_{\text{SA,static}} A_{\text{piston}} \tag{2.20}$$

By substituting Equation 2.20 into Equation 2.16, Equation 2.21 is obtained, which can be used to calculate the static shock absorber stroke $x_{\text{SA,static}}$.

$$x_{\text{SA,static}} = \frac{1}{A_{\text{piston}}} \left(V_0 - V_0 \left(\frac{P_0}{P_1} \right)^{\frac{1}{\gamma}} \right) \tag{2.21}$$

2.4.4. Airport Compatibility

Airport compatibility is a key aspect of landing gear design, encompassing several key considerations. The aircraft must have sufficient control authority to independently manoeuvre itself on the airport, and must have sufficient means to safely come to a stop after landing or in case of a rejected take-off. The aircraft landing gear track and wheelbase must not surpass intended airport runway and taxiway limits, and ground reaction loads must be sufficiently distributed, such that the aircraft can operate from the intended airport surface. Lastly, it is highly beneficial if the aircraft service points are not too high above the ground, such that it can be serviced with ground support equipment already present at those airports.

Gear Load Limits

To ensure the aircraft has sufficient directional control, the static load on the nose gear should be at least 5% of the total aircraft weight [9, 12]. However, Airbus A330 and A350 airport planning manuals suggest that 4% can also provide satisfactory performance [42, 43]. On the other side of the spectrum, the static nose gear load should also not be too high. In absolute terms, high nose gear loads result in larger structural mass, and in relative terms, a high nose gear load fraction implies a low main gear load fraction, negatively affect braking performance. As such, the static nose gear load should not exceed 20% of the total aircraft weight [20], with 15% often being used as a practical limit [12, 20, 41]. To minimise nose gear loads and associated structural mass, and maximise braking and performance, the nose gear is typically positioned as far forward as the minimum load and stowage constraints allow [12]. The nose gear load fraction β_{nlg} can be calculated using Equation 2.22, with dimensions as defined in Figure 2.14.

$$\beta_{\text{nlg}} = \frac{l_{x,\text{mlg/CG}}}{l_{x,\text{nlg/CG}} + l_{x,\text{mlg/CG}}} \tag{2.22}$$

The maximum static load on each tyre is defined by the load rating of the respective tyre, which can be found in tyre specification sheets, such as those provided by Schmidt [12]. Tyres can withstand a load that is 1.5 times higher than the static load when dynamically loaded, e.g., during braking [12]. For both static and dynamic loading, a 1.07 safety factor needs to be applied, as stipulated by CS25.733 [17].

Braking

Landing gear brakes need to be designed such that they can bring the aircraft to a full stop after landing or in case of a rejected take-off [12]. The consideration of thrust reversal is not permitted by regulations [17]. As a conservative estimate, it may be assumed that all kinetic energy of the aircraft is absorbed by the brakes, neglecting the effect of tyre rolling resistance, aerodynamic drag, and runway slope. The energy that needs to be absorbed by the brakes can be calculated using Equation 2.23. The rejected take-off case describes the largest energy to be absorbed, with V = V_1, and m = MTOM.

$$E_{\text{kin}} = \frac{1}{2} m V^2 \tag{2.23}$$

Braking causes a pitch down moment that needs to be resisted by the nose gear and its tyres. The maximum vertical reaction of the nose gear during constant deceleration can be calculated using Equation 2.24 [8]. Here, dimensions l are defined as specified in Figure 2.14, W is the respective aircraft weight and g is the gravitational acceleration. The deceleration due to braking a_x, needs to be at least 3.1 m/s^2 at maximum landing weight, or 1.8 m/s^2 at maximum take-off weight, as stipulated by CS25.735 [17].

$$F_{\text{nlg}} = \frac{l_{x,\text{mlg/CG}} + \frac{a_x}{g} l_{z,\text{mlg/CG}}}{l_{x,\text{nlg/CG}} + l_{x,\text{mlg/CG}}} W \tag{2.24}$$

Taxiway Design Groups

Airport taxiways are typically designed according to recommended practices outlined by aviation authorities. The Federal Aviation Administration specifies taxiway design groups (TDGs) in Advisory Circular 150/5300-13B, outlining taxiway and taxilane width, clearance and fillet design standards depending on the aircraft outer main gear width (MGW) and the cockpit to main gear distance (CMG) [44]. Whenever a taxiway is designed according to a TDG standard, this ensures that an aircraft belonging to that TDG is able to operate from that taxiway. The other way around, if a landing gear is designed to be within the limits set by the intended TDG, it ensures that the aircraft can operate from airports designed according to that TDG standard. Taxiway design group dimensions are displayed in Figure 2.16.

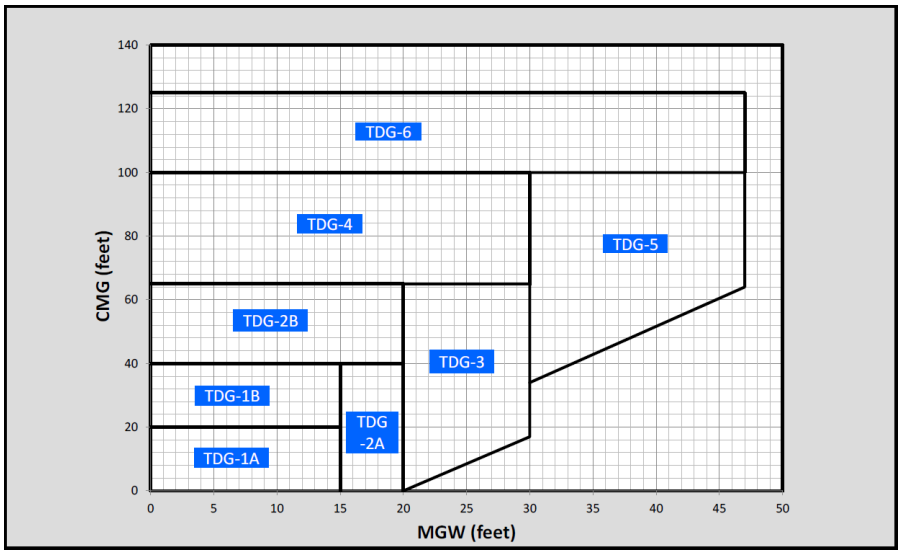

Figure 2.16: Taxiway design groups (TDGs), as specified by FAA AC 150/5300-13B [44].

Minimum Turn Width

The International Civil Aviation Organization (ICAO) mandates that aircraft need to be able to make a $180°$ turn on the runway [45]. Generally, runways need to have turn pads to facilitate the turn, as runways are typically not wide enough. Turn pad widths are not specifically mandated, however ICAO does recommend a clearance distance between any of the aircraft wheels and the turn pad edge.

Prescribed clearance dimensions depend on the outer main gear width and wheelbase, and are outlined in Table 2.5.

Table 2.5: Turn pad clearance distance as recommended by ICAO Annex 14 [45]

	MGW			
	Up to but not including 4.5 m	4.5 m up to but not including 6 m	6 m up to but not including 9 m	9 m up to but not including 15 m
Clearance	1.50 m	2.25 m	3 m[1] or 4 m[2]	4 m

[1] For aircraft with a wheelbase less than 18 m.
[2] For aircraft with a wheelbase equal to or greater than 18m.

An aircraft is capable of making a $180°$ turn on a turn pad or runway, when its minimum turn width l_{turn} plus two times its respective clearance distance (both sides), is smaller than the width of a turn pad or runway. The minimum turn width can be calculated using Equation 2.26, where l_{tc} is the turn centre location, which is the neutral point around which the aircraft rotates (Equation 2.25), $l_{\text{wheelbase}}$ is the wheelbase length, and $\lambda_{\text{steering}}$ is the nose gear steering angle. Compliance with the $180°$ turn requirement may be shown by comparing the minimum turn width of the design aircraft with that of aircraft that already operate on intended airports. Minimum turn widths can typically be found in aircraft airport planning manuals, such as [43]. Some examples are shown in Table 2.6. Interestingly, the A380-800 has a turn width that is smaller than that of the A350, which can be attributed to the presence of main gear steering.

$$l_{\text{tc}} = l_{\text{wheelbase}} \tan(90° - \lambda_{\text{steering}}) \tag{2.25}$$

$$l_{\text{turn}} = \frac{1}{2}(l_{\text{S,mlg,single}} + l_{\text{S,nlg,single}}) + l_{\text{T,mlg}} + l_{\text{tc}} + \sqrt{(l_{\text{tc}})^2 + (l_{\text{wheelbase}})^2} \tag{2.26}$$

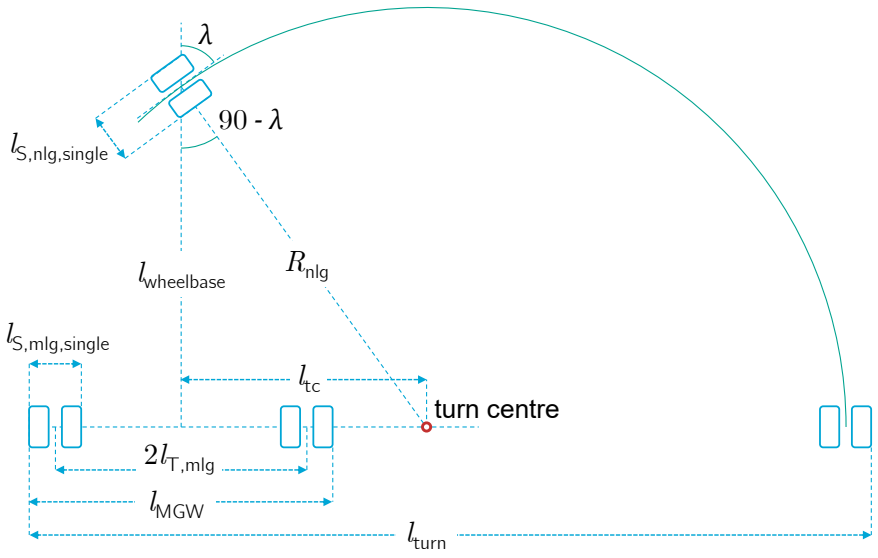

Figure 2.17: Turn centre definition

Turning Radii and Separation Distance

Airports are designed such that runways, taxilanes, taxiways and objects are sufficiently separated. Margins are included to prevent collisions should pilots deviate from the centreline [45]. Usually, separation distances and clearance margins are prescribed based on the intended ICAO reference code letter, which categorises aircraft based on their wing span. Reference code letters and critical minimum separation distances as defined by ICAO Annex 14 [45] are outlined in Table 2.7.

Table 2.6: Examples of minimum turn widths [18, 42, 43, 46].

Aircraft	l_{turn} (m)
A320-200	22.8
A330-200	45.6
A330-300	50.7
A350-900	51.1
A350-1000	59.2
A380-800	50.9

Table 2.7: Aerodrome reference code letters and critical minimum taxiway separation distances as recommended by ICAO Annex 14 [45]

Code letter	Wing span (m)	Taxiway centre line to centre line (m)	Aircraft stand taxilane centre line to centre line (m)
A	< 15	15.5	19.5
B	15 < 24	20	28.5
C	24 < 36	26	40.5
D	36 < 52	37	59.5
E	52 < 65	43.5	72.5
F	65 < 80	51	87.5

While using these separation distance values may ensure sufficient margin to prevent collisions when moving straight ahead, this may no longer be true when turning. This is particularly the case for aircraft with high-sweep angle wings, where the distance between the wing tip and the turn centre is significantly larger compared to conventional aircraft, causing the wing tip to swing out considerably during turns. In such instances, standard separation distances may not be sufficient to allow for safe operation of the aircraft, even if the aircraft falls under the ICAO reference code letter for which the airport was designed. Therefore, it becomes necessary to evaluate turning radii of critical aircraft components, such as the wing tip, tail, and nose, in addition to the minimum turn width. By using the turning radii and turn centre location, the maximum centreline deviation distance for each component can be determined. If this maximum deviation distance violates the maximum permissible deviation distance, the landing gear positions may need to be adjusted in order to have a different turn centre location. Alternatively, this might impose operational limitations.

Flotation

Ground loads need to be sufficiently distributed such that the intended airport surface can reliably and repetitively support the weight of the aircraft. This characteristic, commonly known as flotation, has a major impact on the operational limitations of the aircraft [12]. Hence, flotation is an important metric to consider in landing gear design. Parameters affecting flotation characteristics are the landing gear load distribution, the number of tyres, the wheel spacing and the tyre contact patch area. The latter is affected by the tyre specification and inflation pressure [8].

Due to the wide variety of pavement types and qualities, flotation analysis is not straightforward [12]. For initial landing gear design, wheel arrangements may be selected based on that of comparable aircraft, ensuring similar flotation, mitigating the need for flotation analysis [9, 20]. However, this approach requires the existence of comparable aircraft and would not allow for evaluating different wheel configurations, making it unsuitable for physics-based design explorations. Alternatively, flotation performance may be confirmed using the ICAO ACR/PCR method [47]. The method allocates Aircraft Classification Ratings (ACR) to aircraft and calculates required pavement thickness. The calculation takes into account factors such as wheel arrangement, tyre pressure, tyre loads, and the type and subgrade strength of the pavement surface. If the ACR is lower than the Pavement Classification Rating (PCR) of the respective pavement, the aircraft can use the pavement without any restrictions [12]. Although the ACR/PCR method does not specifically calculate aircraft flotation, it can be used to compare pavement requirements for different aircraft and different gear arrangements [20]. Aircraft Classification Ratings and minimum required pavement thickness for both rigid (concrete) and flexible (asphalt) surfaces with different subgrade strengths can be calculated using the ICAO-ACR tool [47].

The results for the A350-900 are shown in Table 2.8.

Table 2.8: A350-900 ACR numbers and required pavement thickness, obtained from the ICAO-ACR tool [47].

		Flexible		Rigid	
Subgrade category	Subgrade modulus (MPa)	ACR number	Thickness (mm)	ACR number	Thickness (mm)
D	50.0	884	978	1031	506
C	80.0	742	793	918	458
B	120.0	692	665	825	418
A	200.0	680	546	729	372

Ground Service Accessibility

The landing gear should be designed in a way that, when the shock absorbers and tyres are in their static position, the height of the cabin floor allows the aircraft to be serviced using existing ground support equipment (GSE) [9]. Although in theory, GSE could be modified to accommodate novel aircraft requirements, it is generally beneficial to ensure compatibility with existing equipment. This avoids the need for costly investments in new GSE fleets, thereby enhancing commercial viability of the aircraft. Examples of door sill heights of various existing wide-body aircraft are outlined in Table 2.9.

Table 2.9: Aircraft door sill heights. Height ranges displayed in this table are based on maximum ramp weight, operational empty weight, variation in centre of gravity location and difference due to static aircraft incidence angle (sill heights of doors located at the front are generally lower than that of doors located at the rear).

Aircraft	Main deck door sill height (m)	Upper deck door sill height (m)	Cargo hold door sill height (m)
Airbus A330-200 [42]	4.4 - 5.7	N/A	2.6 - 3.7
Airbus A330-200F [42]	4.8 - 5.1	N/A	2.9 - 3.6
Airbus A350-900 [43]	5.0 - 5.5	N/A	3.1 - 3.5
Airbus A380-800 [46]	5.1 - 5.4	7.9 - 8.2	3.1 - 3.4

2.4.5. Retraction, Stowage and Extension

Most large transport aircraft have landing gear that retract within the wings or fuselage to decrease aerodynamic drag during cruise flight. When designing such landing gear, it is important to verify that selected gear locations allow the gear to be retracted without interfering with other aircraft components. Regulations require that tyres always have sufficient clearance from surrounding structures and systems, taking into account the maximum tyre dimensions expected in service [17]. For radial ply tyres, the minimum required radial clearance may be calculated using Equation 2.27, and the minimum required lateral clearance may be calculated using Equation 2.28 [12]. Here d_{rim} is the wheel rim ledge diameter, d_{grown} is the maximum grown outside tyre diameter, w_{grown} is the maximum grown tyre width, and w_{rim} is the width between the wheel rim flanges, all measured in inches. V is the aircraft speed in miles per hour.

$$s_{\text{rad,min}} = 0.029\sqrt{d_{\text{grown}} - d_{\text{rim}}}\sqrt{w_{\text{grown}} - w_{\text{rim}}}\sqrt{\frac{V}{d_{\text{grown}}}} + 0.15 \tag{2.27}$$

$$s_{\text{lat,min}} = 0.01 w_{\text{grown}} \tag{2.28}$$

In addition, regulations prescribe that locking means must be provided to make sure the gear remains in the down position when extended, and remains in the up position when retracted. Moreover, there must be alternative methods to extend the gear in case it cannot be extended using the primary extension mechanism [17].

2.5. Mass Estimation

It is crucial to have insight in landing gear mass early in the design process for good design decision making and to be able to accurately estimate aircraft flight performance and payload capacity. In this section, landing gear mass estimation methods are discussed.

2.5.1. General

Mass estimation methods are typically grouped into classes [48]. Class 1 methods offer the lowest fidelity estimate, and relies solely on statistics and top-level aircraft requirements on an aircraft category level. Class 2 methods provide a slightly better estimate, relying on semi-empirical equations and statistics to estimate the mass of the main aircraft components. Typically, the baseline geometry, aircraft level properties and load factors need to be available for a class 2 method. Class 3 methods introduce physics-based estimations, based on extensive structural analysis and multibody simulations. They provide the highest fidelity estimate, but are by far the most computationally and labour intensive, typically making them unsuitable for the conceptual aircraft design phase.

2.5.2. Class 1 and Class 2 Methods

Historically, landing gear mass estimations are based on statistical Class 1 and Class 2 methods. Torenbeek [41], Roskam [49], Raymer [50] all present statistics based gear mass estimation equations, the latter being used by Bourget [9] to estimate the mass of the landing gear of the Flying-V. Main gear mass can be estimated using Equation 2.29 and nose gear mass can be estimated using Equation 2.30 [50]. Both equations are corrected from imperial to SI units.

$$m_{\text{mlg}} = 0.045 K_{\text{mp}} m_{\text{MLM}}^{0.888} N_{\text{l}}^{0.25} l^{0.4} N_{\text{mlg,wheels}}^{0.321} N_{\text{mlg,ss}}^{-0.5} V_{\text{S}_\text{R}}^{0.1} \tag{2.29}$$

$$m_{\text{nlg}} = 0.152 K_{\text{np}} m_{\text{MLM}}^{0.646} N_{\text{l}}^{0.2} l^{0.5} N_{\text{nlg,wheels}}^{0.45} \tag{2.30}$$

Where:

- K_{mp}: correction factor, equal to 1.126 for kneeling gear, otherwise it is equal to 1.0.
- K_{np}: correction factor, equal to 1.15 for kneeling gear, otherwise it is equal to 1.0.
- l: gear strut length (m)
- m_{MLM}: maximum aircraft landing weight (kg)
- m_{mlg}: main landing gear group mass (kg)
- m_{nlg}: nose landing gear group mass (kg)
- N_{l}: ultimate landing load factor (limit loading factor, or reaction factor times 1.5)
- $N_{\text{mlg,ss}}$: number of main landing gear shock struts
- $N_{\text{mlg,wheels}}$: total number of main gear wheels (all struts combined)
- $N_{\text{nlg,wheels}}$: total number of nose gear wheels
- V_{SR}: reference stall speed (m/s)

However, it is important to note that these methods, which are based on data from the 1960s and 1970s, only provide accurate results for aircraft and landing gear from that era [12]. Furthermore it was found that the data sets typically only contain a few aircraft with a maximum take-off mass exceeding 225 tonnes, making it difficult to establish proper trends for heavy aircraft [8].

2.5.3. Class 2.5 Methods

As an alternative means to estimate landing gear mass, methods have been proposed that bridge the gap between computationally expensive Class 3 methods and low-fidelity Class 2 methods [8, 38]. These so-called Class 2.5 methods use physics-based structural analysis to obtain a structural mass estimation. The mass of other components that contribute to the overall gear group mass is determined using statistical and empirical relationships. This approach has been adopted in various landing gear design studies [14, 29, 32, 34, 35].

Structural Mass
The structural mass of structural components can be estimated by calculating the minimum required material volume to support the loads to be expected during service. Typically, these loads are specified by regulations. Structural analysis can be performed using analytical methods [8, 14, 32, 38], as well as finite element methods (FEM) [29, 51]. In both cases, typically, the analysis is based on a simplified representation of the landing gear structure. However, when dealing with more complex, possibly statically indeterminate, structural arrangements, FEM is considered to be more suitable [12]. Most computer-aided design (CAD) software come equipped with finite element analysis (FEA) packages. This integration allows for a quick comparison between different gear designs, enhancing the efficiency of the design process [12].

Group Mass
An overview of a typical landing gear group mass breakdown (Boeing 707) is given in Table 2.10. Here, the shock strut mass describes the mass of the primary structure including the trunnion, shock strut cylinder, shock strut piston and if applicable, the bogie beam. The total landing gear group mass may be estimated using the structural mass estimate and the relative contributions of rolling stock and controls outlined in the table [8, 20].

Table 2.10: Boeing 707 gear mass breakdown, modified from Currey [20].

Component	Main gear	Nose gear
Rolling stock	35%	2%
Wheels	8%	1%
Tyres	11%	1%
Brakes	16%	-
Structure	46%	3%
Shock strut	27%	2%
Fittings	14%	-
Braces	4%	1%
Misc.	1%	-
Controls	11%	3%
Total	92%	8%

For a more representative estimate of rolling stock mass, empirical equations and tyre specification sheets can be used. Equation 2.31 provides an estimate of brake assembly mass for carbon brakes, where m_{brakes} is the brake assembly mass (in kg) for a single braked wheel, and E_{kin} the maximum kinetic energy to be absorbed (in MJ) [12]. Similarly, Equation 2.32 estimates wheel mass m_{wheel} (in kg) based on the wheel rim diameter d_{rim} (in inches) [12]. Tyre specification sheets with tyre mass data can be found in the book of Schmidt [12].

$$m_{\text{brakes}} = 0.8653 E_{\text{kin}} + 12.722 \tag{2.31}$$

$$m_{\text{wheel}} = 0.0202 d_{\text{rim}}^3 - 0.3936 d_{\text{rim}}^2 + 3.1364 d_{\text{rim}} - 5.707 \tag{2.32}$$

3
Methodology

The primary objective of this research is to compare various Flying-V landing gear concepts to identify the best solution for the Flying-V, using a dynamic, physics-based approach to conceptual design and mass estimation. This chapter outlines the landing gear design exploration methodology. It begins with a description of the design exploration setup, followed by a discussion of the conceptual landing gear design method. The chapter concludes with a detailed explanation of the landing gear analysis method.

3.1. Landing Gear Design Exploration

During the conceptual aircraft design phase, in particular that of novel aircraft concepts such as the Flying-V, landing gear design is a dynamic process, involving rapid changes in aircraft properties and requirements [12, 28]. Moreover, the objective of any aircraft landing gear design is multi-dimensional. While one might simply prioritise minimising landing gear mass, doing so at the expense of overall aircraft mass or aerodynamic performance does not result in the best possible aircraft design. Specifically for the Flying-V, it might be beneficial or even necessary to revisit design trade-offs that have been well established for traditional aircraft in order to get a feasible and potentially better overall design.

Exploration Setup

In this research, a Flying-V landing gear design exploration is presented. A physics-based landing gear design and analysis methodology is developed that allows for exploring various Flying-V landing gear concept designs as well as family design commonality implications. This supports further design trade-offs and contributes to the best possible compromise. As discussed in Chapter 2, physics-based landing gear design routines have proved to be effective in performing rapid design iterations, ensuring a better optimised design and reducing experience dependency, making them suitable for designing landing gear for Flying-V aircraft [8, 9, 14, 29–33].

The design exploration starts with the development of a baseline gear design for all members of the Flying-V family. The baseline gear is designed for maximum aircraft and gear design commonality, sharing the same structural components across the family, which are sized based on the requirements of the FV-1000, e.g., the largest and heaviest Flying-V family member. The baseline gear design serves as the basis for a comparison with gear concept variations, which involve adjusting the baseline design to explore the potential benefits or drawbacks of various gear design considerations. The following design aspects are explored:

- **Strut configuration:** The benefit of utilising a drop link strut arrangement over a conventional single folding strut arrangement is evaluated. Generally, drop link arrangements are more complex and have a higher mass, but allow for more compact stowage [12].
- **Bogie configuration:** The benefit of utilising a 6-wheel bogie configuration instead of a 4-wheel bogie configuration is evaluated. Generally, 6-wheel bogie configurations are longer but narrower, which could be beneficial depending on the stowage concept.
- **Bogie articulation:** The benefit of utilising a bogie articulation mechanism is evaluated. Similar to the strut shortening mechanism, an articulation mechanism is beneficial for stowage, but adds complexity and mass to the gear.

- **Strut shortening:** The benefit of utilising a strut shortening mechanism is evaluated. Shortening mechanisms reduce stowage volume, but add mass and complexity.
- **Stowage concept:** Generally, landing gear are retracted in forward direction such that drag loads do not prevent the gear from extending in case of extension mechanism failure. However, for the Flying-V, retracting in backward direction could be more beneficial in terms of structural integration and stowage.
- **Family design:** The benefits of having landing gear specifically tailored for each Flying-V family member are compared to the advantages of using a common gear design for all aircraft.

The design aspects are used to formulate a set of landing gear concepts, which are evaluated based on primary Flying-V design concerns:

- **Feasibility:** The landing gear needs to be feasible in order to have a viable Flying-V aircraft. The feasibility study includes an evaluation of the retraction path and kinematics, structural integration, and complexity.
- **Mass:** Landing gear mass is estimated to be able to quantitatively compare different landing gear concepts and allow for future aircraft performance evaluations and design trade-offs.
- **Stowage performance:** Stowage performance is assessed by evaluating the stowed gear volume, width, length and frontal surface area. Stowage volume needs to be minimised as it conflicts with the available fuel tank volume. Stowed gear width, length and frontal surface area affect the aerodynamic efficiency of the landing gear fairing.
- **Design commonality**: The design should maximise commonality with other members of the aircraft family or similar aircraft types in order to limit design and certification cost and enhance the commercial viability of the aircraft.

For each landing gear concept, the design process starts with the conceptual landing gear design, during which a landing gear gear concept is developed into a 3D landing gear model. Each concept is then systematically evaluated in the landing gear analysis module, following the key design concerns outlined above. Different inputs for the conceptual landing gear design module lead to different landing gear designs and subsequent analysis results, contributing to the design exploration study. An overview of the process is visualised in Figure 3.1. To provide context for the subsequent methodology description, a brief summary of each phase is outlined here. The methodologies are described in more detail in their respective sections.

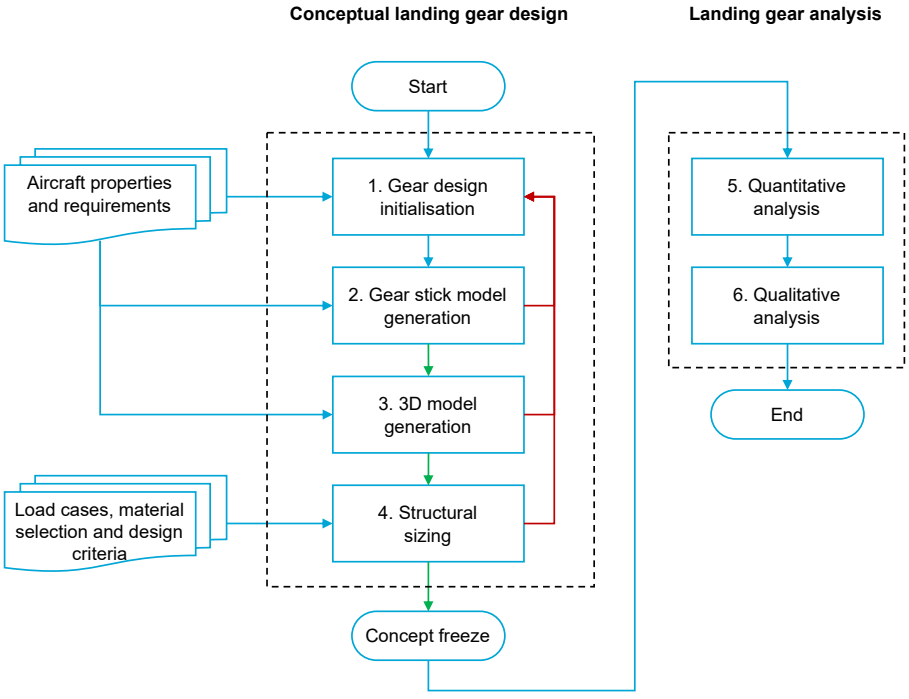

Figure 3.1: Concept design and analysis methodology flow chart, conducted for each landing gear concept.

Conceptual Landing Gear Design
The conceptual landing gear design module is structured into four distinct submodules: gear design initialisation, gear stick model generation, 3D model generation, and structural sizing. In the gear design initialisation submodule, the designer has to formulate the gear concept and define the programme of requirements, which serve as inputs for the stick model generation submodule. The stick model generation submodule utilises a multidisciplinary design optimisation (MDO) algorithm to generate a stick model of the gear concept, optimised for maximum aircraft rotation ability and minimum length. Optimising for minimum length instead of mass is a simplification, as it allows to remove structural analysis from the optimisation algorithm. Given the strong correlation between gear mass and length [8, 12, 29, 50], this approach is anticipated to produce results that are sufficiently accurate. Moreover, it should be noted that the objective is not to have an optimised gear, but rather to obtain a feasible gear that satisfies design constraints and requirements as specified in the initialisation module. After the stick model is found to be feasible, the geometry is refined in the 3D model generation submodule using computer-aided design (CAD) software. Based on the 3D model, an initial assessment of gear kinematics, integration and structural feasibility can be made. The minimum required wall-thickness of the primary structural components is determined in the structural sizing submodule, after which feasibility can be checked once again. After each submodule, the designer needs to assess whether the design is good enough to progress to the next submodule, or if it is necessary to reiterate with adjusted gear design initialisation submodule inputs. Finally, if all concept landing gear design submodules are completed, the concept design is frozen and ready to be analysed in more detail.

Landing Gear Analysis
After the conceptual landing gear design is completed, landing gear concepts are evaluated and compared in the landing gear analysis module. The feasibility of the gear is assessed qualitatively. After a concept is found to be feasible, also its mass, stowage performance and resulting cabin floor height are determined, allowing for a comparison based on quantitative metrics.

3.2. Gear Design Initialisation

The development of a landing gear concept starts with the gear design initialisation submodule. It stipulates and limits the design space and defines the constraints of the MDO algorithm in the geometry generation submodule. Landing gear design involves many different variables when it comes to sizing, positioning and integration, introducing design space complexity, which negatively affects computational efficiency and design algorithm robustness [32].

The methodology for conceptual landing gear design proposed in this research employs a mix of fixed design parameters and free design variables. Free design variables are varied by the optimiser to obtain the best design, and are bounded by limits set by the designer. Fixed design parameters, on the other hand, can only be adjusted by the designer, and represent aircraft characteristics, design constraints and requirements, as well as gear properties and dimensions that are excluded from optimisation. Adding gear properties and dimensions as fixed design design parameters reduces design space complexity, thereby enhancing computational efficiency, optimiser robustness, and design feasibility. In addition, it serves to incorporate gear properties and dimensions that cannot be optimised by the optimiser, but do have have a significant impact on the gear design characteristics and performance. For instance, a different joint location or different tyre selection may not affect landing gear length, but inherently affect gear kinematics and flotation.

The process of formulating a specific landing gear concept involves adjusting fixed design parameters and free design variable bounds as desired, resulting in a different gear stick model. This contributes to the design exploration. The selection of design variables and the resulting concepts is not only based on the design requirements outlined in Section 2.4. In order to have a feasible landing gear for a commercial viable aircraft, the method also relies on engineering judgement and creativity. The list below describes a list of design recommendations and considerations that serve to support the designer:

- **Compactness**: The landing gear must be as compact as possible in the stowed position in order to minimise aerodynamic drag.
- **Complexity**: Landing gear complexity must be limited as much as possible to reduce mass,

maintenance cost and reliability [8, 12].

- **Structural efficiency**: The landing gear structure must be designed in a way that it has efficient load transfer to the airframe, as well as within the structure itself. This limits structural mass and maximises fatigue life [12].
- **Interfaces**: The number of interfaces with other aircraft systems and components must be minimised in order to limit design and maintenance costs [8].
- **Risk**: Any risk imposed by the landing gear must be minimised to reduce certification cost and difficulty. The landing gear should be designed to ensure that drag loads do not prevent the gear from extending in the event of primary extension mechanism failure [12, 32].

The gear design initialisation submodule process is divided into five distinct input categories, as depicted in Figure 3.2. These categories collectively produce a set of input files, which in turn serve as the defining parameters for the stick model generation submodule. This section provides a description of inputs that need to be specified by the designer in each input category.

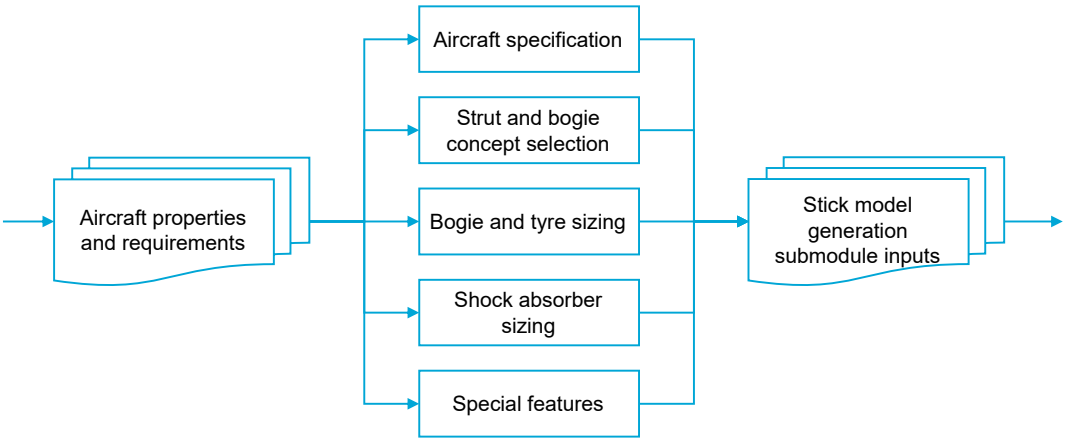

Figure 3.2: Gear design initialisation process flowchart.

3.2.1. Aircraft Specification

The configuration of a landing gear largely depends on the specific aircraft it is designed for. Input data related to aircraft geometry, mass properties and operational properties is discussed in this section.

Geometry

The stick model generation submodule requires aircraft geometry information to allow for landing gear positioning and to facilitate the evaluation of stowage properties, ground clearance and turning radii. All aircraft dimensions are measured in a standard aircraft design reference frame, with the x-axis positive from nose to tail, and the z-axis pointing upwards, as illustrated in Figure 3.3. The origin of the reference frame is aligned with the nose of the aircraft, unless specified otherwise.

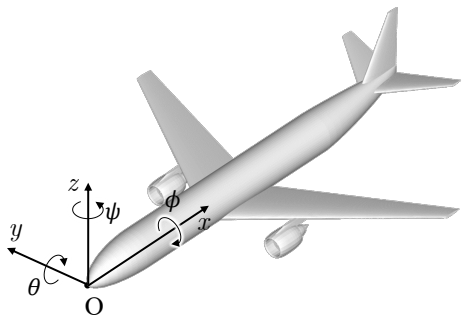

Figure 3.3: Aircraft design reference frame.

The landing gear is attached to the aircraft at a point within the designated main or nose gear attachment

design space. The main gear attachment design space is parameterised by either a parallelogram surface, defined by four design space coordinates, or a triangular surface, defined by three design space coordinates, as illustrated in Figures 3.4a and 3.4b, respectively. Normalised gear positioning parameters $x_{\text{mlg,DS}}$ and $y_{\text{mlg,DS}}$ describe any point on this surface. Positioning parameter $x_{\text{mlg,DS}}$ represents the longitudinal placement between coordinates A and B, while $y_{\text{mlg,DS}}$ describes the lateral position, as shown in the figures. The nose gear design space is parameterised by a line coincident with the aircraft centreline, with the attachment location defined by the normalised nose gear positioning parameter $x_{\text{nlg,DS}}$, as illustrated in Figure 3.4c. The positioning parameters can be varied by the optimiser to change the landing gear attachment locations relative to the design space. The main and nose gear design spaces for the FV-1000 are marked in blue in Figure 3.5.

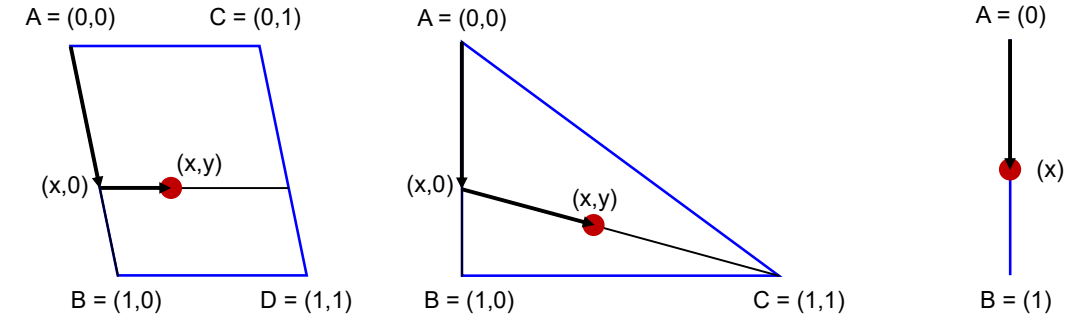

(a) Main landing gear, parallelogram-shaped. **(b)** Main landing gear, triangle-shaped. **(c)** Nose landing gear.

Figure 3.4: Landing gear attachment design space parameterisation.

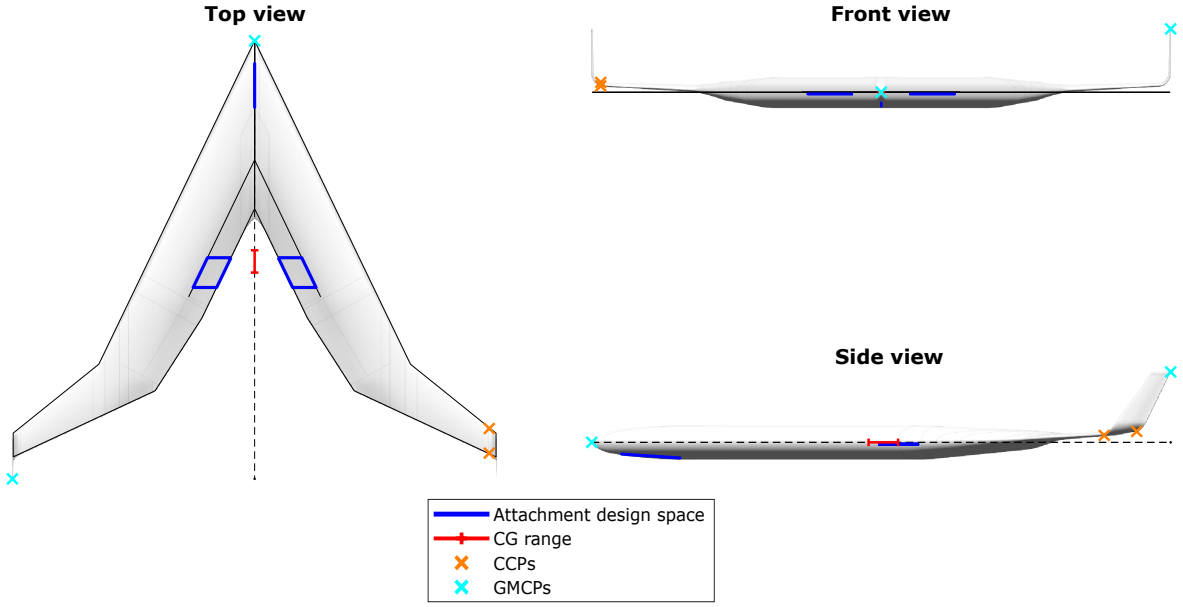

Figure 3.5: FV-1000 geometric aircraft representation for conceptual landing gear design

In addition to the attachment design space, also the stowage design space needs to be considered. The main landing gear stowage design space is defined by the imaginary triangle spanned by the aircraft centreline and the rear wing spar. This is illustrated by the shaded yellow area in Figure 3.6a for the Flying-V, and in Figure 3.6b for conventional aircraft. The main landing gear must remain clear of the rear spar by a distance $s_{\text{rs,min}}$. Similarly, the main landing gear must remain clear of the aircraft centreline by a distance $s_{\text{cl,min}}$ to avoid colliding with the landing gear mounted on the opposite wing or keel beam, if applicable. The nose landing gear stowage design space is defined by an imaginary rectangle located at a distance s_{fpb} from the aircraft front pressure bulkhead, as illustrated by the shaded yellow area in Figure 3.6c. The front pressure bulkhead is located at a distance l_{fpb} from the nose of the

aircraft and can be determined from scaled drawings in aircraft airport planning manuals [42, 43, 46]. Minimum clearance values $s_{\text{rs,min}}$, $s_{\text{cl,min}}$ and $s_{\text{fpb,min}}$ can be obtained using Equation 2.27. Additional clearance may be added based on engineering judgement.

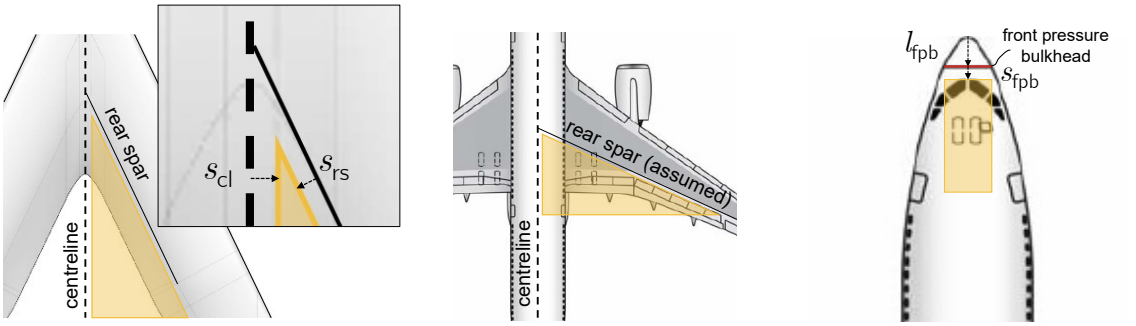

(a) Main gear stowage design space, Flying-V

(b) Main gear stowage design space, regular aircraft, modified from [43].

(c) Nose gear stowage design space, modified from [43].

Figure 3.6: Landing gear stowage design space specification.

The optimiser needs to be able to verify whether the selected gear configuration allows the aircraft to remain clear of the ground during landing and take-off. Evaluating clearance for the entire outer mold line is computationally expensive and deemed unnecessary. Instead, it is assumed that clearance can be evaluated based on a set of discrete clearance critical points (CCPs), which are defined by the most adverse locations on the wing tips, tail and engine nacelles. Ground clearance critical points for the right wing of the FV-1000 are indicated by an orange x in Figure 3.5.

Similarly, for ground manoeuvring, evaluating turning radii is assumed to only be relevant for the wing tip, horizontal stabiliser, nose, cockpit and nose gear, in line with turning radii typically provided by aircraft airport planning manuals [42, 43, 46]. The stick model generation submodule evaluates turning radii for ground manoeuvring critical points (GMCPs) provided by the designer. Ground manoeuvring critical points for the left wing of the FV-1000 are indicated by a cyan x in Figure 3.5.

An overview of aircraft geometry related inputs is provided in Table 3.1.

Table 3.1: Aircraft geometry specifications.

Item	Unit	Description	Type
MDS_A	m	MLG attachment design space coordinate A (x, y, z)	Fixed
MDS_B	m	MLG attachment design space coordinate B (x, y, z)	Fixed
MDS_C	m	MLG attachment design space coordinate C (x, y, z)	Fixed
MDS_D	m	MLG attachment design space coordinate D (x, y, z)	Fixed
$x_{\text{mlg,DS}}$	-	Longitudinal main gear positioning parameter	Free
$y_{\text{mlg,DS}}$	-	Lateral main gear positioning parameter	Free
NDS_A	m	NLG attachment design space coordinate A (x, y, z)	Fixed
NDS_B	m	NLG attachment design space coordinate B (x, y, z)	Fixed
$x_{\text{nlg,DS}}$	-	Longitudinal nose gear positioning parameter	Free
$s_{\text{rs,min}}$	m	Minimum rear spar clearance	Fixed
$s_{\text{cl,min}}$	m	Minimum centreline clearance	Fixed
$s_{\text{fpb,min}}$	m	Minimum front pressure bulkhead clearance	Fixed
l_{fpb}	m	Front pressure bulkhead location	Fixed
CCP_1	m	Clearance critical point 1 (x, y, z)	Fixed
CCP_n	m	Clearance critical point n (x, y, z)	Fixed
GMCP_1	m	Ground manoeuvring critical point 1 (x, y, z)	Fixed
GMCP_n	m	Ground manoeuvring critical point n (x, y, z)	Fixed

Mass Properties

Aircraft mass properties are required to be able to evaluate ground stability, ground loads and shock absorber dimensions. The aft and forward centre of gravity (CG) limits need to be provided, both

in absolute x, y and z dimensions measured from the aircraft nose, as well as relative to the mean aerodynamic chord, such that gear locations and loading diagrams of various aircraft and gear concepts can effectively be compared. In addition, the maximum ramp mass (MRM), maximum take-off mass (MTOM), maximum landing mass (MLM) and operational empty mass (OEM) need to be specified. The CG range for the FV-1000 is depicted by the red line in Figure 3.5.

Aircraft loading diagrams, such as Figure 2.11b for the FV-900, suggest that maximum mass data may not always apply to the full centre of gravity range. For instance, the Flying-V can physically not reach its maximum take-off mass at the forward centre of gravity limit, as maximum take-off mass can only be achieved at high fuel loads. Due to the location of the fuel tanks, high fuel loads inherently cause the centre of gravity to move aft. Consequently, for landing gear design, the nose gear tyres do not need to be sized for the maximum take-off mass at the forward CG limit. Maximum expected mass ranges need to be provided by the designer in order for the stick model generation submodule to account for this phenomenon. The maximum ramp mass range MRM_{range}, maximum take-off mass range $MTOM_{range}$ and maximum landing mass range MLM_{range} define the forward and aft limit at which a specific mass may occur, relative to the full centre of gravity range, where 0 equals the forward CG limit (0%), and 1 equals the aft CG limit (100%). Figure 3.7 illustrates an example of a loading diagram of an aircraft that can only be at MRM or MTOM between 50% and 100% of the full CG range, but can be at MLM over the full CG range. Transitions between specified ranges are assumed to be linear.

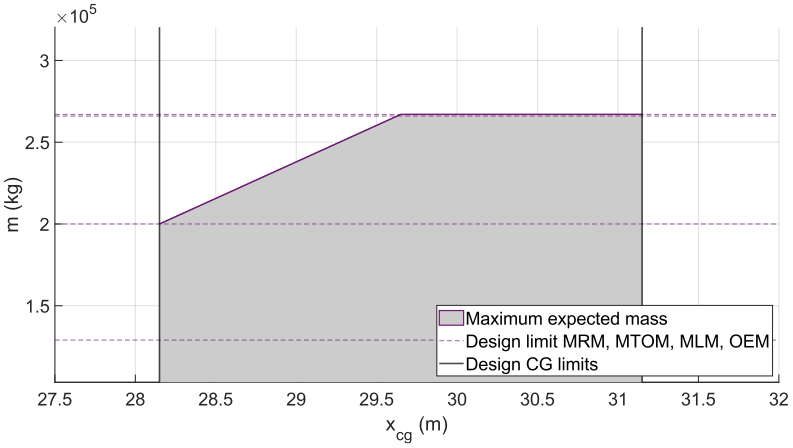

Figure 3.7: Aircraft loading diagram example.

An overview of aircraft mass related inputs is provided in Table 3.2.

Table 3.2: Aircraft mass specifications.

Item	Unit	Description	Type
CG_{fwd}	m	Forward CG limit (x, y, z)	Fixed
$CG_{fwd,\%MAC}$	%MAC	Forward CG limit relative to the mean aerodynamic chord	Fixed
CG_{aft}	m	Aft CG limit (x, y, z)	Fixed
$CG_{aft,\%MAC}$	%MAC	Aft CG limit relative to the mean aerodynamic chord	Fixed
MRM	kg	Maximum ramp mass	Fixed
MTOM	kg	Maximum take-off mass	Fixed
MLM	kg	Maximum landing mass	Fixed
OEM	kg	Operating empty mass	Fixed
MRM_{range}	-	MRM range relative to CG range (fwd, aft)	Fixed
$MTOM_{range}$	-	MTOM range relative to CG range (fwd, aft)	Fixed
MLM_{range}	-	MLM range relative to CG range (fwd, aft)	Fixed

Operational Properties

In addition to physical aircraft properties, the designer needs to specify operational requirements or constraints. Stability requirements as outlined in Section 2.4 prescribe a minimum tipback angle $\theta_{tpb,min}$ and

maximum lateral turnover angle $\psi_{tno,max}$ to prevent push-back tipover and lateral turnover. In addition, the static aircraft pitch attitude θ_{stat}, the maximum aircraft pitch attitude with shock absorbers in static and extended position $\theta_{max,extSA}$ and $\theta_{max,statSA}$, and the maximum aircraft roll angle ϕ_{max} need to be provided to be able to evaluate static stability, rotated stability and ground clearance. Target minimum and maximum nose gear weight fractions $\hat{\beta}_{nlg,min}$ and $\hat{\beta}_{nlg,max}$ need to be provided for shock absorber sizing, with the optimiser ensuring consistency between the target nose gear weight fractions and the actual nose gear weight fractions. The maximum main gear load fraction $\beta_{mlg,max}$ can be used to account for downforce generation when on the ground. The intended taxiway design group (TDG) and maximum nose gear steering angle $\lambda_{steering}$ need to be specified to ensure compatibility with intended airports. The take-off decision speed V_1 is used for brake sizing. An overview of operational aircraft requirements and constraints is provided in Table 3.3.

Table 3.3: Aircraft operational requirements.

Item	Unit	Description	Type
$\theta_{tpb,min}$	°	Minimum tipback angle	Fixed
ϕ_{max}	°	Maximum aircraft roll angle	Fixed
$\psi_{tno,max}$	°	Maximum lateral turnover angle	Fixed
θ_{stat}	°	Static aircraft pitch attitude	Fixed
$\theta_{max,statSA}$	°	Maximum aircraft pitch attitude with static shock absorber	Fixed
$\theta_{max,extSA}$	°	Maximum aircraft pitch attitude with extended shock absorber	Fixed
$\hat{\beta}_{nlg,min}$	-	Minimum nose gear load fraction, guess value	Free
$\hat{\beta}_{nlg,max}$	-	Maximum nose gear load fraction, guess value	Free
$\beta_{mlg,max}$	-	Maximum main gear load fraction	Fixed
TDG	-	Taxiway design group	Fixed
$\lambda_{steering}$	°	Maximum nose gear steering angle	Fixed
V_1	m/s	Take-off decision speed	Fixed

3.2.2. Strut and Bogie Concept Selection

The landing gear designer may select four different main gear strut concepts, as illustrated in Figure 3.8. Concept A describes a single folding strut with a total shock strut cylinder length l_{ss} and a shock absorber piston length l_{piston}. Shock strut length l_{ss} is a free design variable. Concept B describes a double folding strut which features a shock strut and an upper strut with a length l_{us}. Such a concept may be used to represent a gear with a drop-link arrangement. The upper strut length is a fixed design parameter that needs to be adjusted by the designer to obtain a feasible design. Concept C and D present a variation to Concept A and B respectively, where the shock absorber piston is connected to the bogie using a 'hockey stick' arrangement as described in Section 2.1.3. , requiring lower and upper bounds, as well as an initial guess from the designer. Piston length l_{piston} is calculated by the stick model generation submodule. The 'hockey stick' connector dimensions l_{hs} and θ_{hs} need to be provided by the designer based on engineering judgement.

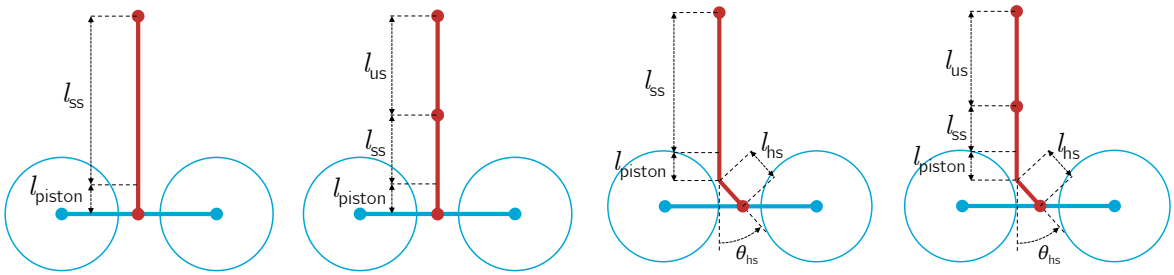

(a) Concept A: Single folding strut, regular bogie attachment. **(b)** Concept B: Double folding strut, regular bogie attachment. **(c)** Concept C: Single folding strut, 'hockey-blade' bogie attachment. **(d)** Concept D: Double folding strut, 'hockey-blade' bogie attachment.

Figure 3.8: Strut concept variations supported by the stick model generation submodule.

Extended and retracted orientation angles need to be specified for the main gear and nose gear shock strut, and if present, for the main gear upper strut as well. In the extended position, the shock strut

and upper strut may be raked with respect to the vertical aircraft axis. In the retracted position, the orientation angles must align the gear to fit the intended stowage space and satisfy stowage clearance constraints. The orientation angles of the retracted upper strut have a major effect on the retraction path of the gear. The following angles are defined:

- $\theta_{\text{us,ext}}$, $\theta_{\text{ss,ext}}$ and $\theta_{\text{nlg,ret}}$: describe the extended main gear upper strut, main gear shock strut and nose gear shock strut rake angle around the lateral aircraft axis, measured from the vertical aircraft axis. Angle θ is illustrated in Figure 3.9a.
- $\phi_{\text{us,ext}}$, $\phi_{\text{ss,ext}}$ and $\phi_{\text{nlg,ext}}$: describe the extended main gear upper strut, main gear shock strut and nose gear shock strut rake angle around the longitudinal aircraft axis, measured from the vertical aircraft axis. Angle ϕ is illustrated in Figure 3.9b.
- $\psi_{\text{us,ext}}$, $\psi_{\text{ss,ext}}$ and $\psi_{\text{nlg,ext}}$: describe the extended main gear upper strut, main gear shock strut and nose gear shock strut orientation angle around the vertical aircraft axis, measured from the longitudinal aircraft axis. Angle ψ is illustrated in Figure 3.9c.
- $\theta_{\text{us,ret}}$, $\theta_{\text{ss,ret}}$ and $\theta_{\text{nlg,ret}}$: describe the retracted main gear upper strut, main gear shock strut and nose gear shock strut orientation angle around the lateral aircraft axis, measured from the vertical aircraft axis. Angle θ is illustrated in Figure 3.9a.
- $\phi_{\text{us,ret}}$, $\phi_{\text{ss,ret}}$ and $\phi_{\text{nlg,ret}}$: describe the retracted main gear upper strut, main gear shock strut and nose gear shock strut orientation angle around the longitudinal aircraft axis, measured from the vertical aircraft axis. Angle ϕ is illustrated in Figure 3.9b.
- $\psi_{\text{mlg,ret}}$ and $\psi_{\text{nlg,ret}}$: describe the retracted main gear upper strut, main gear shock strut (mlg) and nose gear shock strut (nlg) orientation angle around the vertical aircraft axis, measured from the longitudinal aircraft axis. Angle ψ is illustrated in Figure 3.9c.

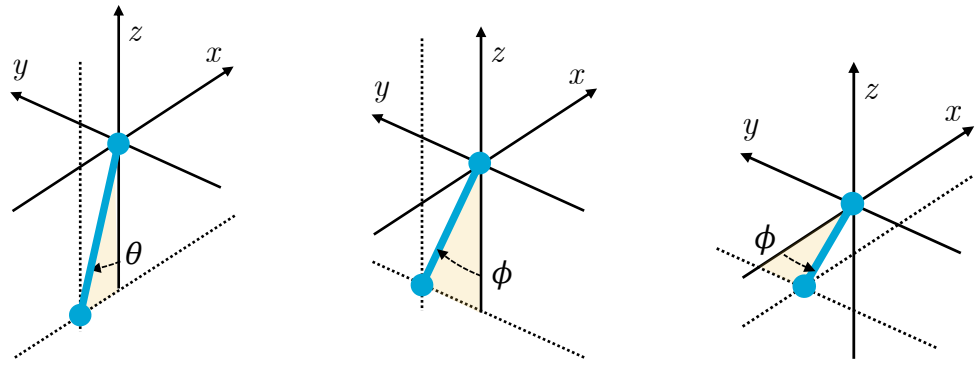

(a) Strut orientation angle θ. **(b)** Strut orientation angle ϕ. **(c)** Strut orientation angle ψ.

Figure 3.9: Strut orientation angle definitions.

Any geometry represented by a vector **r** or matrix **A** (e.g., the landing gear struts) can be rotated by elemental rotations ϕ, θ and ψ. Equation 3.1 describes the elemental rotation matrices that can be multiplied to obtain the rotation matrix **R**, representing the aggregated rotation in Euclidean space. The matrix multiplication order follows the standard aircraft yaw-pitch-roll convention, as shown by Equation 3.2.

$$\mathbf{R_z}(\psi) = \begin{bmatrix} \cos\psi & -\sin\psi & 0 \\ \sin\psi & \cos\psi & 0 \\ 0 & 0 & 1 \end{bmatrix}, \mathbf{R_y}(\theta) = \begin{bmatrix} \cos\theta & 0 & \sin\theta \\ 0 & 1 & 0 \\ -\sin\theta & 0 & \cos\theta \end{bmatrix}, \mathbf{R_x}(\phi) = \begin{bmatrix} 1 & 0 & 0 \\ 0 & \cos\phi & -\sin\phi \\ 0 & \sin\phi & \cos\phi \end{bmatrix} \tag{3.1}$$

$$\mathbf{r}^{\text{rot}} = \mathbf{R}\mathbf{r} = \mathbf{R_z}(\psi)\mathbf{R_y}(\theta)\mathbf{R_x}(\phi)\mathbf{r} \tag{3.2}$$

The extended shock strut sideward rake angle $\phi_{\text{ss,ext}}$ must be equal to zero to ensure that the main gear wheel span remains constant during shock absorber extension or compression, preventing lateral loading on the tyres and structure. Similarly, $\psi_{\text{us,ext}}$, $\psi_{\text{ss,ext}}$ and $\psi_{\text{nlg,ext}}$ must be set to zero to have the

wheels aligned with the aircraft moving direction. The extended nose gear angles $\theta_{\text{nlg,ret}}$ and $\phi_{\text{nlg,ext}}$ are selected by the optimiser such that the nose gear strut is perpendicular to the ground surface in static position. Retracted nose gear orientation angles $\phi_{\text{nlg,ret}}$ and $\psi_{\text{nlg,ret}}$ are selected such that the nose gear strut folds around the aircraft y-axis only. The angles $\theta_{\text{us,ret}}$, $\theta_{\text{ss,ret}}$, $\theta_{\text{nlg,ret}}$, $\phi_{\text{us,ret}}$ and $\phi_{\text{ss,ret}}$ are fixed design parameters, and may be adjusted by the designer. The remaining angles are free design variables which are adjusted by the optimiser within their respective bounds to achieve the optimal gear arrangement.

Similar to the strut concepts, two different bogie concepts may be selected by the designer. The different concepts are illustrated in Figure 3.10. Concept A describes a regular arrangement where the strut is connected at the centre of the bogie beam. Concept B describes an alternative, where the strut is connected at an offset above the bogie beam, allowing the bogie to be 'flat-packed'. The offset distance is given by the fixed design parameter l_{offset}.

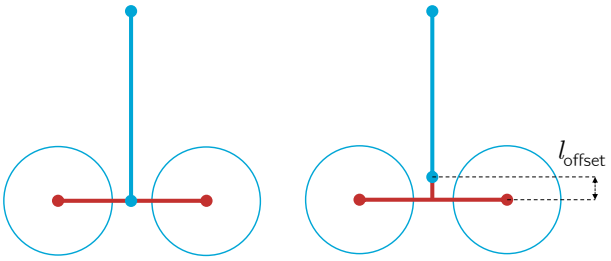

(a) Concept A: Regular strut attachment.

(b) Concept B: Offset strut attachment.

Figure 3.10: Bogie concept variations supported by the stick model generation submodule.

In Figures 3.8, piston length l_{piston} is defined as the node to node distance between the shock strut cylinder and the bogie joint, or in case of the 'hockey stick' arrangement, as the distance between the shock strut cylinder and the hockey stick kink. This piston length can not be equal to the shock absorber stroke length x_{SA}, as the piston length needs to account for fully compressed margins and bogie connector element length. This ineffective piston length $l_{\text{ineffective}}$ needs to be specified by the designer, and is defined as illustrated in Figure 3.11.

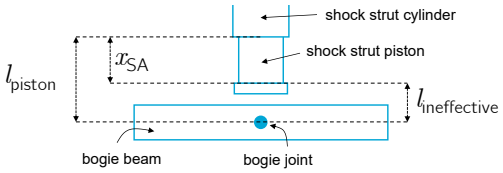

Figure 3.11: Ineffective piston length.

An overview of inputs related to the strut and bogie concept specification is provided in Table 3.4.

3.2.3. Bogie and Tyre Sizing

After selecting the strut and bogie concept, the designer must specify the dimensions of the main landing gear bogie, the nose gear wheel span, and the tyre selections. Initially, the designer can refer to the bogie and tyre sizes of similar existing aircraft, as discussed in Section 2.4.4. At a later stage, this may be adjusted based on flotation and gear load analysis results. Figure 3.12 illustrates both a 4-wheel and a 6-wheel bogie configuration, with bogie length (l_{bogie}) and bogie width or wheel span (w_{bogie}). The total number of main gear wheels (all struts combined) is denoted by $N_{\text{mlg,wheels}}$, and the number of main gear shock struts is denoted by $N_{\text{mlg,ss}}$. Similarly, for the nose gear, the wheel span w_{nlg} and the number of nose gear wheels $N_{\text{nlg,wheels}}$ need to be specified. The main gear tyre size Tyre_{mlg} and nose gear tyre size Tyre_{nlg} can be selected from the tyre tables provided by Schmidt [12], which specify loaded and unloaded tyre radii, tyre width, tyre mass and wheel dimensions. The designer may specify a design deceleration rate $a_{x,\text{des}}$, allowing dynamic gear loads under braking to be evaluated at the actual design deceleration rate in addition to the minimum deceleration rates specified by regulations.

Table 3.4: Strut and bogie concept specifications.

Item	Unit	Description	Type
Strut	-	Main gear strut concept selection	Fixed
l_{ss}	m	Main gear shock strut cylinder length	Free
$\theta_{ss,ext}$	°	Extended mlg shock strut rake angle around y-axis	Free
$\theta_{ss,ret}$	°	Retracted mlg shock strut orientation angle around y-axis	Fixed
$\phi_{ss,ret}$	°	Retracted mlg shock strut orientation angle around x-axis	Fixed
$\psi_{mlg,ret}$	°	Retracted mlg orientation angle around z-axis	Free
l_{us}	m	Main gear upper strut length	Fixed
$\theta_{us,ext}$	°	Extended mlg upper strut rake angle around y-axis	Free
$\phi_{us,ext}$	°	Extended mlg upper strut rake angle around x-axis	Free
$\theta_{us,ret}$	°	Retracted mlg upper strut orientation angle around y-axis	Fixed
$\phi_{us,ret}$	°	Retracted mlg upper strut orientation angle around x-axis	Fixed
l_{hs}	m	Hockey stick connector length	Fixed
θ_{hs}	°	Hockey stick connector length	Fixed
Bogie	-	Bogie concept selection	Fixed
l_{offset}	m	Bogie joint offset distance	Fixed
$l_{ineffective}$	m	Ineffective shock strut piston length	Fixed
$\theta_{nlg,ret}$	°	Retracted nlg shock strut orientation angle around y-axis	Fixed

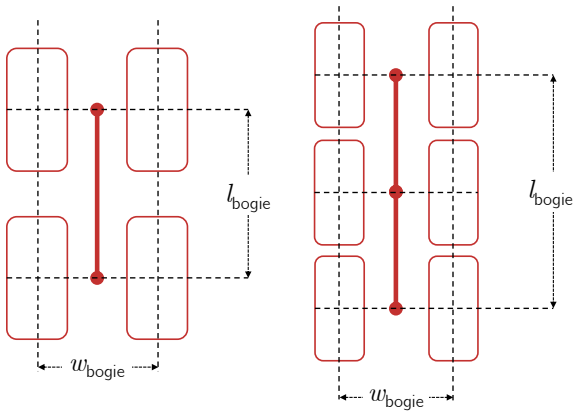

(a) 4-wheel bogie **(b)** 6-wheel bogie

Figure 3.12: Bogie dimensions specification.

An overview of inputs related to bogie and tyre sizing is provided in Table 3.5.

Table 3.5: Bogie and tyre sizing specifications.

Item	Unit	Description	Type
$N_{mlg,wheels}$	-	Total number of main gear wheels, all struts combined	Fixed
$N_{mlg,ss}$	-	Number of main gear shock struts	Fixed
l_{bogie}	m	Bogie length	Fixed
w_{bogie}	m	Bogie width or wheel span	Fixed
$Tyre_{mlg}$	-	MLG tyre size	Fixed
$N_{nlg,wheels}$	-	Total number of nose gear wheels	Fixed
w_{nlg}	m	Nose gear wheel span	Fixed
$Tyre_{nlg}$	-	NLG tyre size	Fixed
$a_{x,des}$	m/s^2	Design deceleration	Fixed

3.2.4. Shock Absorber Sizing

Designing shock absorbers involves balancing various performance factors, allowing designers significant flexibility to adjust the design to specific aircraft requirements. This typically necessitates numerous iterations to find the optimal trade-off [12]. In this research, shock absorber specifications must be provided such that ground reaction loads, shock absorber strokes, and extended and static gear lengths can be estimated.

Shock absorber (SA) strokes are calculated using the the SA reaction factors λ_{mlg} and λ_{nlg} (Equation 2.15). In order to be able to calculate the SA spring curves and resulting static and extended SA positions, the desired shock absorber pressures in static position and breakout load fractions need to be provided. The breakout load fraction b describes the load at which the shock absorber starts to compress as fraction of the static load on the gear at maximum landing mass. Additionally, for structural analysis, the designer needs to specify the shock absorber compression s_{Fmax} as fraction of the total stroke x_{a} at which the maximum vertical reaction load occurs.

An overview of inputs related to shock absorber sizing is provided in Table 3.6.

Table 3.6: Shock absorber sizing specifications.

Item	Unit	Description	Type
λ_{mlg}	-	Main gear SA reaction factor	Fixed
$P_{\text{mlg,static}}$	MPa	Main gear SA static pressure	Fixed
b_{mlg}	-	Main gear SA breakout load as % of static load at MLM	Fixed
λ_{nlg}	-	Main gear SA reaction factor	Fixed
$P_{\text{nlg,static}}$	MPa	Nose gear SA static pressure	Fixed
b_{nlg}	-	Nose gear SA breakout load as % of static load at MLM	Fixed
s_{Fmax}	-	% SA compression at maximum vertical reaction	Fixed

3.2.5. Special Features

The landing gear may have bogie articulation mechanisms and strut shortening mechanisms, reducing the required stowage volume, as described in Section 2.1. Bogie articulation input specifications are illustrated in Figure 3.13a. The figure shows the articulation angle θ_{bogie}, which is measured from the longitudinal aircraft axis. Please note that the angle of the bogie with respect to the ground also depends on the pitch attitude of the aircraft. The bogie articulation pivot is at a distance $l_{\text{x,pivot}}$ behind, and $l_{\text{z,pivot}}$ above the forward wheel axle, which both need to be specified by the designer. It is assumed that when the bogie is articulated, e.g., when the bogie rotates due to shock absorber extension or compression , the vertical location of the pivot remains constant. The pivot location and the angle between the bogie and the ground geometrically define the articulation shock absorber stroke $x_{\text{a,articulation}}$, which is the amount of shock absorber compression required to have all wheels in the horizontal position.

Maximum vertical reaction loads on the landing gear result from the reaction factor λ_{mlg} (Equation 2.12). When the bogie is articulated, only the aft wheels are in contact with the ground, limiting the maximum landing gear reaction factor to not overload the tyres and bogie. On the contrary, the reaction factor must be high enough to cause the aircraft to pitch down immediately after touch-down. This is needed because after touch-down, the shock absorber starts to compress, de-articulating the bogie, effectively reducing the available ground clearance. Therefore, an additional reaction factor $\lambda_{\text{mlg,art}}$ needs to be defined, which defines the maximum vertical load on the gear when the bogie is articulated, e.g., when $x_{\text{SA}} < x_{\text{SA,art}}$. The articulated reaction factor $\lambda_{\text{mlg,art}}$ needs to be lower than the fraction of the total main gear wheels on the ground multiplied by the reaction factor with all wheels on ground, as shown by Equation 3.3.

$$\lambda_{\text{mlg,art}} < \frac{N_{\text{mlg,w,art}}}{N_{\text{mlg,wheels}}} \lambda_{\text{mlg}} \tag{3.3}$$

When the aircraft is at its lowest mass, the static compression of the shock absorber must be large enough to have all wheels on the ground, e.g., the shock absorber must be larger than the articulation stroke $x_{\text{SA,art}}$. The designer needs to specify a dearticulation margin $l_{\text{margin,art}}$, which together with

the articulation shock absorber stroke describes the minimum static shock absorber compression, as shown by Equation 3.4. Adding a margin ensures that the bogie can move freely when all wheels are on the ground and needs to be selected based on engineering judgement.

$$x_{\text{SA,static}} > x_{\text{SA,art}} + l_{\text{margin,art}} \tag{3.4}$$

For strut shortening, only the shortening amount $l_{\text{shortening}}$ needs to be specified, as illustrated in Figure 3.13b.

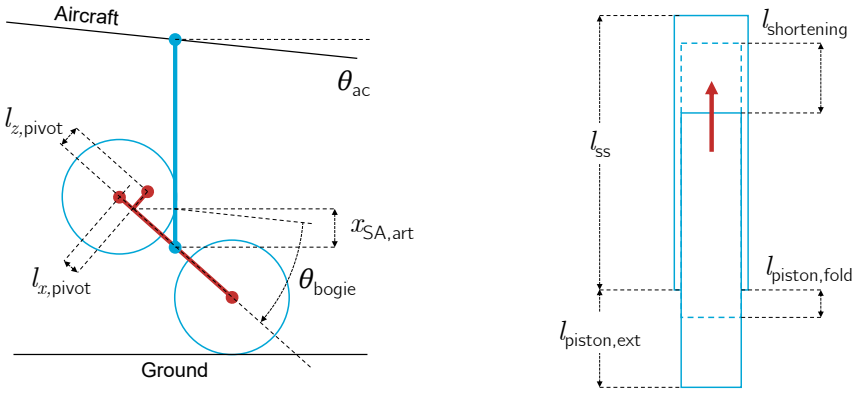

(a) Bogie articulation mechanism. **(b)** Strut shortening mechanism.

Figure 3.13: Special landing gear feature specifications.

Table 3.7: Special landing gear feature specifications.

Item	Unit	Description	Type
Articulation	-	Boolean input to trigger articulated bogie	Fixed
$\lambda_{\text{mlg,art}}$	-	Articulated main gear SA reaction factor	Fixed
θ_{bogie}	°	Bogie articulation angle	Free
$l_{\text{x,pivot}}$	m	Articulation pivot x-distance from forward wheel axle	Fixed
$l_{\text{z,pivot}}$	m	Articulation pivot z-distance from forward wheel axle	Fixed
$l_{\text{margin,art}}$	m	Dearticulation margin	Fixed
Shortening	-	Boolean input to trigger strut shortening	Fixed
$l_{\text{shortening}}$	m	Dearticulation margin	Fixed

3.3. Gear Stick Model Generation

After the gear design initialisation, the conceptual landing gear design process continues with the gear stick model generation submodule. This section presents a hybrid landing gear stick model optimisation approach, which utilises both a gradient-based optimisation algorithm and manual operations to achieve a feasible design. Free design variables, as introduced in Section 3.2, are adjusted by the gradient-based optimisation algorithm according to predefined design objectives and constraints. Manual operations, on the other hand, allow for the adjustment of fixed design parameters, which may involve both continuous and discrete design decisions. Some landing gear requirements, such as flotation, cannot easily be evaluated by the optimisation algorithm directly. Therefore, manual evaluations are necessary to ensure overall design feasibility.

3.3.1. Gradient-Based Optimisation

The extended design structure matrix (XDSM) shown in Figure 3.14 illustrates the optimisation architecture used to obtain suitable landing gear stick model size and positions. Specifically, the XSDM presents an Individual Design Feasible (IDF) multidisciplinary design optimisation (MDO) architecture, which can be distinguished from a Multi Discipline Feasible (MDF) architecture by the absence of a multidisciplinary analysis coordinator, and the presence of consistency constraints. The design vector

is varied by the optimiser, which is then used to generate landing gear stick models in the landing gear positioning and sizing block. The stick models are evaluated following the objective and constraint specifications. Consistency between design variables and analysis outputs is coordinated by the optimiser. It must be noted that because there is only one analysis block, implementation of an MDF architecture instead of IDF would be very similar and equally suitable, only differing from IDF in the way it reaches convergence.

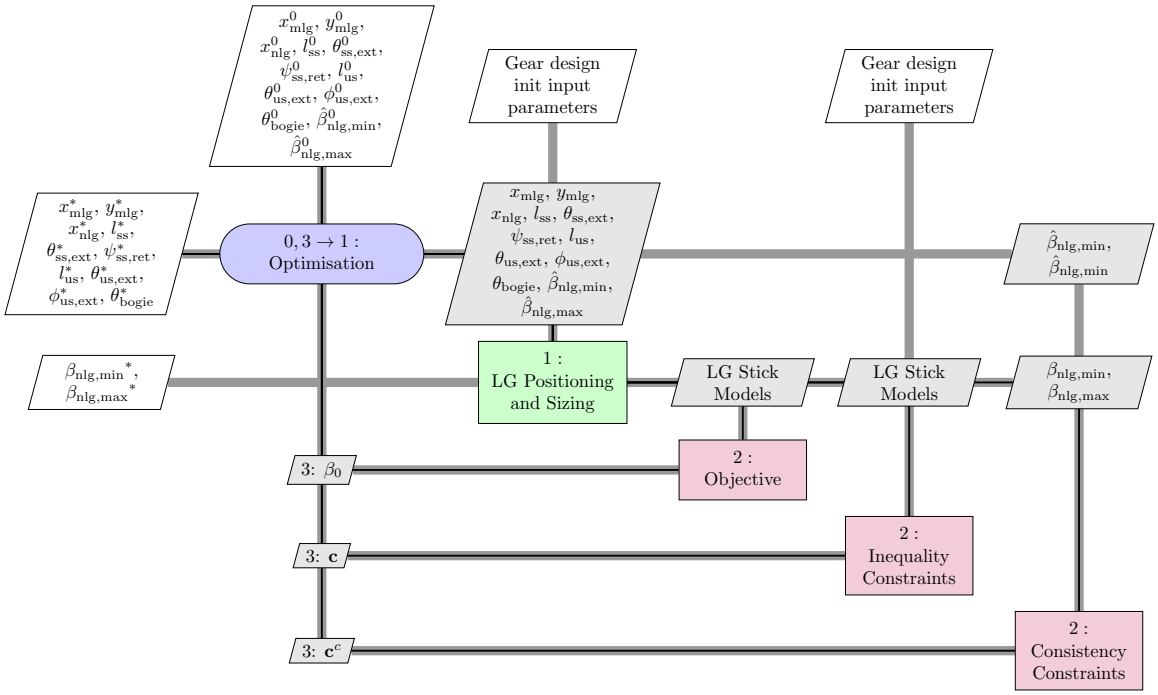

Figure 3.14: Gear stick model optimisation extended design structure matrix.

To solve the problem, MATLAB fmincon with a sequential quadratic programming (SQP) solving algorithm is utilised. The SQP algorithm is well-suited for the gear stick model optimisation, as it provides good speed and accuracy for problems with a relatively low number of design variables and smooth constraints [52]. In addition, it can recover from NaN and Inf results, and maintains feasibility by satisfying bounds at all iterations.

3.3.2. Design Variables

The design variables, chosen as described in Section 3.2, define the size and position of the landing gear, with the exception of $\hat{\beta}_{\text{nlg,min}}$ and $\hat{\beta}_{\text{nlg,max}}$, which describe the minimum and maximum nose gear load target values. An overview is provided in Table 3.8. To ensure that all design variables are on a comparable scale, they are normalised using their respective lower and upper bounds.

3.3.3. Landing Gear Positioning and Sizing

Landing gear positioning and sizing describes the process in which fixed input parameters and design variable are used to define a main and nose gear stick models.

Landing Gear Positioning

The process begins with positioning the landing gear. Main gear positioning parameters x_{mlg} and y_{mlg}, and nose gear positioning parameter x_{nlg} are used to determine gear attachment locations within their respective attachment design space. For the main gear, the design space is represented by either a triangle or a parallelogram, as detailed in Section 3.2.1. In case of the former, the attachment location is defined by Equation 3.5. In case of the latter, the attachment location O_{mlg} is defined by Equation 3.6. The design space coordinates are represented by MDS_A, MDS_B, MDS_C and MDS_D.

Table 3.8: Overview of stick model generation design variables.

Variable	Unit	Description
x_{mlg}	-	Longitudinal main gear positioning parameter
y_{mlg}	-	Lateral main gear positioning parameter
x_{nlg}	-	Longitudinal nose gear positioning parameter
l_{ss}	m	Main gear shock strut cylinder length
$\theta_{\text{ss,ext}}$	$^\circ$	Extended mlg shock strut rake angle around y-axis
$\psi_{\text{mlg,ret}}$	$^\circ$	Retracted mlg shock strut orientation angle around z-axis
l_{us}	m	Main gear upper strut length
$\theta_{\text{us,ext}}$	$^\circ$	Extended mlg upper strut rake angle around y-axis
$\phi_{\text{us,ext}}$	$^\circ$	Extended mlg upper strut rake angle around x-axis
θ_{bogie}	$^\circ$	Bogie articulation angle
$\hat{\beta}_{\text{nlg,min}}$	-	Minimum nose gear load fraction target value
$\hat{\beta}_{\text{nlg,max}}$	-	Maximum nose gear load fraction target value

$$\begin{aligned} \text{AB} &= \text{MDS}_\text{B} - \text{MDS}_\text{A} \\ O_{\text{mlg}} &= (\text{MDS}_\text{C} - (\text{AB}x_{\text{mlg}} + \text{MDS}_\text{A}))y_{\text{mlg}} + \text{AB}x_{\text{mlg}} + \text{MDS}_\text{A} \end{aligned} \tag{3.5}$$

$$\begin{aligned} \text{AB} &= \text{MDS}_\text{B} - \text{MDS}_\text{A} \\ \text{AC} &= \text{MDS}_\text{C} - \text{MDS}_\text{A} \\ O_{\text{mlg}} &= \text{AB}x_{\text{mlg}} + \text{AC}y_{\text{mlg}} + \text{MDS}_\text{A} \end{aligned} \tag{3.6}$$

For the nose gear, the design space is represented by a line. The attachment location O_{nlg} is determined using Equation 3.7, where NDS_A and NDS_B describe the design space coordinates.

$$O_{\text{nlg}} = (\text{NDS}_\text{B} - \text{NDS}_\text{A})x_{\text{nlg}} + \text{NDS}_\text{A} \tag{3.7}$$

Shock Absorber Stroke Evaluations

Once the landing gear attachment locations are established, the shock absorber is sized to determine the static and fully extended strut length. These lengths depend on the shock absorber stroke and sizing parameters.

For a conventional bogie configuration, the shock absorber starts to compress as soon as all wheels touch the ground. The wheel axle stroke required to absorb vertical kinetic energy is then calculated using Equation 2.13, based on the descent conditions outlined in Table 2.4. However, for an articulated bogie, only two wheels touch the ground initially after touchdown. This limits the allowable shock strut reaction load and thus energy absorption. Additionally, the vertical stroke is now defined by the movement of the aft wheel axle, projecting a different stroke on the shock absorber depending on the articulation pivot point location. Figures 3.15a and 3.15b illustrate the difference.

To account for this, an initial phase is defined where the stroke is determined by the geometric stroke required for de-articulation, i.e., the stroke required to have all wheels touch the ground. The second part of the stroke is derived from the residual energy to be absorbed by the shock absorber, as described by Equation 3.8. Here, E_{kin} represents the total vertical kinetic energy calculated using the descent conditions in Table 2.4 (Equation 2.9), while $E_{\text{abs,phase1}}$ and $E_{\text{abs,phase2}}$ represent the energies absorbed during the initial and second shock absorber compression phase, respectively (Equation 2.11). All strokes are corrected such that there always is sufficient stroke available to absorb the energy, regardless of the shock strut orientation angle with respect to the ground (Equation 2.15, as discussed in Section 2.4.3).

$$E_{\text{abs,phase2}} = E_{\text{kin}} - E_{\text{abs,phase1}} \tag{3.8}$$

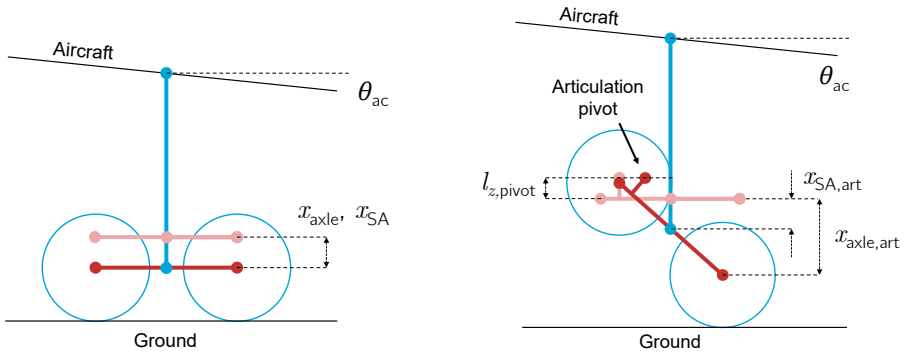

(a) Conventional bogie, axle and shock strut stroke. **(b)** Articulated bogie, axle and shock strut stroke.

Figure 3.15: Axle and shock strut strokes. Please note that the figures illustrate the case where the shock strut is perfectly perpendicular to the ground surface, such that $x_{SA} = x_{axle}$ ($\alpha = 0°$ in Equation 2.15).

Although the reserve energy test condition typically demands the largest stroke, the shock absorber does not need to be specifically sized for this condition, as it is generally permissible for the shock absorber to bottom out during a reserve energy test [12]. Instead, the shock absorber is sized for the 3.05 m/s limit landing condition, with a 10% stroke margin to accommodate low-temperature operations.

Shock Absorber Sizing

The target minimum nose gear load fraction $\hat{\beta}_{nlg,min}$ is used to calculate the maximum main gear load at maximum ramp mass. This, along with the intended static shock absorber pressure, is then used to determine the piston surface area (Equation 3.9) and corresponding piston diameter.

$$A_{piston} = \frac{MRM g(1 - \hat{\beta}_{nlg,min})}{2P_{mlg,static}} \tag{3.9}$$

In shock absorber sizing, the piston diameter is typically selected to accommodate standard seals [12]. Therefore, the calculated piston diameter is adjusted to the nearest standard seal dimension as specified by AS4832 Aerospace Standards [53]. After this adjustment, the piston cross-section area and static pressure are recalculated accordingly.

The maximum shock absorber load is defined by the 1.7g bump load at maximum ramp mass, as discussed in Section 2.4.3. For the Flying-V specifically, also the 1.7g bump load with an additional 0.6g downforce at maximum take-off mass needs to be considered, representing a ground surface bump during braking after a rejected take-off. The minimum shock absorber load is defined by the shock absorber breakout load. With the minimum and maximum shock absorber loads known, the fully extended (minimum) and fully compressed (maximum) shock absorber pressures can be calculated. Shock absorber compression chamber volumes are calculated using Equation 2.16, which can then be used to calculate the fully extended, static, and fully compressed shock absorber positions (Equation 2.20).

The nose gear shock absorber is sized in a similar way, with the target maximum nose gear load fraction $\hat{\beta}_{nlg,max}$ defining the maximum static load on the nose gear.

Main Gear Strut Sizing

Three primary gear configurations are defined: the static configuration, the fully extended configuration, and the retracted configuration. The configurations describe the shock absorber positions and orientation angles of the shock strut and, if applicable, the upper strut, as discussed in Section 3.2.2.

First, the strut lengths are determined. For the static configuration, the shock strut length is the sum of the shock strut cylinder length l_{ss} and the corrected static shock absorber length. For both the fully extended and retracted configurations, the shock strut length is the sum of the shock strut cylinder length l_{ss} and the corrected fully extended shock absorber length. If the gear features a strut shortening

mechanism, the strut shortening amount $l_{\text{shortening}}$ is subtracted from the retracted shock strut length. In the case of a double folding strut type, an upper strut is added, which has a certain upper strut length l_{us}. Both the shock strut length l_{ss} and the upper strut length l_{us} are part of the design vector as shown in Table 3.8.

Main Gear Extended Strut Rotation

Once the strut lengths are defined, the struts are rotated about their origin using angles θ_{ext}, ϕ_{ext} and ψ_{ext}, as detailed in Section 3.2.2, applied in the order as defined by Equation 3.2. In this phase, all three gear configurations are rotated according to the angles specified for the extended gear, resulting in each configuration having the same orientation. The retracted configuration is rotated to have the retracted gear configuration in a later step, after the rolling stock has been attached. For double folding struts, each strut is rotated independently. Following the rotation, the coordinates of the shock strut are translated such that its origin aligns with the bottom of the upper strut.

Main Gear Rolling Stock Positioning

After the length and orientation of the extended gear have been determined, the rolling stock is attached. Bogie length, width and joint location, together with loaded and unloaded tyre radii are used to define a certain rolling stock geometry. The bogie length describes the location of the front and aft wheel axles, whereas the width and loaded tyre radius describe the ground contact point locations. The rolling stock geometry is rotated around the bogie joint as required. The bogie joint only allows rotations around the lateral aircraft axis.

In the static configuration, the rolling stock rotation must account for the aircraft static pitch attitude, $\theta_{\text{ac,static}}$, as shown in Figure 3.16a. In the fully extended configuration, the rolling stock rotation must consider either the aircraft pitch attitude θ_{ac}, such that all wheels remain on the ground, or the bogie articulation angle, θ_{bogie}, with only the aft wheels touching the ground. The latter is illustrated in Figure 3.16b. For the retracted configuration, the rolling stock needs to be rotated so that, once the gear is fully folded, the bogie and tyres align with the aircraft's longitudinal axis for efficient stowage. After rotating the rolling stock, its geometry is translated to align the bogie joint with the bottom of the shock strut.

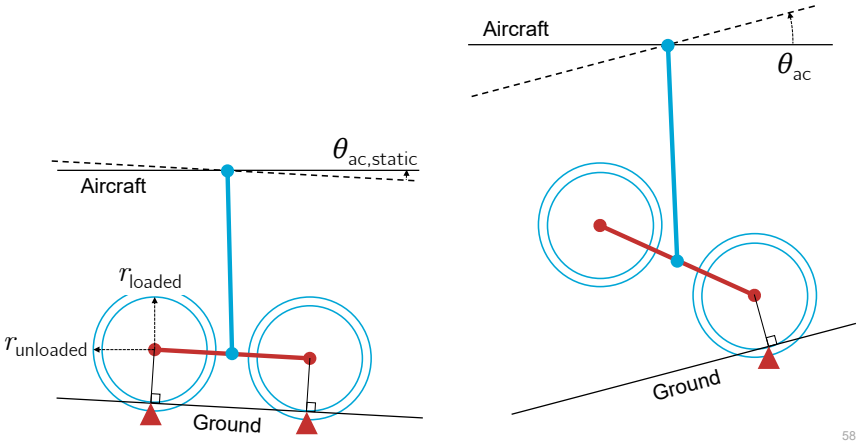

(a) Static configuration, rolling stock rotated to account for static aircraft pitch attitude.

(b) Fully extended configuration, rolling stock rotated to represent articulated bogie. Orientation is representative for landing or take-off manoeuvre.

Figure 3.16: Rolling stock positioning.

Main Gear Folding

With the extended gear configurations established, the retracted gear configuration can be folded to represent the retracted gear. Importantly, the shock strut and rolling stock are rotated as a single structure, maintaining the orientation of the bogie relative to the shock strut as defined during the rolling stock positioning. This ensures that the bogie rotation axle for the retracted configuration remains aligned with that for the extended configuration as defined by the lateral aircraft axis. First, the shock

strut, now including the rolling stock, is rotated back to its neutral position using angles $\theta_{\text{ss,ext}}$, $\phi_{\text{ss,ext}}$ and $\psi_{\text{ss,ext}}$. Then, it is rotated about its origin to obtain the retracted orientation, using angles $\theta_{\text{ss,ret}}$, $\phi_{\text{ss,ret}}$ and $\psi_{\text{ss,ret}}$, applied in the order as defined by Equation 3.2.

For a double folding strut, the upper strut is rotated independently of the shock strut. Similar to the shock strut, it is first rotated back to the neutral position and then to the correct retracted orientation, but using angles $\theta_{\text{us,ret}}$, $\phi_{\text{us,ret}}$ and $\psi_{\text{us,ret}}$. After the rotation, the coordinates of the shock strut are translated to align its origin with the bottom of the upper strut.

Nose Gear Sizing and Rotation
The nose gear strut is sized such that the combined length of the strut and the static shock absorber, e.g., the static configuration, results in the intended static aircraft pitch attitude. The nose gear strut is raked with respect to the longitudinal aircraft axis to be perpendicular to the ground. The fully extended nose gear configuration is then defined by the combined length of the strut and the fully extended shock absorber. This fully extended configuration is rotated by an angle $\theta_{\text{nlg,ret}}$ to achieve the retracted nose gear configuration.

3.3.4. Objective

As with many engineering problems, landing gear need to be designed with multiple objectives in mind. Specifically, the gear must be positioned as far forward as possible for rotation performance, while its length needs to be as short as possible to have the lowest mass. The main gear needs to be stowed as close to the primary aircraft structure as possible for efficient integration and additionally, the nose gear needs to be positioned as far forward as possible to minimise nose gear loads.

The multi-objective, or Pareto, landing gear stick model optimisation is performed by minimising the objective function 3.10, employing an objective weighted sum approach [54]. This approach involves combining multiple objectives f_{i} into a single objective function $f_{\text{weighted sum}}$ using a set of weight factors w_{i} that represent the relative importance of each objective. An overview of weight factors is presented in Table 3.9.

$$\text{minimise: } f_{\text{weighted sum}}(\bar{x}) = \sum_{\text{i}=1}^{\text{m}} w_{\text{i}} f_{\text{i}}(\bar{x}) = w_1 \frac{l_{\text{mlg,ext}}}{l_{\text{mlg,ext,0}}} + w_2 \frac{s_{\text{to,stat}}}{s_{\text{to,stat,0}}} + w_3 \frac{s_{\text{fpb}}}{s_{\text{fpb,0}}} + w_4 \frac{s_{\text{rs}}}{s_{\text{rs,0}}} \tag{3.10}$$

In the objective function, $s_{\text{to,stat}}$ represents the static tipover margin, which is defined as the distance between the aft centre of gravity and the main gear pivot. Minimising the static tipover margin positions the gear as far forward as stability allows, thereby maximising aircraft rotation ability, which is the primary objective. The secondary objective is to minimise the extended gear length $l_{\text{mlg,ext}}$, which is the combined length of the upper strut (if applicable) and the shock strut with a fully extended shock absorber. Landing gear length and mass are strongly correlated [8, 12, 29, 50]. It is assumed that optimising for minimum length also results in minimum mass. This approach significantly simplifies the optimisation algorithm by eliminating the need for integrated structural analysis.

Minimisation of the nose gear to front pressure bulkhead clearance distance s_{fpb} is added as a tertiary objective to ensure that the nose gear is positioned as far forward as possible. This should, however, not affect the design of the main gear and is therefore given a low weight factor. For Flying-V aircraft, minimisation of the main gear to rear spar clearance distance s_{rs} is added as a fourth objective. This ensures that the stowed main gear is positioned as close to the rear spar as possible, resulting in better structural and aerodynamic integration. Each objective is normalised using their respective initial evaluation value, ensuring that all objectives have a similar scale.

Table 3.9: Optimisation objective function weight factors.

Weight factor	w_1	w_2	w_3	w_4
Value	3	5	1	1

3.3.5. Inequality Constraints

To ensure the feasibility of the landing gear stick model, it must satisfy a set of design constraints that address aircraft stability, ground clearance, airfield compatibility, and airframe integration. All constraints are normalised such that they have a similar scale.

Stability

Stability constraints ensure that the aircraft is longitudinally and laterally stable, as discussed in Section 2.4.1. Push-back tipover is prevented by ensuring that the tipback angle θ_{tpb} is larger than the minimum tipback angle $\theta_{\text{tpb,min}}$, resulting in the constraint formulated by Equation 3.11.

$$c_{\text{pb tipover}} = 1 - \frac{\theta_{\text{tpb}}}{\theta_{\text{tpb,min}}} \leq 0 \tag{3.11}$$

The rotated tipover constraint is defined by Equation 3.12, where $s_{\text{to,rot}}$ represents the rotated tipover margin. The rotated tipover margin is the horizontal distance between the aft centre of gravity and the main landing gear pivot, measured with the aircraft and rolling stock oriented as corresponding to the maximum pitch attitude condition. The main landing gear pivot is defined by the joint connecting the strut to the bogie for both conventional and articulated bogie configurations. Physically, bogie articulation shifts the pivot point from the bogie joint to the aft wheel axle during articulation. However, taking the bogie joint as pivot for stability constraint evaluations ensures that the gear is positioned slightly further aft. While this marginally affects rotation ability, it also induces a pitch-down moment upon touchdown, facilitating derotation. Immediate derotation is required to ensure adequate ground clearance when all wheels contact the ground. Further optimisation of the landing gear position for optimal landing and take-off performance can be explored in future research. The impact is not expected to be significant enough to justify it being included in this research.

$$c_{\text{rot tipover}} = -\frac{s_{\text{to,rot}}}{|s_{\text{to,rot,0}}|} \leq 0 \tag{3.12}$$

Lateral stability is ensured by imposing a constraint on the lateral turnover angle ψ_{tno}. The lateral turnover angle, which can be calculated using Equation 2.5, needs to smaller than the maximum lateral turnover angle $\psi_{\text{tno,max}}$ as stipulated by Equation 3.13.

$$c_{\text{lat turnover}} = 1 - \frac{\psi_{\text{tno,max}}}{\psi_{\text{tno}}} \leq 0 \tag{3.13}$$

Ground Clearance

Ground clearance is evaluated for the static gear configuration, as well as for the fully extended gear configuration. For the static configuration, the maximum pitch attitude is $\theta_{\text{max,statSA}}$, whereas for the fully extended configuration, the maximum pitch attitude is $\theta_{\text{max,extSA}}$. For both configurations, the minimum pitch attitude is θ_{stat}. The roll angles vary from 0° to ϕ_{max}. For all possible combinations of pitch and roll, the z-coordinate of any clearance critical point CCP_i may not be lower than the z-coordinate of the ground contact point, both measured in the inertial frame.

The vector $\mathbf{r}_{\text{CCP}_\text{i}}$, which describes the location of the clearance-critical point CCP_i relative to the ground contact point, is rotated around the ground contact point with angles ϕ and θ, as described by Equation 3.14. In this equation, $\mathbf{R_y}(\theta)$ and $\mathbf{R_x}(\phi)$ are the elemental rotation matrices (Equation 3.1), and $\mathbf{r}^{\text{rot}}_{\text{CCP}_\text{i}}$ is the rotated vector $\mathbf{r}_{\text{CCP}_\text{i}}$. For each clearance evaluation, the location of the ground contact point is updated to reflect the orientation of the rolling stock corresponding to the aircraft orientation to be evaluated. The aircraft is considered to roll around the outboard tyre centroid, and is considered to pitch around the bogie pivot joint, or the aft wheel axle when the bogie is articulated.

$$\mathbf{r}^{\text{rot}}_{\text{CCP}_\text{i}} = \mathbf{R_y}(\theta)\mathbf{R_x}(\phi)\mathbf{r}_{\text{CCP}_\text{i}} \tag{3.14}$$

The ground clearance constraint is defined by Equation 3.14, where z_{CCP_i} is the z-component of the vector $\mathbf{r}^{\text{rot}}_{\text{CCP}_\text{i}}$.

$$c_{\text{clearance}_i} = -\frac{z_{\text{CCP}_i}}{|z_{\text{CCP}_i,0}|} \leq 0 \tag{3.15}$$

Airfield Compatibility

Airfield compatibility constraints ensure that the landing gear stick model complies with airfield compatibility requirements as outlined in Section 2.4.4. The minimum and maximum nose gear load constraints are defined by Equations 3.16 and 3.17 respectively. Here $\beta_{\text{nlg,aftCG}}$ is the nose gear load fraction for the aft centre of gravity condition, and $\beta_{\text{nlg,fwdCG}}$ is the nose gear load fraction for the forward centre of gravity condition. Nose gear load fractions are calculated using Equation 2.22.

$$c_{\beta\text{nlg,min}} = 1 - \frac{\beta_{\text{nlg,aftCG}}}{\beta_{\text{nlg,min}}} \leq 0 \tag{3.16}$$

$$c_{\beta\text{nlg,max}} = 1 - \frac{\beta_{\text{nlg,max}}}{\beta_{\text{nlg,fwdCG}}} \leq 0 \tag{3.17}$$

The intended taxiway design group (TDG) imposes constraints on the outer main gear width (MGW) and cockpit to main gear distance (CMG). The MGW constraint is expressed by Equation 3.18, whereas the CMG constraint is defined as shown by Equation 3.19.

$$c_{\text{TDG,MGW}} = 1 - \frac{\text{MGW}_{\text{max}}}{\text{MGW}} \leq 0 \tag{3.18}$$

$$c_{\text{TDG,CMG}} = 1 - \frac{\text{CMG}_{\text{max}}}{\text{CMG}} \leq 0 \tag{3.19}$$

In addition, the aircraft needs to be able to make a 180° turn on a runway or turn pad. The turn width constraint as defined by Equation 3.20 ensures that the turn with l_{turn} is smaller or equal to the turn width of a reference aircraft $l_{\text{turn,ref}}$. The turn width is calculated using Equation 2.26, examples of turn widths are shown in Table 2.6.

$$c_{\text{turn}} = 1 - \frac{l_{\text{turn,ref}}}{l_{\text{turn}}} \leq 0 \tag{3.20}$$

Airframe Integration

Stowage constraints ensure that the nose gear and main gear can be stowed without colliding into each other or other aircraft components and structures. For all clearance distance evaluations, the maximum grown tyre width and diameter are considered, accounting for inflation pressure stress and centrifugal loads when spinning [12]. Equation 3.21 describes the nose gear stowage constraint ensuring that the front pressure bulkhead clearance distance s_{fpb} is larger than the minimum distance $s_{\text{fpb,min}}$.

$$c_{\text{nlg,fpb}} = 1 - \frac{s_{\text{fpb}}}{s_{\text{fpb,min}}} \leq 0 \tag{3.21}$$

The main gear tyres are kept clear of the aircraft centreline at a distance s_{cl}, which must be larger than $s_{\text{cl,min}}$ as described by Equation 3.22.

$$c_{\text{mlg,cl}} = 1 - \frac{s_{\text{cl}}}{s_{\text{cl,min}}} \leq 0 \tag{3.22}$$

For Flying-V aircraft, an additional constraint is added to prevent the main gear from colliding with the rear spar in the retracted position. The constraint is formulated by Equation 3.23, where s_{rs} is the main gear to rear spar clearance distance.

$$c_{\text{mlg,rs}} = 1 - \frac{s_{\text{rs}}}{s_{\text{rs,min}}} \leq 0 \tag{3.23}$$

3.3.6. Consistency Constraints

The consistency constraints imposed by Equation 3.24 and 3.25 ensure that the target nose gear load values $\hat{\beta}_{\text{nlg,min}}$ and $\hat{\beta}_{\text{nlg,max}}$ selected by the optimiser are consistent with the actual nose gear load values $\beta_{\text{nlg,min}}$ and $\beta_{\text{nlg,max}}$.

$$c^c_{\beta_{\text{nlg,min}}} = 1 - \frac{\hat{\beta}_{\text{nlg,min}}}{\beta_{\text{nlg,min}}} = 0 \tag{3.24}$$

$$c^c_{\beta_{\text{nlg,max}}} = 1 - \frac{\hat{\beta}_{\text{nlg,max}}}{\beta_{\text{nlg,max}}} = 0 \tag{3.25}$$

3.3.7. Manual Design Evaluations and Adjustments

Some design requirements are not included in the optimisation algorithm, as their complexity or limited impact on the optimisation result does not justify the additional effort given the scope of this research. Instead, after the optimiser has found a feasible optimum, additional manual design evaluations are required to ensure the final design meets all requirements before progressing to structural sizing and further gear design analysis. Specifically, tyre loads, flotation and turning radii are evaluated. If the landing gear features an articulated bogie, also the de-articulation margin is assessed. If needed, the design initialisation inputs need to be adjusted in order to get a satisfactory gear stick model.

Tyre Loads

While tyre loads can be evaluated using the optimisation algorithm, tyre load limits are defined by a discrete tyre selection, which adds significant complexity to the otherwise gradient-based process. Instead, the tyre selection is adjusted by the designer, simply requiring a single iteration to adjust to the maximum loads calculated by the algorithm. Following the optimisation, a loading diagram is created, allowing the designer to visually inspect the maximum mass an aircraft may have without overloading the tyres. Both static and dynamic loading conditions are considered, with the centre of gravity ranging from the forward to aft limit corresponding to each mass condition, as discussed in Section 3.2.1. If the expected maximum mass exceeds the permissible maximum mass on either the nose or main gear, adjustments to the tyre selection are necessary. Tyres can withstand 1.5 times the static load rating under dynamic loading. A 1.07 safety factor is considered [12].

Flotation

In addition to gear loading, also flotation is evaluated. As discussed in Section 2.4.4, in initial landing gear design, using the wheel arrangement of a comparable aircraft in the initial landing gear design typically ensures adequate flotation performance. However, even for aircraft that seem very similar, different gear locations can lead to different gear loads and, consequently, different Aircraft Classification Ratings (ACR). Therefore, as an additional feasibility check, flotation performance is evaluated and compared with a reference aircraft. To limit complexity, flotation analysis is not included within the optimisation algorithm. Instead, it is evaluated using the ICAO-ACR tool.

Turning Radii

Although turning radius evaluations are crucial for ensuring airport compatibility, they are excluded from the optimisation algorithm because the gear design has only a marginal impact on turning radii. The turning radius of an aircraft component depends on its distance from the turn centre, as discussed in Section 2.4.4. For locations far from the turn centre, such as the wing tip, changes in the turn centre location result in minor relative changes to the turning radius. Consequently, specifically imposing turning radius constraints may prevent the optimiser from finding a feasible solution.

Instead, wing tip, nose and tail plane turning radii are only determined after the optimisation is completed. If any of the turning radii is not satisfactory, this may either impose operational limitations, require adjustments to aircraft geometry, or necessitate the implementation of a steering main gear.

De-Articulation Margin

For aircraft with landing gear that includes an articulation mechanism, it is crucial to verify that the static shock absorber compression is sufficient to have all wheels touch the ground when the aircraft

is at its minimum mass. After optimisation, the static compression is compared with the geometric dearticulation stroke defined in Section 3.3.3. The static compression needs to be larger than the de-articulation stroke with a margin to account for ground operations (e.g., bumps). The shock absorber reaction factors for the initial de-articulation compression phase and second compression phase can be modified to change the amount of energy absorbed in each phase. A decrease in energy absorption in the initial phase necessitates a larger energy absorption in the second phase, thereby increasing the length of the static stroke, and vice versa.

3.4. 3D Model Generation

Once the stick model is completed, the design is detailed in Computer Aided Design (CAD) software such that kinematic feasibility can be verified, and structural sizing can be performed. In this section, the 3D model generation submodule is discussed.

3.4.1. Folding Axes

The 3D model generation starts with an evaluation of folding axis orientations, which are required for analysing the gear retraction path and load resolutions. For gear configurations with a single folding axis, the orientation axis is described by a line representing the intersection of two planes that are orthogonal to the retraction movement vectors $\mathbf{r}_{\mathbf{AA'}}$ and $\mathbf{r}_{\mathbf{BB'}}$. The movement vectors are defined as illustrated in Figure 3.17a. The folding axis orientation vector is obtained by taking the cross product of both movement vectors, as outlined by Equation 3.26 [8, 12].

$$\mathbf{r}_{\text{folding axis}} = \mathbf{r}_{\mathbf{AA'}} \times \mathbf{r}_{\mathbf{BB'}} \tag{3.26}$$

For gear configurations with a double folding axis, two additional movement vectors are defined, as illustrated in Figure 3.17b. First, the orientation of the upper strut folding axis (folding axis 1) is determined by taking the cross product of the movement vectors $\mathbf{r}_{\mathbf{AA'}}$ and $\mathbf{r}_{\mathbf{BB'}}$, as formulated by Equation 3.27. The movement vectors describe the movement of any wheel axle from the extended position to an imaginary retracted position, which describes the orientation of that wheel axle as if not only the upper strut, but also the lower strut and rolling stock are rotated with the upper strut folding angles $\theta_{\text{us,ret}}$, $\phi_{\text{us,ret}}$ and $\psi_{\text{us,ret}}$.

$$\mathbf{r}_{\text{folding axis 1}} = \mathbf{r}_{\mathbf{AA'}} \times \mathbf{r}_{\mathbf{BB'}} \tag{3.27}$$

Subsequently, the orientation of the lower strut folding axis (folding axis 2) is determined by taking the cross product of the movement vectors $\mathbf{r}_{\mathbf{A'A''}}$ and $\mathbf{r}_{\mathbf{B'B''}}$, as defined in Equation 3.28. The movement vectors describe the movement of the wheel axle from the imaginary retracted orientation to the actual retracted orientation.

$$\mathbf{r}_{\text{folding axis 2}} = \mathbf{r}_{\mathbf{A'A''}} \times \mathbf{r}_{\mathbf{B'B''}} \tag{3.28}$$

3.4.2. Design Refinement

During the landing gear design refinement, the stick model is developed into a three-dimensional gear model in 3DEXPERIENCE CATIA [55]. At this point, only gear strut and bogie dimensions and folding axes orientations are known. In order to be able to evaluate gear clearance, feasibility and mass, the gear needs to be detailed such that it includes tyres and primary structural components. In the context of this research, primary structural components are the shock strut cylinder, shock strut piston, trunnion beam, bogie beam, wheel axles, a drag brace and a side brace. If the gear is of the double folding type, also the upper strut and an additional support brace are considered. Similar to previous landing gear mass estimation studies, torque links are excluded, as their influence on the overall mass estimate is insufficient to justify the effort required [8, 32]. Articulation and shortening mechanisms are included such that the mass benefits of using them can effectively be evaluated.

For each structural member, either the minimum or maximum dimensions are defined as a function of the shock strut piston diameter or wheel rim diameter, similar to Chai and Mason [8]. This is required

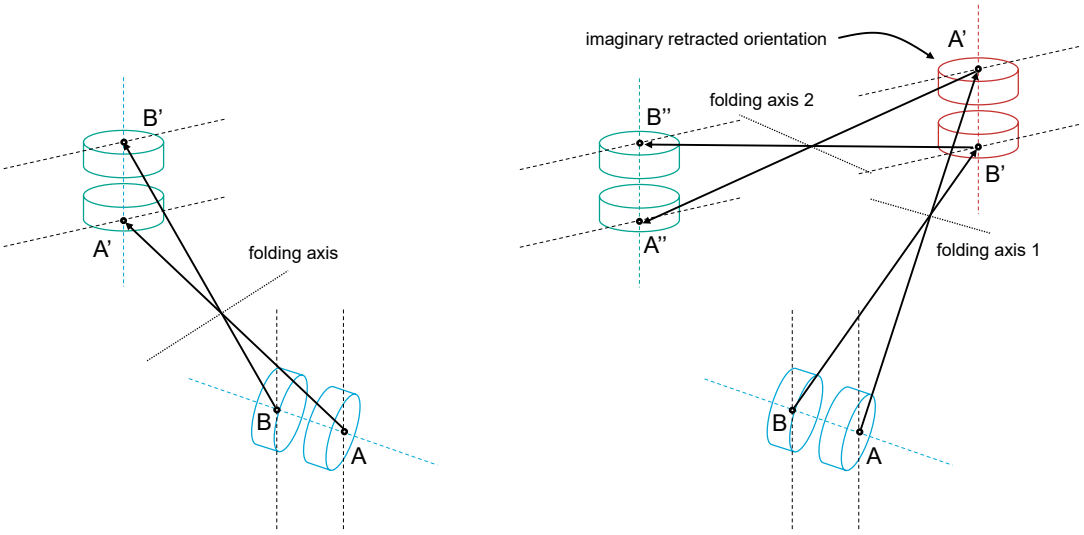

(a) Single folding strut folding axis [8].

(b) Double folding strut folding axes.

Figure 3.17: Gear retraction movement vectors.

as otherwise, wall thickness optimisation will increase member diameters indefinitely for a larger area moment of inertia, resulting in infeasible structures. As an initial sizing estimate, each structural component is assumed to have a wall thickness of 15 mm.

Shock Strut

The shock strut cylinder and piston are modelled as tubes connecting the bogie beam to the trunnion beam. The inner cylinder diameter must be equal to the outer piston diameter, which is defined by shock absorber sizing. While the cylinder length can be directly derived from the stick model, this is not true for the piston, as bearing overlap is required for smooth operation. The piston length is defined as the fully extended stroke plus 2.75 times the piston diameter [8, 12]. The cylinder has a connector that is either fixed to or pivotably connected to the trunnion beam (Figure 3.18a), depending on the brace configuration. In addition, the cylinder features connectors connecting to one or multiple support braces or an articulation mechanism if applicable. The piston is pivotably connected to the bogie beam, as illustrated in Figure 3.18b, allowing the bogie to pivot around the lateral aircraft axis.

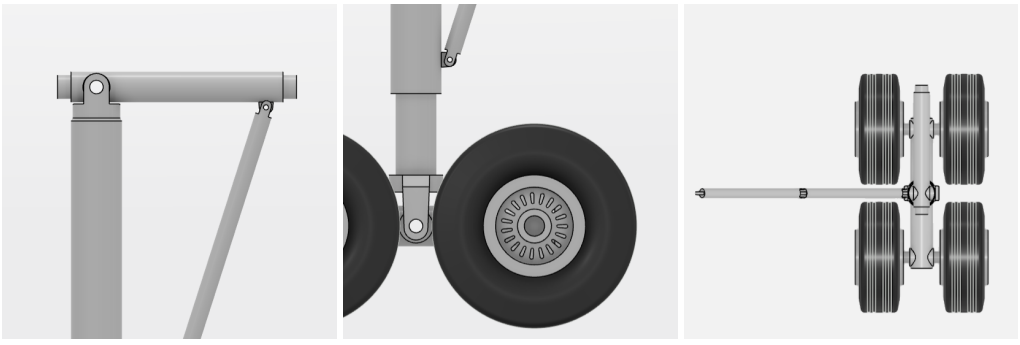

(a) Main gear trunnion design refinement.

(b) Main gear bogie beam design refinement.

(c) Main gear side brace design refinement.

Figure 3.18: Landing gear design refinement.

Trunnion Beam

The trunnion beam serves as the connecting element between the shock strut cylinder and the aircraft attachment structure or upper strut assembly, and is aligned with the shock strut folding axis. The trunnion features multiple connection points, which allow for attaching the cylinder as well as one or multiple support braces, as illustrated in Figure 3.18a. The trunnion length is chosen to achieve a

reasonable compromise between trunnion mass, brace loads and aircraft integration. The trunnion is modelled as a tube with an outer trunnion diameter assumed to be equal to the shock absorber piston diameter [8]. When the landing gear is of the double folding type, the trunnion is modelled as a tube with an outer diameter that is 80% of piston diameter to account for loads being distributed over a larger number of components.

Bogie Beam
The bogie beam connects the shock absorber piston to the wheel axles, which are evenly distributed along its length. It is modelled as a tube with an outer diameter that is 85% of the piston diameter (estimated from Schmidt [12]). Depending on the configuration, the bogie beam may feature an offset shock absorber piston joint and a connector for an articulation mechanism.

Wheel Axles
The wheel axles connect the rolling stock to the bogie beam, and are modelled as tubes with an outer diameter that is 25% of the wheel rim diameter (estimated from Schmidt [12]).

Upper Strut Assembly
When the landing gear is of the double folding type, also the upper strut assembly is included in the model. The design of the upper strut assembly is derived from the B-58 drop link arrangement, where the upper strut is represented by two fixed length linkages, linking the shock strut trunnion to to the drop link assembly trunnion as shown in Figure 3.19. The linkages flare out slightly from bottom to top, providing stability. Additionally, two diagonal linkages are incorporated to provide extra support. All upper strut linkages are modelled as tubes with the outer diameter equal to 40% of the shock strut piston diameter (estimated from Schmidt [12]).

Figure 3.19: Upper strut assembly design.

Braces
Braces are added to support the gear in all intended loading directions. Many different brace arrangements exist, each with varying levels of complexity as discussed in Chapter 2. The brace configurations considered in this research are based on those found in existing landing gear to ensure proven feasibility and reliability. Each brace is modelled as either a tube or a square I-beam (with equal width and height) and can be of either the fixed or planar folding type to minimise complexity and mass [12]. The maximum outer diameter, or section height, is initially limited to 50% of the shock strut piston diameter (estimated from Schmidt [12]), but may be adjusted based on structural analysis, e.g., to satisfy buckling or machinability constraints.

Brace positioning involves several key considerations, such as kinematic feasibility, structural integration, load transfer, and mass. Previous work has included brace positioning in an optimisation algorithm, optimising for minimum mass [34]. In this research, braces are positioned based on engineering judgement for simplicity. It is ensured that the brace does not collide with existing aircraft or landing gear structure when retracted, and that there is airframe structure available to attach the brace. Moreover, the brace is positioned such that it provides appropriate leverage to the strut, benefiting load distribution and sizing. Tension loading is preferred over compression to avoid buckling, which is a common sizing mode for braces [8, 12].

The brace configuration supporting a single folding strut is based on the that of the Airbus A310-200 and Boeing 707-320. A fixed length brace prevents the shock strut from moving relative to the trunnion, as illustrated by Figures 3.18a and 3.18b. Additionally, a folding brace is added perpendicular to the folding axis as shown in Figure 3.18c, providing support to the gear when extended and locked, but permitting retraction when unlocked and folded.

Brace configurations supporting a double folding strut are inspired by the design of the B-58 main landing gear drop link arrangement, which is shown in Figure 2.7. The upper strut assembly is supported by two planar folding braces, providing a rigid attachment platform for the shock strut trunnion. Two fixed braces connect the shock strut to the trunnion. A third fixed length brace is added, directly connecting the shock strut to the airframe, such that the gear only has a single degree of freedom. Consequently, the gear can be retracted with a single actuator, limiting complexity.

Special Features
The design of the articulation mechanism is based on that of the Airbus A330/A340 family (Figure 2.5a). The lengths of the linkages are adjusted to achieve the correct articulation orientation and to ensure the right stowage orientation can be obtained when retracted. The shortening mechanism is modelled as a single tube with a length corresponding to the required shortening amount. All linkages are modelled as tubes, with the outer diameter assumed to be equal to 30% of the shock strut piston diameter, as estimated from Schmidt [12] and Figures 2.5a and 2.6.

3.4.3. Feasibility Evaluation
Feasibility of the three-dimensional gear model is assessed by conducting a retraction path and swept volume analysis in CATIA software to identify any structural interference. The landing gear must not collide with itself or other aircraft structures throughout its range of motion. This is evaluated by simulating the retraction kinematics, utilising collision detection features in CATIA and performing visual inspection.

3.5. Structural Sizing
After a feasible geometry has been generated, the minimum wall-thickness, volume and mass of primary structural components is determined in the structural sizing submodule. This section outlines the structural sizing methodology, which includes generating a finite element model, calculating external loads, performing finite element analysis to determine internal member loads, and conducting cross-section sizing to determine the required wall thickness. The process is illustrated by the flowchart in Figure 3.20.

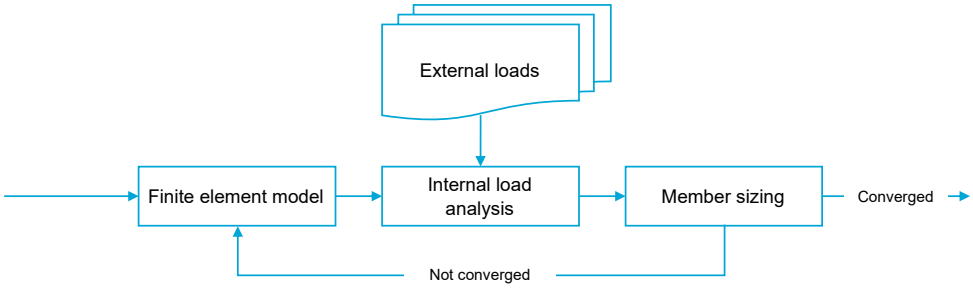

Figure 3.20: Structural sizing process flowchart.

In the context of this research, the structural sizing is conducted only for the main landing gear. As discussed in Section 2.5, traditional landing gear mass estimations are unsuitable for unconventional aircraft and unconventional gear designs. Insights from the conceptual design phase and previous studies on the Flying-V landing gear [9, 11] indicate that the design and integration of the main gear differ from those of conventional aircraft, necessitating a (quasi) physics-based mass estimation method. Conversely, the design and integration of the nose gear is rather conventional, justifying the use of traditional, statistics-based, mass estimation methods. As an additional justification, the contribution of the nose landing gear to the total landing gear mass is typically around 10% [8, 12], implying that

potential errors arising due to the simplification would only have a minor effect on total gear group mass estimations.

3.5.1. Finite Element Model

Structural sizing is based on a (1D) stick model representation of the three-dimensional gear model. This model is fundamentally different from the stick model which was created in the stick module generation submodule (Section 3.3), as it incorporates the design refinement described in Section 3.4.2. The refined stick model includes a trunnion, braces, wheel axles, tyres, and if applicable, an upper strut and articulation mechanism. The shortening mechanism is excluded from the finite element model, as it can be sized directly using the vertical force on the shock absorber piston, with the assumption that all lateral forces, bending moments and torque are transferred to the cylinder.

Brace and articulation mechanism attachments are modelled as shown in Figure 3.21, illustrating a side view of a three-dimensional gear model with a beam model representation in orange. The beam representing the brace is not directly connected to the strut, as this would overestimate the leverage provided by the brace. Instead, an imaginary connector beam element AB is added, representing the distance between the brace joint and strut centreline. The resulting load in the shock strut cylinder is a result of the combined action of brace reaction loads F_x and F_z, and induced bending moment $F_z l_{\text{AB}}$. The connector beam is infinitely stiff, and is not included in the mass estimation.

Regulations prescribe that some external loads need to be applied to the ground contact point, requiring the tyres to be included in the refined stick model as well [17, 29]. Similar to the connector beams, tyres are modelled by an infinitely stiff beam element that is not included in the mass estimation. The beam element represents the loaded tyre radius, its length depending on the actual loading condition.

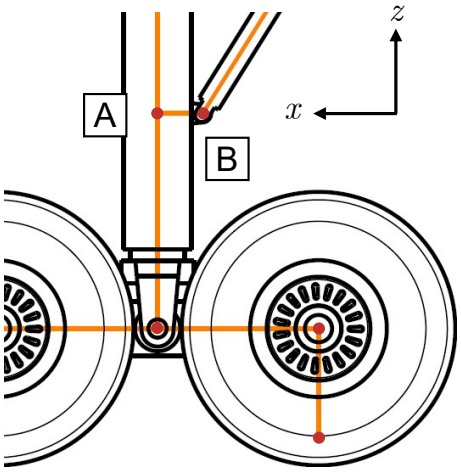

Figure 3.21: Brace attachment and tyre modelling.

All stick model elements except the tyres and connector elements are modelled as tubes, similar to Chai and Mason [8]. Dimensions are dictated by the three-dimensional model. Nodes may either be of the beam, hinge or universal type. A beam type node describes a joint that transfers all translations and all rotations, e.g., a rigid connection. A hinge type transfers all translations and all rotations except the rotation around the x-axis, defined according to its local coordinate system. Lastly, the universal type transfers all translations, but no rotations. Similar to previous landing gear design and mass estimation studies, all structural members are made of 300M high-strength steel [8, 32]. Material properties are outlined in Table 2.3.

3.5.2. External Load Analysis

The stick model is subjected to the CS-25 landing and ground handling load cases outlined in Table 2.2. Table A.1 in Appendix A provides a detailed overview of conditions and loads corresponding to each load case. Regulations prescribe that vertical loads and drag loads are applied to the wheel axles while lateral loads need to be applied to the ground contact points, as illustrated in Figure 3.22 for the

right aft wheel.

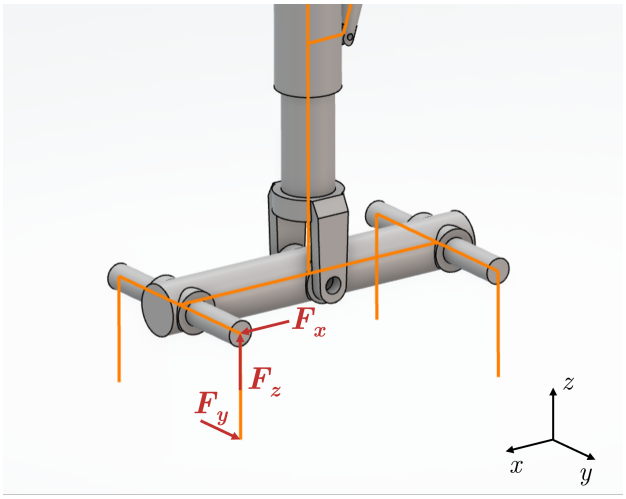

Figure 3.22: External landing gear loads on right aft main gear wheel.

Asymmetric loading in multi-wheel gear units is not considered, except for asymmetric loading caused by bogie articulation. Structural deflections of the aircraft and the dynamic behaviour of shock absorbers and tyres are also not taken into account. Instead, load cases are evaluated using quasi-static approximations, as discussed in Section 2.4.2. Tyre and shock absorber deflections are assumed constant, depending on the vertical reaction load and the total available deflection.

Landing Loads

For landing load cases, the maximum vertical reaction load is proportional to the shock absorber reaction factor λ_{mlg} as defined in Equation 2.12. Drag loads and side loads are expressed as fractions of the maximum vertical reaction load. As a conservative estimate, all prescribed loads are assumed to occur simultaneously.

Tyre deflections are estimated to be 90% of the value obtained through linear interpolation or extrapolation between the unloaded and loaded tyre radii, as detailed in Equation 3.29 [12]. The maximum vertical reaction is estimated to occur at 25% of the corrected 3.05 m/s descent velocity design landing shock absorber stroke [12].

$$\begin{aligned} x_{\text{tyre}} &= 0.9 \left(\frac{r_{\text{tyre,unloaded}} - r_{\text{tyre,loaded}}}{F_{\text{gear,rated}}} \right) F_{\text{gear,max}} \\ r_{\text{tyre}} &= r_{\text{tyre,unloaded}} - x_{\text{tyre}} \end{aligned} \tag{3.29}$$

Spin-up and spring-back loads are obtained using a simplified method from Schmidt [12], suitable for initial sizing calculations. For spin-up, it is assumed that peak spin-up occurs when the vertical reaction load is 80% of the maximum vertical reaction load. Taking a maximum tyre-to-ground friction coefficient of 0.8, maximum spin-up loads are estimated to be $0.8 \times 0.8 = 0.64$ times the maximum vertical reaction load. The maximum spring-back load is equal to the spin-up load, but in opposite direction. Spin-up and spring-back loads are only considered if they impose a more significant wheel load than the drag load specified by the applicable CS-25 load case.

For conventional bogie configurations, loads are applied to all wheels simultaneously. However, for articulated bogie configurations, the landing load case needs to be split in two phases. In the initial phase, the bogie is articulated, such that only the aft wheels are subjected to landing loads (including spin-up and spring-back). The maximum vertical reaction being proportional to the articulated gear reaction factor $\lambda_{\text{mlg,art}}$. In the second phase, all wheels are subjected to landing loads, with the maximum

vertical reaction again being proportional to the shock absorber reaction factor λ_{mlg}. At this stage, spin-up and spring-back are no longer relevant for the aft wheels as they are already up to speed, making CS-25 drag loads dominant for these wheels.

Ground Handling Loads
For ground handling loads, the maximum vertical reaction is proportional to a load factor prescribed by CS-25 load cases. For aircraft that feature means to generate downforce to enhance braking performance, this is added to the vertical reaction. Specifically, this is only done for the taxi, take-off and landing roll, and braked roll load cases, as these load cases describe conditions where the aircraft has sufficient airspeed to generate downforce. Side and drag loads are proportional to the vertical reaction. As for the landing load cases, tyre deflections are calculated using Equation 3.29. The shock absorber position is taken as the static position corresponding to the aircraft mass dictated by the load case condition.

3.5.3. Internal Load Analysis

The maximum internal loads on individual structural members are calculated using finite element analysis software. Once the model is set up within the software, it allows for efficient evaluation and comparison of complex arrangements that may feature skewed folding axes or statically indeterminate structures. For this research, 3DEXPERIENCE SIMULIA is utilised. As part of the same platform as 3DEXPERIENCE CATIA, it facilitates a smooth transition from design to analysis. Modifications made in the CATIA model can be seamlessly updated in the SIMULIA analysis, saving time and reducing the risk of errors.

The loads are calculated for each load case, determining the maximum shear loads V_x and V_y, axial load N_z, bending moments M_x and M_y, and torque T_z for each structural member, as defined and illustrated in Figure 3.23.

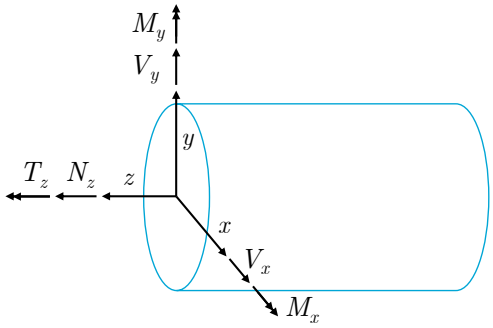

Figure 3.23: Structural analysis load definitions.

Finite element analysis consider member deflections to determine loads in statically indeterminate structures, which inherently depend on member stiffness and, consequently, wall thickness. Iterations are required to make sure that the wall thicknesses of the stick model members match those calculated using the internal loads.

3.5.4. Member Sizing

Member cross-sections need to be sized such that members do not yield when the landing gear is subjected to limit loads, and not fracture when the landing gear is subjected to ultimate loads. Moreover, the safe-life design principle requires that cyclic stresses as a result of normal operating loads do not cause the members to fail due to fatigue during their intended design life.

For each structural member, a critical (sizing) load case is identified, which is the load case that requires the largest wall-thickness to satisfy the design criteria outlined in this section. The wall-thickness, node-to-node member length and material density are then used to determine the minimum mass of each member.

Tube Stress

If the tube wall thickness is much smaller than the tube, typically $t/r \leq 0.1$, the tube may be approximated as a thin-walled tube, simplifying stress calculations. Although this may be the case for large components such as the shock strut cylinder and piston, this criterion is not expected to hold for smaller but major components, such as braces and wheel axles.

General tube stress equations have been derived by Heerens [32]. The maximum normal stress due to combined axial loads and bending moments is calculated using Equation 3.30, where r_o and r_i are the outer and inner tube radii, as illustrated in Figure 3.24. The maximum shear stress due to combined torque and transverse shear is calculated using Equation 3.31, where b is the the effective local cross-section width normal to the respective transverse shear force [39]. For a tube, b = 2t, accounting for both sides of the tube wall.

$$\sigma_{zz} = \frac{N_z}{\pi(r_o^2 - r_i^2)} \pm \frac{4r_o\sqrt{M_x^2 + M_y^2}}{\pi(r_o^4 - r_i^4)} \tag{3.30}$$

$$\tau_{zs} = \frac{2}{\pi(r_o^4 - r_i^4)} \left(T_z r_o \pm \frac{4(r_o^3 - r_i^3)\sqrt{V_x^2 + V_z^2}}{3b} \right) \tag{3.31}$$

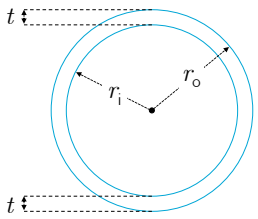

Figure 3.24: Tube definitions.

Substituting σ_{zz} and τ_{zs} into Equation 2.6, the equivalent von Mises stress σ_{Mises} is obtained, which is used for structural sizing.

Design Criteria

Similar to preceding landing gear structural sizing studies, members are sized for minimal mass while subjected to limit loads prescribed by the specified load cases, with a 1.5 safety factor applied to the resulting equivalent von Mises stress (Equation 3.32) [8, 29, 32]. Limit loads describe the maximum load expected during service. Normal operating loads, e.g., the loads relevant to fatigue failure, are lower than the limit loads, practically imposing an additional safety margin. Assuming a linear load-stress relationship [40], and recalling that ultimate loads are limit loads with a 1.5 multiplication factor, adding a 1.5 safety factor ensures that ultimate loads do not cause stress above the material yield strength. The margin between the material yield and ultimate stress limits and the safety factor together add a safety margin to account for nonlinearities, component stress concentrations and fatigue.

$$F.S. = \frac{\sigma_y}{\sigma_{\text{Mises}}} = 1.5 \tag{3.32}$$

For slender members loaded in compression, such as drag and side stays in certain loading conditions, Euler's critical buckling load is evaluated as well. The critical buckling load is calculated using 2.7, using the second area moment I for a tube as defined by Equation 3.33. For members making up the upper strut, it is assumed that the ends are rigidly connected (K = 0.5). All other buckling sensitive members are assumed to have pin-ended supports (K = 1). Members are sized such that the critical buckling load is higher than the axial compressive load in the member. A 1.5 safety factor is applied here as well.

$$I = \frac{\pi}{4}(r_{\mathsf{o}}^4 - r_{\mathsf{i}}^4) \tag{3.33}$$

Machinablity constraints are accounted for by imposing a maximum machinability factor $k \leq 40$, as defined by Equation 3.34 where d_{m} is the mean tube diameter and t is the wall thickness [8].

$$k = \frac{d_{\mathsf{m}}}{t} \tag{3.34}$$

3.6. Landing Gear Analysis

Each landing gear concept is assessed using qualitative and quantitative analyses, such that different concepts can effectively be compared. The landing gear analysis method is outlined in this section.

3.6.1. Quantitative Analysis

Quantitative analyses include the landing gear group mass estimation, stowage volume evaluation, and an estimation of resulting cabin floor height.

Landing Gear Group Mass Estimation

In the context of this research, landing gear group mass is defined as the combined mass of the nose gear and main gear assemblies, excluding the attachment structure. Nose gear mass is estimated using a statistics-based method formulated by Equation 2.30, which is justified given the conventional characteristics of the nose gear as discussed in Section 3.5. Conversely, the main gear mass is estimated using a combination of physics-based structural sizing, empirical equations, and tabulated data.

Main gear mass consists of rolling stock mass, structural mass and controls mass. The combined mass of brakes, wheels and tyres make up the main gear rolling stock mass. Mass of brake assemblies and wheels is estimated using Equation 2.31 and 2.32 respectively, whereas tyre mass is obtained from tyre tables provided by Schmidt [12]. Controls system mass is estimated to be 8% of the total main gear mass [20]. Structural main gear mass includes a contribution of the primary gear structure and a contribution of fittings and miscellaneous components, following the gear mass breakdown outlined in Table 2.10. It is assumed that, similar to the table, fittings and miscellaneous components together always have a 33% contribution to the total structural mass of a single main gear. The primary structure mass is defined by the combined mass of all structural members of a single main gear, as evaluated during structural sizing.

Generally, finite element based mass-estimations are based on simplified geometric shapes that do not consider fillets, detailed manufacturing constraints, material overlap and surface finishings [8, 56]. In this research, the FEM-based mass estimate excludes torque links, locking mechanisms, and internal shock strut mechanisms and components. Only node-to-node member lengths are considered, leading to a further underestimation of the mass. In order to obtain an accurate primary structure mass estimate, the FEM-based mass estimate is corrected using a correction factor f_{c}, which is determined during the mass estimation method calibration in Section 4.4. For landing gear, the FEM to actual (engineering) mass correction factor typically ranges between 1.2 and 1.9 [8]. Equation 3.35 describes the resulting structural mass of a single main gear.

$$m_{\text{mlg structure}} = \frac{f_{\mathsf{c}} m_{\text{FEM}}}{1 - 0.33} = \frac{m_{\text{FEM,corrected}}}{1 - 0.33} \tag{3.35}$$

Stowage Volume

In addition to landing gear group mass, also the stowage volume determined. The stowage volume is evaluated by measuring the width, height, and length, occupied by the retracted landing gear. A smaller volume indicates a more compact stowed gear, and vice versa.

Cabin Floor Height

Lastly, the resulting cabin floor height is evaluated, which naturally depends on the landing gear length. The landing gear design cannot easily be adjusted to have a shorter length, as length is a direct result

of the centre of gravity location and the required ground clearance. However, having insight in cabin floor height allows for an assessment of compatibility with existing ground support equipment. This may incentivise the implementation of special landing gear features such as articulation or kneeling mechanisms to reduce the static cabin floor height, if necessary.

Landing gear length varies slightly depending on the aircraft mass and centre of gravity location. The least favourable condition, e.g., the condition with the largest cabin floor height, is evaluated in this research. For aircraft with a pitch down attitude in static, such as the Flying-V [9], the largest cabin floor height is observed at the aft cabin doors, with the aircraft at operating empty mass and the centre of gravity at the forward limit.

3.6.2. Qualitative Analysis

Many landing gear characteristics are not easily quantifiable, necessitating qualitative analyses to fully understand the feasibility, performance, drawbacks and benefits of each concept. In this research, landing gear complexity, integration, design commonality and level of understanding are assessed.

Complexity and Level of Understanding

Minimising landing gear complexity is crucial, as it significantly impacts reliability, production cost, maintenance cost, and mass [8, 12]. Complexity evaluations are based on engineering judgement, comparing the gear arrangement with existing designs and considering the number of components, such as joints, actuators, and structural members. In addition, the level of understanding of the landing gear concept is assessed. This involves evaluating the similarity of the gear with existing landing gear systems, which can leverage existing knowledge, reduce development time, and ensure proven feasibility. Conversely, if the design significantly deviates from existing systems, it may require more extensive research and development efforts, making the feasibility more uncertain.

Integration

The integration of landing gear is evaluated by examining how well the stowage bay, attachment points, and gear structures integrate with the aircraft. Key considerations include ensuring short load paths and minimising interference with other components. These evaluations rely on engineering judgement.

Risk

CS25.729 requires provisions to ensure that the landing gear can extend when the primary extension mechanism fails [17]. Risk assessments involve a high-level qualitative evaluation of emergency gear extension, which is then compared to existing landing gear systems.

Design Commonality

When the landing gear is designed for a family of aircraft, maximising commonality is desirable to enhance the commercial viability of the aircraft. In this research, design commonality is evaluated from both the aircraft perspective as well as the gear perspective. For aircraft design commonality, it is crucial to ensure that attachment and stowage positions relative to a common reference point or section are consistent. This allows the same stowage bay fairing and attachment structure to be used across different models within the aircraft family. For landing gear design commonality, it is important to ensure that the same landing gear components can be used across various aircraft models. Standardising components simplifies production and maintenance, and reduces costs.

4

Verification, Validation and Calibration

Before the proposed gear design and analysis methods can be utilised to explore and compare various Flying-V landing gear concepts, it is important to ensure that the methods yield feasible and reliable results. This chapter describes the verification and validation of the conceptual landing gear design method, as well as the verification and calibration of the gear mass estimation method.

4.1. General Setup

In this research, method verification involves assessing the correct implementation of the model. During the development phase of the stick model generation algorithm, continuous verification is carried out to immediately address any modelling errors and become familiar with modelling artefacts. Once the model is completed, the model is verified by comparing optimised and non-optimised results to evaluate how the optimiser adjusts the gear to meet limitations set by constraints and design requirements. For the mass estimation method, the structural analysis FEM-model is verified by comparing finite element analysis results with manually calculated results for a simplified structure subjected to simplified loads.

Contrary to verification, validation requires a comparison with actual real-world data to evaluate how results correspond to reality. Because this research explores landing gear concepts for the Flying-V, which in itself is a conceptual aircraft, real-world data cannot be obtained. Consequently, Flying-V gear concepts cannot specifically be validated. However, the methods can be validated for existing aircraft where actual landing gear data is available. Validation of the computed stick model generation method is conducted by comparing gear dimensions and positions with those specified on scaled drawings in airport planning manuals for various existing aircraft. Similarly, the mass estimation method is validated by comparing mass results with actual gear mass data. If results appear to be accurate but not precise, the models can be calibrated to account for this error.

The following reference aircraft are used for verification, validation and calibration in this research:

- **Airbus A350-900**: Used for stick model generation method verification and validation. Specifically selected because its landing gear features a four-wheel bogie [43] and because it is one of the main Flying-V reference aircraft [6].
- **Airbus A350-1000**: Used for stick model generation method verification and validation. Specifically selected because its landing gear features a six-wheel bogie [43] and because it is one of the main Flying-V reference aircraft [22].
- **Airbus A330-300**: Used for stick model generation method verification and validation. Specifically selected because its landing gear features bogie articulation and strut shortening [12].
- **Airbus A310-200**: Used for mass estimation method calibration. Specifically selected because it features a bogie landing gear with gear mass data available in [57].
- **Boeing 707-320**: Used for mass estimation method calibration. Specifically selected because it features a bogie landing gear with gear mass data available in [8].

4.2. Reference Aircraft Gear Design Initialisation

Before verification, validation or calibration can be performed, reference aircraft gear design input data needs to be gathered, formalising the initialisation submodule as discussed in Section 3.2. In this section, the gear design initialisation for aircraft used for gear stick model generation method validation is discussed. The tables in this section present final design input parameters, which result in the gear models presented in Section 4.3 and 4.4. Gear design initialisation data for aircraft used in gear mass validation is included in Appendix C. This data is derived using methods similar to those discussed here.

4.2.1. Reference Aircraft Specifications

For all reference aircraft used to verify, validate and calibrate the methods employed in this research, aircraft specifications are extracted from their respective Aircraft Characteristics for Airport Planning manuals [42, 43, 58, 59]. Dimensions are measured in a standard aircraft design reference frame, with the x-axis positive from nose to tail, and the z-axis pointing upwards, as illustrated in Figure 3.3. The reference frame origin is at the aircraft nose, with z = 0 at the fuselage centreline as illustrated in Figure 4.1.

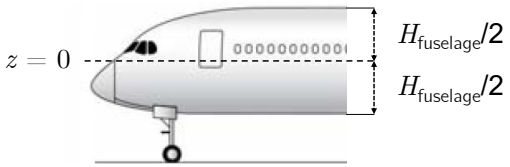

Figure 4.1: Design reference frame, x-axis coincident (y=0, z=0) with fuselage centreline, modified from [43].

Geometry

Geometry specifications for the A350-900, A350-1000 and A330-300 are outlined in Table 4.1.

Table 4.1: Reference aircraft geometry specifications, based on Airport Planning Manuals as discussed in the section text [42, 43].

Item	Unit	Format	A350-900	A350-1000	A330-300
MDS_A	m	(x, y, z)	(30.1, 3.0, -2.1)	(33.9, 3.0, -2.1)	(30.0, 2.8, -2.0)
MDS_B	m	(x, y, z)	(33.3, 3.0, -2.1)	(37.1, 3.0, -2.1)	(-31.3, 2.8, 2.0)
MDS_C	m	(x, y, z)	(33.5, 10.2, -0.5)	(37.3, 10.2, -0.5)	(32.1, 8.7, -0.8)
$x_{\text{mlg,DS}}$	-	$x_{\text{lb}} \leq x_0 \leq x_{\text{ub}}$	$0.0 \leq 0.5 \leq 1.0$	$0.0 \leq 0.5 \leq 1.0$	$0.0 \leq 0.5 \leq 1.0$
$y_{\text{mlg,DS}}$	-	$x_{\text{lb}} \leq x_0 \leq x_{\text{ub}}$	$0.0 \leq 0.5 \leq 1.0$	$0.0 \leq 0.5 \leq 1.0$	$0.0 \leq 0.5 \leq 1.0$
NDS_A	m	(x, y, z)	(1.4, 0.0, -2.5)	(1.4, 0.0, -2.5)	(1.4, 0.0, -1.4)
NDS_B	m	(x, y, z)	(6.4, 0.0, -2.9)	(6.4, 0.0, -2.9)	(7.4, 0.0, -2.5)
$x_{\text{nlg,DS}}$	-	$x_{\text{lb}} \leq x_0 \leq x_{\text{ub}}$	$0.0 \leq 0.5 \leq 1.0$	$0.0 \leq 0.5 \leq 1.0$	$0.0 \leq 0.5 \leq 1.0$
$s_{\text{rs,min}}$	m	-	0.02	0.02	0.02
$s_{\text{cl,min}}$	m	-	0.27	0.27	0.27
$s_{\text{fpb,min}}$	m	-	0.02	0.02	0.02
l_{fpb}	m	-	1.4	1.4	1.4
CCP_1	m	(x, y, z)	(62.9, 0.0, 0.5)	(69.8, 0.0, 0.5)	(61.4, 0.0, 1.3)
CCP_2	m	(x, y, z)	(49.8, 0.0, -2.6)	(56,4, 0.0, -2.5)	(50.6, 0.0, -1.9)
CCP_3	m	(x, y, z)	(44.1, 30.2, 1.4)	(47.9, 30.2, 1.4)	(41.8, 28.8, 1.1)
CCP_4	m	(x, y, z)	(24.8, 10.5, -4.9)	(28.6, 10.5, -4.9)	(23.4, 9.4, -4.5)
$GMCP_1$	m	(x, y, z)	(46.7, -32.4, 3.8)	(50.6, -32.4, 3.8)	(42.2, -30.2, 2.8)
$GMCP_2$	m	(x, y, z)	(0.0, 0.0, -1.4)	(0.0, 0.0, -1.4)	(0.0, 0.0, -0.2)
$GMCP_3$	m	(x, y, z)	(66.8, -9.4, 2.0)	(73.8, -9.4, 2.0)	(63.7, -9.7, 2.4)

Scaled aircraft drawings from Airport Planning manuals [42, 43, 58, 59] are used to estimate suitable main and nose landing gear attachment design space coordinates. For all aircraft, the main gear is attached to a virtual triangle-shaped plane, constrained by the fuselage on the inboard side, and

constrained by assumed rear wing spar and control surface locations on the front and rear side, respectively. The design space has a varying height, parallel to the lower surface of the wing. The nose gear design spaces are defined as straight lines coincident with the aircraft centreline, starting from the front pressure bulkhead, extending five meters aft. Vertically, the line roughly follows the outer mold line of the aircraft, such that nose gear strut length for a given static aircraft attitude can be estimated appropriately. The main and nose gear attachment design spaces are defined as shown by the blue lines in Figure 4.2 for the A350-900, Figure 4.3 for the A350-1000, and Figure 4.4 for the A330-300. Normalised gear positioning parameters x_{mlg}, y_{mlg} and x_{nlg}, have a lower bound equal to 0, an upper bound equal to 1, and an initial guess value of 0.5.

Main gear stowage clearance distances $s_{\text{rs,min}}$ and $s_{\text{cl,min}}$ are derived using the main gear tyre dimensions substituted into the radial tyre clearance equation (Equation 2.27). Similarly, nose gear stowage clearance distance $s_{\text{fpb,min}}$ is derived using the nose gear tyre dimensions substituted in the same equation. A 0.25 m margin is added to the main gear stowage centreline clearance distance $s_{\text{cl,min}}$ to account for the keel beam, allowing for a total keel beam width of 0.50 m. The tyre selection for each reference aircraft is specified in Table 4.5. Tyre dimensions of the tyres used are extracted from tyre tables [12]. The front pressure bulkhead locations l_{fpb}, clearance critical points CCP, and ground manoeuvring critical points GMCP, are estimated from scaled drawings and dimensions stipulated by airport planning manuals. Here, CCP_1 and CCP_2 represent extremes of the aft fuselage section, CCP_3 represents the wing tip (lower surface extreme), and CCP_4 represents the engine nacelle, each indicated by an orange x in Figures 4.2, 4.3 and 4.4. GMCP_1, GMCP_2 and GMCP_3 represent extremes on the wing tip (winglet), nose and horizontal stabiliser, each indicated by a cyan x in Figures 4.2, 4.3 and 4.4.

Mass Properties

Mass properties of the A350-900, A350-1000 and A330-300 are outlined in Table 4.2.

Table 4.2: Reference aircraft mass specifications, based on Airport Planning Manuals as discussed in section text [42, 43].

Item	Unit	Format	A350-900	A350-1000	A330-300
CG_{fwd}	m	(x, y, z)	(30.3, 0.0, -0.8)	(33.9, 0.0, -0.8)	(29.1, 0.0, -0.7)
$\text{CG}_{\text{fwd,\%MAC}}$	% MAC	-	20	20	15
CG_{aft}	m	(x, y, z)	(32.1, 0.0, -0.8)	(35.8, 0.0, -0.8)	(31.0, 0.0, -0.7)
$\text{CG}_{\text{aft,\%MAC}}$	% MAC	-	40	40	40
MRM	kg	-	2.76×10^5	3.17×10^5	2.43×10^5
MTOM	kg	-	2.75×10^5	3.16×10^5	2.42×10^5
MLM	kg	-	2.07×10^5	2.36×10^5	1.87×10^5
OEM	kg	-	1.39×10^5	1.58×10^5	1.25×10^5
$\text{MRM}_{\text{range}}$	-	$(x_{\text{fwd}}, x_{\text{aft}})$	(0.0, 1.0)	(0.0, 1.0)	(0.0, 1.0)
$\text{MTOM}_{\text{range}}$	-	$(x_{\text{fwd}}, x_{\text{aft}})$	(0.0, 1.0)	(0.0, 1.0)	(0.0, 1.0)
$\text{MLM}_{\text{range}}$	-	$(x_{\text{fwd}}, x_{\text{aft}})$	(0.0, 1.0)	(0.0, 1.0)	(0.0, 1.0)

The longitudinal location of the forward and aft centre of gravity limit are derived from the gear locations and forward and aft centre of gravity gear weight distributions as specified in [42, 43, 58, 59]. Although this approach may initially appear to involve circular reasoning, with the centre of gravity later being used to position the landing gear, it is justified in this research context. Using the gear locations to determine the CG limits does not necessarily result in the optimiser placing the gear in the same locations. The optimiser must satisfy several constraints, and multiple gear locations can yield the same weight distribution. Furthermore, the objective of the validation study is to generate a gear stick model for a given CG location, not to estimate the CG locations specifically. A different CG limit naturally leads to a different gear length and location. The centre of gravity limits of the A350-900, A350-1000 and A330-300 are indicated by the red lines in Figures 4.2, 4.3 and 4.4. The forward and aft centre of gravity limits are also expressed relative to the aircraft nose, as well as relative to the mean aerodynamic chord (MAC) using the method outlined in Appendix B.1.1.

The vertical weight distributions of the reference aircraft are assumed to be similar to the weight distribution estimated for the A300-B2, resulting in a similar centre of gravity height. The A300-B2 centre of gravity height is expressed relative to the fuselage centreline, and normalised using the fuselage

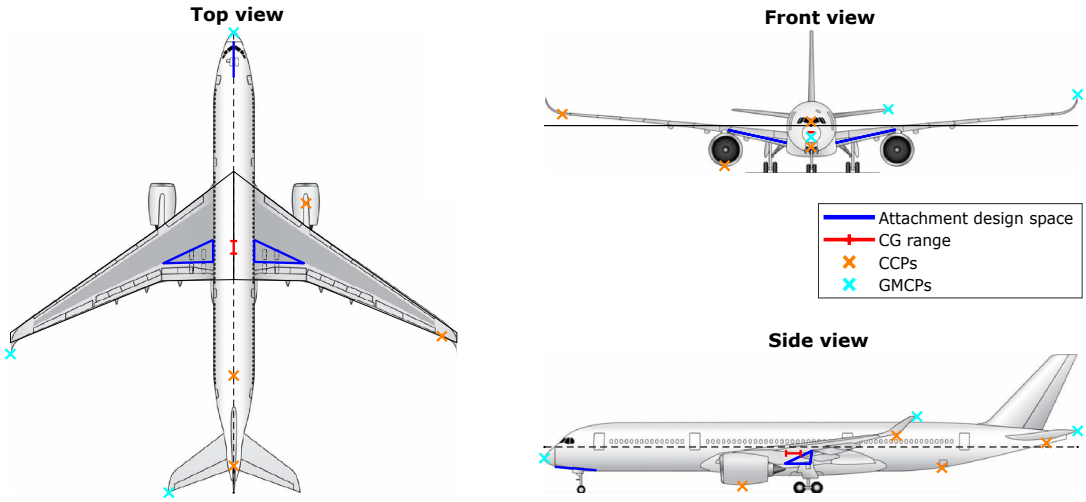

Figure 4.2: A350-900 gear attachment design spaces, critical points, and centre of gravity range. Image modified from [43].

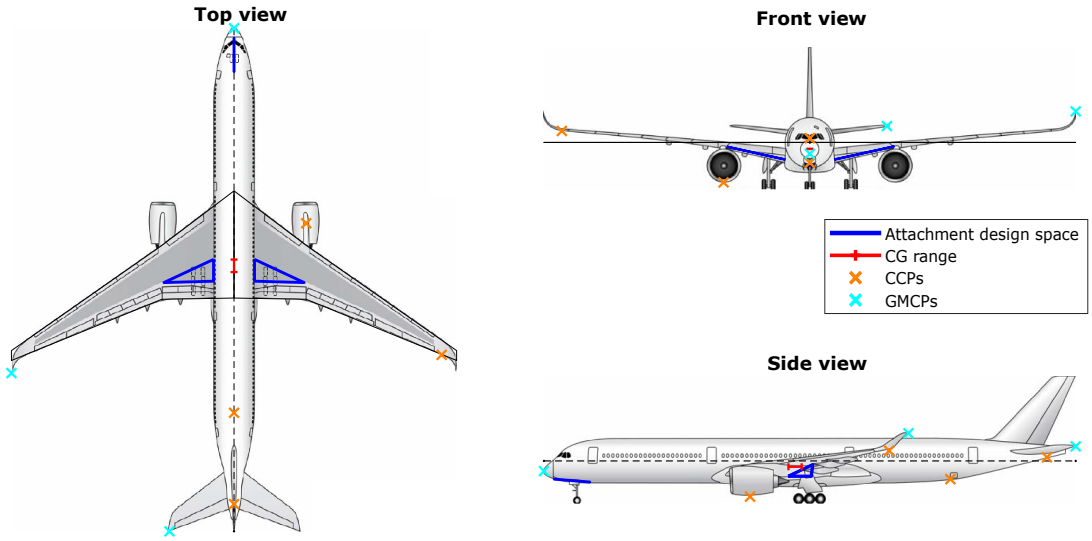

Figure 4.3: A350-1000 gear attachment design spaces, critical points, and centre of gravity range. Image modified from [43].

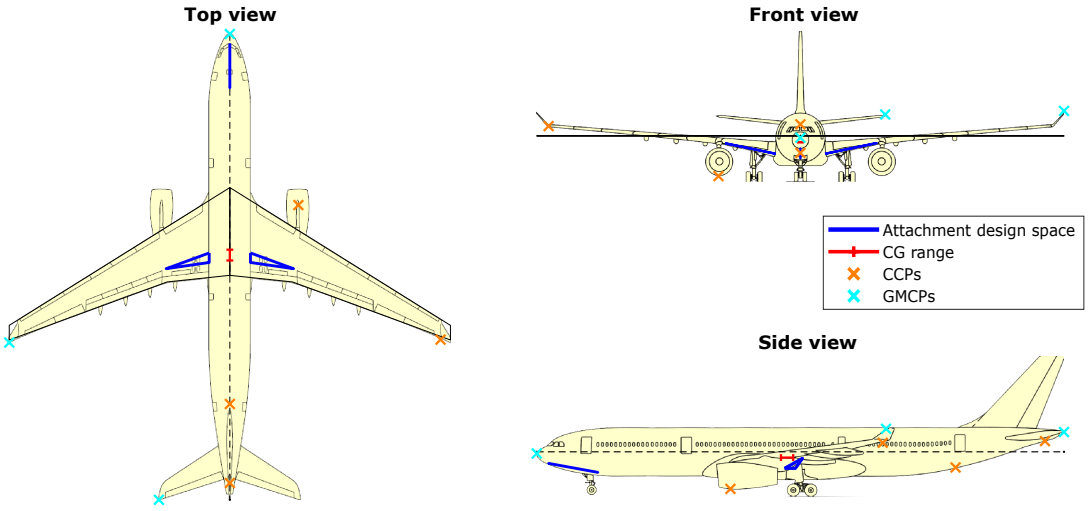

Figure 4.4: A330-300 gear attachment design spaces, critical points, and centre of gravity range. Image modified from [42].

height H_{fuselage}, resulting in z_{CG} = 0.13H_{fuselage}. The derivation can be found in Appendix B.1.2. The lateral location of the centre of gravity is assumed to be at y = 0.

The maximum ramp mass (MRM), maximum take-off mass (MTOM) and maximum landing mass (MLM) are obtained from [42, 43, 58, 59]. Operational empty mass (OEM) highly depends on the specific configuration used by the operator, and is therefore generally not always provided in Aircraft Characteristics for Airport Planning manuals. Estimated OEM values could only be obtained for the A310-200 and the Boeing 707-320 [58, 59]. It is found that for these aircraft, the operational empty mass is typically between 65% and 69% of the maximum landing mass. It is assumed that the A350-900, A350-1000 and A330-300 have an operational empty mass that is 67% of their maximum landing mass. For all reference aircraft, it is assumed that the aircraft can be at MRM, MTOM and MLM throughout the full centre of gravity range, similar to the Airbus A310 [58].

Operational Properties

Operational properties of the Airbus A350-900, A350-1000 and A330-300 are outlined in Table 4.3.

Table 4.3: Reference aircraft operational requirements, based on landing gear background study (Section 2.4) and Airport Planning Manuals, as discussed in section text [42, 43].

Item	Unit	Format	A350-900	A350-1000	A330-300
$\theta_{\text{tpb,min}}$	°	-	15.0	15.0	15.0
$\psi_{\text{tno,max}}$	°	-	63.0	63.0	63.0
ϕ_{max}	°	-	8.0	8.0	8.0
θ_{static}	°	-	-0.2	-0.2	-0.9
$\theta_{\text{max,statSA}}$	°	-	10.0	9.5	10.1
$\theta_{\text{max,extSA}}$	°	-	11.8	11.3	14.2
$\hat{\beta}_{\text{nlg,min}}$	-	$x_{\text{lb}} \leq x_0 \leq x_{\text{ub}}$	$0.04 \leq 0.10 \leq 0.15$	$0.04 \leq 0.10 \leq 0.15$	$0.04 \leq 0.10 \leq 0.15$
$\hat{\beta}_{\text{nlg,max}}$	-	$x_{\text{lb}} \leq x_0 \leq x_{\text{ub}}$	$0.04 \leq 0.10 \leq 0.15$	$0.04 \leq 0.10 \leq 0.15$	$0.04 \leq 0.10 \leq 0.15$
$\beta_{\text{mlg,max}}$	-	-	N.A.	N.A.	N.A.
TDG	-	-	5	6	5
$\lambda_{\text{steering}}$	°	-	72.0	75.0	72.0
V_1	m/s	-	90.0	90.0	90.0

The minimum tipback angle $\theta_{\text{tpb,min}}$ and maximum turnover angle $\psi_{\text{tno,max}}$ are selected as required for stability (Section 2.4.1).

Regardless of the aircraft pitch attitude, the landing gear must permit the aircraft to roll with an angle ϕ_{max} of at least $8°$, as discussed in Section 2.4.3. The static pitch attitudes θ_{static} are derived from Airport Planning manuals [42, 43, 58, 59]. Both the maximum aircraft pitch attitude with a fully compressed shock absorber $\theta_{\text{max,statSA}}$ and the maximum aircraft pitch attitude with a fully extended shock absorber $\theta_{\text{max,extSA}}$ could only be obtained from [60] for the A340-300. Because the A340-300 gear and fuselage are similar to that of the A330-300 [12], it is assumed that the A330-300 has similar maximum pitch attitudes. For the other reference aircraft, $\theta_{\text{max,statSA}}$ is estimated using scaled drawings provided in the Airport Planning manuals, as illustrated in Appendix B.1.3. The maximum pitch attitudes with fully extended shock absorbers on the other hand cannot be derived from the manuals. Instead, it is assumed that the A350-900, A350-1000, A310-200 and Boeing 707-320 have a similar $\Delta\theta_{\text{max}}$ compared to reference aircraft that have maximum pitch attitudes specified in [60]. $\Delta\theta_{\text{max}}$ defines the difference between both maximum pitch attitudes, as specified in Equation 4.1. Naturally, $\Delta\theta_{\text{max}}$ is rather large for the A330-300 as it employs bogie articulation for additional tail clearance [12]. Maximum pitch attitudes are, however, also provided for the A320 (which does not employ bogie articulation), which has $\Delta\theta_{\text{max}}$ equal to $1.8°$ [60]. The A350-900, A350-1000, A310-200 and Boeing 707-320 are assumed to have a $\theta_{\text{max,extSA}}$ that is $1.8°$ larger than $\theta_{\text{max,statSA}}$.

$$\Delta\theta_{\text{max}} = \theta_{\text{max,extSA}} - \theta_{\text{max,statSA}} \tag{4.1}$$

The target minimum and maximum nose gear weight fractions $\hat{\beta}_{\text{nlg,min}}$ and $\hat{\beta}_{\text{nlg,max}}$ are selected as discussed in Section 2.4.3. The maximum steering angle $\lambda_{\text{steering}}$, main gear width (MGW) and cockpit

to main gear distance (CMG) are obtained from [42, 43, 58, 59]. The MGW and CMG are then used to derive the taxiway design group (TDG) from Figure 2.16. The take-off decision speed V_1 is assumed to be equal to that of the A350-1000 for all reference aircraft, and is obtained from de Zoeten [22].

4.2.2. Reference Aircraft Strut and Bogie Concept Selection

Reference aircraft strut and bogie concept specifications are outlined in Table 4.4.

Table 4.4: Reference aircraft strut and bogie concept specifications.

Item	Unit	Format	A350-900	A350-1000	A330-300
Strut	-	-	Concept A	Concept A	Concept A
l_{ss}	m	$x_{lb} \leq x_0 \leq x_{ub}$	1.0 $\leq$ 2.0 $\leq$ 6.0	1.0 $\leq$ 2.0 $\leq$ 6.0	1.0 $\leq$ 2.0 $\leq$ 6.0
$\theta_{ss,ext}$	$^\circ$	$x_{lb} \leq x_0 \leq x_{ub}$	-9.0 $\leq$ -5.0 $\leq$ 0.0	-9.0 $\leq$ -5.0 $\leq$ 0.0	-9.0 $\leq$ -5.0 $\leq$ 0.0
$\theta_{ss,ret}$	$^\circ$	-	0.0	0.0	0.0
$\phi_{ss,ret}$	$^\circ$	-	-80.0	-80.0	-80.0
$\psi_{mlg,ret}$	$^\circ$	$x_{lb} \leq x_0 \leq x_{ub}$	0.0 $\leq$ 0.0 $\leq$ 0.0	0.0 $\leq$ 0.0 $\leq$ 0.0	0.0 $\leq$ 0.0 $\leq$ 0.0
l_{us}	m	-	N.A.	N.A.	N.A.
$\theta_{us,ext}$	$^\circ$	$x_{lb} \leq x_0 \leq x_{ub}$	N.A.	N.A.	N.A.
$\phi_{us,ext}$	$^\circ$	$x_{lb} \leq x_0 \leq x_{ub}$	N.A.	N.A.	N.A.
$\theta_{us,ret}$	$^\circ$	-	N.A.	N.A.	N.A.
$\phi_{us,ret}$	$^\circ$	-	N.A.	N.A.	N.A.
l_{hs}	m	-	N.A.	N.A.	N.A.
θ_{hs}	$^\circ$	-	N.A.	N.A.	N.A.
Bogie	-	-	Concept A	Concept A	Concept A
l_{offset}	m	-	N.A.	N.A.	N.A.
$l_{ineffective}$	m	-	0.45	0.45	0.45
$\theta_{nlg,ret}$	$^\circ$	-	105	105	110

All reference aircraft have a single folding strut (strut concept A) and a regular bogie attachment (bogie concept A). Consequently, all inputs related to the double folding strut, or the offset bogie attachment are not required. The main gear shock strut length l_{ss} must be between 1 and 6 metres long and may be raked at an angle not smaller than -9° and not larger than 0°. The main gear is designed to only retract inward with an angle $\phi_{ss,ret}$ that is suitable for stowage within the aircraft belly fairing. The ineffective piston length $l_{ineffective}$ is estimated from A330-300 bogie attachment drawings, accounting for the bogie connector, torque link connector and piston end stop. The nose gear strut folding angle $\theta_{nlg,ret}$ is selected such that the nose gear folds into the aircraft fuselage entirely.

4.2.3. Reference Aircraft Bogie and Tyre Sizing

Reference aircraft bogie and tyre sizing specifications are outlined in Table 4.5.

Table 4.5: Reference aircraft bogie and tyre sizing specifications.

Item	Unit	Format	A350-900	A350-1000	A330-300
$N_{mlg,w}$	-	-	8	12	8
$N_{mlg,ss}$	-	-	2	2	2
l_{bogie}	m	-	2.04	2.80	1.98
w_{bogie}	m	-	1.74	1.47	1.40
$Tyre_{mlg}$	-	-	1400x530R23 (42 ply)	50x20R22 (34 ply)	1400x530R23 (36 ply)
$N_{nlg,w}$	-	-	2	2	2
w_{nlg}	m	-	0.75	0.75	0.71
$Tyre_{nlg}$	-	-	1050x395R16 (28 ply)	1050x395R16 (28 ply)	1050x395R16 (28 ply)
$a_{x,des}$	m/s^2	-	3.5	3.5	3.5

Bogie and tyre sizing specifications are extracted from Aircraft Characteristics for Airport Planning man-

uals [42, 43, 58, 59]. Specifically, the Airbus A350-900 and A330-300 are equipped with a 4-wheel bogie, while the A350-1000 features a 6-wheel bogie configuration. The design deceleration $a_{x,\text{des}}$ could be derived from [22] for the A350-1000. This deceleration factor is assumed to be similar for the other reference aircraft considered in this study.

4.2.4. Reference Aircraft Shock Absorber Sizing

Reference aircraft shock absorber sizing specifications are outlined in Table 4.6.

Table 4.6: Reference aircraft shock absorber sizing specifications.

Item	Unit	Format	A350-900	A350-1000	A330-300
λ_{mlg}	-	-	1.10	1.10	1.10
$P_{\text{mlg,static}}$	MPa	-	13.8	13.8	13.8
b_{mlg}	-	-	0.10	0.10	0.10
λ_{nlg}	-	-	1.30	1.30	1.30
$P_{\text{nlg,static}}$	MPa	-	13.8	13.8	13.8
b_{nlg}	-	-	0.10	0.10	0.10
s_{Fmax}	-	-	0.30	0.30	0.30

Shock absorber sizing specifications are determined based on the criteria outlined in Section 2.4.3. For all reference aircraft, a main gear reaction factor (λ_{mlg}) of 1.1 is chosen to minimise loads on the gear and aircraft structure. For the nose gear, a reaction factor of 1.3 is selected to minimise the stroke length, thus reducing the extended gear length. A shorter extended gear length reduces the required nose gear stowage volume, allowing the gear to be positioned further forward, thereby decreasing gear loads. All shock absorbers are sized for a static pressure of 2000 psi (13.8 MPa), and a breakout load fraction of 0.10. The vertical load on the landing gear is estimated to be largest at 30% (0.30) of the total vertical axle travel [12].

4.2.5. Reference Aircraft Special Features

Reference aircraft special landing gear feature specifications are outlined in Table 4.7.

Table 4.7: Reference aircraft special landing gear feature specifications.

Item	Unit	Format	A350-900	A350-1000	A330-300
Articulation	-	Boolean	False	False	True
$\lambda_{\text{mlg,art}}$	-	-	N.A.	N.A.	0.38
θ_{bogie}	$^\circ$	$x_{\text{lb}} \leq x_0 \leq x_{\text{ub}}$	N.A.	N.A.	$0.00 \leq 0.00 \leq 25.0$
$l_{\text{x,pivot}}$	m	-	N.A.	N.A.	0.22
$l_{\text{z,pivot}}$	m	-	N.A.	N.A.	0.26
$l_{\text{margin,art}}$	m	-	N.A.	N.A.	0.10
Shortening	-	Boolean	False	False	True
$l_{\text{shortening}}$	m	-	N.A.	N.A.	0.50

Of the reference aircraft considered in this study, only the A330-300 has special landing gear features. It features bogie articulation for additional tail clearance during take-off and landing [12]. The articulated bogie shock absorber reaction factor $\lambda_{\text{mlg,art}}$ is selected such that all wheels are on the ground in the static position at operational empty mass. A 0.1 m 'de-articulation' margin is added to account for ground operations and aircraft mass below the operational empty mass (e.g., manufacturers empty mass). The maximum bogie articulation angle θ_{bogie} measured from the longitudinal aircraft axis is found to be 25°, which is selected as the design variable upper bound [12]. The articulated bogie pivots around a point located 0.2 m behind and 0.2 m above the front wheel axle, as estimated from Schmidt [12].

In addition to the bogie articulation mechanism, the A330-300 is equipped with a strut shortening mechanism. This mechanism not only reduces the required stowage space but also returns the bogie to its

neutral position after articulation by retracting the shock absorber, which further aids in stowage. According to Schmidt [12], the shortening amount $l_{\text{shortening}}$ is nearly as large as the full shock absorber travel. The A330-300 shock absorber travel is calculated to be 0.61 m (Equations 2.13 and 2.15) for the 3.05 m/s limit landing case. Following that, the strut shortening amount is estimated to be 0.50 m.

4.3. Stick Model Generation Verification and Validation

In this section, the stick model generation method verification and validation are discussed. First, the method is verified by comparing optimised and non-optimised gear stick models for the A350-900. After that, gear stick models for the A350-900, A350-1000 and A330-300 are validated using scaled drawings and dimensions from Aircraft Characteristics for Airport Planning manuals. Stick models generated for the A310-200 and Boeing 707-320, which are later used for gear mass validation, are shown in Appendix C.2.

4.3.1. Model Verification

A comparison of non-optimised and optimised reference aircraft gear stick models for the A350-900 is conducted to verify whether the model is capable of adjusting the design vector to obtain a feasible gear stick model. In addition, design vector bound and constraint violations are checked for all reference aircraft considered in this research.

Figure 4.5 illustrates the A350-900 gear stick model generated using initial design vector inputs x_0, as provided by Table 4.8. Figures 4.6 and 4.7 display the A350-900 most critical ground clearance attitudes with shock absorbers in static position. It can directly be concluded from the figures that before optimisation, the gear is too short to provide sufficient ground clearance. Even when the aircraft is in its static position, there is not sufficient ground clearance for the engine nacelles. When the pitch attitude is increased, tail clearance is insufficient as well. Constraint violations are outlined in Table 4.9. It becomes clear that in addition to insufficient ground clearance, the main gear is positioned too far forward to provide a stable platform when braking after push-back. Moreover, the nose gear load is too low for sufficient steering authority, and the wheel track is too wide for the intended taxiway design group.

After optimisation, the gear locations and lengths have been adjusted to not violate the constraints, optimised according to the optimisation objective which can be found in Section 3.3. Figure 4.8 illustrates the optimised Airbus A350-900 gear stick model resulting from the A350-900 design vector provided by Table 4.8. Figures 4.9 and 4.10 illustrate the A350-900 at attitudes most critical for ground clearance. Constraint violations are shown in Table 4.9.

Compared to the gear stick model before optimisation, the longitudinal position of the main gear has been adjusted to meet stability constraints. The gear length is increased, such that the aircraft has sufficient ground clearance for all possible combinations of pitch and roll. Only the ground clearance with static shock absorbers remains critical, as can be seen for the engine nacelle in maximum roll condition illustrated in Figure 4.9, and the tail in maximum pitch condition illustrated in Figure 4.10. Furthermore, the main gear is positioned further inboard. Interestingly, however, the taxiway design group constraint, which stipulates the maximum main gear width, is not active. This could be explained by the shape of the main landing gear attachment design space. Because the design space follows the wing dihedral angle, positioning the gear further inboard allows for a shorter gear strut while maintaining similar tail clearance. Lastly, also the location of the nose gear is adjusted such that it satisfies load and stowage constraints.

The optimiser has found a feasible solution for all reference aircraft considered in this research. Resulting design vectors for the Airbus A350-900, A350-1000 and A330-300 are outlined in Table 4.8, constraint activity is shown in Table 4.9. Similar tables for the A310-200 and Boeing 707-320 can be found in Appendix C.2.

4.3.2. Model Validation

Gear stick models are validated using dimensions and scaled drawings from Aircraft Characteristics for Airport Planning manuals [42, 43, 58, 59]. Validation results for the Airbus A350-900, A350-900 and A330-300 are presented in this Section. Results for the Airbus A310-200 and Boeing 707-320 are

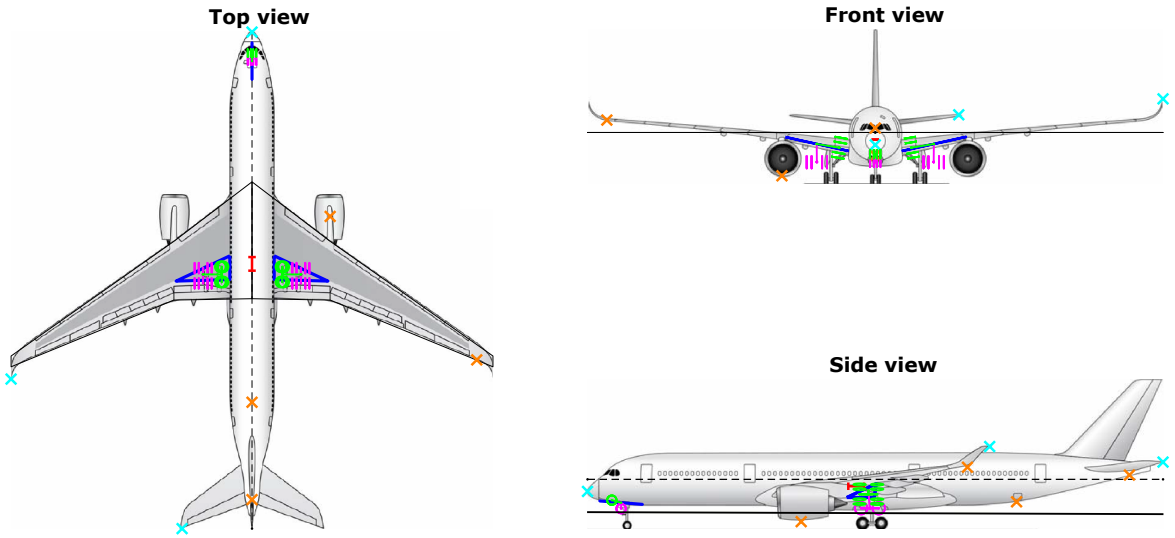

Figure 4.5: Airbus A350-900 gear stick model results before optimisation (x = x_0).

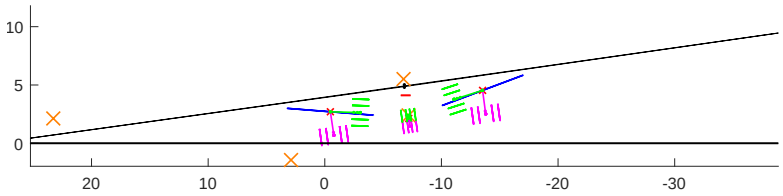

Figure 4.6: Airbus A350-900 front view, critical ground clearance attitude (θ = $-0.2°$, ϕ = $8.0°$), static shock absorber position, before optimisation.

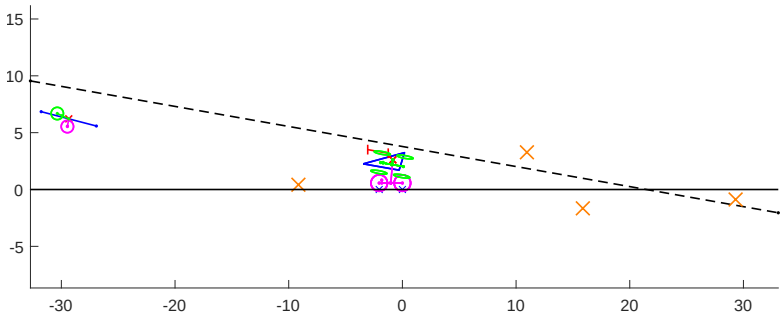

Figure 4.7: Airbus A350-900 side view, critical ground clearance attitude (θ = $10.0°$, ϕ = $0.0°$), static shock absorber position, before optimisation.

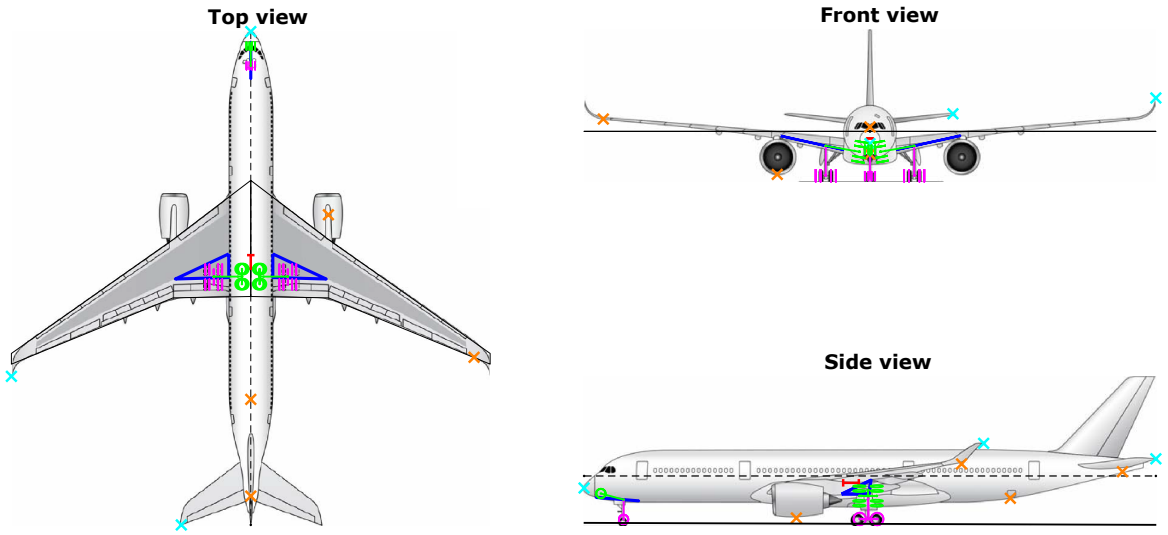

Figure 4.8: A350-900 gear stick model results after optimisation.

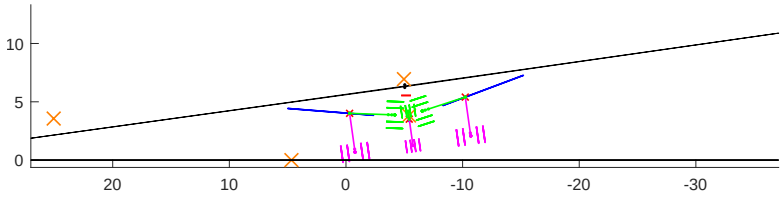

Figure 4.9: A350-900 front view, critical ground clearance attitude (θ = $-0.2°$, ϕ = $8.0°$), static shock absorber position, after optimisation.

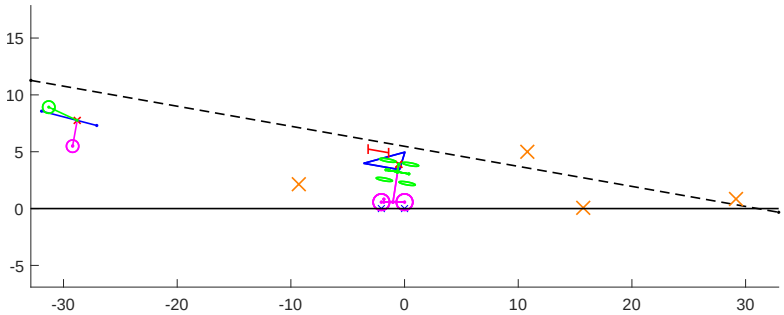

Figure 4.10: A350-900 side view, critical ground clearance attitude (θ = $10.0°$, ϕ = $0.0°$), static shock absorber position, after optimisation.

Table 4.8: Design vector before and after optimisation.

Variable	Unit	x_{lb}	x_0	x_{ub}	A350-900	A350-1000	A330-300
x_{mlg}	-	0.00	0.50	1.00	0.92	0.90	1.00
y_{mlg}	-	0.00	0.50	1.00	0.28	0.30	0.35
x_{nlg}	-	0.00	0.50	1.00	0.65	0.78	0.54
l_{ss}	m	1.50	2.00	8.00	3.31	3.55	3.04
$\theta_{\text{ss,ext}}$	$^\circ$	-9.00	-5.00	0.00	-0.96	-1.32	-9.00
$\psi_{\text{mlg,ret}}$	$^\circ$	0.00	0.00	0.00	0.00	0.00	0.00
$\theta_{\text{us,ext}}$	$^\circ$	0.00	0.00	0.00	N.A.	N.A.	N.A.
$\phi_{\text{us,ext}}$	$^\circ$	0.00	0.00	0.00	N.A.	N.A.	N.A.
θ_{bogie}	$^\circ$	0.00	0.00	25.0	N.A.	N.A.	24.2
$\hat{\beta}_{\text{nlg,min}}$	-	0.040	0.100	0.150	0.040	0.040	0.041
$\hat{\beta}_{\text{nlg,max}}$	-	0.040	0.100	0.150	0.104	0.098	0.108

Table 4.9: Stick model generation constraint activity.

Constraint	Before optimisation	After optimisation		
	A350-900	A350-900	A350-1000	A330-300
Longitudinal stability - minimum nlg load	Violated	Active	Active	Inactive
Longitudinal stability - maximum nlg load	Inactive	Inactive	Inactive	Inactive
Longitudinal stability - rotated tipover	Inactive	Inactive	Inactive	Active
Longitudinal stability - push-back tipover	Violated	Active	Active	Inactive
Lateral stability - lateral turnover	Inactive	Inactive	Inactive	Inactive
Ground clearance - static shock absorber	Violated	Active	Active	Active
Ground clearance - extended shock absorber	Violated	Inactive	Inactive	Active
Airframe integration - nlg stowage	Inactive	Active	Inactive	Active
Airframe integration - mlg stowage	Inactive	Active	Active	Inactive
Ground manoeuvring - taxiway design group	Violated	Inactive	Inactive	Inactive
Ground manoeuvring - 180° turn	Inactive	Inactive	Active	Inactive

provided in Appendix C.2.

Figure 4.8 illustrates the A350-900 stick model on top of scaled aircraft drawings. The two most critical ground clearance attitudes are illustrated in Figures 4.9 (maximum roll, static shock absorber position) and 4.10 (maximum pitch, static shock absorber position). Similar illustrations are provided in Figures 4.11, 4.12 and 4.13 for the A350-1000, and in Figures 4.14, 4.15 and 4.16 for the A330-300. For the latter, an additional ground clearance illustration is provided in Figure 4.17, showing ground clearance while the bogie is articulated. Estimated and actual gear locations along with estimated static and extended gear lengths are outlined in Table 4.10, 4.11 and 4.12 for the A350-900, A350-1000 and A330-300 respectively. Gear lengths are measured from the attachment location to the wheel or bogie axle.

The optimisation model accurately determined the longitudinal location of the main gear for all reference aircraft. Notably, the model estimated a strut rake angle of -9° for the A330-300 (Table 4.8), which matches the actual configuration [12]. Although a rake angle adds length and therefore mass to the gear, the main gear attachment design space for the A330-300 is situated closer to the aft centre of gravity limit compared to other aircraft (Figure 4.4). To satisfy stability constraints, implementing a rake angle was necessary to achieve a feasible solution.

The lateral positions of the main gear, however, show a slight inboard deviation compared to actual data. Looking at the constraint activities in Table 4.9, it appears that for the A350-900 and A350-1000, the main gear is positioned as much inboard as stowage constraints allow. Although positioning the gear further inboard reduces engine nacelle ground clearance in maximum roll condition, normally

necessitating a longer gear, still this results in a shorter gear as caused by the shape of the attachment design space (Section 4.3). The inboard deviation must then be caused by either a too small centreline clearance distance (keel beam), or by an overestimated benefit of positioning the gear further inboard. For the A330-300, the main gear stowage constraint is not active, indicating that the lateral location of the gear is fully determined by ground clearance in maximum roll condition. In this case, the deviation is likely caused by aircraft family design constraints. The A330-300 has the same fuselage and landing gear as the A340-300 [12]. However, the A340-300 features two more engines that are located further outboard, requiring additional roll ground clearance, thereby pushing the gear further outboard.

The estimated longitudinal location of the nose gear shows good agreement with the actual nose gear location for the A350-900, however shows a deviation for both the A350-1000 and A330-300, the latter being most significant. Naturally, the nose gear load percentage is very sensitive to main gear location discrepancies. For the A350-1000, the main gear location is estimated to be slightly ahead of the actual location. Consequently, the minimum nose gear load constraint caused the nose gear to be positioned further aft. Conversely, for the A330-300, the nose gear location is not affected by load constraints. Instead, the optimiser positioned the nose gear as much forward as allowed by stowage constraints. Possibly, more stringent nose gear load or stowage constraints have been used by Airbus when designing the A330.

Actual gear lengths could not be obtained and could therefore not explicitly be validated. It can only be concluded from Figures 4.8, 4.11 and 4.14 that the height of the stick model wheel axles roughly correspond to the wheel axles on the drawing. However, this does not necessarily mean that the gear lengths are similar, as the length is also affected by the lateral attachment location due to the orientation of the attachment design space. The largest lateral attachment location deviation is found for the A330-300, having a deviation of 0.48 m (Table 4.12). With the main gear attachment location becoming 0.20 m higher for every 1.00 m the gear is positioned further outboard (Table 3.1), and assuming that required the aircraft to ground distance remains equal, the gear length would be 0.09 m larger than estimated using the model when positioned at the actual lateral location. For $l_{\text{mlg,static}}$, this results in a 2.9% deviation for the A330-300, which is considered acceptable for the scope of this research.

Noteworthy is the 24.2° bogie articulation angle that has been added by the optimiser to obtain additional extended shock absorber tail clearance for the A330-300 (Table 4.8, illustrated in Figure 4.17). This roughly corresponds to the 25° bogie articulation angle estimated from figures in Schmidt [12].

Table 4.10: A350-900 gear stick model validation

Item	Estimated (m)	Actual (m)	Est/Act (-)
X_{mlg}	33.3	33.3	1.00
Y_{mlg}	5.01	5.30	0.95
$l_{\text{mlg,static}}$	3.35	-	-
$l_{\text{mlg,extended}}$	3.87	-	-
X_{nlg}	4.64	4.63	1.00
$l_{\text{nlg,static}}$	2.30	-	-
$l_{\text{nlg,extended}}$	2.76	-	-

Table 4.11: A350-1000 gear stick model validation

Item	Estimated (m)	Actual (m)	Est/Act (-)
X_{mlg}	37.0	37.1	1.00
Y_{mlg}	5.15	5.37	0.96
$l_{\text{mlg,static}}$	3.59	-	-
$l_{\text{mlg,extended}}$	4.11	-	-
X_{nlg}	5.33	4.63	1.15
$l_{\text{nlg,static}}$	2.39	-	-
$l_{\text{nlg,extended}}$	2.85	-	-

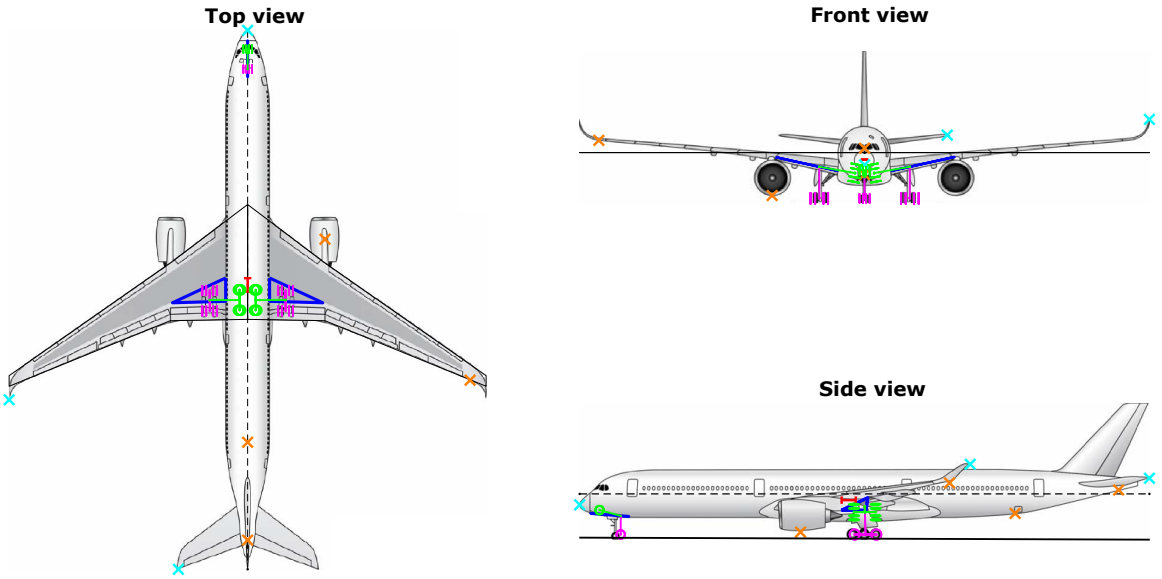

Figure 4.11: A350-1000 gear stick model results after optimisation.

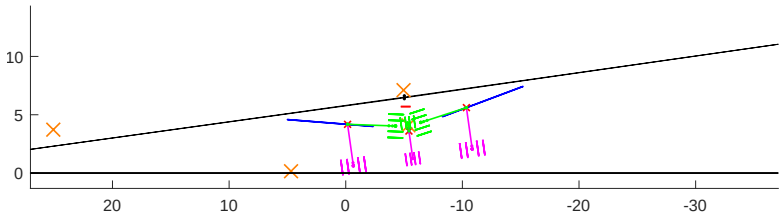

Figure 4.12: A350-1000 front view, critical ground clearance attitude (θ = $-0.2°$, ϕ = $8.0°$), static shock absorber position, after optimisation.

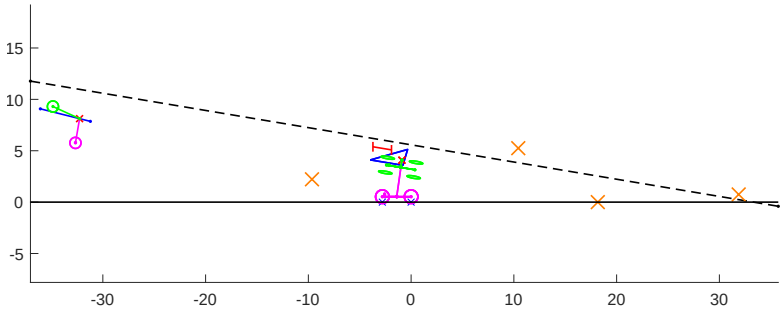

Figure 4.13: A350-1000 side view, critical ground clearance attitude (θ = $9.5°$, ϕ = $0.0°$), static shock absorber position, after optimisation.

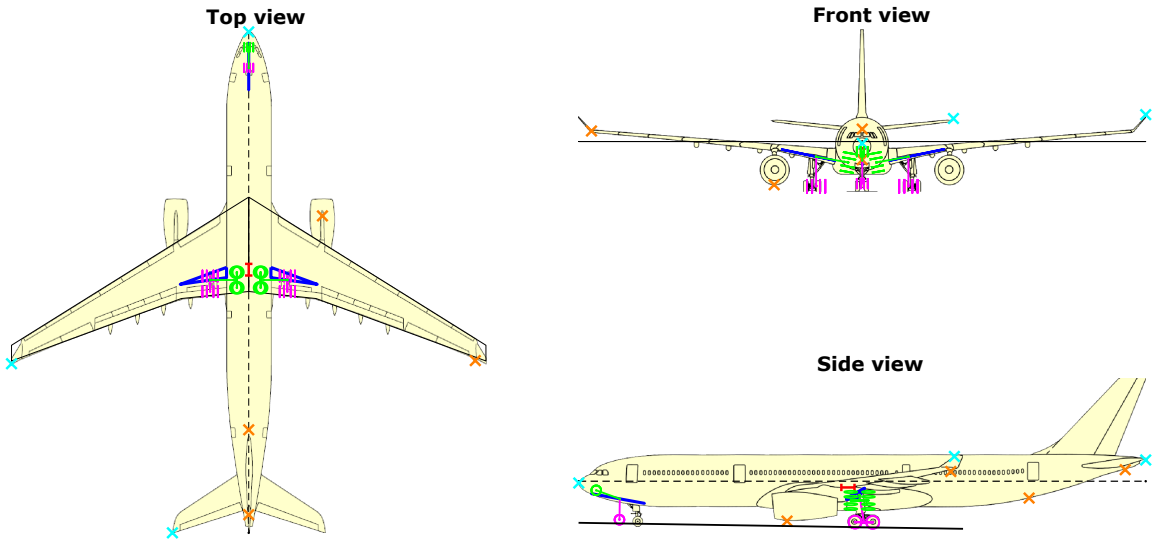

Figure 4.14: A330-300 gear stick model results after optimisation.

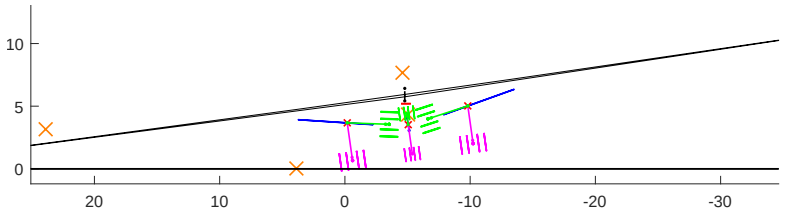

Figure 4.15: A330-300 front view, critical ground clearance attitude (θ = $-0.9°$, ϕ = $8.0°$), static shock absorber position, after optimisation.

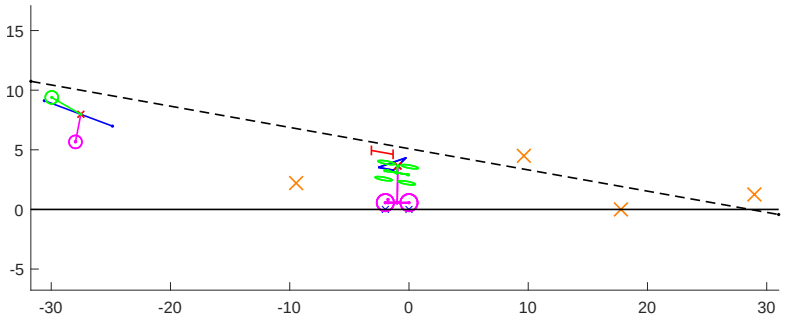

Figure 4.16: A330-300 side view, critical ground clearance attitude (θ = $10.1°$, ϕ = $0.0°$), static shock absorber position, after optimisation.

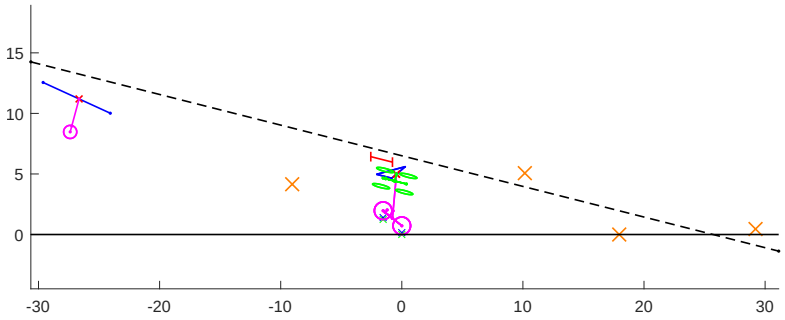

Figure 4.17: A330-300 side view, critical ground clearance attitude (θ = $14.2°$, ϕ = $0.0°$), extended shock absorber position, after optimisation.

Table 4.12: A330-300 gear stick model validation

Item	Estimated (m)	Actual (m)	Est/Act (-)
X_{mlg}	32.1	32.1	1.00
Y_{mlg}	4.86	5.34	0.91
$l_{\text{mlg,static}}$	3.09	-	-
$l_{\text{mlg,extended}}$	3.66	-	-
X_{nlg}	4.64	6.67	0.70
$l_{\text{nlg,static}}$	2.36	-	-
$l_{\text{nlg,extended}}$	2.82	-	-

Figure 4.18 presents the A350-900 gear loading diagram. The shaded grey area represents the maximum expected aircraft mass across the entire centre of gravity range, expressed relative to the nose and mean aerodynamic chord. Blue lines indicate the nose gear load limits, while red lines show the main gear load limits. Both static and dynamic tyre load limits are considered. The diagram indicates that the tyre selection for both the main and nose gear is driven by static load limits. For the main gear, the most critical mass condition logically occurs at the aft centre of gravity limit at maximum ramp mass. Conversely, for the nose gear, the critical mass condition is a result of maximum ramp mass at the forward centre of gravity limit.

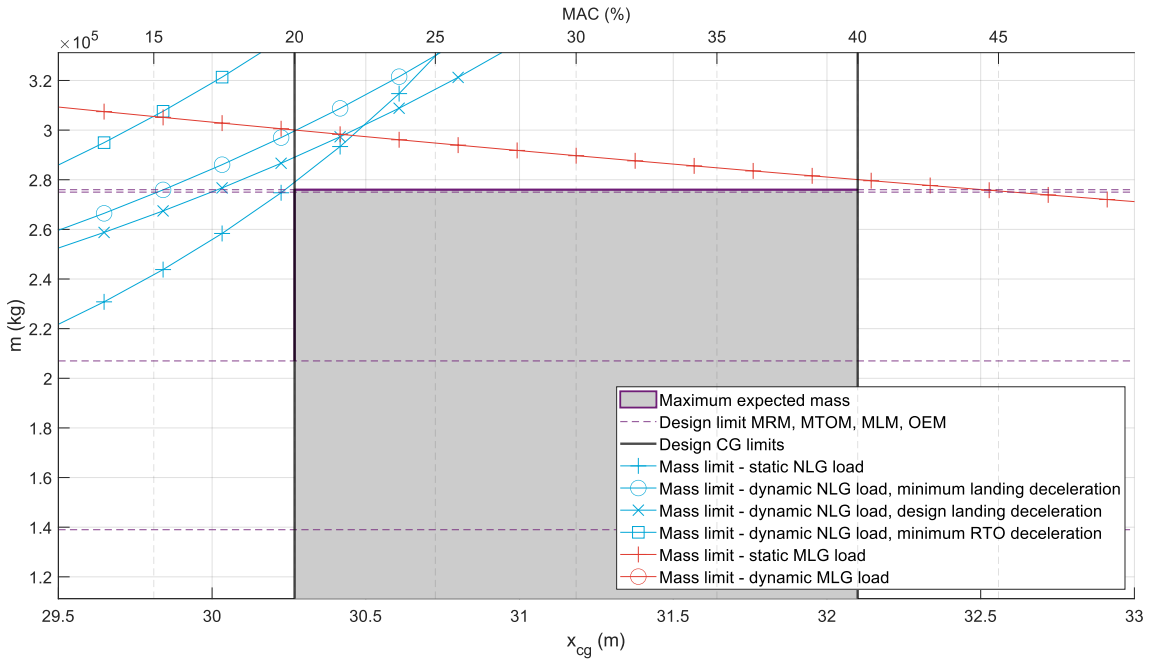

Figure 4.18: A350-900 gear loading diagram.

Figure 4.19 displays the turning radii of the wing tip, tail plane, nose, and landing gear for an A350-900 executing a right turn with a nose gear steering angle of $72°$. Vertical lines indicate the taxiway width and separation distances typically specified for a Code E aircraft. It can be concluded that, given the estimated turn centre location and assuming the aircraft remains on the taxiway centreline, the A350-900 can execute its sharpest turn without the wing tips trespassing the airport design separation distance. This ensures that the wing tip does not collide with any object or aircraft taxiing on a parallel taxiway or taxilane.

Flotation is not specifically evaluated in the validation study. Flotation performance is primarily influenced by the bogie width, length, and tyre pressure, which are directly obtained from Airport Planning Manuals, naturally resulting in consistent flotation.

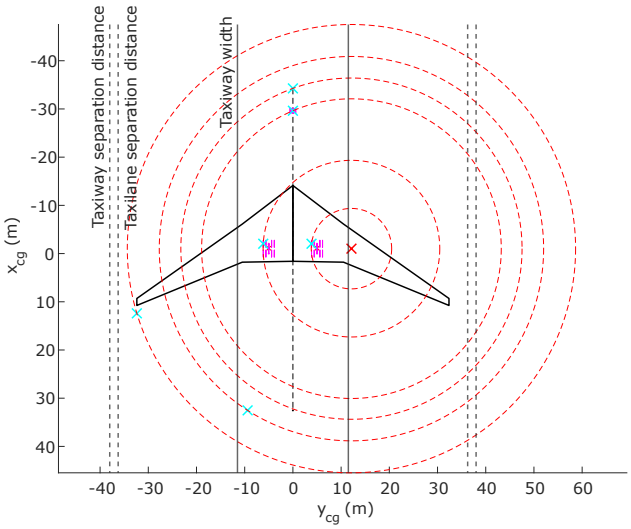

Figure 4.19: A350-900 wing tip, nose, nose gear, tail plane, left main gear and right main gear turning radii for a right turn with maximum nose gear steering angle.

4.4. Mass Estimation

In this section, the verification, validation and calibration of the gear mass estimation method are discussed. First, the finite element model is verified by comparing manual load calculations with loads resulting from the finite element analysis. After that, the gear mass estimation method validation is outlined, including a description of the 3D model generation, structural sizing, and the gear group mass analysis. Lastly, the mass estimation calibration is discussed.

4.4.1. Finite Element Model Verification

Verification is performed to ensure that the finite element model, including geometries, mesh, boundary conditions and loads, is correctly implemented. Figure 4.20 illustrates a generic main landing gear model and a corresponding 1D (stick) model in orange, which is used for finite element model verification in this study. Specifically, the model features a bogie beam with four wheels, a shock strut cylinder, a shock strut piston, a trunnion, a drag brace and a side brace.

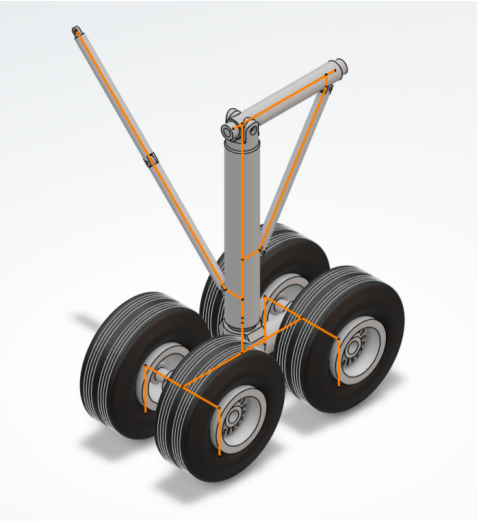

Figure 4.20: Generic gear 3D model and 1D finite element model (in orange) for verification and validation, isometric view.

In the verification experiment, the landing gear stick model is subjected to two different verification load cases. Internal forces and moments in the bogie beam, shock strut and drag brace are evaluated using

both analytical calculations and finite element analysis. The stick model nodes are defined as illustrated in Figure 4.21. Node coordinates and type specifications relevant to the analysis of the bogie beam (KL), shock strut (OC) and drag brace (HG) are shown in Table 4.13. Coordinates are measured from the stick model origin (O) following the reference frame depicted in the figure. The shock absorber is considered to be in the static position. Node type specifications describe beam to beam interactions, and are described in detail in Section 3.5. Table C.12 in Appendix C.3 provides a full overview of all verification gear model node coordinates and type specifications.

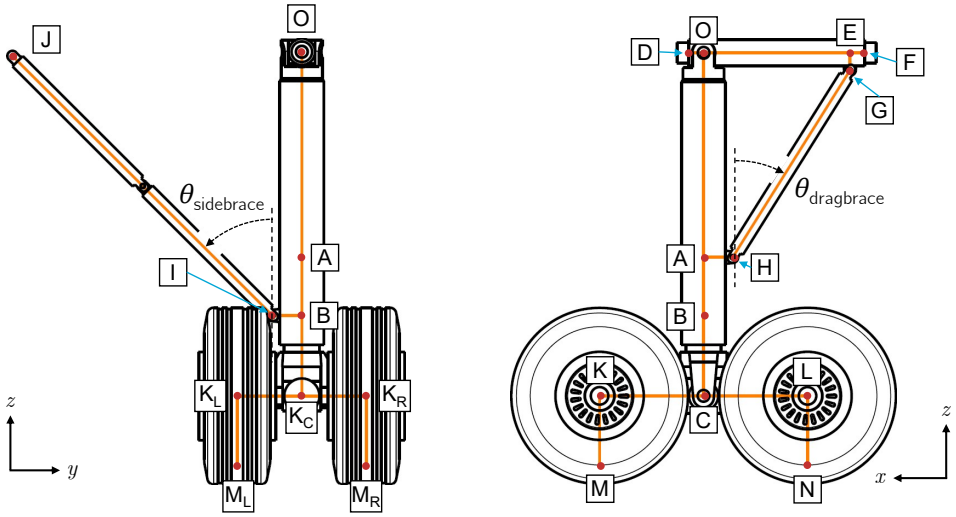

(a) Right main landing gear back view. **(b)** Right main landing gear side view.

Figure 4.21: Generic gear model node definitions.

Table 4.13: Generic gear model node specifications.

Node	x (m)	y (m)	z (m)	Type
O	0.00	0.00	0.00	Hinge
A	0.00	0.00	-1.40	Beam
C	0.00	0.00	-2.35	Hinge
D	0.10	0.00	0.00	-
E	1.00	0.00	0.00	Beam
F	1.10	0.00	0.00	-
G	1.00	0.00	-0.12	Hinge
H	0.20	0.00	-1.40	Hinge
K_C	0.71	0	-2.35	Beam
L_C	-0.71	0	-2.35	Beam

Boundary conditions are defined as shown in Table 4.14. Trunnion nodes D, F and side brace node J are all subjected to a zero translation boundary condition. Node D and F may only rotate around a local z-axis, which is aligned with the longitudinal axis of the trunnion as illustrated in Figure 4.22a. Similarly, node J may only rotate around a local x-axis, which is defined by the hinge axis as shown in Figure 4.22b. Loads are applied to either side of the bogie beam, represented by node K_C and L_C. The first load case exposes the nodes to a vertical load of 100 kN. In the second load case, this vertical load is combined with a drag load of 50 kN. The load cases are defined as shown in Table 4.15, with F_x, F_y and F_z in the directions as illustrated in Figure 4.22c. Load directions are always aligned with the earth reference frame, such that F_z is always perpendicular to the ground, irrespective of the bogie orientation.

Table 4.16 shows maximum internal loads in the bogie beam, shock strut and drag brace loads resulting from verification case 1. Similarly, verification case 2 results are shown in Table 4.17. Internal loads

Table 4.14: Generic gear model boundary conditions.

Node	δ_x (m)	δ_y (m)	δ_z (m)	θ_x	θ_y	θ_z
D	Fixed	Fixed	Fixed	Fixed	Fixed	Free
F	Fixed	Fixed	Fixed	Fixed	Fixed	Free
J	Fixed	Fixed	Fixed	Free	Fixed	Fixed

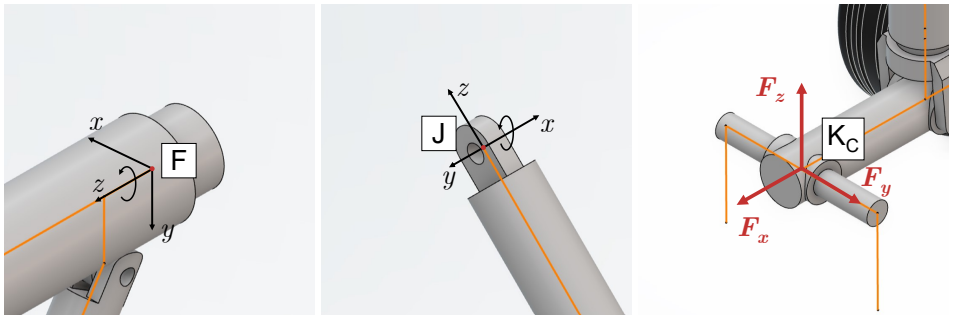

(a) Trunnion (node D and F) boundary condition.

(b) Side brace (node J) boundary condition.

(c) Bogie beam (node K_C) load condition.

Figure 4.22: Generic gear model boundary condition and load definitions.

Table 4.15: Verification load case definitions.

Load case	Node	F_x (N)	F_y (N)	F_z (N)
Verification 1	K_C	0.00	0.00	1.00×10^5
	L_C	0.00	0.00	1.00×10^5
Verification 2	K_C	0.00	5.00×10^4	1.00×10^5
	L_C	0.00	5.00×10^4	1.00×10^4

are defined as illustrated in Figure 3.23. Free body diagrams and derivations used for the analytical calculations can be found in Appendix C.3.

Table 4.16: Finite element model verification case 1 maximum internal load results.

	Bogie beam (KL)		Shock strut (OC)		Drag brace (GH)	
Load	Analytical	FEM	Analytical	FEM	Analytical	FEM
V_x (N)	0.00	0.00	0.00	5.00	0.00	5.00
V_y (N)	1.00×10^5	1.00×10^5	0.00	-81.0	0.00	0.00
N_z (N)	0.00	0.00	-2.00×10^5	-2.00×10^5	0.00	-136
M_x (Nm)	7.10×10^4	7.10×10^4	0.00	-22.0	0.00	0.00
M_y (Nm)	0.00	0.00	0.00	3.67	0.00	5.40
T_z (Nm)	0.00	0.00	0.00	-76.2	0.00	1.71

Table 4.17: Finite element model verification case 2 maximum internal load results.

	Bogie beam (KL)		Shock strut (OC)		Drag brace (GH)	
Load	Analytical	FEM	Analytical	FEM	Analytical	FEM
V_x (N)	0.00	0.00	5.00×10^4	5.00×10^4	0.00	-2.87
V_y (N)	1.00×10^5	1.00×10^5	0.00	-2.87	0.00	0.00
N_z (N)	2.50×10^4	2.50×10^4	-3.09×10^5	-3.09×10^5	1.29×10^5	1.28×10^5
M_x (Nm)	7.10×10^4	7.10×10^4	0.00	2.10	0.00	0.00
M_y (Nm)	0.00	0.00	-4.75×10^4	-4.75×10^4	0.00	3.10
T_z (Nm)	0.00	0.00	0.00	-43.8	0.00	0.98

Comparing the results, it can be concluded that loads calculated using finite element methods are similar to the loads calculated manually. Results for the bogie beam align perfectly. Discrepancies are noticeable for the shock strut and drag brace. These can be attributed to the fact that FEM incorporates the impact of structural deformations, which have been assumed negligible in the analytical calculations. The compressive strain experienced by the shock strut induces compression in both the side brace and drag brace, consequently introducing shear forces and bending moments into the strut. Crucially, load analysis results depend on the deflections, which in its turn depend on the selected cross-sectional properties of the stick model members determined during structural sizing. Therefore, iterative processes are imperative to achieve convergence and ensure that the analysis reflects the true behaviour of the structure.

4.4.2. Mass Estimation Validation

The mass estimation method is validated by comparing the landing gear mass data of the Airbus A310-200 and Boeing 707-320 with the mass derived using the conceptual landing gear design methodology proposed in this research. Gear stick models are generated for both aircraft, and can be found in Appendix C.2. Prior to structural sizing, these stick models must be refined with secondary supports, such as the drag brace and side brace. Additionally, initial estimates of structural member dimensions are required to evaluate structural deformations and loads. For both validation aircraft, the dimensions and positions of the trunnion, drag brace, and side brace were estimated from drawings provided by Currey [20]. These estimations are illustrated in Figures C.9 and C.11 in Appendix C.4.

Figure 4.23a shows the A310-200 right main landing gear refined using computer aided design (CAD) software. Similarly, the CAD model of the right main landing gear of the Boeing 707-320 is shown in Figure 4.23b. Node definitions and coordinates for both models can be found in Appendix C.4.

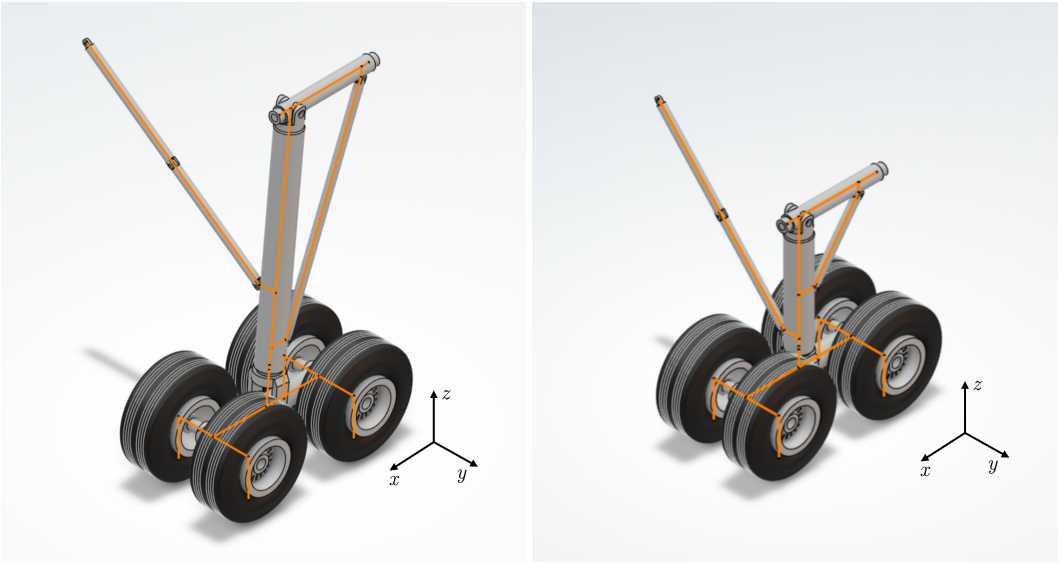

(a) A310-200 right main landing gear 3D model and stick model in orange.

(b) Boeing 707-320 right main landing gear 3D model and stick model in orange.

Figure 4.23: Reference aircraft 3D gear models and 1D finite element models.

Structural Sizing

Now the support structures are added, and initial estimates of cross-sectional dimensions are provided, structural sizing needs to be performed such that the structural mass can be estimated. The right main landing gear of the A310-200 and Boeing 707-320 are subjected to the load cases outlined in Table 2.2. A detailed overview of external loads associated with each load case can be found in Tables C.15 and C.17 in Appendix C.4. Additionally, calculated internal loads corresponding to the the most critical load case for each structural member are outlined Tables C.16 and C.18 in the same appendix. For illustrative purposes, Figure 4.24a shows the internal force F_y in the bogie beam of the A310-200 for the level landing load case with spin-up loads. Similarly, Figure 4.24b illustrates the internal moment

magnitude in the full 1D gear model. Iterations have been performed to ensure that the load results are sufficiently converged.

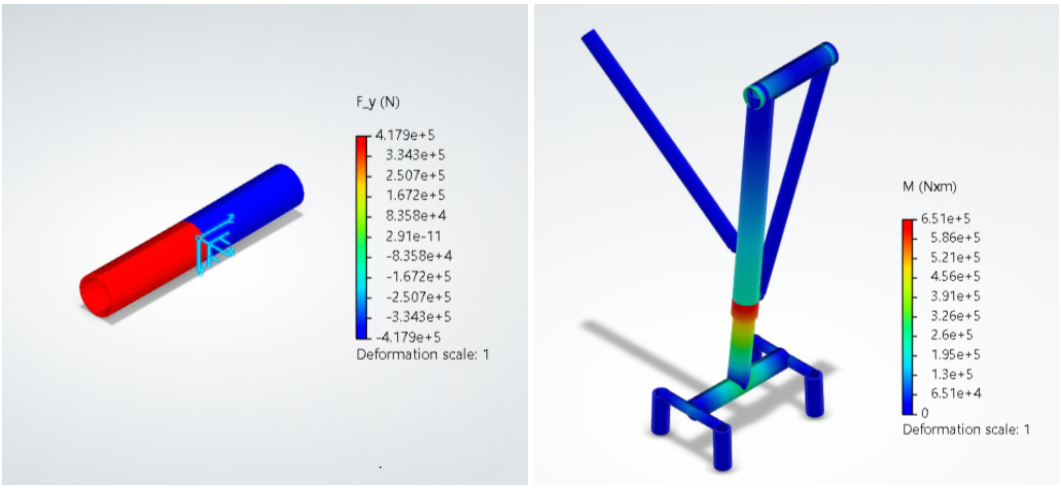

(a) Trunnion shear loads. **(b)** Full model bending moments.

Figure 4.24: Internal loads (illustrative purposes only).

The resulting structural dimensions and mass are presented in Table 4.18 for the A310-200 and in Table 4.19 for the Boeing 707-320. The inner and outer radii are denoted by r_i and r_o. Dimensions shown in bold are fixed, based on either the piston diameter or wheel rim diameter, as described in Section 3.5. The section thickness, cross-sectional area, and stick model member mass are given by t, A and m respectively.

Table 4.18: A310-200 right main landing gear structural member sizing.

Member	l (m)	r_i (m)	r_o	t (m)	A (m^2)	m (kg)
Trunnion	1.250	0.1104	**0.1240**	0.0136	0.0100	97.9
Cylinder	2.818	**0.1240**	0.1389	0.0149	0.0123	271.4
Piston	1.197[1]	0.1100	**0.1240**	0.0140	0.0103	96.6
Bogie beam	1.397	0.0923	**0.1054**	0.0131	0.0079	86.0
Wheel axle (2x)	0.927	0.0508	**0.0640**	0.0132	0.0048	34.6
Drag brace	2.664	0.0711	**0.0850**	0.0079	0.0040	84.3
Side brace	2.800	0.0809	**0.0850**	0.0041	0.0022	48.2
Total	-	-	-	-	-	754

[1] Extended length plus a margin of 2.75 times the respective piston diameter (Section 3.4.2).

Table 4.19: Boeing 707-320 right main landing gear structural member sizing.

Member	l (m)	r_i (m)	r_o (m)	t (m)	A (m^2)	m (kg)
Trunnion	1.200	0.1176	**0.1270**	0.0094	0.0072	67.7
Cylinder	1.520	**0.1270**	0.1417	0.0147	0.0124	147.6
Piston	1.230[1]	0.1167	**0.1270**	0.0103	0.0079	76.1
Bogie beam	1.420	0.0879	**0.1016**	0.0137	0.0082	91.2
Wheel axle (2x)	0.880	0.0511	**0.0640**	0.0129	0.0047	32.4
Drag brace	1.000	0.0585	**0.0635**	0.0050	0.0019	14.9
Side brace	2.502	0.0592	**0.0635**	0.0043	0.0017	33.3
Total	-	-	-	-	-	496

[1] Extended length plus a margin of 2.75 times the respective piston diameter (Section 3.4.2).

Gear Group Mass Analysis

Landing gear group mass is estimated following the methodology outlined in Section 3.6 and is validated using actual gear mass data obtained from literature.

Main landing gear structural mass breakdowns are shown in Table 4.20. The primary structure mass represents uncorrected FEM-based mass estimates based on structural member sizing results outlined in Table 4.18 and 4.19. Total structural mass is estimated using an assumed constant relative contribution of fittings and miscellaneous components of 33%, derived from the typical gear mass breakdown shown in Table 2.10. Please note that the mass presented in Table 4.20 applies to a single main landing gear.

Table 4.20: Validation aircraft main landing gear structural mass estimations.

Structural mass	Share	A310-200	B707-320
Primary structure	0.67	754	496
Fittings and misc. components	0.33	365	240
Total	1.00	1119	736

Group mass validation results are shown in Table 4.21 for the A310-200, and in Table 4.22 for the Boeing 707-320. The actual gear group mass of the A310-200 is 6110 kg [57], whereas the actual gear group mass of the Boeing 707-320 is 5087 kg [8]. For the Boeing 707-320, actual mass contributions of the nose gear, main gear rolling stock, structure and controls are derived using the Boeing 707-320 gear mass breakdown shown in Table 2.10. A similar mass breakdown could not be obtained for the A310-200, with only the total main gear mass (2710 kg each) and total nose gear mass (690 kg) specifically available. However, looking at the differences between both aircraft, it appears that both aircraft have a similar maximum take-off mass [58, 59], and that both aircraft have a similar four-wheel bogie configuration with similar dimensions. Only the gear of the A310-200 is taller than the gear of the Boeing 707-320 to facilitate the larger engine bypass ratio and associated fan diameter. It is therefore assumed that the absolute mass contribution of the rolling stock of the A310-200 is equal to that of the Boeing 707-320. A310-200 main gear controls are estimated to take up 8% of the total main gear mass [20]. Further differences in main gear mass between both aircraft are fully attributed to the structure.

Table 4.21: A310-200 landing gear group mass validation.

Item	Estimated (kg)	Actual (kg)	Est/Act (-)
Main gear (each)	2187	2710	0.81
Rolling stock	896	890	1.00
Structure	1119	1603	0.70
Controls	172	217	0.79
Nose gear	588	690	0.85
Total (% MTOM)	4.96×10^3 (3.49)	6.11×10^3 (4.30)	0.82

Table 4.22: Boeing 707-320 landing gear group mass validation.

Item	Estimated (kg)	Actual (kg)	Est/Act (-)
Main gear (each)	1900	2340	0.81
Rolling stock	884	890	0.99
Structure	736	1170	0.63
Controls	220	280	0.79
Nose gear	463	407	1.14
Total (% MTOM)	4.26×10^3 (3.00)	5.09×10^3 (3.58)	0.85

It can be concluded from Tables 4.21 and 4.22 that statistics-based rolling stock mass estimations can reliably be used. As expected, estimated structural mass, which is directly proportional to the FEM-based primary structure mass estimate, underestimates the actual structural mass as discussed in Section 3.6. The error aligns with typical FEM to actual mass correction factors [8, 56]. Interestingly,

the deviation is larger for the Boeing 707-320 than it is for the A310-200. This can be explained by the Boeing 707-320 having a much shorter gear (Appendix C.4), leading to a larger relative contribution of torque links and locking mechanisms, which have not been considered in the structural analysis. In addition, only node to node member lengths were considered, which inherently has a larger relative impact on the mass estimate if members are shorter. Naturally, estimated control mass deviates from actual mass, as it is directly derived using the total main gear mass, and is therefore affected by the structural mass estimate. Nose gear mass is underestimated for the A310-200, and overestimated for the Boeing 707-320. Nose gear mass is estimated using Equation 2.30, which considers nose gear strut length. Looking at the A310-200 gear stick model results in Figure C.3, it is found that the nose gear is positioned further aft than the scaled aircraft drawing suggests, leading to a shorter nose gear strut, lowering the mass estimate. Similarly, for the B707-320, the nose gear is positioned further forward than suggested by the drawing (Figure C.4), leading to a longer gear strut and consequently, a higher mass.

4.4.3. Mass Estimation Calibration

Using the estimated and actual primary structure mass (67% of main gear structural mass, Section 3.6), mass correction factors f_c can be determined, as shown in Table 4.23. Linear regression is used to derive a general equation for the correction factor. The extended strut length $l_{\text{mlg,ext}}$ is selected as independent variable to account for the reduction in relative contributions of torque links and locking mechanisms as the strut length increases. It is assumed that the Airbus A310-200 and Boeing 707-320 main gear primary structure mass estimates are sufficiently representative.

Table 4.23: Primary structure mass correction factors.

	Primary structure (kg)			
Aircraft	Estimated	Actual	f_c (-)	$l_{\text{mlg,ext}}$ (m)
A310-200	754	1080	1.43	3.80
Boeing 707-320	496	789	1.59	2.31

The primary structure mass correction factor can be calculated using Equation 4.2.

$$f_c = 1.84 - 0.107 l_{\text{mlg,ext}} \tag{4.2}$$

Corrected landing gear group mass estimations are shown in Table 4.24 and 4.25.

Table 4.24: Corrected A310-200 landing gear group mass.

Item	Corrected (kg)	Actual (kg)	Est/Act (-)
Main gear (each)	2716	2710	1.00
Rolling stock	896	890	1.00
Structure	1603	1603	1.00
Controls	217	217	1.00
Nose gear	588	690	0.85
Total (% MTOM)	6.02×10^3 (4.24)	6.11×10^3 (4.30)	0.97

Table 4.25: Corrected Boeing 707-320 landing gear group mass.

Item	Corrected (kg)	Actual (kg)	Est/Act (-)
Main gear (each)	2334	2340	1.00
Rolling stock	884	890	0.99
Structure	1170	1170	1.00
Controls	280	280	1.00
Nose gear	463	407	1.14
Total (% MTOM)	5.13×10^3 (3.61)	5.09×10^3 (3.58)	1.01

5

Flying-V Implementation

In this chapter, the conceptual design method implementation is discussed. First, the Flying-V family baseline gear concept is formulated. After that, the gear design initialisation is discussed, followed by the baseline gear design. Finally, variations to the baseline concept are developed as discussed in Section 3.1.

5.1. Baseline Gear Concept Formulation

Based on previous research, it is concluded that the Flying-V requires a long and heavy landing gear due to its high sweep angle wing and stringent landing and take-off clearance angle requirements [9, 22]. In addition, the Flying-V is significantly limited in stowage volume availability [10]. Lacking a suitable stowage area within the fuselage, the retracted landing gear must be contained within fairings, which need to be as compact as possible to maximise aerodynamic performance. Moreover, landing gear stowage conflicts with fuel tank capacity, which is limited already. Lastly, maximising commonality between different Flying-V family members is essential for enhancing commercial viability.

A baseline Flying-V family landing gear is formulated, defining the basis for further comparison. The baseline concept design principles apply to all family members, and are defined as follows:

- The gear design facilitates maximum aircraft and gear design commonality between the Flying-V family members.
- The gear features a double folding strut to increase stowed compactness.
- The gear incorporates two skewed folding axes to achieve an aerodynamically efficient stowed position and feasible retraction path.
- The gear includes a mechanism that folds the bogie parallel to the strut when retracted, allowing for more efficient stowage.
- The shock strut features a shortening mechanism to increase stowed position compactness.
- The bogie and wheels retract forward with respect to the attachment position, such that drag loads do not oppose gear extension. This is beneficial for compliance with emergency requirements and actuator sizing.
- The gear features a four-wheel bogie configuration, similar to the Airbus A330 and A350-900. This ensures similar airport compatibility.

The baseline landing gear is sized and positioned based on the the requirements of the FV-1000 for all family members. Consequently, each landing gear shares the same structural components and attachment structure. The FV-800 and FV-900 landing gear only differ from that of the FV-1000 in the absence of a bogie articulation mechanism. The FV-1000 features a bogie articulation mechanism to increase ground clearance during landing and take-off, effectively reducing gear length and stowage requirements at the expense of adding complexity. Because the FV-800 and FV-900 require less ground clearance, including an articulation mechanism is not justified for those aircraft. For all aircraft, the amount of strut shortening is adjusted to achieve the same bogie position relative to the airframe attachment when retracted, allowing for a common fairing design. This aligns with the common family section philosophy presented by Oosterom [10]. Rolling stock is sized for each aircraft individually.

5.2. Gear Design Initialisation

This section outlines the Flying-V gear design initialisation, presenting the final stick model generation inputs which have been adjusted to obtain a feasible gear. For all family members, this results in the baseline designs as presented in Section 5.3.

5.2.1. Flying-V Aircraft Specifications

Landing gear design inputs related to the Flying-V geometry, mass and operational properties are presented and discussed in this section. For all Flying-V family members, dimensions were extracted from the Flying-V - Version 1 3DEXPERIENCE CATIA model, which is described by Jorge [61]. Dimensions were measured in a standard aircraft design reference frame, with the x-axis positive from nose to tail, and the z-axis pointing upwards, as illustrated in Figure 3.3. The reference frame origin coincides with the aircraft planform nose as defined in the CATIA model.

Geometry

Table 5.1 outlines FV-1000, FV-800 and FV-900 geometry specifications.

Table 5.1: Flying-V geometry specifications [61].

Item	Unit	Format	FV-1000	FV-800	FV-900
MDS_A	m	(x, y, z)	(29.2, 3.17, -0.25)	(23.8, 0.62, -0.25)	(26.7, 1.99, -0.25)
MDS_B	m	(x, y, z)	(33.2, 5.10, -0.25)	(27.8, 2.54, -0.25)	(30.7, 3.92, -0.25)
MDS_C	m	(x, y, z)	(29.2, 6.32, -0.25)	(23.8, 3.77, -0.25)	(26.7, 5.15, -0.25)
MDS_D	m	(x, y, z)	(33.2, 8.25, -0.25)	(27.8, 5.70. -0.25)	(-30.7, 7.07, -0.25)
$x_{mlg,DS}$	-	$x_{lb} \leq x_0 \leq x_{ub}$	$0.0 \leq 0.5 \leq 1.0$	$0.0 \leq 0.5 \leq 1.0$	$0.0 \leq 0.5 \leq 1.0$
$y_{mlg,DS}$	-	$x_{lb} \leq x_0 \leq x_{ub}$	$0.0 \leq 0.5 \leq 1.0$	$0.0 \leq 0.5 \leq 1.0$	$0.0 \leq 0.5 \leq 1.0$
NDS_A	m	(x, y, z)	(3.0, 0.0, -1.2)	(3.0, 0.0, -1.2)	(3.0, 0.0, -1.2)
NDS_B	m	(x, y, z)	(9.0, 0.0, -1.6)	(9.0, 0.0, -1.6)	(9.0, 0.0, -1.6)
$x_{nlg,DS}$	-	$x_{lb} \leq x_0 \leq x_{ub}$	$0.0 \leq 0.5 \leq 1.0$	$0.0 \leq 0.5 \leq 1.0$	$0.0 \leq 0.5 \leq 1.0$
$s_{rs,min}$	m	-	0.02	0.02	0.02
$s_{cl,min}$	m	-	0.02	0.02	0.02
$s_{fpb,min}$	m	-	0.02	0.02	0.02
l_{fpb}	m	-	1.4	1.4	1.4
CCP_1	m	(x, y, z)	(55.4, 31.5, 1.1)	(45.5, 26.6, 1.1)	(50.9, 29.2, 1.1)
CCP_2	m	(x, y, z)	(52.1, 31.5, 0.7)	(42.2, 26.6, 0.7)	(47.6, 29.2, 0.7)
$GMCP_1$	m	(x, y, z)	(58.9, -32.5, 7.1)	(49.0, -27.7, 7.1)	(54.4, -30.4, 7.1)
$GMCP_2$	m	(x, y, z)	(0.0, 0.0, 0.0)	(0.0, 0.0, 0.0)	(0.0, 0.0, 0.0)

The main landing gear attachment design space is defined by a parallelogram, with a front and aft edge parallel to the lateral aircraft axis, the inboard edge coincident with the Flying-V trailing edge, and the outboard edge coincident with the rear spar as illustrated in Figure 5.1. Naturally, the optimiser positions the main gear ground contact points aft of the aft centre of gravity for stability. This, however, does not necessarily require the gear to also be attached aft of the aft centre of gravity limit, as this may also be achieved by implementing a strut rake angle. To account for that, the front edge of the design space is positioned 2.0 m in front of the aft centre of gravity limit. The rear edge is positioned 2.0 m aft of aft centre of gravity limit, providing the optimiser with sufficient gear positioning freedom. The design space height z is selected such that the gear attachment and stowed tyres remain below the upper surface of the wing. Resulting right main landing gear attachment design space is described by coordinates MDS_A, MDS_B, MDS_C and MDS_D.

The nose gear attachment design space is defined by a single line coincident with the aircraft centreline. Vertically, the line roughly follows the outer mold line. The nose gear attachment design space is the same for all family members.

Normalised main gear positioning variables x_{mlg}, y_{mlg} and x_{nlg} may range from 0.0 to 1.0, with an initial estimate of 0.5.

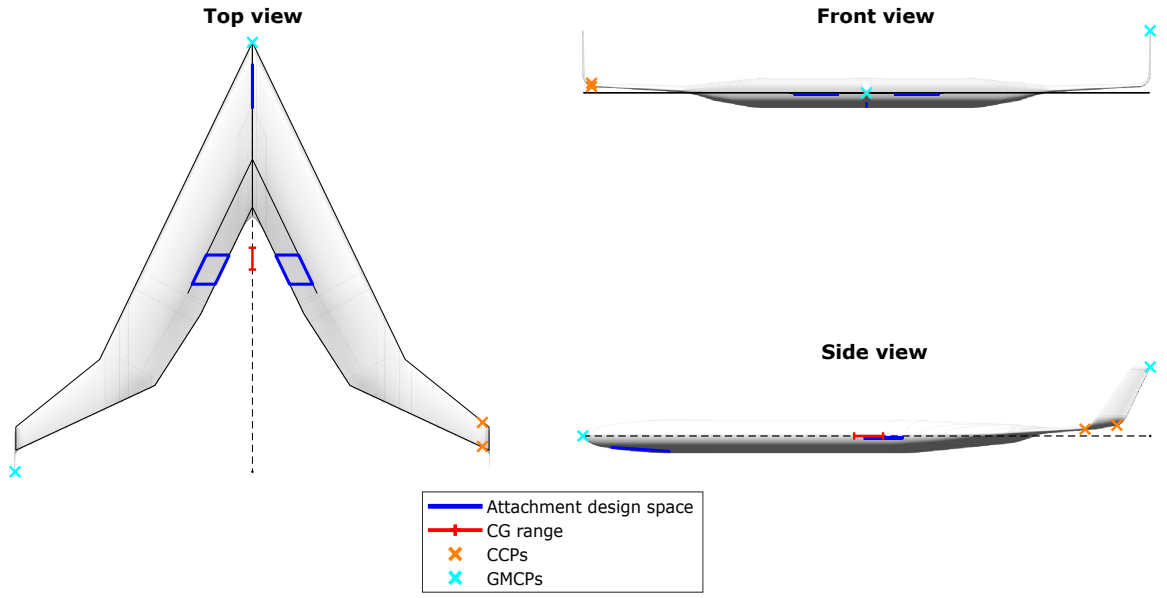

Figure 5.1: Flying-V gear attachment design spaces, critical points, and centre of gravity range.

Minimum stowage clearance distances are calculated using Equation 2.27. The equation requires tyre dimensions of selected main and nose gear tyres, which are obtained from tyre tables [12], as well as the aircraft take-off speed, which is derived from de Zoeten [22].

Coordinates of clearance critical points CCP and ground manoeuvring critical points GMCP are extracted from the Flying-V - Version 1 CATIA model. CCP_1 and CCP_2 represent the wing tip trailing edge and leading edge, as indicated by the orange x in Figure 5.1. $GMCP_1$ and $GMCP_2$ represent the tip of the winglet and the aircraft nose respectively. Ground manoeuvring critical points are indicated by a cyan x in Figure 5.1.

Mass Properties

Flying-V mass properties are outlined in Table 5.2.

Table 5.2: Flying-V aircraft mass specifications [10, 21, 27, 61].

Item	Unit	Format	FV-1000	FV-800	FV-900
CG_{fwd}	m	(x, y, z)	(28.2, 0.0, 0.0)	(23.3, 0.0, 0.0)	(26.2, 0.0, 0.0)
$CG_{fwd,\%MAC}$	% MAC	-	30.8	30.7	32.2
CG_{aft}	m	(x, y, z)	(31.2, 0.0, 0.0)	(25.8, 0.0, 0.0)	(28.7, 0.0, 0.0)
$CG_{aft,\%MAC}$	% MAC	-	47.5	45.9	46.5
MRM	kg	-	2.67×10^5	1.86×10^5	2.35×10^5
MTOM	kg	-	2.66×10^5	1.85×10^5	2.34×10^5
MLM	kg	-	2.00×10^5	1.39×10^5	1.76×10^5
OEM	kg	-	1.29×10^5	0.99×10^5	1.15×10^5
MRM_{range}	-	(x_{fwd}, x_{aft})	(0.5, 1.0)	(0.5, 1.0)	(0.5, 1.0)
$MTOM_{range}$	-	(x_{fwd}, x_{aft})	(0.5, 1.0)	(0.5, 1.0)	(0.5, 1.0)
MLM_{range}	-	(x_{fwd}, x_{aft})	(0.0, 1.0)	(0.0, 1.0)	(0.0, 1.0)

The feasible centre of gravity (CG) range for all Flying-V family members is estimated by van der Toorn [21]. However, unpublished work suggests that the CG is located further aft than initially estimated. In this research, the aft CG limit for the FV-1000 is assumed to be the average of van der Toorn's aft limit (29.9) and the centre of pressure estimated by Laar [27] (32.4). For the FV-800 and FV-900, it is assumed that the actual aft CG deviates from van der Toorn's estimate by a similar percentage of the mean aerodynamic chord (%MAC) as for the FV-1000. The mean aerodynamic chord (MAC) and mean

aerodynamic chord leading edge (LEMAC) are calculated for each aircraft using Equations B.1 and B.2 in Appendix B.1.1. The forward centre of gravity limits are obtained by applying the CG excursions from van der Toorn [21] relative to the newly obtained aft limits. Both the lateral and vertical centre of gravity locations are assumed to be aligned with the aircraft centreline.

Maximum take-off mass (MTOM) and operational empty mass (OEM) are obtained from Oosterom [10] for all family members. It is assumed that the maximum ramp mass (MRM) and maximum landing mass (MLM) are 100.5% and 75% of the maximum take-off mass respectively, similar to the A350-900 [43]. Upon inspection of the FV-900 loading diagram in Figure 2.11b, it is found that MRM and MTOM cannot reasonably occur at a forward CG position. Therefore, as a conservative estimate, it is estimated that for all family members, maximum ramp mass and maximum take-off mass can only occur when the CG is aft of 50% of the full CG range, alleviating nose gear sizing requirements.

Operational Properties

Operational properties of the FV-1000, FV-800 and FV-900 are outlined in Table 5.3.

Table 5.3: Flying-V aircraft operational requirements, based on landing gear background study (Section 2.4) and [22, 23].

Item	Unit	Format	FV-1000	FV-800	FV-900
$\theta_{\text{tpb,min}}$	°	-	15.0	15.0	15.0
$\psi_{\text{tno,max}}$	°	-	63.0	63.0	63.0
ϕ_{max}	°	-	8.0	8.0	8.0
θ_{stat}	°	-	-3.0	-3.0	-3.0
$\theta_{\text{max,statSA}}$	°	-	9.9	9.9	9.9
$\theta_{\text{max,extSA}}$	°	-	14.0	14.0	14.0
$\hat{\beta}_{\text{nlg,min}}$	-	$x_{\text{lb}} \leq x_0 \leq x_{\text{ub}}$	$0.04 \leq 0.10 \leq 0.20$	$0.04 \leq 0.10 \leq 0.20$	$0.04 \leq 0.10 \leq 0.20$
$\hat{\beta}_{\text{nlg,max}}$	-	$x_{\text{lb}} \leq x_0 \leq x_{\text{ub}}$	$0.04 \leq 0.10 \leq 0.20$	$0.04 \leq 0.10 \leq 0.20$	$0.04 \leq 0.10 \leq 0.20$
$\beta_{\text{mlg,max}}$	-	-	1.5	1.5	1.5
TDG	-	-	6	6	6
$\lambda_{\text{steering}}$	°	-	75.0	75.0	75.0
V_1	m/s	-	80.0	80.0	80.0

The minimum tipback angle $\theta_{\text{tpb,min}}$ and maximum lateral turnover angle $\psi_{\text{tno,max}}$ are selected as discussed in Section 2.4.

The Flying-V must be able to roll with 8° while maintaining sufficient ground clearance. All family members have a static pitch attitude of -3° [22]. Without flaps, the maximum pitch attitude with fully extended shock absorbers $\theta_{\text{max,extSA}}$ is 17° [22]. For the baseline gear design, the use of flaps is anticipated, reducing the maximum pitch attitude by 3° to 14° [24]. It is assumed that the difference between $\theta_{\text{max,extSA}}$ and $\theta_{\text{max,statSA}}$, the maximum pitch attitude with shock absorbers in the static position is 4.1°, similar to the A330-300 [60]. Consequently, the permissible static pitch attitude must be at least 9.9°. It must be noted that this is a rough estimation, and that a larger clearance angle is desirable.

The nose gear load target values $\hat{\beta}_{\text{nlg,min}}$ and $\hat{\beta}_{\text{nlg,max}}$ have a lower bound of 0.04, similar to the aircraft used for verification and validation. The upper bound, however, is increased to 0.20 to account for the larger CG range compared to the reference aircraft, inherently increasing the nose gear load fraction at the forward centre of gravity limit. It must be noted that for an aircraft with two nose gear tyres and eight main gear tyres in total, a nose gear load fraction of 0.20 implies that all tyres are loaded equally. Typically, the nose gear tyres are smaller and have a lower load rating compared to the main gear tyres. This is only possible if either the maximum nose gear load fraction is sufficiently small (e.g., smaller than 0.20 for aforementioned configuration), or if the nose gear load at forward centre of gravity is lower in absolute terms. The latter is the case for the Flying-V (Table 5.2). The maximum main gear load fraction $\beta_{\text{mlg,max}}$ is 1.5, representing downforce generated by the spoilers after touchdown [22].

The taxiway design group (TDG) and maximum steering angle $\lambda_{\text{steering}}$ are selected to be similar to that of the A350-1000. The take-off decision speed V_1 is obtained from de Zoeten [22].

It must be noted that the minimum tipback angle, maximum lateral turnover angle, maximum roll and

pitch attitudes and nose gear load fractions only impose design limitations, and only represent actual performance if the respective constraints are active. Actual performance characteristics are evaluated after the optimisation to gain insight in actual operational performance even when constraints are inactive.

5.2.2. Flying-V Strut and Bogie Concept Selection

Flying-V baseline gear design strut and bogie concept selections are outlined in Table 5.4.

Table 5.4: Flying-V strut and bogie concept specifications.

Item	Unit	Format	FV-1000	FV-800	FV-900
Strut	-	-	Concept B	Concept B	Concept B
l_{ss}	m	$x_{lb} \leq x_0 \leq x_{ub}$	1.0 $\leq$ 2.0 $\leq$ 6.0	1.0 $\leq$ 2.0 $\leq$ 6.0	1.0 $\leq$ 2.0 $\leq$ 6.0
$\theta_{ss,ext}$	$^\circ$	$x_{lb} \leq x_0 \leq x_{ub}$	-4.0 $\leq$ -2.0 $\leq$ 0.0	-4.0 $\leq$ -2.0 $\leq$ 0.0	-6.0 $\leq$ -4.0 $\leq$ 0.0
$\theta_{ss,ret}$	$^\circ$	-	90.0	90.0	90.0
$\phi_{ss,ret}$	$^\circ$	-	0.0	0.0	0.0
$\psi_{mlg,ret}$	$^\circ$	$x_{lb} \leq x_0 \leq x_{ub}$	0.0 $\leq$ 20.0 $\leq$ 45.0	0.0 $\leq$ 20.0 $\leq$ 45.0	0.0 $\leq$ 20.0 $\leq$ 45.0
l_{us}	m	-	2.10	2.10	2.10
$\theta_{us,ext}$	$^\circ$	$x_{lb} \leq x_0 \leq x_{ub}$	-24.0 $\leq$ -22.0 $\leq$ -20.0	-24.0 $\leq$ -22.0 $\leq$ -20.0	-24.0 $\leq$ -22.0 $\leq$ -20.0
$\phi_{us,ext}$	$^\circ$	$x_{lb} \leq x_0 \leq x_{ub}$	0.0 $\leq$ 0.0 $\leq$ 0.0	0.0 $\leq$ 0.0 $\leq$ 0.0	0.0 $\leq$ 0.0 $\leq$ 0.0
$\theta_{us,ret}$	$^\circ$	-	-70.0	-70.0	-70.0
$\phi_{us,ret}$	$^\circ$	-	-10.0	-10.0	-10.0
l_{hs}	m	-	N.A.	N.A.	N.A.
θ_{hs}	$^\circ$	-	N.A.	N.A.	N.A.
Bogie	-	-	Concept B	Concept B	Concept B
l_{offset}	m	-	0.28	0.28	0.28
$l_{ineffective}$	m	-	0.40	0.40	0.40
$\theta_{nlg,ret}$	$^\circ$	-	102.0	102.0	102.0

Following the baseline gear concept formulation, the gear needs to have a double folding strut, and the bogie needs to be folded parallel to the strut when retracted. This can either be achieved by selecting strut concept D together with bogie concept A ('hockey stick' arrangement), or by selecting strut concept B together with bogie concept B. The latter is selected because it offers lower strut bending moments, a shorter strut, a simpler design, and more kinematics design freedom.

The main gear shock strut length l_{ss} must be between 1 and 6 metres long and may be raked at an angle not smaller than -4° and not larger than 0°. Given that the Flying-V static rake angle is -3°, a shock strut range angle of -4° results in a rake angle of -7° relative to the ground, which is the maximum recommended rake angle, as discussed in Section 2.4.3. Imposing an upper bound of 0° prevents excessively high strut bending moments during landing. The retracted shock strut angles are selected such that the strut and wheels are aligned with the aircraft centreline for efficient stowage.

The upper strut length l_{us} is selected to ensure that when the gear is retracted, tyres remain clear of other landing gear components. The upper strut rake angle $\theta_{us,ext}$ is bounded such that it may be adjusted by the optimiser to achieve a 20° rake angle relative to the shock strut, similar to the Convair B-58 [12]. The sideward rake angle $\phi_{us,ext}$ is constrained to zero. While the optimiser could theoretically adjust this angle to shift the ground contact points further outboard than the gear attachment position, thereby potentially reducing the required gear length to achieve ground clearance, this adjustment would also result in increased bending moments in the upper strut. Additionally, such a modification would bring the shock strut closer to the attachment point of the fixed-length shock strut brace, thereby diminishing its mechanical leverage. The angle between the retracted shock strut and upper strut is set to 20°, offering a good compromise between compactness, actuator loads, and kinematic feasibility. Consequently, the retracted upper strut angle $\theta_{us,ret}$ must be -70°, $\phi_{us,ret}$ is selected to obtain a feasible retraction path.

The bogie pivot to bogie centreline offset distance l_{offset} is selected to be as small as possible to minimise

bogie pitching moments during spin-up and brake rod loads during braking, while still allowing flat-packing during retraction. The ineffective piston length $l_{\text{ineffective}}$ is assumed to be similar to that of the A310-200. The nose gear strut folding angle $\theta_{\text{nlg,ret}}$ ensures that the strut folds entirely into the aircraft fuselage.

5.2.3. Flying-V Bogie and Tyre Sizing

Flying-V bogie and tyre sizing specifications are outlined in Table 5.5.

Table 5.5: Flying-V bogie and tyre sizing specifications.

Item	Unit	Format	FV-1000	FV-800	FV-900
$N_{\text{mlg,w}}$	-	-	8	8	8
$N_{\text{mlg,ss}}$	-	-	2	2	2
l_{bogie}	m	-	2.02	2.02	2.02
w_{bogie}	m	-	1.62	1.62	1.62
Tyre_{mlg}	-	-	1400x530R23 (42 ply)	50x20R22 (32 ply)	54x21R23 (38 ply)
$N_{\text{nlg,w}}$	-	-	2	2	2
w_{nlg}	m	-	0.75	0.75	0.75
Tyre_{nlg}	-	-	43x17.5R17 (32 ply)	43x17.5R17 (32 ply)	43x17.5R17 (32 ply)
$a_{x,\text{des}}$	m/s^2	-	3.9	3.9	3.9

The baseline concept features two main gear struts, both with a four-wheel bogie configuration. The length and width of the FV-1000 are determined through linear interpolation between the dimensions of the A330-300 and A350-900, based on the maximum take-off mass of each aircraft. The FV-800 and FV-900 share the same bogie design. Main and nose gear tyre selections are based on the tyre loading diagrams (Figure 5.11 for the FV-1000) and are aligned with those used on current wide-body aircraft, including the Airbus A330, A350, and Boeing 777 and 787. Similar to most large transport aircraft, the Flying-V will have a single nose gear strut with two wheels. The nose gear wheel span is based on that of the A350-900. The design deceleration $a_{x,\text{des}}$ is obtained from de Zoeten [22].

5.2.4. Flying-V Shock Absorber Sizing

Flying-V shock absorber sizing specifications are outlined in Table 5.6, and are similar to those specified for the reference aircraft used for validation, as shown in Table 4.6.

Table 5.6: Flying-V shock absorber sizing specifications.

Item	Unit	Format	FV-1000	FV-800	FV-900
λ_{mlg}	-	-	1.10	1.10	1.10
$P_{\text{mlg,static}}$	MPa	-	13.8	13.8	13.8
b_{mlg}	-	-	0.10	0.10	0.10
λ_{nlg}	-	-	1.30	1.30	1.30
$P_{\text{nlg,static}}$	MPa	-	13.8	13.8	13.8
b_{nlg}	-	-	0.10	0.10	0.10
s_{Fmax}	-	-	0.30	0.30	0.30

5.2.5. Flying-V Special Features

Flying-V special landing gear feature specifications are outlined in Table 5.7.

Following the baseline concept formulation, the FV-1000 incorporates both bogie articulation and strut shortening, while the FV-800 and FV-900 feature only strut shortening. The specifications for FV-1000 bogie articulation and strut shortening are similar to those of the A330-300, as detailed in Table 4.7. Only the articulated bogie reaction factor $\lambda_{\text{mlg,art}}$ is lowered slightly to have the de-articulation margin larger than 0.1 m. The shortening amounts of the FV-800 and FV-900 are adjusted to achieve the same retracted bogie position as the FV-1000, measured relative to the gear attachment origin.

Table 5.7: Flying-V special landing gear feature specifications.

Item	Unit	Format	FV-1000	FV-800	FV-900
Articulation	-	Boolean	True	False	False
$\lambda_{\text{mlg,art}}$	-	-	0.35	N.A.	N.A.
θ_{bogie}	$^\circ$	$x_{\text{lb}} \leq x_0 \leq x_{\text{ub}}$	$0.00 \leq 0.00 \leq 25.0$	N.A.	N.A.
$l_{\text{x,pivot}}$	m	-	0.22	N.A.	N.A.
$l_{\text{z,pivot}}$	m	-	0.26	N.A.	N.A.
$l_{\text{margin,art}}$	m	-	0.10	N.A.	N.A.
Shortening	-	Boolean	True	True	True
$l_{\text{shortening}}$	m	-	0.50	0.35	0.35

5.3. Baseline Gear Design

In this section, the implementation of the baseline landing gear concept is outlined. First, baseline landing gear stick models are generated, which is then followed by the 3D model generation and structural sizing. As detailed in Section 5.1, the baseline concept is based on the requirements of the FV-1000, and includes both bogie articulation and strut shortening. For the FV-800 and FV-900, bogie articulation is eliminated, and the strut shortening is modified to ensure the bogie maintains the same relative position to the gear attachment point as it does in the FV-1000 configuration.

5.3.1. Stick Model Generation

First, a stick model is generated for the FV-1000, following the objective and constraints as specified in Section 3.3. The resulting design vector values subsequently serve as fixed inputs for generating the stick models of the FV-800 and FV-900. Gear positioning parameters x_{mlg} and y_{mlg} define the main gear attachment location within the attachment design space, which maintains consistent dimensions and placement relative to the centre of gravity across all family members. Consequently, using the same positioning parameters for each family member ensures that the gear attachment remains consistently aligned with both the centre of gravity and the rear spar. Furthermore, by applying the same stick model design variables l_{ss}, $\theta_{\text{ss,ext}}$, $\psi_{\text{mlg,ret}}$, $\theta_{\text{us,ext}}$, $\phi_{\text{us,ext}}$, stick model lengths and orientations are uniform across all family members. The bogie articulation angle θ_{bogie} does not need to be specified for the FV-800 and FV-900, as bogie articulation is omitted for these aircraft.

However, an exception is made for the nose gear positioning parameter x_{nlg} and target nose gear load fractions $\hat{\beta}_{\text{nlg,min}}$ and $\hat{\beta}_{\text{nlg,max}}$. Because of the -3° static pitch attitude, constant main gear length, and variation in aircraft length between the Flying-V family members, the FV-800 and FV-900 inherently require a longer nose gear than the FV-1000. Consequently, the FV-800 and FV-900 require the nose gear to be positioned further aft in order to have sufficient clearance from the front pressure bulkhead when stowed. This also affects the nose gear load fraction. Instead of fixing FV-800 and FV-900 nose gear positioning parameters and target nose gear load fractions to that of the FV-1000 design vector outputs, they are limited by their original bounds as specified in Tables 5.1 and 5.3.

The final design vector and an overview of constraint activity are presented in Tables 5.8 and 5.9, respectively. The gear positioning parameters and shock strut length are well within their respective bounds, indicating that the design space has been positioned appropriately. Interestingly, the shock strut is raked aft at -4° (-7° relative to the ground), even though this is not specifically needed for feasible attachment, e.g., there is still room to move the attachment point further aft, which would result in a shorter gear for the same ground contact point. This can be explained by the optimiser optimising for maximum rotation ability, which moves the static main gear pivot as much forward as possible, and the rotated tipover constraint being active. When the strut is raked, the pivot point moves aft as the shock absorber extends, effectively adding to the rotated tipover margin (extended shock absorber) whilst not affecting the pivot location for initial rotation (static shock absorber). The bogie articulation angle θ_{bogie} is bounded by its upper bound to maximise the articulation benefit. The upper strut rake angle $\theta_{\text{us,ext}}$ is selected to achieve a 20° difference with the shock strut rake angle, as discussed in Section 5.2. The sideward rake angle $\phi_{\text{us,ext}}$ is maintained at 0° because increasing it would unnecessarily lengthen the gear. As the outboard gear location is constrained by taxiway design group limits, implementing a

rake angle would require adjusting the lateral positioning parameter y_{mlg} to move the attachment further inboard.

FV-800 and FV-900 design vector changes and constraint violations are indicated in bold. Interestingly, using the FV-1000 design vector for the FV-800 and FV-900 does not yield a feasible design. Even though both the FV-800 and FV-900 have a smaller CG excursion compared to the FV-1000 (Table 5.2), the larger nose gear length and resulting nose gear repositioning results in the FV-800's nose gear load fraction being larger than 20% at forward CG. For the FV-900, the nose gear load fractions fall within the acceptable range, however, ground clearance is insufficient to allow the aircraft to achieve a combined $14.0°$ pitch and $8.0°$ degree roll attitude.

Table 5.8: Flying-V baseline concept stick model generation design vectors.

Variable	Unit	x_{lb}	x_0	x_{ub}	FV-1000	FV-800	FV-900
x_{mlg}	-	0.00	0.50	1.00	0.61	0.61	0.61
y_{mlg}	-	0.00	0.50	1.00	0.55	0.55	0.55
x_{nlg}	-	0.00	0.50	1.00	0.55	**0.60**	**0.57**
l_{ss}	m	1.00	2.00	6.00	3.55	3.55	3.55
$\theta_{\text{ss,ext}}$	°	-4.00	-2.00	0.00	-4.00	-4.00	-4.00
$\psi_{\text{mlg,ret}}$	°	0	20.0	45.00	14.4	14.4	14.4
$\theta_{\text{us,ext}}$	°	-24.0	-22.0	-20.0	-24.0	-24.0	-24.0
$\phi_{\text{us,ext}}$	°	0.00	0.00	0.00	0.00	0.00	0.00
θ_{bogie}	°	0.00	0.00	25.0	25.0	N.A.	N.A.
$\hat{\beta}_{\text{nlg,min}}$	-	0.04	0.10	0.20	0.07	**0.09**	**0.08**
$\hat{\beta}_{\text{nlg,max}}$	-	0.04	0.10	0.20	0.18	**0.21**	0.18

Table 5.9: Flying-V baseline concept stick model generation constraint activity.

Constraint	FV-1000	FV-800	FV-900
Longitudinal stability - minimum nlg load	Inactive	Inactive	Inactive
Longitudinal stability - maximum nlg load	Inactive	**Violated**	Inactive
Longitudinal stability - rotated tipover	Active	Inactive	Inactive
Longitudinal stability - push-back tipover	Inactive	Inactive	Inactive
Lateral stability - lateral turnover	Inactive	Inactive	Inactive
Ground clearance - static shock absorber	Inactive	Inactive	Inactive
Ground clearance - extended shock absorber	Active	Inactive	**Violated**
Airframe integration - nlg stowage	Active	Active	Active
Airframe integration - mlg stowage	Active	Active	Active
Ground manoeuvring - taxiway design group	Active	Inactive	Inactive
Ground manoeuvring - $180°$ turn	Inactive	Inactive	Inactive

Resulting extended and retracted baseline concept gear stick models are shown in Figures 5.2, 5.3 and 5.4 for the FV-1000, in Figures 5.5, 5.6 and 5.7 for the FV-800, and in Figures 5.8, 5.9 and 5.10 for the FV-900. Specifically, for each aircraft, the latter two figures illustrate ground clearance for a combined $14.0°$ pitch and $8.0°$ roll attitude. An overview of stick model results is provided in Table 5.10, with unsatisfactory results indicated in bold.

It can be observed that the FV-1000 utilises bogie articulation to achieve sufficient ground clearance under combined pitch and roll conditions. With fully extended shock absorbers (SA), the FV-1000 can attain a pitch attitude of $14.0°$, whereas in the static position, only a $10.5°$ pitch attitude is available. The FV-800 and FV-900 do not feature bogie articulation and hence, they naturally have a smaller difference between the static and fully extended SA maximum pitch attitudes ($\theta_{\text{max,statSA}}$ and $\theta_{\text{max,extSA}}$, respectively). For the FV-800, the gear allows the aircraft to achieve a $16.0°$ pitch attitude when the SA is fully extended, or $13.9°$ when the SA is in the static position. For the FV-900, only a $13.7°$ pitch attitude is available when the SA is fully extended, which is lower than the $14.0°$ pitch attitude requirement. This necessitates either an increase in the landing and take-off speed or an extension of the gear length.

Alternatively, bogie articulation could be implemented for the FV-900 as well. The FV-900 can achieve a 11.9° pitch attitude when the SA is in the static position. In all cases, a roll angle of 8.0° is considered.

Because bogie articulation requires the shock absorber to exert a reduced vertical reaction during the initial phase of its compression stroke to avoid overloading the tyres, a slightly longer total stroke is needed to absorb all vertical landing energy. Consequently, the FV-1000 has a slightly longer SA stroke, which translates to a longer main gear length $l_{\text{mlg,extended}}$ compared to the FV-800 and FV-900.

It can also be observed that for the FV-800 and FV-900, the nose gear attachment has to be moved aft with 0.35 m and 0.11 m, respectively, in order to have sufficient room for retracting the longer nose gear. Instead of relocating the attachment point, a nose gear strut shortening mechanism could be implemented. Typically, such mechanisms can reduce the strut length by nearly the full SA stroke [12], which is approximately 0.45 m. This means that the increase in gear length can effectively be countered by strut shortening, negating the need to relocate the attachment point, enhancing family design commonality. Additionally, moving the gear forward would reduce the nose gear load fraction, which is currently too high for the FV-800.

Lastly, it must be noted that when it comes to lateral stability, the FV-800 only marginally has its lateral turnover angle ψ_{tno} below 63.0°. Although it is sufficient for lateral stability, a smaller lateral turnover angle is generally recommended to increase the operational envelope (Section 2.4).

Table 5.10: Flying-V baseline concept stick model results.

Item	Unit	FV-1000	FV-800	FV-900
X_{mlg}	m	31.6	26.3	29.2
Y_{mlg}	m	6.08	3.52	4.90
$l_{\text{mlg,static}}$	m	5.71	5.70	5.70
$l_{\text{mlg,extended}}$	m	6.38	6.22	6.22
X_{nlg}	m	6.15	6.40	6.26
$l_{\text{nlg,static}}$	m	3.37	3.64	3.50
$l_{\text{nlg,extended}}$	m	3.83	4.09	3.95
θ_{tpb}	$^\circ$	18.1	18.1	18.1
ψ_{tno}	$^\circ$	49.0	61.6	54.1
ϕ_{max}	$^\circ$	8.0	8.0	8.0
$\theta_{\text{max,statSA}}$	$^\circ$	10.5	13.9	11.9
$\theta_{\text{max,extSA}}$	$^\circ$	14.0	16.0	**13.7**
$\beta_{\text{nlg,aftCG}}$	-	0.070	0.088	0.077
$\beta_{\text{nlg,fwdCG}}$	-	0.183	**0.207**	0.181

The resulting FV-1000 gear loading diagram is shown in Figure 5.11. Similar diagrams for the FV-800 and FV-900 are shown in Figures D.1 and D.2 in Appendix D. The diagrams illustrate nose gear and main gear tyre load limits (blue lines and red lines, respectively), indicating the maximum allowable aircraft mass at any centre of gravity location under specific loading conditions. It can be concluded that for the FV-1000, the nose gear tyre selection is driven by both the static load limit and dynamic (design landing deceleration) load limit (Table 5.5). The main gear tyre selection is only driven by the dynamic load limit, which can be attributed to the generation of downforce.

It is important to note that the analysis considers a maximum main gear load fraction $\beta_{\text{mlg,max}}$ of 1.5 (Table 5.3) to account for downforce generation, whereas de Zoeten [22] suggests a range of 1.5 to 1.7. Specifically for the FV-1000, the baseline concept is already equipped with the strongest tyres commonly available [12], and can thus not further be upgraded. Consequently, the main gear load fraction must be limited to 1.5 when the aircraft is at MTOM, e.g., during a rejected take-off. However, this limitation is unlikely to yield unsatisfactory operational performance, as the FV-1000 balanced field length is significantly shorter than that of the A350-1000 [22], not requiring a larger main gear load fraction for better braking.

Figure 5.12a and 5.12b show FV-1000 and FV-800 turning radii when executing a right turn with a 75° nose gear steering angle. A similar figure for the FV-900 can be found in Appendix D. Vertical

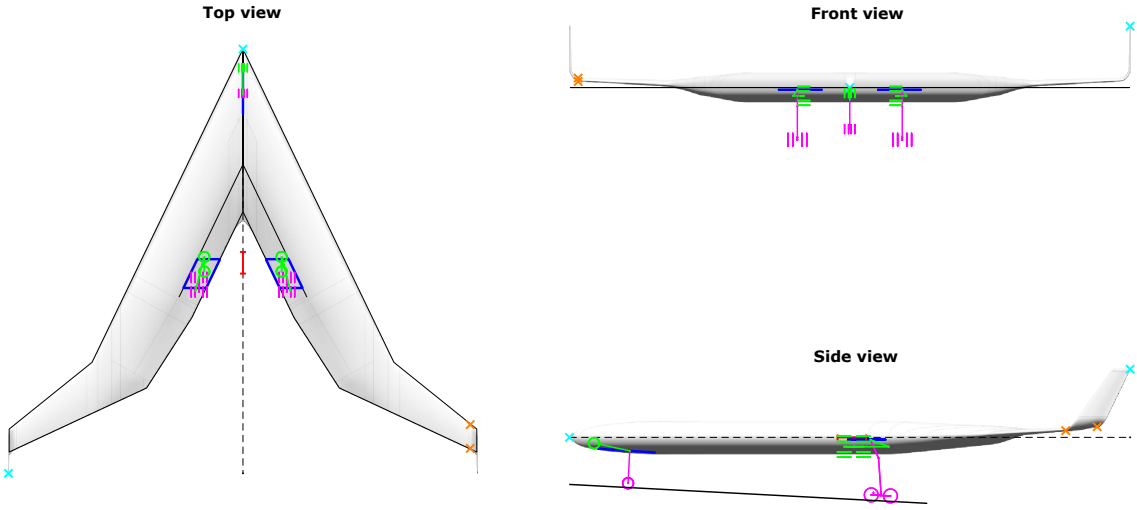

Figure 5.2: FV-1000 baseline concept landing gear stick model.

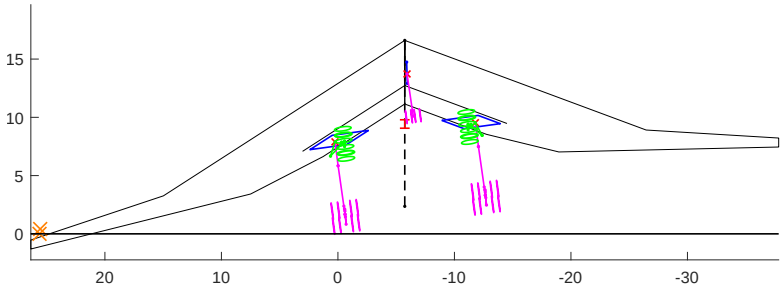

Figure 5.3: FV-1000 baseline concept front view, critical ground clearance attitude (θ = $14.0°$, ϕ = $8.0°$), extended shock absorber position.

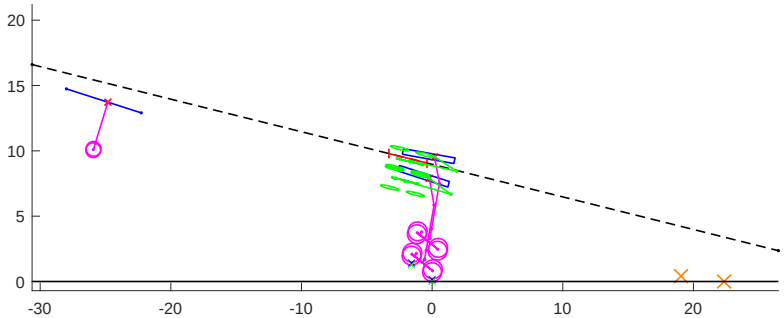

Figure 5.4: FV-1000 baseline concept side view, critical ground clearance attitude (θ = $14.0°$, ϕ = $8.0°$), extended shock absorber position.

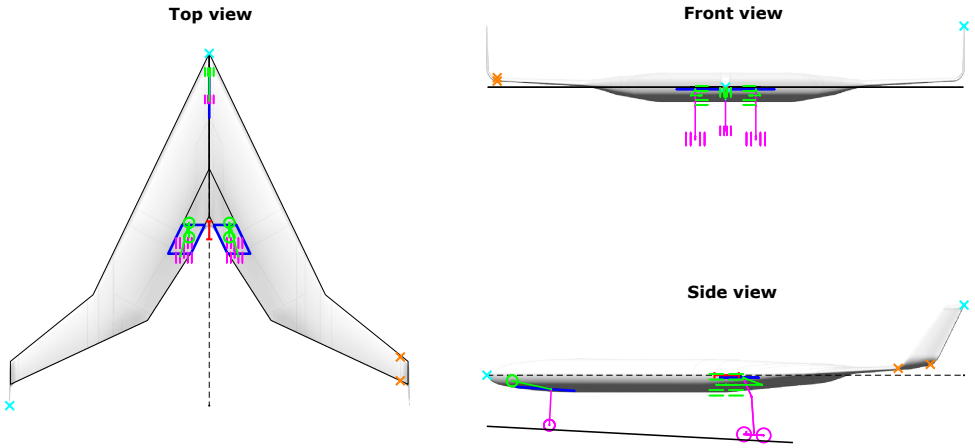

Figure 5.5: FV-800 baseline concept landing gear stick model.

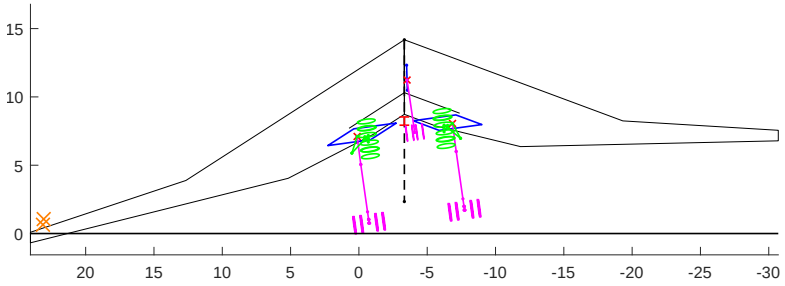

Figure 5.6: FV-800 baseline concept front view, critical ground clearance attitude (θ = $14.0°$, ϕ = $8.0°$), extended shock absorber position.

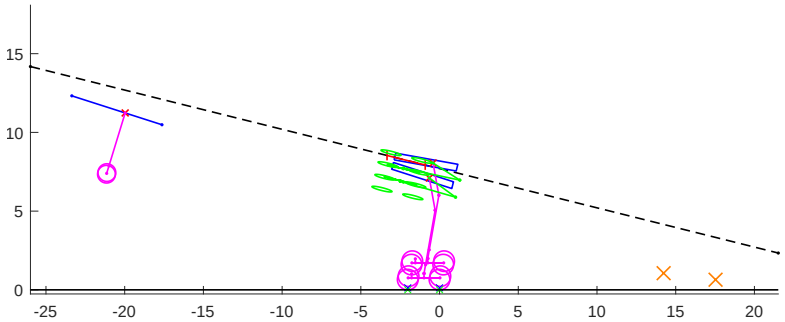

Figure 5.7: FV-800 baseline concept side view, critical ground clearance attitude (θ = $14.0°$, ϕ = $8.0°$), extended shock absorber position.

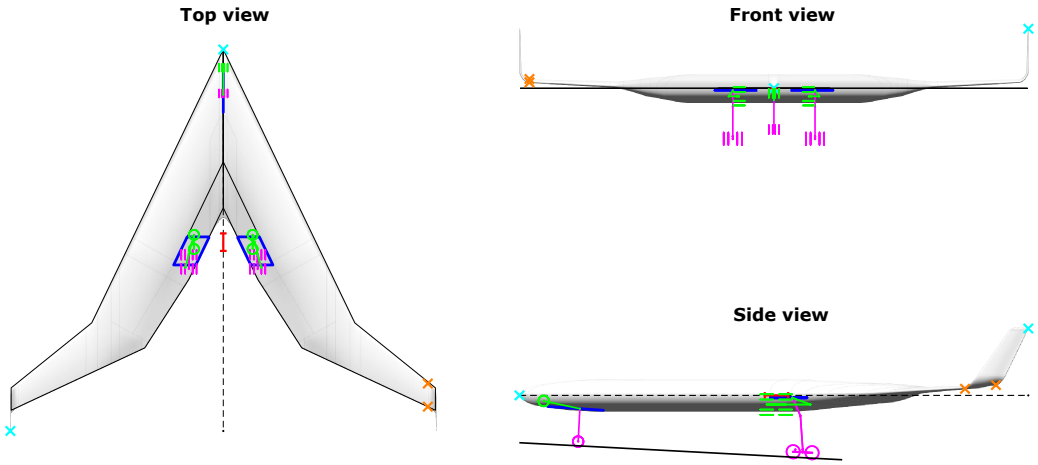

Figure 5.8: FV-900 baseline concept landing gear stick model.

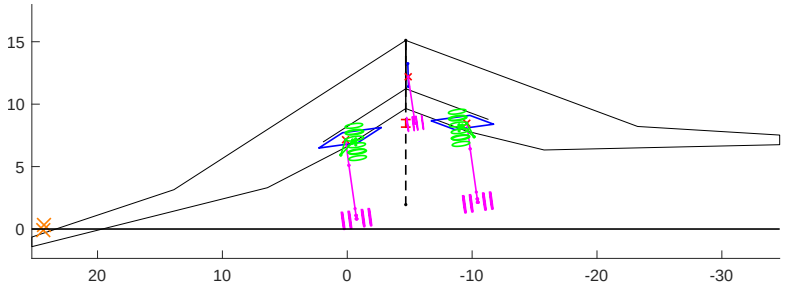

Figure 5.9: FV-900 baseline concept front view, critical ground clearance attitude (θ = $14.0°$, ϕ = $8.0°$), extended shock absorber position.

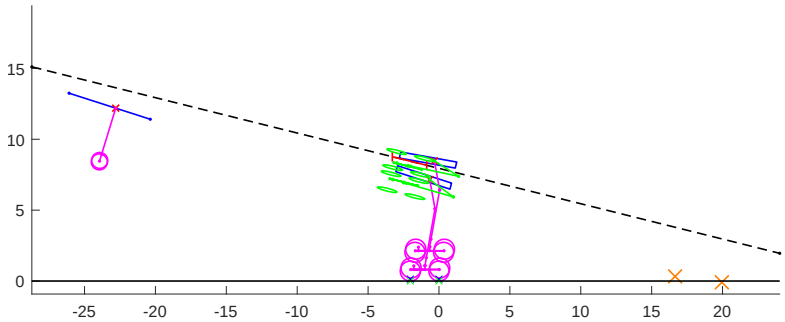

Figure 5.10: FV-900 baseline concept side view, critical ground clearance attitude (θ = $14.0°$, ϕ = $8.0°$), extended shock absorber position.

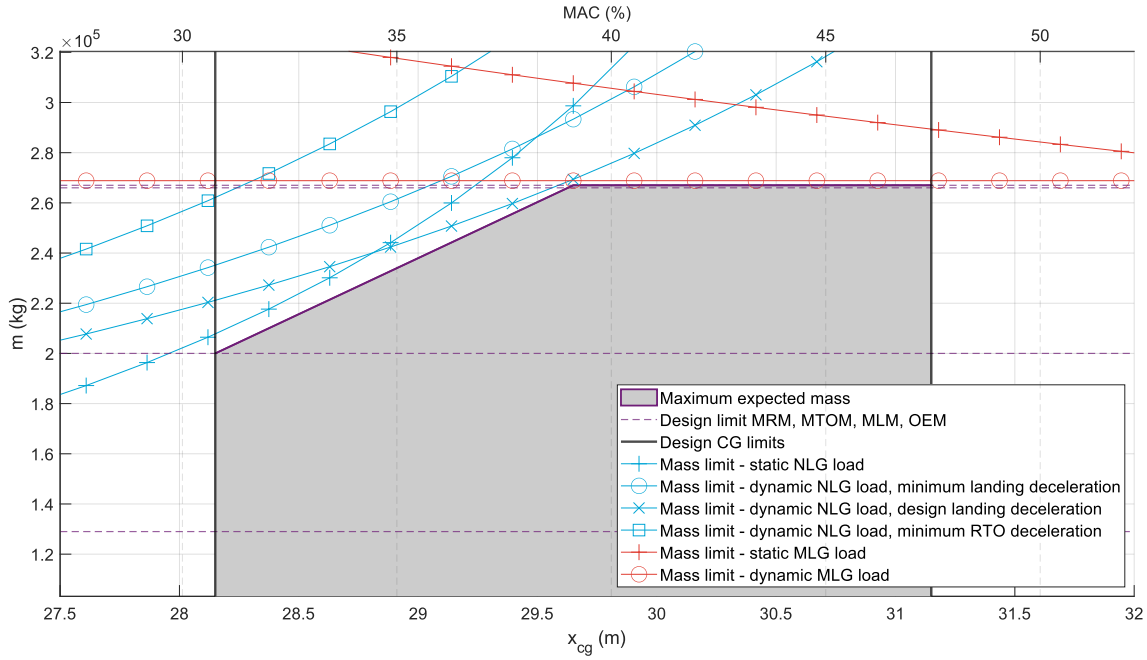

Figure 5.11: FV-1000 baseline gear loading diagram.

lines indicate the minimum taxiway separation distance, minimum taxilane separation distance and the taxiway width for a Code E aircraft, which are used for airport design (Table 2.7). It can be concluded that when the FV-1000 turns, its wing tip trespasses both minimum separation distances, potentially leading to collisions with objects or other aircraft. The FV-900 only trespasses the taxilane separation distance, while the FV-800 does not trespass any of the minimum separation distances. It must be noted that the wing tip turning radius is defined by the distance between the wing tip and the turning centre, which is only marginally affected by landing gear positioning. Therefore, operational limitations may need to be imposed on the FV-900 and FV-1000 to ensure safe ground operations.

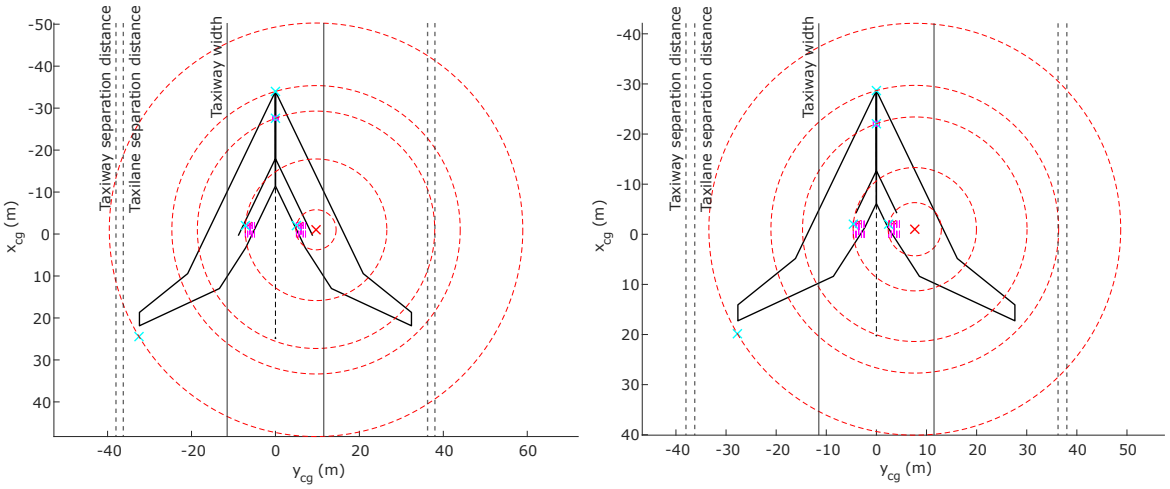

(a) FV-1000 baseline gear concept.

(b) FV-800 baseline gear concept.

Figure 5.12: Flying-V wing tip, nose, nose gear, left main gear and right main gear turning radii for a right turn with maximum nose gear steering angle.

Table 5.11 presents A350-900, FV-1000, FV-800 and FV-900 Aircraft Classification Ratings (ACR), which are calculated using the ICAO-ACR tool [47]. It is found that all Flying-V family members have a lower ACR compared to the A350-900 on both rigid and flexible pavements across all subgrade categories. This implies that all Flying-V family members have similar or better flotation performance

compared to the A350-900. However, it is important to note that these findings are based on static loads, without considering the effects of downforce generation after landing or during a rejected take-off.

Table 5.11: Flying-V baseline concept flotation (ACR) comparison, obtained using the ICAO-ACR tool [47].

Subgrade category	Flexible ACR				Rigid ACR			
	A350-900	FV-1000	FV-800	FV-900	A350-900	FV-1000	FV-800	FV-900
D	884	868	510	703	1031	1003	597	827
C	742	723	462	609	918	894	533	735
B	692	670	449	575	825	803	487	663
A	680	655	450	569	729	708	449	594

5.3.2. 3D Model Generation

The stick model of the FV-1000 right main landing gear is refined in 3DEXPERIENCE CATIA, enabling further analysis. This refinement process is not necessary for the FV-800 and FV-900 models, as they share the same fundamental landing gear design as the FV-1000. Figures 5.13a and 5.13b illustrate the final baseline concept 3D gear model and the refined stick model, from a left isometric and a right isometric perspective.

(a) Left isometric view. **(b)** Right isometric view.

Figure 5.13: FV-1000 baseline concept right main landing gear 3D model and refined stick model in orange.

The upper strut and shock strut folding axis orientations are given by the unit vectors $\hat{\mathbf{v}}_1$ and $\hat{\mathbf{v}}_2$, respectively, in Equation 5.1.

$$\hat{\mathbf{v}}_1 = \begin{pmatrix} 0.28 \\ -0.95 \\ 0.14 \end{pmatrix}, \quad \hat{\mathbf{v}}_2 = \begin{pmatrix} 0.73 \\ -0.62 \\ 0.30 \end{pmatrix} \tag{5.1}$$

Further design refinement is conducted as discussed in Section 3.4.2. The lengths of the upper strut and shock strut trunnion have been selected to provide maximal support to the gear without increasing the stowed volume already occupied by the struts and bogie assembly. A similar approach is followed when determining the brace attachment locations. Special care is taken in positioning the brace that connects the shock strut to the airframe. Since the brace has a fixed length, the distance between

the airframe and the strut attachment point when the gear is extended must be equal to the distance when the gear is retracted. During retraction, the brace attachment locations significantly influence the gear retraction path, thereby affecting concept feasibility. Tyres and wheels are added to the model to enable a stowage and retraction path analysis. Outer tyre dimensions correspond to the maximum grown dimensions, as specified in tyre tables [12]. Refined baseline gear concept stick model nodes are illustrated in Figures 5.14a and 5.14b. Node locations and type specifications are provided in Table D.1 in Appendix D.

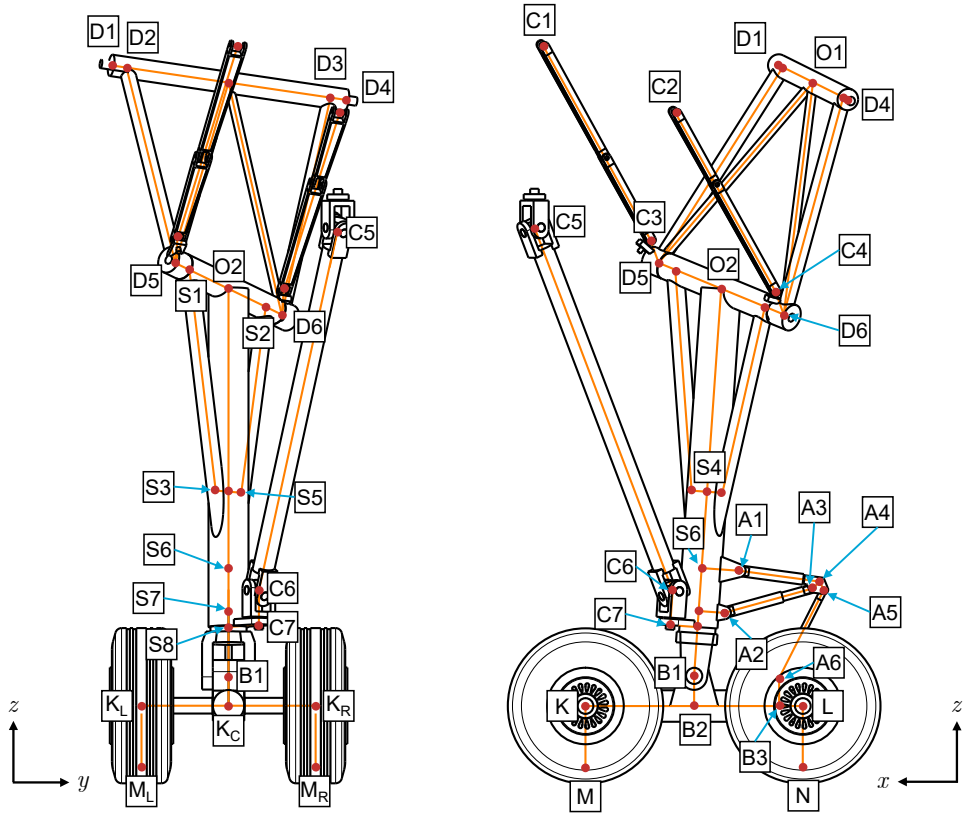

(a) Right main landing gear back view.

(b) Right main landing gear side view.

Figure 5.14: Baseline gear model node definitions.

The baseline gear retraction path is illustrated in Figure 5.15. From left to right, the Figure shows the gear in the static position, articulated position, half-retracted position, and fully retracted position. For the FV-1000, the articulation mechanism serves a dual purpose: it articulates the bogie for landing and take-off, and flat-packs the bogie for stowage. In contrast, the FV-800 and FV-900 require a dedicated bogie positioning mechanism for stowage as they do not have an articulation mechanism. It is found that the gear is able to retract from the extended to folded position without colliding with itself or the rear spar. However, special care must be taken when timing the bogie folding during retraction. As can be observed in the figures representing the half-retracted position, the front or rear tyres may get far inboard relative to the gear attachment point, depending on the bogie rotation angle. While this is not an issue for the FV-1000 and FV-900, for the FV-800 incorrect timing of bogie folding during retraction could result in the left and right gears colliding.

5.3.3. Structural Sizing

Finite element analysis is conducted to determine minimum required size and mass of the main landing gear primary structure. The refined stick model is subjected to the boundary conditions outlined in Table 5.12, representing the airframe attachment. The upper strut trunnion and drop link assembly braces are allowed to hinge around their respective rotation axis. The shock strut support brace is connected to the airframe using an universal joint, only preventing translations, but allowing rotations in all directions.

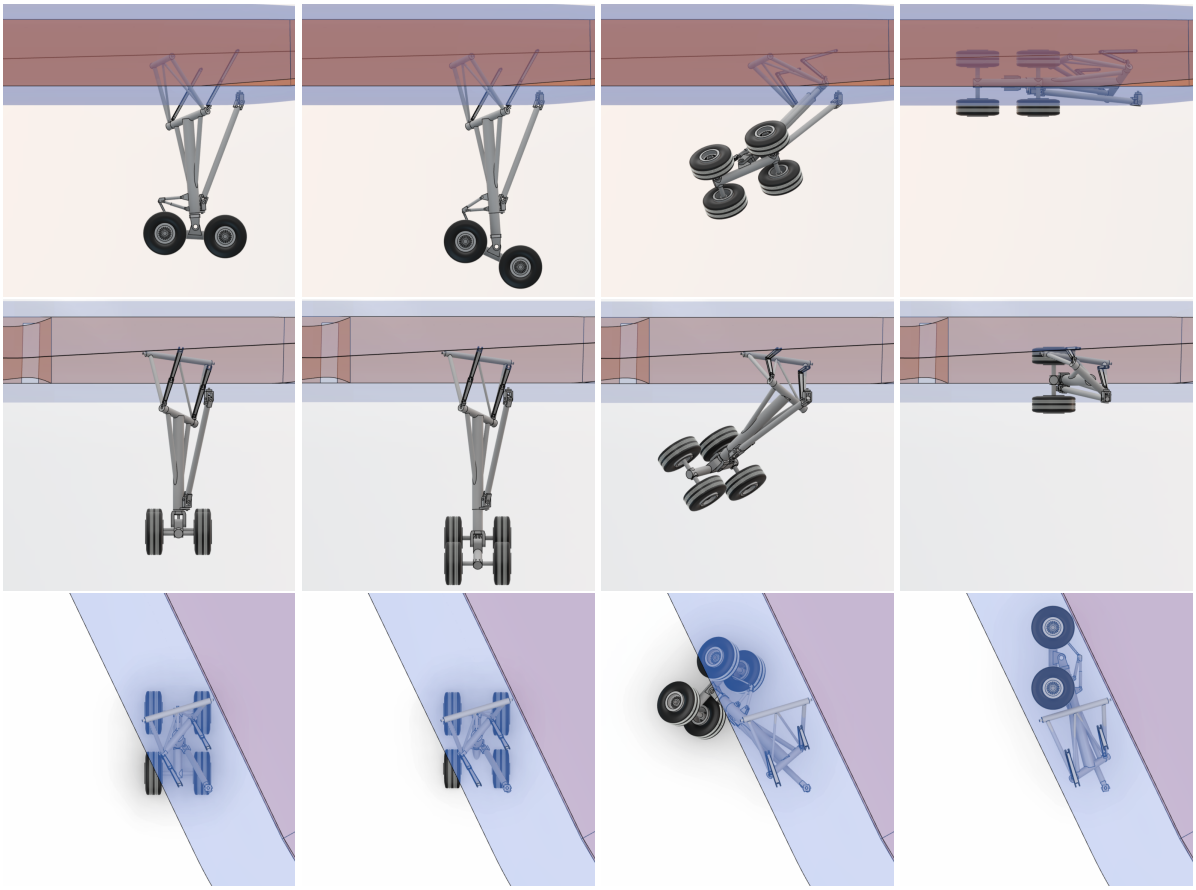

Figure 5.15: FV-1000 main landing gear baseline concept retraction kinematics, left view, back view and top view.

Table 5.12: Flying-V gear model boundary conditions.

Node	δ_x (m)	δ_y (m)	δ_z (m)	θ_x	θ_y	θ_z
D1	Fixed	Fixed	Fixed	Fixed	Fixed	Free
D4	Fixed	Fixed	Fixed	Fixed	Fixed	Free
C1	Fixed	Fixed	Fixed	Free	Fixed	Fixed
C2	Fixed	Fixed	Fixed	Free	Fixed	Fixed
C5	Fixed	Fixed	Fixed	Free	Free	Free

The structure is subjected to the load cases outlined in Table 2.2, applied in a manner similar to the verification and validation gear models described in Section 4.4. A detailed description of load cases and an overview of resulting external gear loads is presented in Table A.1 in Appendix A and Table D.3 in Appendix D, respectively.

For each member, the most critical load case is identified. Resulting internal member loads are detailed in Table D.2. The critical load cases are visualised in Figure 5.16, where 'LVL', 'SSL', 'GRO' and 'BRR' represent variations of the level landing, side load loading, general ground handling, and braked roll load cases, respectively. For landing load cases, 'P1' describes the initial (de-articulation) shock absorber compression phase, with only two wheels on the ground, while 'P2' represents the second phase, with all wheels on the ground. 'SU', 'SB', 'IB' and 'OB' describe spin-up, spring-back, inboard and outboard load conditions, respectively.

It can be observed that, apart from the articulation mechanism, all primary structural components are sized based on ground handling load cases, whereas for the validation gear models, this was only true for the bogie and wheel axles. First, bogie articulation significantly reduces the landing loads experienced by the gear. During landing, initially only the aft two wheels make contact with the ground,

preventing simultaneous spin-up and spring-back of all wheels. In addition, by the time all wheels are on the ground, the shock absorber is already partially compressed, reducing the leverage arm and associated bending moments. Second, the generation of downforce comes with a significant increase in gear loads during ground operations.

It must be noted that the FV-800 and FV-900 baseline concepts do not feature bogie articulation, making the first argument invalid. Despite this, ground handling loads are still higher than the landing loads. Naturally, the ground handling loads for the FV-800 and FV-900 are lower compared to those for the FV-1000 due to the lower aircraft mass. Consequently, the landing gear, which is sized to handle the FV-1000 ground handling load cases, is suitable for all aircraft in the family.

Figure 5.16: FV-1000 baseline concept right main landing gear critical load cases.

Baseline concept sizing results are presented in Table 5.13, where l,r_i, r_o, t, A and m denote the node-to-node member length, tube inner diameter, outer diameter, thickness, cross-sectional area and mass, respectively. Dimensions shown in bold are fixed, based on either the piston diameter or wheel rim diameter, as described in Section 3.5. The bogie and wheel axle outer diameters were initially sized to 80% of the piston diameter and 25% of the wheel rim diameter, respectively, as discussed in Section 3.4.2. However, to accommodate the larger loads resulting from downforce generation, this sizing was adjusted to 100% of the piston diameter and 40% of the wheel rim diameter, respectively. Additionally, the diameter of the brace connecting the shock strut to the airframe (shock strut brace 3) is increased to increase its resistance to buckling, as this brace is particularly long and therefore more susceptible to buckling under compressive loading.

The resulting total finite element mass of a single FV-1000 main landing gear is 2519 kg. For the FV-800 and FV-900, the combined mass of the articulation mechanism members is subtracted. The shock strut cylinder stands out as the largest contributor, but the bogie beam, trunnions, fixed length shock strut brace (shock strut brace 3) and wheel axles also make a significant contribution.

5.4. Gear Concept Variations

This section investigates several modifications to the FV-1000 baseline landing gear concept, contributing to the design exploration as discussed in Section 3.1. Modifications considered include substituting the double folding strut with a single folding strut, transitioning from a 4-wheel to a 6-wheel bogie, and eliminating both the articulation and strut shortening mechanisms. Additionally, the potential benefits

Table 5.13: FV-1000 baseline concept right main landing gear structural member sizing.

Member	Nodes	l (m)	r_i (m)	r_o (m)	t (m)	A (m^2)	m (kg)
Upper strut trunnion	D1-D2-O1-D3-D4	2.300	0.121	**0.134**	0.013	0.011	191.2
Drop link member 1	D2-D5	2.203	0.055	**0.067**	0.012	0.005	77.6
Drop link member 2	O1-D5	2.292	0.063	**0.067**	0.004	0.002	27.9
Drop link member 3	O1-D6	2.257	0.064	**0.067**	0.003	0.001	23.7
Drop link member 4	D3-D6	2.140	0.057	**0.067**	0.010	0.004	64.6
Drop link brace 1	C2-C4	2.201	0.064	**0.067**	0.003	0.001	23.1
Drop link brace 2	C1-C3	2.132	0.057	**0.067**	0.010	0.004	65.1
Shock strut trunnion	D5-S1-O2-S3-D6	1.750	0.115	**0.134**	0.019	0.015	206.8
Shock strut cylinder	O2-S4-S6-S7-S8	3.153	**0.168**	0.190	0.021	0.024	622.5
Shock strut piston	S8-B1	1.930[1,2]	0.149	**0.168**	0.018	0.018	280.9
Shock strut brace 1	S1-S3	2.101	0.072	**0.084**	0.012	0.006	99.8
Shock strut brace 2	S2-S5	1.786	0.072	**0.084**	0.012	0.006	79.8
Shock strut brace 3	C5-C6	3.687	0.101	**0.109**	0.007	0.005	151.2
Bogie beam	K-B2-L	2.020	0.151	**0.168**	0.017	0.017	275.3
Aft wheel axle	K_L-K_R	1.620	0.102	**0.117**	0.015	0.010	132.2
Front wheel axle	L_L-L_R	1.620	0.102	**0.117**	0.015	0.010	132.2
AM member 1[3]	A1-A4	1.272[1]	0.039	**0.050**	0.011	0.003	30.8
AM member 2[3]	A2-A3	1.103[1]	0.045	**0.050**	0.005	0.002	13.6
AM member 3[3]	A5-A6	0.920	0.045	**0.050**	0.005	0.002	11.3
Shortening members	-	0.500	0.042	**0.050**	0.009	0.003	9.8
Total	-	-	-	-	-	-	2519

[1] Extended length plus a margin of 2.75 times the respective piston diameter (Section 3.4.2).
[2] Includes the bogie pivot offset distance l_offset is added here.
[3] Articulation mechanism.

of folding the bogie backward rather than forward for stowage are explored. Each modification is evaluated separately, with the baseline FV-1000 gear design serving as the starting point for each variation. The five resulting concept variations are identified as shown in Table 5.14.

Table 5.14: Overview of FV-1000 landing gear concepts included in the design exploration.

Concept ID	Description
BL	Baseline concept
C1	Single folding strut concept
C2	6-wheel bogie concept
C3	Bogie articulation exclusion concept
C4	Strut shortening exclusion concept
C5	Backward stowage concept

5.4.1. Gear Model Generation

In this section, concept variation input adjustments, stick models, as well as their respective 3D models are discussed. For each concept variation, the final design vector, constraint violations and stick model results are outlined. Specifically, for the 6-wheel bogie concept, the flotation and tyre loading diagrams are compared with the baseline configuration. This comparison is relevant only for this concept, as the bogie and tyre sizing differ from the baseline, whereas for the other concepts, this remains unchanged. No further examination of the turning radii is performed, as the strut locations virtually remain the same compared to the baseline, resulting in similar turning radii.

An overview of design vector results, constraint activity, and results is presented in Tables 5.15, 5.16 and 5.17, respectively.

Table 5.15: Flying-V concept variations stick model generation design vectors.

Variable	Unit	x_{lb}	x_0	x_{ub}	BL	C1	C2	C3	C4	C5
x_{mlg}	-	0.00	0.50	1.00	0.61	0.81	0.63	0.61	0.59	0.96
y_{mlg}	-	0.00	0.50	1.00	0.55	0.43	0.56	0.55	0.56	0.34
x_{nlg}	-	0.00	0.50	1.00	0.55	0.55	0.51	0.67	0.56	0.55
l_{ss}	m	1.00	2.00	6.00	3.55	4.76	3.48	4.03	3.34	3.54
$\theta_{ss,ext}$	°	-4.00	-2.00	0.00	-4.00	-4.00	-4.00	-4.00	-4.00	-4.00
$\psi_{mlg,ret}$	°	0	20.0	45.00	14.4	17.8	21.1	14.5	15.8	10.0
$\theta_{us,ext}$	°	-24.0	-22.0	-20.0	-24.0	N.A.	-24.0	-24.0	-24.0	16.0
$\phi_{us,ext}$	°	0.00	0.00	0.00	0.00	N.A.	0.00	0.00	0.00	0.00
θ_{bogie}	°	0.00	0.00	25.0	25.0	25.0	18.1	N.A.	25.0	25.0
$\hat{\beta}_{nlg,min}$	-	0.04	0.10	0.20	0.07	0.07	0.07	0.08	0.07	0.7
$\hat{\beta}_{nlg,max}$	-	0.04	0.10	0.20	0.18	0.18	0.18	0.19	0.18	0.18

Table 5.16: Flying-V concept variations stick model generation constraint activity.

Constraint	BL	C1	C2	C3	C4	C5
Long. stab. - minimum nlg load	Inactive	Inactive	Inactive	Inactive	Inactive	Inactive
Long. stab. - maximum nlg load	Inactive	Inactive	Inactive	Inactive	Inactive	Inactive
Long. stab. - rotated tipover	Active	Active	Active	Active	Active	Active
Long. stab. - push-back tipover	Inactive	Inactive	Inactive	Inactive	Inactive	Inactive
Lat. stab. - lateral turnover	Inactive	Inactive	Inactive	Inactive	Inactive	Inactive
Ground clearance - stat. SA	Inactive	Inactive	Active	Inactive	Inactive	Inactive
Ground clearance - ext. SA	Active	Active	Active	Active	Active	Active
Integration - nlg stowage	Active	Active	Active	Active	Active	Active
Integration - mlg stowage	Active	Active	Active	Active	Active	Inactive
Ground man. - TDG	Active	Active	Active	Active	Active	Active
Ground man. - $180°$ turn	Inactive	Inactive	Inactive	Inactive	Inactive	Inactive

Table 5.17: Flying-V concept variations stick model results.

Item	Unit	BL	C1	C2	C3	C4	C5
X_{mlg}	m	31.6	32.4	31.7	31.6	31.5	33.0
Y_{mlg}	m	6.08	6.08	6.17	6.08	6.08	6.08
$l_{mlg,static}$	m	5.71	4.81	5.41	6.51	5.79	5.50
$l_{mlg,extended}$	m	6.38	5.48	6.24	7.02	6.45	6.17
X_{nlg}	m	6.15	6.15	5.91	6.80	6.16	6.15
$l_{nlg,static}$	m	3.38	3.37	3.12	4.08	3.38	3.38
$l_{nlg,extended}$	m	3.83	3.83	3.57	4.52	3.83	3.83
θ_{tpb}	°	18.1	18.1	18.4	17.8	18.1	18.1
ψ_{tno}	°	49.0	49.0	47.6	52.3	49.0	49.0
ϕ_{max}	°	8.0	8.0	8.0	8.0	8.0	8.0
$\theta_{max,statSA}$	°	10.5	10.5	9.9	12.4	10.5	10.5
$\theta_{max,extSA}$	°	14.0	14.0	14.0	14.0	14.0	14.0
$\beta_{nlg,aftCG}$	-	0.070	0.070	0.068	0.078	0.070	0.070
$\beta_{nlg,fwdCG}$	-	0.183	0.183	0.180	0.193	0.183	0.183

Single Folding Strut Concept

Baseline design input adjustments for the single folding strut concept are outlined in Table 5.18. For the double folding strut, the upper strut had to be attached above the (horizontal) retracted shock strut to prevent collision between components. This is not needed for single folding strut, and therefore, the gear attachment could be moved down. This leads to a shorter gear, and ensures that the bogie can be stowed beneath the upper wing surface. The single folding strut is represented by strut 'Concept A', as illustrated in Figure 3.8. Parameters related to the upper strut are no longer needed. All other input parameters and design variable bounds remain consistent with those specified for the baseline design.

Table 5.18: Concept variation input adjustments - single folding strut concept (C1).

Item	Unit	Format	Baseline	Concept C1
MDS_A	m	(x, y, z)	(29.2, 3.17, -0.25)	(29.2, 3.17, -0.97)
MDS_B	m	(x, y, z)	(33.2, 5.10, -0.25)	(33.2, 5.10, -0.97)
MDS_C	m	(x, y, z)	(29.2, 6.32, -0.25)	(29.2, 6.32, -0.97)
MDS_D	m	(x, y, z)	(33.2, 8.25, -0.25)	(33.2, 8.25, -0.97)
Strut	-	-	Concept B	Concept A
l_{us}	m	-	2.04	N.A.
$\theta_{us,ext}$	°	$x_{lb} \leq x_0 \leq x_{ub}$	-24.0 $\leq$ -22.0 $\leq$ -20.0	N.A.
$\phi_{us,ext}$	°	$x_{lb} \leq x_0 \leq x_{ub}$	0.0 $\leq$ 5.0 $\leq$ 10.0	N.A.
$\theta_{us,ret}$	°	-	72.0	N.A.
$\phi_{us,ret}$	°	-	-10.0	N.A.

The FV-1000 single folding strut stick model is illustrated in Figure 5.17. Compared to the baseline gear, the gear attachment is positioned further aft. This can be explained by the removal of the upper strut, which possesses a large rake angle. In order to have the same ground contact point locations, the gear attachment has to be moved aft. Although, naturally, the shock strut length is increased, the total gear length is reduced, which is primarily caused by the lower attachment height. Performance parameters concerning stability, clearance angles, and nose gear load fractions, as well as the nose gear sizing itself, remain consistent with the baseline design.

However, comparing the gear stick models of the single folding strut concept (Figure 5.17) with the baseline concept (Figure 5.2), it can be observed that the retracted gear is significantly wider. Assuming a similar attachment structure width, the single folding strut requires a fairing that is roughly 1.1 m wider than the baseline design fairing, compromising aerodynamic efficiency. Moreover, the gear occupies a significant portion of the area inboard of the rear spar, reducing the available fuel tank volume.

To further understand the drawbacks of implementing a single folding strut, stick models are also generated for the FV-800. Figure 5.18 illustrates the FV-800 gear stick model, sized for the FV-1000 but without bogie articulation, following the baseline concept design philosophy. It is found that when retracted, the tyres are only 1.0 m away from the aircraft centreline (compared to 2.1 m for the baseline design), which is significantly less than anticipated by Oosterom [10]. When mounting the engines on top of the landing gear fairing, this implies that engines would have to be mounted very close to each other. Relatively, the gear takes up an even larger portion of the area inboard of the rear spar, compared to the FV-1000. In addition, retraction feasibility is questionable for the FV-800. As can be observed in the baseline gear retraction path visualisation in Figure 5.15, the retraction path extends significantly further inboard than the final retracted position. For a single folding strut, this phenomenon is pronounced, as there is no upper strut to simultaneously move the shock strut pivot axis outboard. Therefore, for the FV-800, the left and right landing gear are likely to collide when retracted simultaneously.

For completeness, another FV-800 stick model is generated, but now specifically sized for the FV-800, not adhering to the design commonality principle. The resulting stick model is illustrated in Figure 5.19. Although tyres are now 1.8 m away from the aircraft centreline, the distance is still smaller than for the baseline design. Also the fairing width can be reduced, but is still needs to be 0.4 larger than that of baseline concept. Still, the retraction feasibility remains questionable. This comes at the expense of having no structural commonality in the gear, as well as the aircraft attachment structure (slightly

different folding angle) and fairing.

In summary, the single folding strut has significant drawbacks. The increased fairing width, reduced fuel tank volume, and family design challenges make the concept infeasible for the Flying-V. Therefore, further exploration of this concept is discontinued.

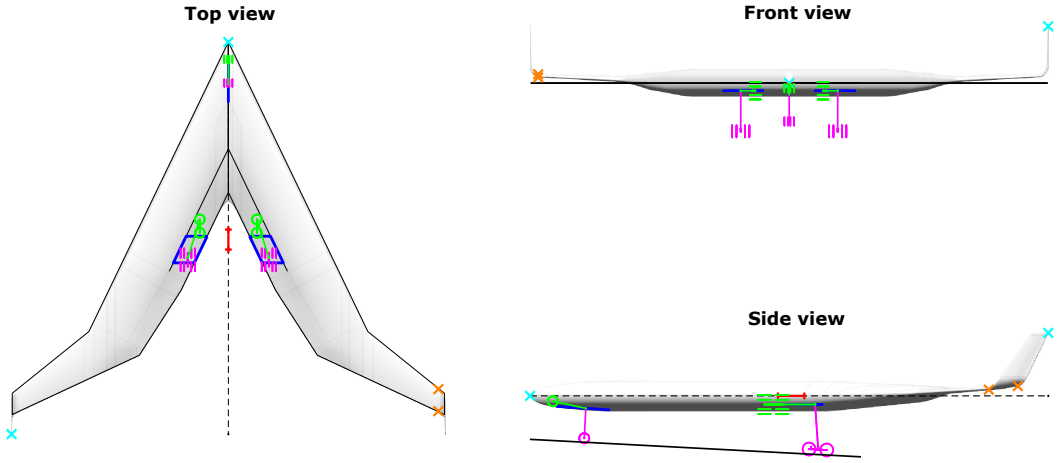

Figure 5.17: FV-1000 single folding strut concept landing gear stick model.

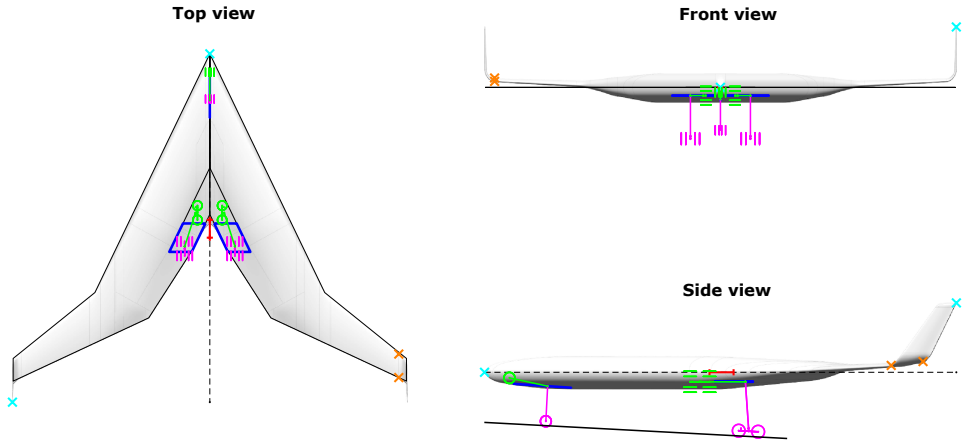

Figure 5.18: FV-800 single folding strut concept landing gear stick model. Gear sized for FV-1000 (maximum commonality).

6-Wheel Bogie Concept

Input adjustments for the 6-wheel bogie concept are outlined in Table 5.18. Compared to the baseline concept, the total number of main gear wheels is increased from 8 to 12. The bogie width, length and tyre selection are aligned with the A350-1000. The gear attachment is lowered to ensure the tyres remain beneath the upper wing surface when retracted. Despite the bogie being narrower, the increase in bogie length causes the aft tyres to be situated closer to the trailing edge, where the upper wing surface is lower. Additionally, the upper strut length is decreased to prevent collision during retraction. As can be observed in Figure 5.15, an increase in bogie length would otherwise cause the gear to collide with the upper strut trunnion when retracted. Reducing the upper strut length effectively positions the retracted bogie further forward.

The FV-1000 6-wheel bogie concept landing gear stick model is illustrated in Figure 5.20, with design vector results, constraint activity, and stick model results outlined in Tables 5.15, 5.16 and 5.17, respectively. Compared to the baseline concept, the reduced bogie width results in the main gear being positioned slightly further outboard. Together with bogie articulation being more effective due to the increased bogie length, this resulted in a shorter main gear. Consequently, also the nose gear is shorter,

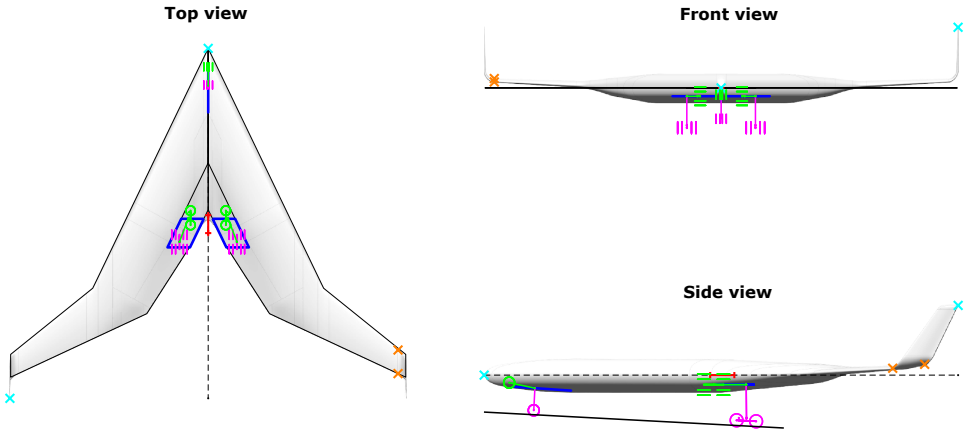

Figure 5.19: FV-800 single folding strut concept landing gear stick model. Gear sized for FV-800 (maximum optimality).

Table 5.19: Concept variation input adjustments - 6-wheel bogie concept (C2).

Item	Unit	Format	Baseline	Concept C2
MDS_A	m	(x, y, z)	(29.2, 3.17, -0.25)	(29.2, 3.17, -0.30)
MDS_B	m	(x, y, z)	(33.2, 5.10, -0.25)	(33.2, 5.10, -0.30)
MDS_C	m	(x, y, z)	(29.2, 6.32, -0.25)	(29.2, 6.32, -0.30)
MDS_D	m	(x, y, z)	(33.2, 8.25, -0.25)	(33.2, 8.25, -0.30)
l_{us}	m	-	2.10	1.92
$N_{mlg,w}$	-	-	8	12
l_{bogie}	m	-	2.02	2.80
w_{bogie}	m	-	1.62	1.47
$Tyre_{mlg}$	-	-	1400x530R23 (42 ply)	50x20R22 (32 ply)

which could therefore be positioned further forward, resulting in a smaller nose gear load fraction. The shorter gears lower the static height of the centre of gravity, which enhances lateral stability as indicated by the lateral turnover angle ψ_{tno}.

It must be noted that, contrary to the other concepts, both the static and extended shock absorber ground clearance constraints are active, and that the articulation angle is only $18.1°$, whereas $25°$ is permitted. This indicates that for the 6-wheel bogie, articulation is so effective that the gear length could be decreased to what is necessary for static ground clearance. The $18.1°$ articulation angle is already sufficient to meet the extended shock absorber ground clearance requirement. A larger angle would result in a longer extended shock absorber gear length, increasing gear mass.

The corresponding 6-wheel bogie tyre loading diagram is shown in Figure 5.21. It can be observed that the nose gear load has been decreased slightly compared to the baseline concept, which can be explained by the nose gear being positioned slightly further forward. Although this results in a larger main gear load fraction, this is more than compensated for by the increase in number of tyres, which have a greater combined load rating. It must be noted that, contrary to the baseline concept, the 6-wheel bogie concept supports a larger main gear load fraction (e.g., more downforce) with the added possibility to upgrade the tyre selection if necessary.

Aircraft Classification Ratings (ACR) for the 6-wheel bogie concept (C2), baseline concept (BL) and A350-900 are outlined in Table 5.20. Values are obtained using the ICAO-ACR tool [47]. Comparing the numbers, it can be concluded that the 6-wheel bogie concept exhibits significantly better flotation performance compared to both the baseline concept and A350-900. As for the baseline results in Table 5.11, it must be noted that these numbers are based on static loads without considering the effect of downforce generation. The table shows that baseline concept results are very close to those of the A350-900, while the 6-wheel bogie concept has some margin, suggesting that the latter is bet-

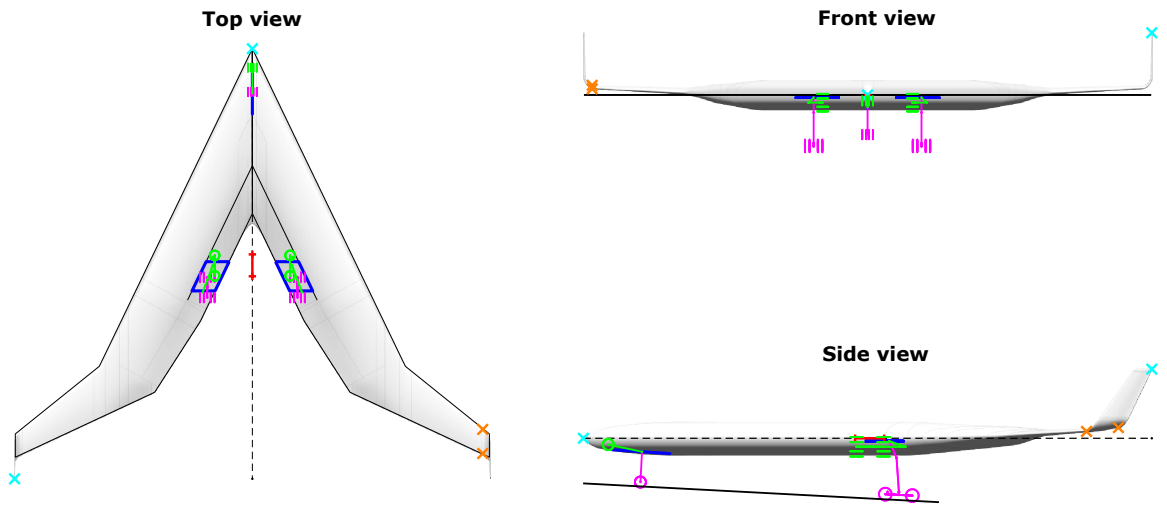

Figure 5.20: FV-1000 6-wheel bogie concept (C2) landing gear stick model. Only shows front and rear main gear tyres.

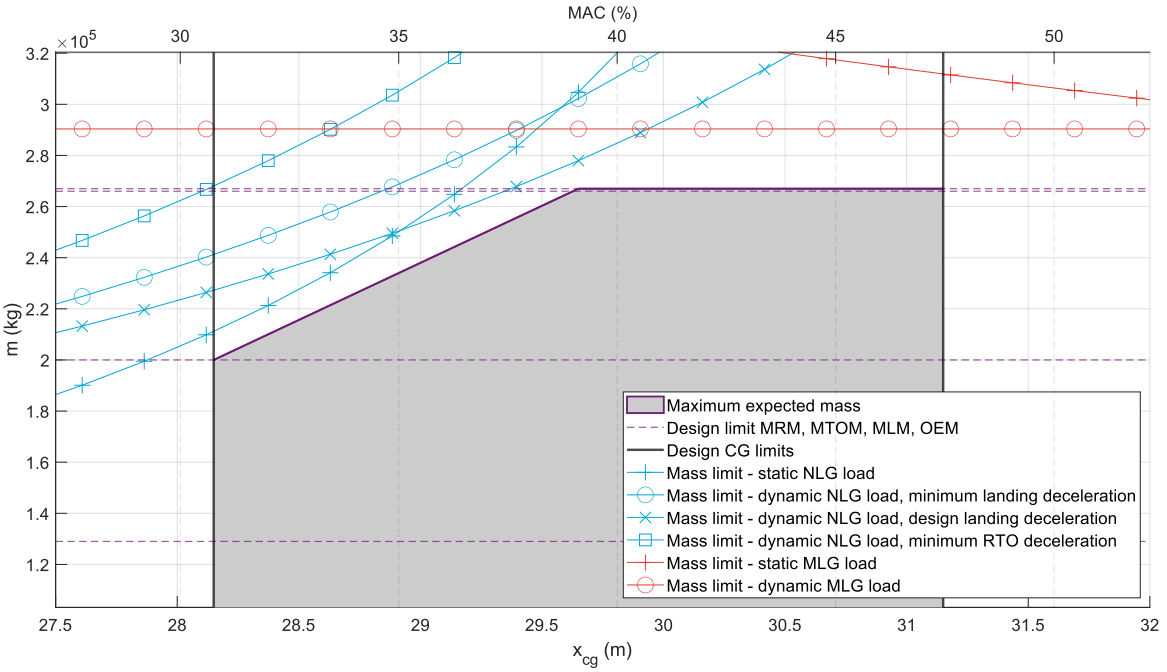

Figure 5.21: FV-1000 6-wheel bogie concept (C2) gear loading diagram.

ter equipped to handle additional loads from downforce generation without leading to unsatisfactory flotation performance.

Table 5.20: FV-1000 6-wheel bogie concept (C2) flotation (ACR) comparison, obtained using the ICAO-ACR tool [47].

Subgrade category	Flexible ACR			Rigid ACR		
	A350-900	BL	C2	A350-900	BL	C2
D	884	868	719	1031	1003	891
C	742	723	509	918	894	752
B	692	670	451	825	803	631
A	680	655	432	729	708	503

Upper strut and shock strut folding axis orientations $\hat{\mathbf{v}}_1$ and $\hat{\mathbf{v}}_2$ corresponding to the 6-wheel bogie concept are specified in Equation 5.2.

$$\hat{\mathbf{v}}_1 = \begin{pmatrix} 0.32 \\ -0.92 \\ 0.24 \end{pmatrix}, \quad \hat{\mathbf{v}}_2 = \begin{pmatrix} 0.73 \\ -0.62 \\ 0.29 \end{pmatrix} \tag{5.2}$$

Figures 5.22a and 5.22b illustrate the 6-wheel bogie concept 3D gear model, along with the corresponding refined stick model (in orange) used for structural analysis. Node locations are outlined in Table D.4 in Appendix D, and are defined similar to Figure 5.14, only with four additional nodes representing the centre wheel axle and tyres. The retraction path is very similar to the baseline concept, and is illustrated in Figure D.4. Compared to the baseline, apart from inherent changes due to the stick model and the added wheel axle, several modifications are made. Bogie articulation linkages need to be longer to facilitate 'flat-packing' of the longer bogie. In addition, braces are repositioned to account for the different folding angles and stick model adjustments.

Notably, the fixed length brace supporting the shock strut is attached further forward, providing more lateral but less longitudinal (drag) support to the gear. This repositioning is a natural effect of the shorter gear. Because the brace length is fixed, and the brace to gear joint location is determined by both the extended and retracted positions of the shock strut, the brace cannot be placed freely. A shorter gear reduces the required brace length, inherently necessitating it to be attached further forward.

(a) Left isometric view. **(b)** Right isometric view.

Figure 5.22: FV-1000 6-wheel bogie concept (C2) right main landing gear 3D model and refined stick model in orange.

Bogie Articulation Exclusion Concept

Table 5.21 outlines the baseline design input adjustments to develop a FV-1000 landing gear configuration without an articulation mechanism (concept C3). The bogie articulation feature is removed, and associated parameters are no longer applicable. To address the subsequent increase in shock strut length, the upper strut length is extended to use the full potential of the double folding strut in terms of stowage. Because the upper strut is raked down in the retracted position, the extension of the upper strut results in the retracted bogie being situated lower than in the baseline configuration. Consequently, the attachment point is repositioned upwards to maintain the aerodynamically efficient placement of the stowed bogie just below the upper wing surface.

The resulting FV-1000 stick model is illustrated in Figure 5.23. Design vector results, constraint activity and stick model results are detailed in Tables 5.15, 5.16 and 5.17, respectively. Comparing the results of concept C3 with the baseline, it is found that excluding the articulation mechanism necessitates a significant increase in gear length (0.6 m for the extended gear). This increase is primarily due to the absence of bogie leverage when the shock absorber extends. The difference in static gear length is

Table 5.21: Concept variation input adjustments - bogie articulation exclusion concept (C3).

Item	Unit	Format	Baseline	Concept C3
MDS_A	m	(x, y, z)	(29.2, 3.17, -0.25)	(29.2, 3.17, -0.20)
MDS_B	m	(x, y, z)	(33.2, 5.10, -0.25)	(33.2, 5.10, -0.20)
MDS_C	m	(x, y, z)	(29.2, 6.32, -0.25)	(29.2, 6.32, -0.20)
MDS_D	m	(x, y, z)	(33.2, 8.25, -0.25)	(33.2, 8.25, -0.20)
l_{us}	m	-	2.10	2.44
Articulation	-	Boolean	True	False
$\lambda_{mlg,art}$	-	-	0.35	N.A.
θ_{bogie}	°	$x_{lb} \leq x_0 \leq x_{ub}$	$0.00 \leq 0.00 \leq 25.0$	N.A.
$l_{x,pivot}$	m	-	0.22	N.A.
$l_{z,pivot}$	m	-	0.26	N.A.
$l_{margin,art}$	m	-	0.10	N.A.

even more pronounced. The absence of articulation allows the shock absorber to sustain a higher reaction force throughout its stroke, thereby reducing the total SA stroke length. Although this shorter stroke benefits the overall length of the shock absorber piston, it ultimately results in an increased static gear length because the gear must be designed to maintain the required ground clearance in its extended state. Having a longer static gear length, concept C3 inherently features a larger static shock absorber ground clearance angle $\theta_{max,statSA}$.

To still obtain a $-3°$ static attitude, also the nose gear length is increased, which necessitates repositioning it further aft to ensure sufficient clearance from the front pressure bulkhead. The increased static height of the aircraft centre of gravity reduces lateral and longitudinal stability, as displayed by the lateral turnover angle θ_{tpb} and tipover angle ψ_{tno}.

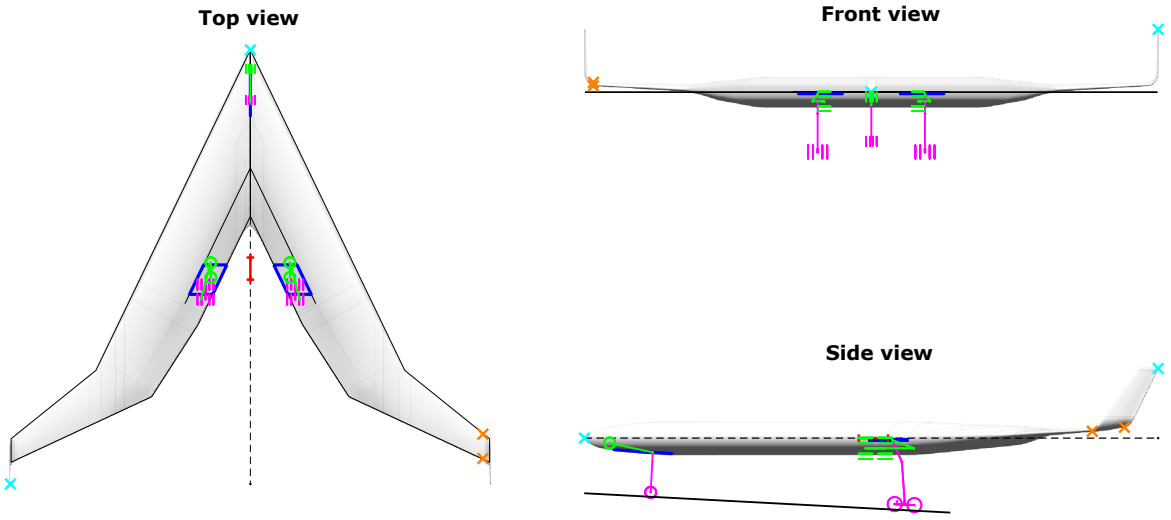

Figure 5.23: FV-1000 bogie articulation exclusion concept (C3) landing gear stick model.

Unit vectors $\hat{\mathbf{v}}1$ and $\hat{\mathbf{v}}2$, which define the orientations of the upper strut and shock strut in concept C3, are presented in Equation 5.3. Since concept C3 shares nearly identical gear folding angles with the baseline concept, folding axis orientations are effectively the same.

$$\hat{\mathbf{v}}_1 = \begin{pmatrix} 0.28 \\ -0.95 \\ 0.14 \end{pmatrix}, \quad \hat{\mathbf{v}}_2 = \begin{pmatrix} 0.73 \\ -0.62 \\ 0.30 \end{pmatrix} \tag{5.3}$$

The bogie articulation exclusion concept 3D gear model is displayed in Figures 5.24a and 5.24b. Based

on the 3D model, the stick model is refined. This is depicted in orange. Node specifications and retraction kinematics are detailed in Table D.5 and Figure D.5, respectively, in Appendix D. Similar to the other concepts, braces are repositioned to match the upper strut and shock strut dimensions. The bogie articulation mechanism is removed from the model.

(a) Left isometric view. **(b)** Right isometric view.

Figure 5.24: FV-1000 bogie articulation exclusion concept (C3) right main landing gear 3D model and refined stick model in orange.

Strut Shortening Exclusion Concept

Baseline concept input parameters are adjusted to eliminate the strut shortening mechanism, as outlined in Table 5.22. The shock strut is no longer shortened during retraction, requiring an increase in upper strut length to maintain an efficient and feasible stowed bogie position. Because the upper strut is raked down in the retracted position, this increase in length results in the bogie being positioned lower when folded. To address this, the attachment height is increased, ensuring that the tyres retain a consistent location beneath the upper wing surface compared to the baseline design.

Table 5.22: Concept variation input adjustments - strut shortening exclusion concept (C4).

Item	Unit	Format	Baseline	Concept C4
MDS_A	m	(x, y, z)	(29.2, 3.17, -0.25)	(29.2, 3.17, -0.20)
MDS_B	m	(x, y, z)	(33.2, 5.10, -0.25)	(33.2, 5.10, -0.20)
MDS_C	m	(x, y, z)	(29.2, 6.32, -0.25)	(29.2, 6.32, -0.20)
MDS_D	m	(x, y, z)	(33.2, 8.25, -0.25)	(33.2, 8.25, -0.20)
l_{us}	m	-	2.10	2.40
Shortening	-	Boolean	True	False
$l_{shortening}$	m	-	0.50	N.A.

The stick model corresponding to the shortening exclusion concept (concept C4) is illustrated in Figure 5.25. Similar to the other concepts, design vector results, constraint activity and stick model results are outlined in Tables 5.15, 5.16 and 5.17, respectively. Fundamentally, the extended gear stick model is very similar to the baseline concept. Effectively, the concept only significantly deviates from the baseline when it comes to the upper strut and shock strut lengths. Notably, the shock strut is shortened to compensate for the lack of strut shortening and increase in upper strut length, maintaining a consistent stowed bogie position. Because the upper strut has a larger rake angle compared to the shock strut, this also results in a slight deviation when it comes to the attachment position and the total gear length, maintaining the same ground contact points.

Concept C4 upper strut and shock strut folding axis orientation vectors $\hat{\mathbf{v}}1$ and $\hat{\mathbf{v}}2$, are specified in Equation 5.4.

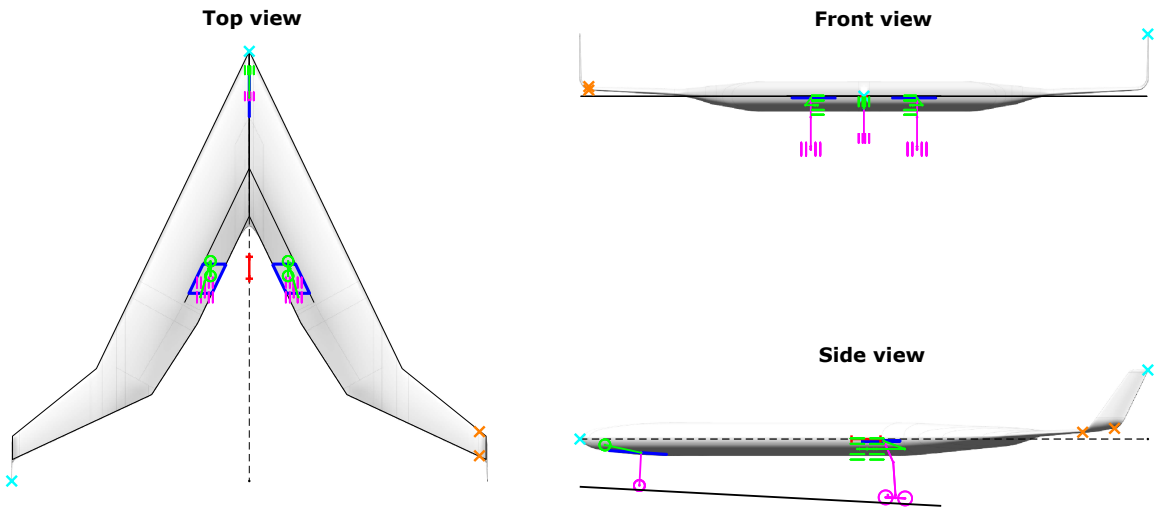

Figure 5.25: FV-1000 strut shortening exclusion concept (C4) landing gear stick model.

$$\hat{\mathbf{v}}_1 = \begin{pmatrix} 0.29 \\ -0.94 \\ 0.17 \end{pmatrix}, \quad \hat{\mathbf{v}}_2 = \begin{pmatrix} 0.73 \\ -0.62 \\ 0.30 \end{pmatrix} \tag{5.4}$$

Figure 5.26 illustrates the resulting 3D gear model and refined stick model in orange. Compared to the baseline, braces are repositioned to accommodate the longer upper strut, shorter shock strut and slightly different folding angles. Without strut shortening, the articulation mechanism linkages need to be longer to be able to achieve the desired retracted bogie position. Concept C4 kinematics and node specifications are outlined in Figure D.6 and Table D.6, respectively, in Appendix D.

(a) Left isometric view. **(b)** Right isometric view.

Figure 5.26: FV-1000 strut shortening exclusion concept (C4) right main landing gear 3D model and refined stick model in orange.

Backward Stowage Concept

Table 5.23 presents baseline concept input adjustments to obtain the backward stowage gear concept. Instead of having the upper strut fold backward, and the shock strut and bogie fold forward, the upper strut now folds forward, and the shock strut and bogie fold backward. This is represented by the

retracted gear orientation angles $\theta_{ss,ret}$ and $\theta_{us,ret}$. Consequently, the drop-link arrangement is reversed, with the upper strut now raked forward instead of backward. The design variable range is adjusted such that the optimiser can keep a $20°$ difference between the shock strut and upper strut, as for the baseline concept.

The baseline design optimisation function includes the objective to minimise the distance between the main gear tyres and rear spar. For the backward stowage concept, this specific objective is disregarded, as this would result in the optimiser maximising the retracted gear angle $\psi_{mlg,ret}$ (Figure 3.9c), thereby requiring a wide fairing for stowage, which is undesirable. Instead, $\psi_{mlg,ret}$ is limited to $10°$, ensuring compact but feasible stowage. The upper strut length and attachment height are adjusted to keep the tyres clear from the upper strut trunnion and upper wing surface, respectively.

Table 5.23: Concept variation input adjustments - backward stowage concept (C5).

Item	Unit	Format	Baseline	Concept C5
MDS_A	m	(x, y, z)	(29.2, 3.17, -0.25)	(29.2, 3.17, -0.35)
MDS_B	m	(x, y, z)	(33.2, 5.10, -0.25)	(33.2, 5.10, -0.35)
MDS_C	m	(x, y, z)	(29.2, 6.32, -0.25)	(29.2, 6.32, -0.35)
MDS_D	m	(x, y, z)	(33.2, 8.25, -0.25)	(33.2, 8.25, -0.35)
$\theta_{ss,ret}$	°	-	90.0	-90.0
$\psi_{mlg,ret}$	°	$x_{lb} \leq x_0 \leq x_{ub}$	$0.0 \leq 20.0 \leq 45.0$	$0.0 \leq 0.0 \leq 10.0$
l_{us}	m	-	2.10	1.90
$\theta_{us,ext}$	°	$x_{lb} \leq x_0 \leq x_{ub}$	$-24.0 \leq -22.0 \leq -20.0$	$16.0 \leq 18.0 \leq 20.0$
$\theta_{us,ret}$	°	-	-70.0	70.0

The resulting landing gear stick model is illustrated in Figure 5.27. The design vector, constraint activity and stick model results are outlined in Tables 5.15, 5.16 and 5.17, respectively. Logically, the ground contact point locations remain unchanged, which can be observed from the taxiway design group constraint activity, and nose gear and stability results. As the upper strut is reversed, this can only be achieved by moving the gear attachment further aft and further inboard relative to the rear spar. Compared to the baseline, the gear is slightly shorter, which can be attributed to the reduced upper strut length. Since the bogie now points aft when retracted, the lateral location of the retracted gear is no longer limited by the rear spar. Other backward stowage gear concept results are very similar to baseline.

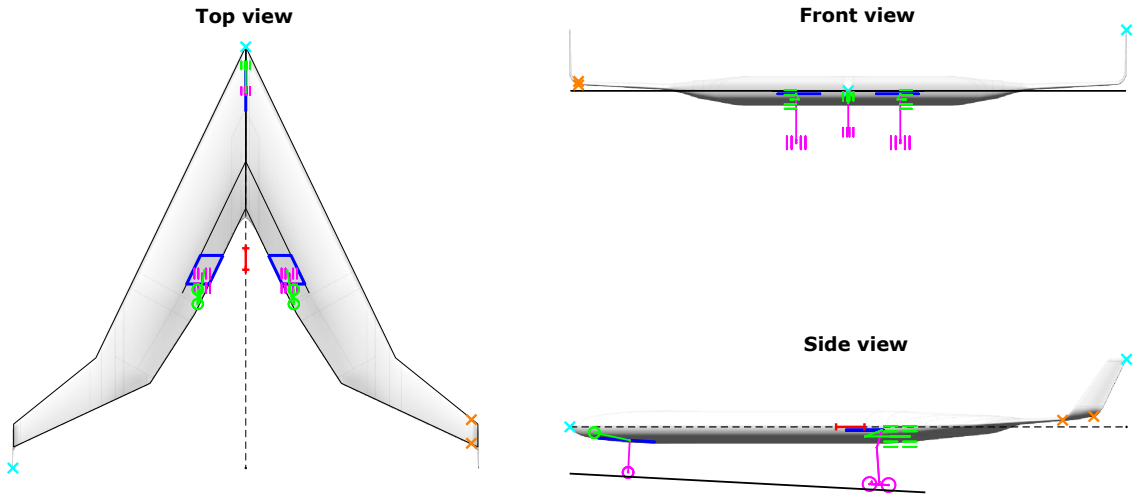

Figure 5.27: FV-1000 backward stowage concept (C5) landing gear stick model.

Folding axis orientations are described by Equation 5.5. The 3D gear model and subsequent refined stick model are shown in Figure 5.28, and retraction kinematics are illustrated in Figure 5.29. Refined stick model node specifications are outlined in Table D.7 in Appendix D.

The bogie articulation mechanism needs to facilitate bogie articulation as well as 'flat-packing' for stowage. For articulation, the mechanism needs to 'pull-up' the leading side of the bogie, while for stowage, this leading side needs to be 'pushed down' to align the bogie with the strut as illustrated in Figure 5.29. In order to have enough room for the mechanism itself, it needs to be placed on the exterior (obtuse) side of the bogie-strut connection. Contrary to the baseline concept, where the leading side of the bogie becomes the obtuse angle side upon retraction, for the reverse stowage concept, this becomes the acute angle side this, as can be observed when comparing the right bottom images in Figures 5.15 and 5.29. Practically, this implies that the bogie orientation needs to be reversed upon retraction, such that the leading side of the bogie in extended position becomes the trailing side when the gear is retracted. Consequently, the folding axes are oriented more aggressively relative to each other compared to the baseline configuration, which can be observed in the Figures. Braces are repositioned accordingly.

$$\hat{\mathbf{v}}_1 = \begin{pmatrix} 0.09 \\ 0.94 \\ 0.34 \end{pmatrix}, \quad \hat{\mathbf{v}}_2 = \begin{pmatrix} 0.78 \\ 0.59 \\ -0.19 \end{pmatrix} \tag{5.5}$$

(a) Left isometric view. **(b)** Right isometric view.

Figure 5.28: FV-1000 reverse stowage concept (C5) right main landing gear 3D model and refined stick model in orange.

A side effect of reversing the bogie orientation direction is that the gear swings further inboard compared to the baseline. Although this does not present any issues for the FV-1000 and FV-900 models, for the FV-800, to prevent the left and right gears from colliding when retracting simultaneously, a significant portion of strut shortening and bogie folding must occur before the bogie reaches its most inboard position.

5.4.2. Structural Sizing

In this section, the structural sizing of the Flying-V baseline gear concept variations is discussed. Structural sizing is conducted for all concept variations except the single folding strut concept. Each gear model is subjected to the same load cases (Table 2.2) and boundary conditions as the baseline gear model (Table 5.12). A detailed description of the load cases can be found in Table A.1 in Appendix A.

Final structural sizing results are outlined in Table 5.24. An overview of external main gear loads, critical load cases, and detailed structural sizing results for each member can be found in Appendix D.2.2 for each concept. As for the baseline concept, most structural members are sized by ground handling load cases, which pose significant loads to the structure due to downforce generation. For all concepts, external loads are virtually the same. Interestingly, however, the differences in structural mass between landing gear concepts are significant.

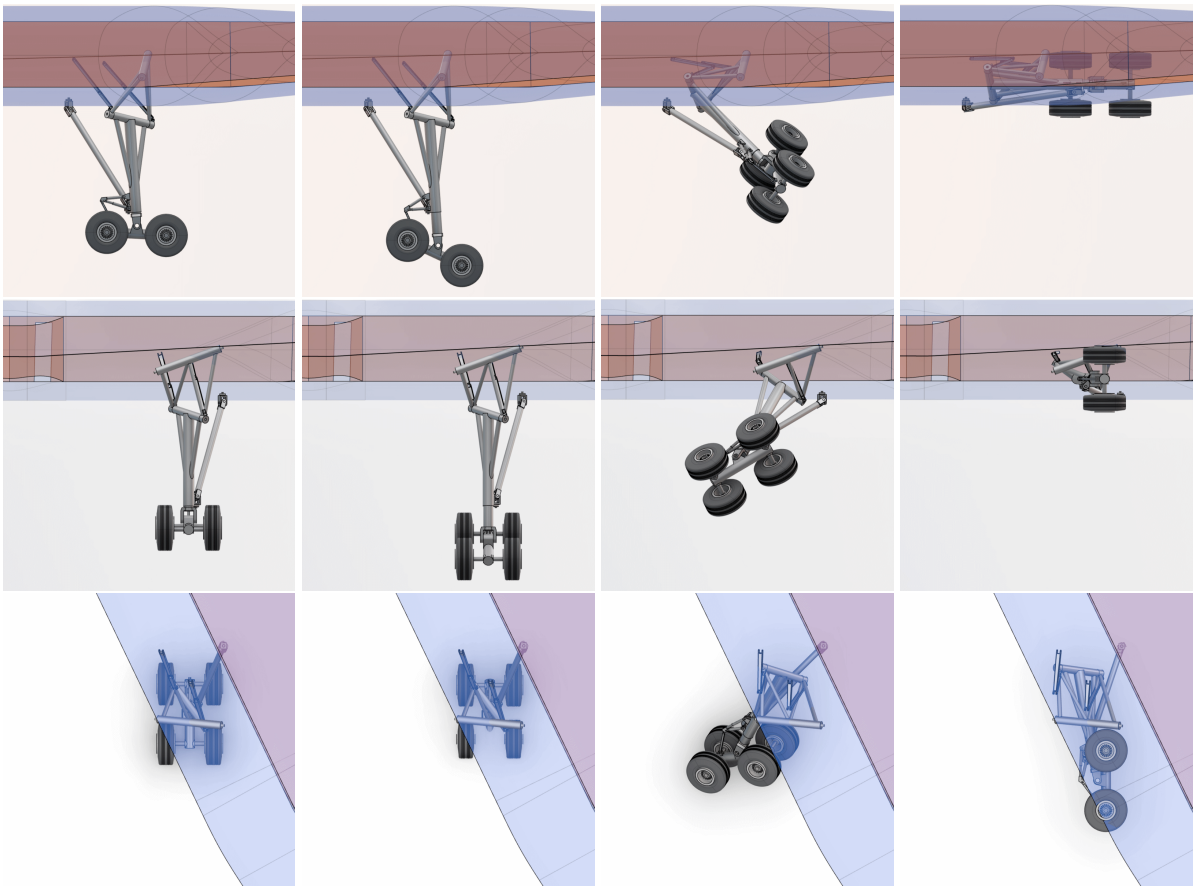

Figure 5.29: FV-1000 main landing gear reverse stowage concept (C5) retraction kinematics, left view, back view and top view.

6-Wheel Bogie Concept

A comparison of 6-wheel bogie concept and baseline concept structural sizing results (Table 5.24) reveals that the structural mass of the 6-wheel bogie concept is higher. Naturally, the distribution of loads over a larger number of tyres results in lighter wheel axles; however, the bogie beam is heavier due to the additional length required to accommodate the third wheel axle. Furthermore, the increased articulation and bogie folding stroke necessitates a longer shock strut piston and extended articulation mechanism members, which also contribute to the increased mass.

Notably, a significant increase in trunnion mass can be observed. Compared to the baseline, the shorter gear requires the fixed length brace connecting the shock strut to the airframe to be attached further forward, providing less support to the gear in longitudinal (drag) direction. Consequently, drag loads, more specifically braking loads and spin-up loads, induce larger reaction loads in the total landing gear structure, most prominently increasing the required wall-thickness of the trunnions. It must be noted that constant wall-thickness is assumed, and that the load increase in the trunnions is only local, suggesting potential for optimisation if variable wall thickness were considered.

Bogie Articulation Exclusion Concept

Structural analysis of concept C3 reveals that removing the articulation mechanism leads to an increase in landing gear primary structure mass. Although the mass of the mechanism itself is eliminated and the shock absorber stroke and associated piston length is reduced, the gear strut needs to be considerably longer. Consequently, the mass of drop link assembly members and the shock strut cylinder is increased. In addition, a longer gear imposes greater leverage for drag and side loads, requiring the trunnions and braces to support higher reaction loads, resulting in greater mass. Notably, the mass of the fixed-length brace connecting the shock strut to the airframe (shock strut brace 3) increases substantially. This is due to the brace having to be longer to connect to the extended landing gear, which naturally increases the material volume while also making it more susceptible to buckling.

Table 5.24: FV-1000 concept variations structural member sizing results. Nodes are defined as illustrated in Figure 5.14.

Member	Nodes	BL (kg)	C2 (kg)	C3 (kg)	C4 (kg)	C5 (kg)
Upper strut trunnion	D1-D2-O1-D3-D4	191.2	250.7	201.8	181.0	319.8
Drop link member 1	D2-D5	77.6	78.9	117.0	93.6	89.5
Drop link member 2	O1-D5	27.9	29.7	46.8	40.1	38.3
Drop link member 3	O1-D6	23.7	21.3	27.1	26.7	42.6
Drop link member 4	D3-D6	64.6	84.0	66.4	44.3	54.7
Drop link brace 1	C2-C4	23.1	23.0	24.8	23.6	82.3
Drop link brace 2	C1-C3	65.1	62.9	89.2	70.5	37.3
Shock strut trunnion	D5-S1-O2-S3-D6	206.8	250.4	220.4	196.4	289.2
Shock strut cylinder	O2-S4-S6-S7-S8	622.5	658.0	775.6	551.9	710.2
Shock strut piston	S8-B1	280.9	313.8	254.0	279.5	283.0
Shock strut brace 1	S1-S3	99.8	90.1	115.0	87.0	114.3
Shock strut brace 2	S2-S5	79.8	110.6	96.6	54.0	67.3
Shock strut brace 3	C5-C6	151.2	128.9	283.6	167.3	108.2
Bogie beam	K-B2-L	275.3	344.7	270.9	275.3	275.5
Aft wheel axle	K_L-K_R	132.2	73.5	130.8	131.4	131.6
Centre wheel axle	P_L-P_R	-	73.5	-	-	-
Front wheel axle	L_L-L_R	132.2	73.5	130.8	131.3	131.6
AM member 1[1]	A1-A4	30.8	54.0	-	51.1	32.1
AM member 2[1]	A2-A3	13.6	19.2	-	28.4	14.0
AM member 3[1]	A5-A6	11.3	11.1	-	13.7	11.0
Shortening members	-	9.8	9.8	9.7	-	9.8
Total	-	2519	2762	2861	2447	2843

[1] Articulation mechanism.

Strut Shortening Exclusion Concept

When the strut shortening mechanism is removed, it leads to a reduction in structural gear mass. While the elimination of the shortening mechanism contributes to this mass reduction, it is not the primary factor. With the removal of the mechanism, the upper strut length is increased to accommodate the longer extended shock strut in the stowed position. However, since the gear does not need to be longer in the extended position, the shock strut length is reduced. The longer upper strut assembly members (drop link members and braces), result in a slight mass increase but this is outweighed by the significant reduction in the mass of the shock strut cylinder.

Backward Stowage Concept

The backward stowage concept is significantly heavier than the baseline concept. For all other concepts, the fixed-length brace connecting the shock strut to the airframe is subjected to compressive stress during braking. Although this results in slightly higher brace mass due to buckling criteria, this compressive force relieves the upward reaction load (compressive stress) and resulting bending moments in the shock strut, upper strut assembly, and trunnions, overall leading to a reduction in mass. In contrast, backward stowage requires the mounting direction of the fixed length brace connecting the shock strut to the airframe to be inverted, causing braking loads to induce tensile stress rather than compressive stress within the brace. Although this is favourable for the mass of the brace itself, as it is no longer sized by buckling, the tensile stress induces additional compressive stress and internal bending moments in the shock strut, upper strut assembly, and trunnions, resulting in higher overall mass.

5.5. Family Design

The baseline gear concept is based on maximum commonality between the Flying-V family members, with the FV-800 and FV-900 landing gear structural sizing and integration being based on the requirements of the FV-1000. Although commonality is favourable for aircraft viability, it is expected to com-

promise FV-800 and FV-900 performance in terms of mass, stowage or even feasibility. In this section, dedicated landing gear concepts for the FV-800 and FV-900 are presented. Being specifically sized and optimised for each aircraft, this allows for the evaluation of the benefits of using dedicated gear for each family member.

5.5.1. Gear Model Generation

Dedicated FV-800 and FV-900 gear models are presented in this section. For both aircraft, single optimisation (SO) input adjustments are outlined, followed by stick model and 3D gear model results. Because single optimisation might impose different gear locations and tyre loads, tyre loading diagrams, flotation comparisons and turning radii are also discussed.

FV-800

Single optimisation input adjustments for the FV-800 are detailed in Table 5.28. The bogie size is reduced to better match the lower mass of the aircraft. The adjusted bogie length l_{bogie} and w_{bogie} are similar to the Boeing 767-300, which has a comparable maximum take-off mass [62]. Only the width is increased slightly to accommodate room for the shock strut support brace when the bogie is folded. The main gear tyre selection is still similar to the baseline FV-800 concept, however, the nose gear tyres are aligned with the lower nose gear load fraction.

With the main gear width no longer constrained by taxiway design group limitations, the optimiser would normally position the gear as far outboard as possible to achieve a shorter gear. However, this results in significant inboard rotation of the gear during retraction to maintain clearance from the rear spar, increasing the stowed gear width and necessitating a wider, less aerodynamic fairing. To prevent this, the strut folding angle $\psi_{\text{mlg,ret}}$ is limited to 14.4° (baseline result), which slightly increases gear length but significantly reduces the fairing width requirement.

Compared to the FV-800 baseline gear, the optimised gear includes bogie articulation. The articulated gear (phase 1) reaction factor has been adjusted to maximise energy absorption during the de-articulation phase while maintaining sufficient margin to ensure that all wheels contact the ground when the aircraft is at its minimum possible mass. The strut shortening amount has been set to 0.5 m, similar to that of the A330-300 and FV-1000.

The upper strut length and attachment height have been adjusted to optimise the position of the tyres relative to the upper strut trunnion and upper wing surface, respectively.

The FV-800 single optimisation landing gear stick model is illustrated in Figure 5.30. The final design vector, constraint activity and stick model results are outlined in Tables 5.25, 5.26 and 5.27, respectively. Compared to the FV-800 baseline gear design, the main gear and nose gear are significantly shorter. Consequently, the single optimisation gear offers a lower aircraft centre of gravity, hence improved lateral stability as reflected by the lateral turnover angle ψ_{tno}. In addition, because the nose gear is shorter, it could be moved further forward, reducing the nose gear load fraction. A lower nose gear load fraction results in lower nose gear loads, allowing for a different tyre selection. The updated tyre loading diagram is shown in Figure D.7 in Appendix D.

Turning radii are shown in Figure D.8. Compared to the FV-800 baseline gear design, the longer wheelbase shifts the turning centre outward, leading to an increase in all turning radii. However, relative to the wing tip, however, this change is only marginal, and consequently, the wing tip turning radius, which poses the greatest limitation, is very similar to the baseline.

Single optimisation gear design Aircraft Classification Ratings (ACR) are compared with the baseline and A350-900 in Table 5.29. The higher main gear load fraction and smaller bogie result in a slightly worse flotation performance compared to the baseline configuration. However, it is important to note that the design still performs significantly better than the A350-900. As with other flotation analyses presented in this study, these results are based on static load assumptions, which do not take into account dynamic factors such as downforce generation after touchdown or during a rejected take-off.

Upper strut and shock strut folding axis orientations are given by unit vectors $\hat{\mathbf{v}}_1$ and $\hat{\mathbf{v}}_1$, respectively, in Equation 5.6. The FV-800 single optimisation folding angles are similar to the baseline, and therefore, have similar folding axis orientations.

Table 5.25: Flying-V family baseline (BL) and single optimisation (SO) gear concept stick model generation design vectors.

Variable	Unit	x_{lb}	x_0	x_{ub}	FV-800 BL	FV-800 SO	FV-900 BL	FV-900 SO
x_{mlg}	-	0.00	0.50	1.00	0.61	0.60	0.61	0.61
y_{mlg}	-	0.00	0.50	1.00	0.55	0.64	0.55	0.56
x_{nlg}	-	0.00	0.50	1.00	0.60	0.43	0.57	0.48
l_{ss}	m	1.00	2.00	6.00	3.55	2.97	3.55	3.27
$\theta_{ss,ext}$	°	-4.00	-2.00	0.00	-4.00	-4.00	-4.00	-4.00
$\psi_{mlg,ret}$	°	0	20.0	45.00	14.4	14.4	14.4	14.4
$\theta_{us,ext}$	°	-24.0	-22.0	-20.0	-24.0	-24.0	-24.0	-24.0
$\phi_{us,ext}$	°	0.00	0.00	0.00	0.00	0.00	0.00	0.00
θ_{bogie}	°	0.00	0.00	25.0	N.A.	25.0	N.A.	25.0
$\hat{\beta}_{nlg,min}$	-	0.04	0.10	0.20	0.09	0.07	0.08	0.07
$\hat{\beta}_{nlg,max}$	-	0.04	0.10	0.20	0.21	0.19	0.18	0.17

Table 5.26: Flying-V family baseline (BL) and single optimisation (SO) gear stick model generation constraint activity.

Constraint	FV-800 BL	FV-800 SO	FV-900 BL	FV-900 SO
Long. stab. - minimum nlg load	Inactive	Inactive	Inactive	Inactive
Long. stab. - maximum nlg load	**Violated**	Inactive	Inactive	Inactive
Long. stab. - rotated tipover	Inactive	Active	Inactive	Active
Long. stab. - push-back tipover	Inactive	Inactive	Inactive	Inactive
Lat. stab. - lateral turnover	Inactive	Inactive	Inactive	Inactive
Ground clearance - stat. SA	Inactive	Inactive	Inactive	Inactive
Ground clearance - ext. SA	Inactive	Active	**Violated**	Active
Integration - nlg stowage	Active	Active	Active	Active
Integration - mlg stowage	Active	Active	Active	Active
Ground man. - TDG	Inactive	Inactive	Inactive	Inactive
Ground man. - $180°$ turn	Inactive	Inactive	Inactive	Inactive

Table 5.27: Flying-V family baseline (BL) and single optimisation (SO) gear concept stick model results.

Item	Unit	FV-800 BL	FV-800 SO	FV-900 BL	FV-900 SO
X_{mlg}	m	26.3	26.2	29.2	29.1
Y_{mlg}	m	3.52	3.79	4.90	4.93
$l_{mlg,static}$	m	5.70	4.69	5.70	5.14
$l_{mlg,extended}$	m	6.22	5.21	6.22	5.80
X_{nlg}	m	6.40	5.45	6.26	5.74
$l_{nlg,static}$	m	3.64	2.64	3.50	2.93
$l_{nlg,extended}$	m	4.09	3.09	3.95	3.39
θ_{tpb}	°	18.1	18.1	18.1	18.2
ψ_{tno}	°	61.6	55.6	54.1	51.5
ϕ_{max}	°	8.0	8.0	8.0	8.0
$\theta_{max,statSA}$	°	13.9	10.8	11.9	10.4
$\theta_{max,extSA}$	°	16.0	14.0	13.7	14.0
$\beta_{nlg,aftCG}$	-	0.088	0.070	0.077	0.069
$\beta_{nlg,fwdCG}$	-	0.207	0.185	0.181	0.171

Table 5.28: FV-800 single optimisation (SO) input adjustments.

Item	Unit	Format	FV-800 BL	FV-800 SO
MDS_A	m	(x, y, z)	(23.8, 0.62, -0.25)	(23.8, 0.62, -0.20)
MDS_B	m	(x, y, z)	(27.8, 2.54, -0.25)	(27.8, 2.54, -0.20)
MDS_C	m	(x, y, z)	(23.8, 3.77, -0.25)	(23.8, 3.77, -0.20)
MDS_D	m	(x, y, z)	(27.8, 5.70. -0.25)	(27.8, 5.70. -0.20)
$\psi_{mlg,ret}$	°	$x_{lb} \leq x_0 \leq x_{ub}$	$0.0 \leq 20.0 \leq 45.0$	$0.0 \leq 0.0 \leq 14.4$
l_{us}	m	-	2.10	1.68
l_{bogie}	m	-	2.02	1.42
w_{bogie}	m	-	1.62	1.40
$Tyre_{nlg}$	-	-	43x17.5R17 (32 ply)	1050x395R16 (28 ply)
Articulation	-	Boolean	False	True
$\lambda_{mlg,art}$	-	-	N.A.	0.54
θ_{bogie}	°	$x_{lb} \leq x_0 \leq x_{ub}$	N.A.	$0.00 \leq 0.00 \leq 25.0$
$l_{x,pivot}$	m	-	N.A.	0.22
$l_{z,pivot}$	m	-	N.A.	0.26
$l_{margin,art}$	m	-	N.A.	0.10
Shortening	-	Boolean	True	True
$l_{shortening}$	m	-	0.35	0.50

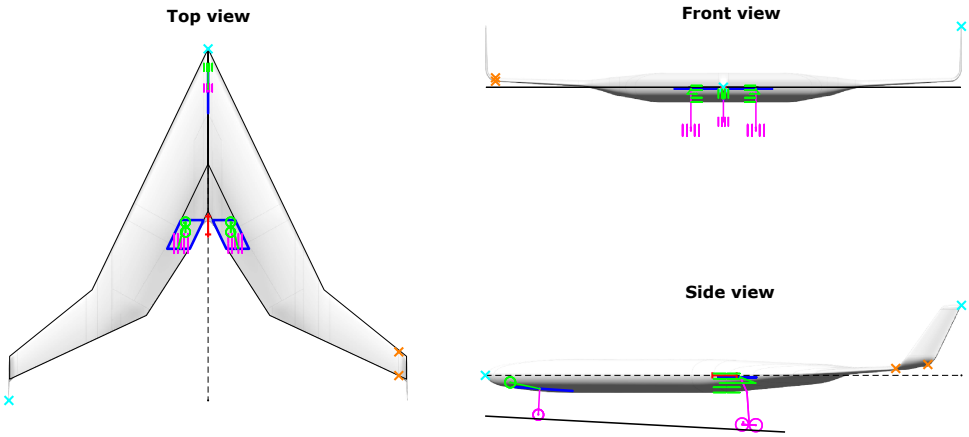

Figure 5.30: FV-800 single optimisation (SO) landing gear stick model.

Table 5.29: FV-800 single optimisation (SO) gear concept flotation (ACR) comparison, obtained using the ICAO-ACR tool [47].

Subgrade category	Flexible ACR			Rigid ACR		
	A350-900	FV-800 BL	FV-800 SO	A350-900	FV-800 BL	FV-800 SO
D	884	510	639	1031	597	733
C	742	462	515	918	533	655
B	692	449	470	825	487	588
A	680	450	453	729	449	512

$$\hat{\mathbf{v}}_1 = \begin{pmatrix} 0.28 \\ -0.95 \\ 0.14 \end{pmatrix}, \quad \hat{\mathbf{v}}_2 = \begin{pmatrix} 0.73 \\ -0.62 \\ 0.30 \end{pmatrix} \tag{5.6}$$

The 3D gear model and refined stick model for structural analysis are illustrated in Figure 5.31. Node specifications and retraction kinematics are detailed in Table D.20 and Figure D.9, respectively, in Appendix D. As for all concept variations, braces are repositioned to match the updated gear geometry.

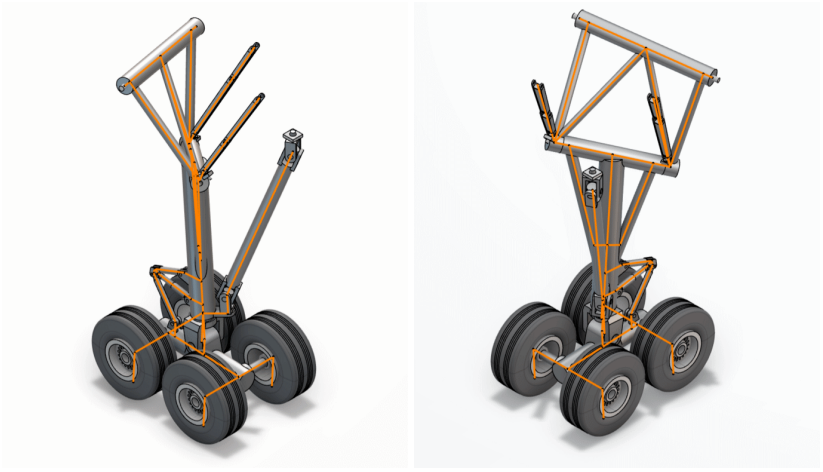

(a) Left isometric view. **(b)** Right isometric view.

Figure 5.31: FV-800 single optimisation (SO) right main landing gear 3D model and refined stick model in orange.

FV-900

Input modifications for the FV-900 gear are outlined in Table 5.30, following a similar approach as for the FV-800. However, this time, the bogie dimensions are based on those of the A330-300 [42], which has a comparable maximum take-off mass to the FV-900.

Table 5.30: FV-900 single optimisation (SO) input adjustments.

Item	Unit	Format	FV-900 BL	FV-900 SO
MDS_A	m	(x, y, z)	(26.7, 1.99, -0.25)	(26.7, 1.99, -0.20)
MDS_B	m	(x, y, z)	(30.7, 3.92, -0.25)	(30.7, 3.92, -0.20)
MDS_C	m	(x, y, z)	(26.7, 5.15, -0.25)	(26.7, 5.15, -0.20)
MDS_D	m	(x, y, z)	(-30.7, 7.07, -0.25)	(-30.7, 7.07, -0.20)
$\psi_{mlg,ret}$	°	$x_{lb} \leq x_0 \leq x_{ub}$	$0.0 \leq 20.0 \leq 45.0$	$0.0 \leq 0.0 \leq 14.4$
l_{us}	m	-	2.10	1.82
l_{bogie}	m	-	2.02	1.98
w_{bogie}	m	-	1.62	1.40
Articulation	-	Boolean	False	True
$\lambda_{mlg,art}$	-	-	N.A.	0.37
θ_{bogie}	°	$x_{lb} \leq x_0 \leq x_{ub}$	N.A.	$0.00 \leq 0.00 \leq 25.0$
$l_{x,pivot}$	m	-	N.A.	0.22
$l_{z,pivot}$	m	-	N.A.	0.26
$l_{margin,art}$	m	-	N.A.	0.10
Shortening	-	Boolean	True	True
$l_{shortening}$	m	-	0.35	0.50

The resulting FV-900 single optimisation stick model is illustrated in Figure 5.32. The final design vector, constraint activity and stick model results are outlined in Tables 5.25, 5.26 and 5.27, respectively. Flotation performance is displayed by the Aircraft Classification Rating comparison in Figure 5.31. A tyre loading diagram and turning radii are shown in Figures D.10 and D.11 in Appendix D. Although numerically different, FV-900 results follow the same fundamental trends as discussed for the FV-800, and consistently fall between those of the FV-800 single optimisation gear concept and FV-900 baseline concept, as expected.

Upper strut and and shock strut folding axis unit vectors are equal to the FV-800 single optimisation gear, as specified in Equation 5.6. The resulting 3D gear model and refined stick model are illustrated in Figure 5.33. FV-900 single optimisation gear node specifications and retraction kinematics are illustrated in Table D.21 and Figure D.12, respectively, in Appendix D.

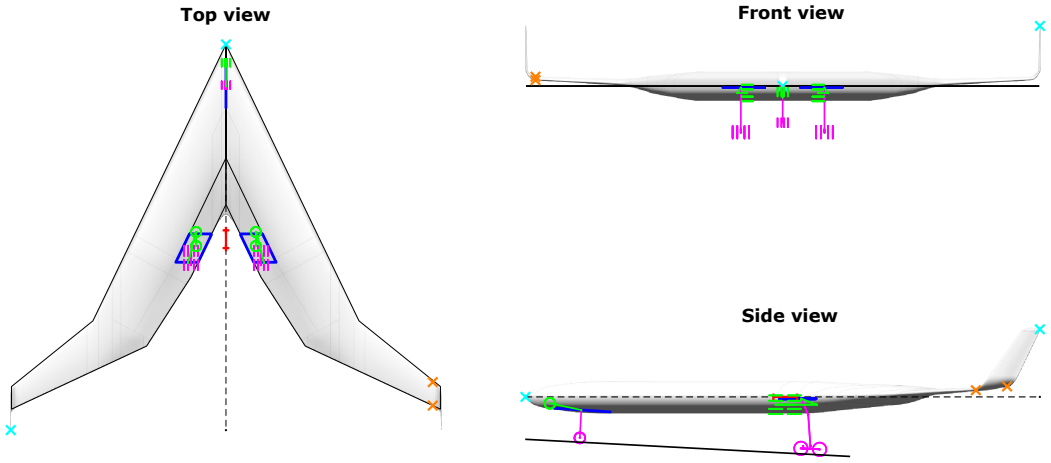

Figure 5.32: FV-900 single optimisation (SO) landing gear stick model.

Table 5.31: FV-900 single optimisation (SO) gear concept flotation (ACR) comparison, obtained using the ICAO-ACR tool [47].

Subgrade category	Flexible ACR			Rigid ACR		
	A350-900	FV-900 BL	FV-900 SO	A350-900	FV-900 BL	FV-900 SO
D	884	703	779	1031	827	889
C	742	609	643	918	735	793
B	692	575	594	825	663	713
A	680	569	577	729	594	630

(a) Left isometric view. **(b)** Right isometric view.

Figure 5.33: FV-900 single optimisation (SO) right main landing gear 3D model and refined stick model in orange.

5.5.2. Structural Sizing

In this section, the structural sizing of dedicated, single optimisation FV-800 and FV-900 main landing gear concepts is discussed. Although each gear model is subjected to the same load cases (Table 2.2) and boundary conditions as the baseline gear model (Table 5.12), specific external loads are aligned with the respective mass and design parameters of the FV-800 and FV-900. Baseline (BL) and single optimisation (SO) structural member sizing results are outlined in Table 5.32. An overview of external main gear loads, critical load cases and sizing results for each member can be found in Appendix D.3.2.

As for the baseline concept, the single optimisation landing gear structures are primarily sized by ground

Table 5.32: Flying-V family baseline (BL) and single optimisation (SO) gear concept structural member sizing results. Nodes are defined as illustrated in Figure 5.14.

Member	Nodes	BL (kg)	FV-800 SO (kg)	FV-900 SO (kg)
Upper strut trunnion	D1-D2-O1-D3-D4	191.2	146.1	187.7
Drop link member 1	D2-D5	77.6	39.1	60.3
Drop link member 2	O1-D5	27.9	15.4	21.3
Drop link member 3	O1-D6	23.7	14.3	19.2
Drop link member 4	D3-D6	64.6	41.7	54.3
Drop link brace 1	C2-C4	23.1	14.3	18.9
Drop link brace 2	C1-C3	65.1	40.7	53.3
Shock strut trunnion	D5-S1-O2-S3-D6	206.8	134.7	170.4
Shock strut cylinder	O2-S4-S6-S7-S8	622.5	360.0	495.4
Shock strut piston	S8-B1	280.9	184.6	247.8
Shock strut brace 1	S1-S3	99.8	55.7	75.8
Shock strut brace 2	S2-S5	79.8	46.7	67.5
Shock strut brace 3	C5-C6	151.2	67.1	103.8
Bogie beam	K-B2-L	275.3	110.0	245.0
Aft wheel axle	K_L-K_R	132.2	70.0	86.7
Front wheel axle	L_L-L_R	132.2	70.0	86.7
AM member 1[1]	A1-A4	-	20.3	29.5
AM member 2[1]	A2-A3	-	9.3	12.8
AM member 3[1]	A5-A6	-	10.5	10.9
Shortening members	-	9.8	6.8	8.6
Total	-	2463	1457	2056

[1] Articulation mechanism.

handling load cases, which impose high external loads due to downforce generation. The added articulation mechanism results in a small mass increase, but the lower overall aircraft mass of the FV-800 and FV-900 is reflected in a mass reduction for all structural members. Consequently, the single optimisation gear achieves a significantly lower overall structural mass compared to the baseline.

Notably, the mass reduction of the upper strut trunnion is smaller than for other structural components. This can be attributed to the shorter gear configuration, which requires the fixed length brace connecting the shock strut to the airframe to be attached further forward. Similar to the trend observed during the structural analysis of the gear concept variations, positioning the brace further forward provides less longitudinal (drag) support, leading to relatively higher reaction loads, particularly during drag, braking, and spin-up conditions. This translates to a relative higher mass of the total landing gear structure, but most prominently in the trunnions. Again, it must be noted that the stress increase in the trunnions is very local, suggesting that there may be potential for mass optimisation through the use of variable wall thickness or other design refinement.

6

Results and Discussion

In this chapter, the analysis of the different landing gear concepts is discussed. First, the baseline gear design is investigated, followed by the concept variations as outlined in Section 3.1. Finally, the most suitable Flying-V family landing gear concept is selected in the design exploration synthesis.

6.1. Baseline Design

This section presents the Flying-V baseline landing gear concept analysis results. It includes an evaluation of landing gear group mass, stowage volume, and cabin floor height for all family members. Additionally, the complexity of the gear, its integration within the overall aircraft design, design commonality, and the level of understanding are discussed. Figures 6.1a and 6.1b visualise the FV-1000 baseline concept right main landing gear in the extended and retracted position, respectively.

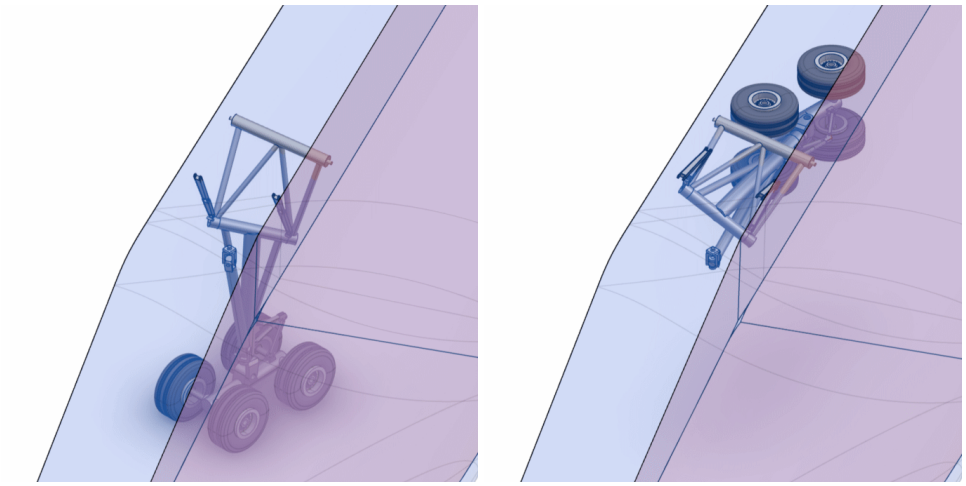

(a) Extended gear. **(b)** Retracted gear.

Figure 6.1: FV-1000 baseline concept right main landing gear isometric views.

6.1.1. Quantitative Analysis

Table 6.1 presents the estimated and corrected FV-1000 main gear primary structure mass, and mass correction factor f_c, which is obtained by substituting the extended gear length $l_{\text{mlg,ext}}$ into Equation 4.2. For the FV-800 and FV-900, the mass of the articulation mechanism (56 kg) is subtracted. It must be noted that this is likely to result in a slight underestimation of FV-800 and FV-900 gear mass. For the FV-1000, the articulation mechanism serves the dual purpose of articulating the bogie for landing and take-off, and flat-packing the bogie for stowage. Although the FV-800 and FV-900 do not require the bogie to be articulated, they still require a mechanism to position the bogie for stowage. However, this stowage mechanism does not need to withstand landing loads, and is therefore expected to be significantly lighter than the articulation mechanism, justifying the subtraction.

Table 6.1: Flying-V baseline concept landing gear, comparison of primary and total structure mass.

Aircraft	Estimated (kg)	$l_{\text{mlg,ext}}$ (m)	f_{c} (-)	Corrected (kg)	Total (kg)
FV-1000	2519	6.38	1.16	2922	4361
FV-800 / FV-900	2463	6.22	1.17	2893	4317

Landing gear group mass contributions are calculated as discussed in Section 3.6.1 and are presented in Table 6.2. Although the FV-800 and FV-900 landing gear mass is slightly lower than that of the FV-1000. Most notably, the different sizing of tyres, wheels, and brakes contributes to significantly lower rolling stock mass. Despite the FV-800 and FV-900 having slightly longer nose gears compared to the FV-1000, their lower overall aircraft mass results in a reduced nose gear mass as well. It must be noted that the baseline concept, which was designed for maximum commonality, comes with a significant mass penalty for the smaller family members, as shown in Table 6.2. The relative contribution of the gear to the maximum take-off mass for the FV-900 and in particular the FV-800, are much higher than for the FV-1000.

Overall, the Flying-V landing gear is estimated to be heavier than the gears used for validation in Section 4.4.3, accounting for 5.12% of the MTOM for the FV-1000, compared to 4.30% for the A310-200 and 3.58% for the Boeing 707-320 (Table 4.24 and 4.25). This was to be expected as generally, the relative contribution of the gear mass increases for increasing aircraft mass [8, 63]. The A310-200 and Boeing 707-320 have a significantly lower mass compared to the FV-1000. In addition, the Flying-V landing gear is longer, and its structure needs to account for larger ground handling loads as a result of downforce generation.

For comparison, the FV-1000 main gear weight is also estimated using the statistics-based method outlined in Section 2.5. Substituting the relevant values into Equation 2.29, the main gear group mass is estimated to be 10.8 tonnes, contributing to a total gear group mass of 11.9 tonnes, which is 4.47% of the FV-1000 maximum take-off mass and is roughly 12% less than the mass estimated in this study (13.6 tonnes). The baseline gear mass estimate is also higher than the prior (statistics-based) Flying-V gear mass estimate by Bourget [9]. It is important to note, however, that this estimate was derived considering different gear requirements and a different aircraft geometry. Furthermore, while Bourget required outriggers to ensure sufficient ground clearance, these were excluded from the mass estimate. In both cases, it should be recognised that statistics-based methods are generally known to underestimate gear mass for heavy aircraft and yield inaccurate results for unconventional aircraft, as discussed in Section 2.5. Moreover, statistics-based methods are incapable of considering increased ground handling loads due to downforce generation.

Table 6.2: Flying-V baseline concept, comparison of landing gear group mass.

Item	FV-1000 (kg)	FV-800 (kg)	FV-900 (kg)
Main gear (each)	6252	5884	6138
Rolling stock	1391	1096	1330
Structure	4361	4317	4317
Controls	500	471	491
Nose gear	1112	908	1042
Total (% MTOM)	13.6×10^3 (5.12)	12.7×10^3 (6.86)	13.3×10^3 (5.68)

Stowage requirements are outlined in Table 6.2, with dimensions defined as indicated in Figures 6.2a and 6.2b, illustrating a top and front view of the stowed FV-1000 landing gear, respectively. The stowed FV-800 and FV-900 gear have equal dimensions. The enclosing box around the gear has a total volume of 35.5 m^3, though this figure does not fully represent the volume of the stowed gear. A portion of the box extends outboard of the rear spar into the cabin. After excluding this outboard section, which accounts for approximately 5 m^3, the actual retracted gear volume $V_{\text{retracted}}$ is 30.5 m^3.

Cabin floor heights at door locations are presented in Table 6.4. Longitudinal locations X_{door} are estimated from Oosterom [10]. Vertical locations Z_{door} are measured from the ground. The Flying-V floor is considered to be 1.08 m below the aircraft centreline, obtained from the CATIA 3DX model. Door

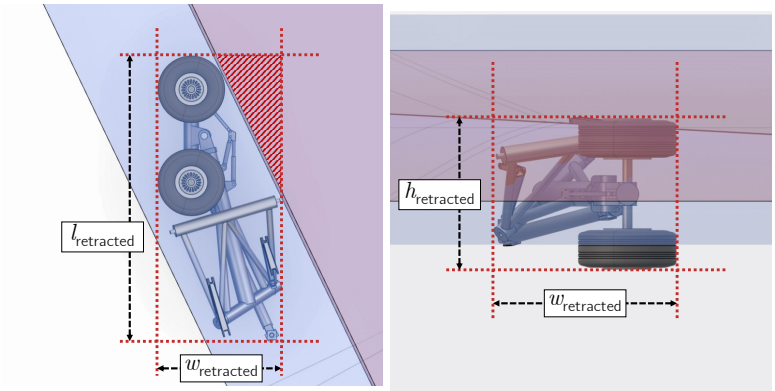

(a) Top view. **(b)** Front view.

Figure 6.2: Flying-V landing gear stowage requirements definitions.

Table 6.3: Flying-V baseline concept stowage requirements.

Item	Unit	FV-1000
$l_{\text{retracted}}$	m	6.2
$w_{\text{retracted}}$	m	2.6
$h_{\text{retracted}}$	m	2.2
V_{box}	m^3	35.5
$V_{\text{retracted}}$	m^3	30.5

sill heights vary between 4.1 and 5.7 m, and depend on the longitudinal location of the door due to the aircraft static pitch attitude. Naturally, the variation is the largest for the FV-1000 because its doors are located at a larger distance from the main gear. The maximum door height of 5.7 meters is comparable to the aft door of the A330, allowing for the use of similar ground support equipment. It should be noted, however, that the table presents values for maximum ramp mass. Door heights will be slightly higher at lower weights due to reduced shock absorber compression.

Table 6.4: Flying-V baseline gear, comparison of cabin floor height at door locations, aircraft at maximum ramp mass.

Item	Unit	FV-1000	FV-800	FV-900
$X_{\text{door,fwd}}$	m	5.8	5.8	5.8
$Z_{\text{door,fwd}}$	m	4.1	4.3	4.2
$X_{\text{door,aft}}$	m	36.6	26.6	32.2
$Z_{\text{door,aft}}$	m	5.7	5.4	5.6

6.1.2. Qualitative Analysis

Compared to a conventional commercial aircraft landing gear, the proposed baseline gear concept is fairly complex. Because it has a double folding strut, it features a larger number of components and a greater number of joints. Despite this added complexity, the gear retains a single degree of freedom, similar to conventional gear systems, allowing it to be extended or retracted with a single actuator. Structurally, the gear is very similar to that of the Convair B-58, with the primary difference being the skewed folding axes, causing the strut and bogie to rotate when the gear extends or retracts. Additionally, the inclusion of bogie articulation and strut shortening adds to the complexity. These features are, however, based on mechanisms that have been successfully utilised on the Airbus A330/A340 families, indicating a proven level of reliability and feasibility.

A landing gear integration proposal is illustrated in Figure 6.3, inspired by the work of Voeten [26] and Oosterom [10]. The fairing, indicated by the red curve, encloses the landing gear stowage bay as well as the gear and engine mounting structures. The fairing and mounting structures can be connected to a common family section to maximise family design commonality. Specifically, the outboard end of the

upper strut trunnion could be connected to the rear spar directly, facilitating efficient load transfer. The engine is mounted on top of the fairing, aft of the landing gear, such that it can be lowered down for maintenance.

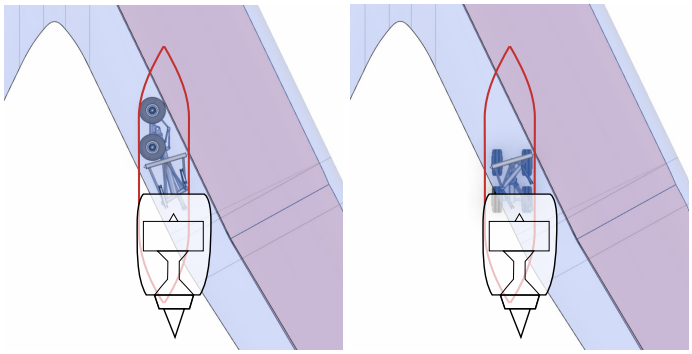

(a) FV-1000 baseline design.

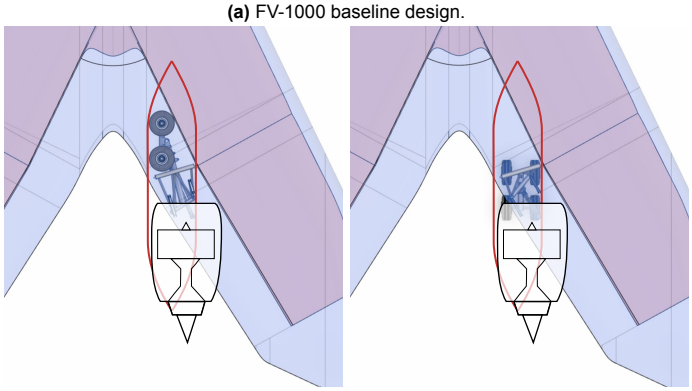

(b) FV-800 baseline design

Figure 6.3: Baseline concept gear integration proposal.

As can be observed from the baseline gear retraction path in Figure 5.15, the bogie assembly extends backward, which is beneficial when it comes to compliance with emergency operation requirements. Of all gear components, the bogie assembly, with tyres, wheels, brakes and the bogie beam itself, presents the largest cross-sectional area perpendicular to the flow direction, making it likely to experience the highest drag loads. In the event of a primary extension mechanism failure, these drag loads, along with gravity, ensure that the gear can still extend.

The baseline concept is designed with a focus on maximising aircraft and landing gear commonality across the family. For each family member, the landing gear shares the same structural components, attachment structure, and fairing dimensions, ensuring a high degree of design consistency, simplifying maintenance and production processes and enhancing overall commercial viability. However, there are differences in nose gear length and attachment location among the family members. These differences could be addressed by implementing a nose gear strut shortening mechanism as discussed in Section 5.3.

6.2. Gear Concept Variations

In this section, gear concept variations analysis results are discussed. Landing gear group mass, stowage requirements and cabin floor height are evaluated and compared. Additionally, qualitative insights into the complexity, integration potential, and compliance with emergency operation requirements are provided. The 6-wheel bogie concept (C2), bogie articulation exclusion concept (C3), strut shortening exclusion concept (C4) and backward stowage concept (C5) are illustrated in Figure 6.4.

6.2.1. Quantitative analysis

Primary structure mass estimates following from the structural analysis need to be corrected using the correction factor f_c, which is obtained by substituting the gear length $l_{mlg,ext}$ into Equation 4.2. Correc-

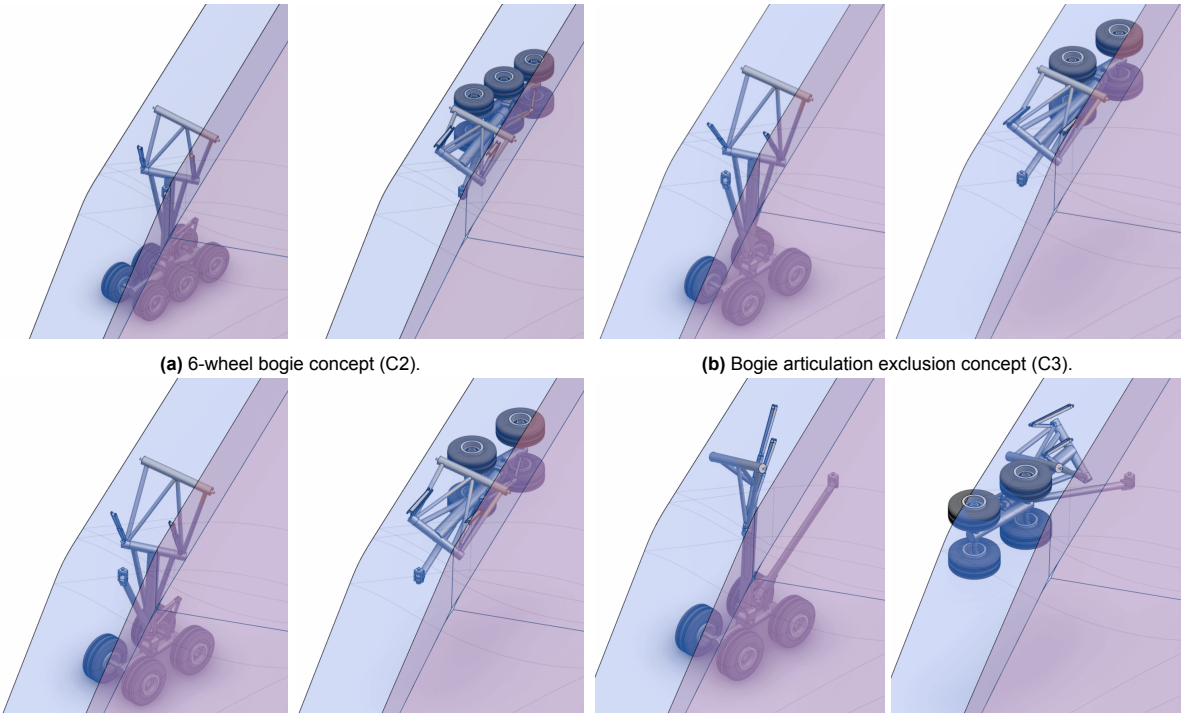

(a) 6-wheel bogie concept (C2).

(b) Bogie articulation exclusion concept (C3).

(c) Strut shortening exclusion concept (C4).

(d) Backward stowage concept (C5).

Figure 6.4: Overview of FV-1000 right main landing gear concept variations.

tion factors and corrected mass values are outlined in Table 6.5. Notably, concept C3, which excludes bogie articulation, has a lower mass correction factor due to its longer gear length. Although it had the highest finite element mass estimate of all concepts, this is not the case anymore after correction. The total structural mass includes contributions from fittings and other miscellaneous structural components, estimated to consistently contribute 33% to the total structural mass throughout this research.

Table 6.5: Flying-V gear concept variations, comparison of primary and total structure mass.

Concept	Estimated (kg)	$l_{mlg,ext}$ (m)	f_c (-)	Corrected (kg)	Total (kg)
BL	2519	6.38	1.16	2922	4361
C2	2762	6.24	1.17	3232	4824
C3	2861	7.02	1.09	3118	4654
C4	2447	6.45	1.15	2813	4200
C5	2843	6.17	1.18	3354	5006

Table 6.6 presents landing gear group mass estimates for each concept, calculated as outlined in Section 2.5. The 6-wheel bogie concept (C2) has the highest group mass, closely followed by the backward stowage concept (C5). While the 6-wheel bogie concept benefits from a slightly lower nose gear mass due to a shorter nose gear strut, its overall mass is significantly higher than the baseline, mainly due to the increased rolling stock and structural mass. For the backward stowage concept (C5), the mass increase is driven entirely by a higher structural mass. Excluding the bogie articulation (Concept C3) also results in a higher group mass, attributed to both increased structural mass and a heavier nose gear. Conversely, Concept C4, which excludes strut shortening, offers the lightest solution, though the mass reduction compared to the baseline is minimal.

It is important to note that the primary structure mass correction equation (Equation 4.2) is derived from a small calibration sample. Additionally, the structure and control mass additions pose constant relative contributions, meaning that any increase in structural mass is further amplified in the total mass estimate. This can disproportionately upscale small structural mass differences between concepts. While the method offers valuable insights for comparative analysis, the results should be interpreted

with an understanding of these limitations, especially when considering absolute mass values. Further validation with larger calibration datasets and design refinements may be required to determine whether the estimates accurately reflect real-world outcomes.

Table 6.6: Flying-V concept variations, comparison of group mass.

Item	BL (kg)	C2 (kg)	C3 (kg)	C4 (kg)	C5 (kg)
Main gear (each)	6252	7013	6571	6077	6953
Rolling stock	1391	1628	1391	1391	1391
Structure	4361	4824	4654	4200	5006
Controls	500	561	525	486	556
Nose gear	1112	1069	1223	1114	1112
Total (% MTOM)	13.6×10^3 (5.12)	15.1×10^3 (5.68)	14.4×10^3 (5.41)	13.3×10^3 (5.00)	15.1×10^3 (5.64)

Stowage requirements are outlined in Table 6.7. The retracted gear volume $V_{\text{retracted}}$ is obtained by subtracting the portion of the box volume outboard of the rear spar, as illustrated in Figure 6.5. Of all concepts, the 6-wheel bogie concept (C2) has the smallest retracted gear volume, which is advantageous from a fuel tank space perspective. However, it also has the largest frontal cross-section, negatively impacting aerodynamic performance. Concepts C3 and C4 (excluding bogie articulation and strut shortening, respectively) exhibit the largest retracted volumes and cross-sections. This is primarily driven by the fixed length shock strut support brace which needs to be attached further aft, increasing the stowage box length as can be observed in the Figures. The backward stowage concept (C5) has a slightly smaller cross-section and box volume compared to the baseline. However, since the box no longer extends outboard of the rear spar, no portion can be subtracted from the total box volume. Consequently, the effective retracted gear volume is not smaller than the box volume, making it significantly larger than that of the baseline.

Table 6.7: Flying-V gear concept variations, comparison of stowage requirements.

Item	BL	C2	C3	C4	C5
$l_{\text{retracted}}$ (m)	6.2	6.2	6.8	7.0	6.4
$w_{\text{retracted}}$ (m)	2.6	2.9	2.7	2.7	2.5
$h_{\text{retracted}}$ (m)	2.2	2.0	2.2	2.2	2.2
V_{box} (m^3)	35.5	36.0	40.4	41.6	35.2
$V_{\text{retracted}}$ (m^3)	30.5	29.5	35.4	36.6	35.2

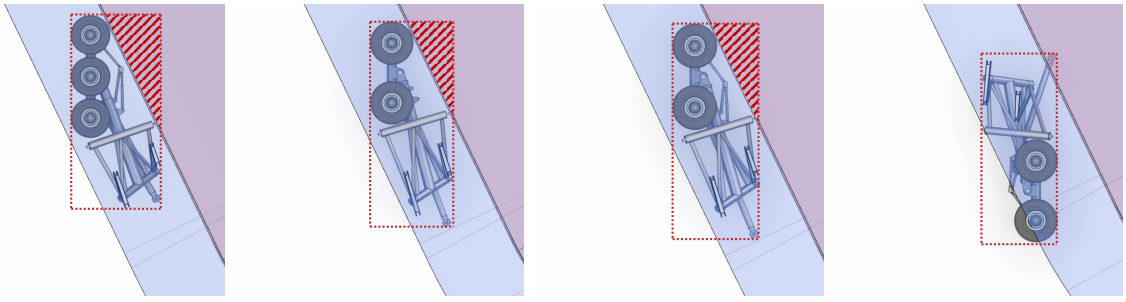

(a) Concept C2. **(b)** Concept C3. **(c)** Concept C4. **(d)** Concept C5.

Figure 6.5: Flying-V gear concept variations, retracted gear volume definitions.

Cabin floor heights are detailed in Table 6.8. Longitudinal locations X_{door} are estimated from Oosterom [10]. Vertical locations Z_{door} are measured from the ground. The Flying-V floor is considered to be 1.08 m below the aircraft centreline, obtained from the CATIA 3DX model. The 6-wheel bogie concept (C2) features a shorter gear, resulting in a lower static cabin floor height. Conversely, eliminating the articulation mechanism in concept C3 requires a longer gear, leading to an increased cabin floor height. The aft door cabin floor height in concept C3 is notably higher than the main deck cabin floors of existing aircraft, but remains below the upper deck floor height of the A380 (Table 2.9. Removing the

strut shortening mechanism (C4) or reversing the stowage direction (C5) does not affect the cabin floor height.

Table 6.8: Flying-V gear concept variations, comparison of cabin floor height at door locations, aircraft at maximum ramp mass.

Item	BL	C2	C3	C4	C5
$X_{\text{door,fwd}}$ (m)	5.8	5.8	5.8	5.8	5.8
$Z_{\text{door,fwd}}$ (m)	4.1	3.9	4.8	4.1	4.1
$X_{\text{door,aft}}$ (m)	36.6	36.6	36.6	36.6	36.6
$Z_{\text{door,aft}}$ (m)	5.7	5.5	6.4	5.7	5.7

6.2.2. Qualitative analysis

The 6-wheel bogie concept (C2) is more complex than the baseline due to the increased number of wheels, which requires additional braking systems, hydraulic components, and introduces more potential points of failure. In contrast, concepts C3 and C4 feature lower complexity, as they do not have bogie articulation and strut shortening mechanisms, respectively, simplifying their design compared to the baseline.

Figures 6.6a and 6.6b illustrate a landing gear integration proposal for the 6-wheel bogie concept (C2) and backward stowage concept (C5), respectively. For maintenance, it must be possible to drop the engine from its mounting structure without colliding with the landing gear. As concept C2 features a longer bogie, the engines need to be mounted slightly further aft, resulting in larger bending moments in the mounting structure. Concepts C3 and C4 are more similar to the baseline in terms of integration but require a longer fairing, as discussed in the stowage analysis. Concept C5 arguably offers the most promising integration from a structural perspective, as the landing gear can be stowed beneath the engine, with the fixed-length shock strut brace connected closer to the rear spar. However, this design introduces a higher risk to the landing gear in the event of engine blade failure.

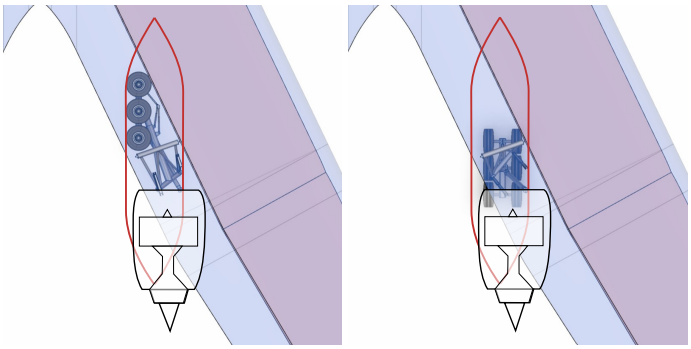

(a) 6-wheel bogie concept (C2).

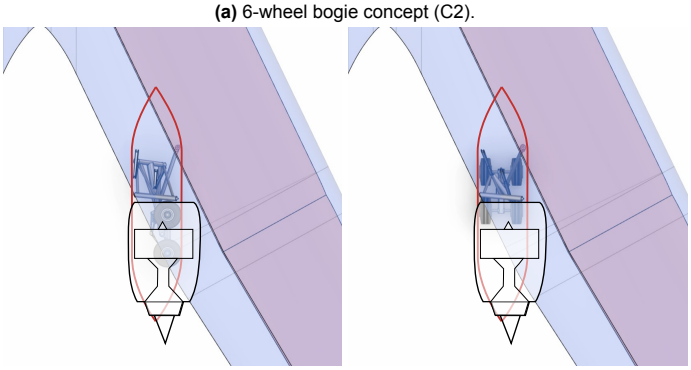

(b) Backward stowage concept (C5).

Figure 6.6: Gear concept variations integration proposals.

Compared to other concepts, concept C5 extends the landing gear forward rather than backward. This configuration is less favourable for emergency operation, as drag loads oppose extension of the gear.

However, as for all other concepts, the extension movement is primarily downward due to the double-folding strut design, making the effect of drag loads less crucial. In addition, it is worth noting that the Convair B-58 Hustler also retracts its main landing gear in backward direction [12]. If concept C5 is selected, further research is required to fully assess the implications for compliance with CS 25.729 [17], and, if needed, address any issues.

6.3. Family Design

Single optimisation FV-800 and FV-900 landing gear analysis results are presented and discussed in this section. The respective gear designs are illustrated in Figure 6.7.

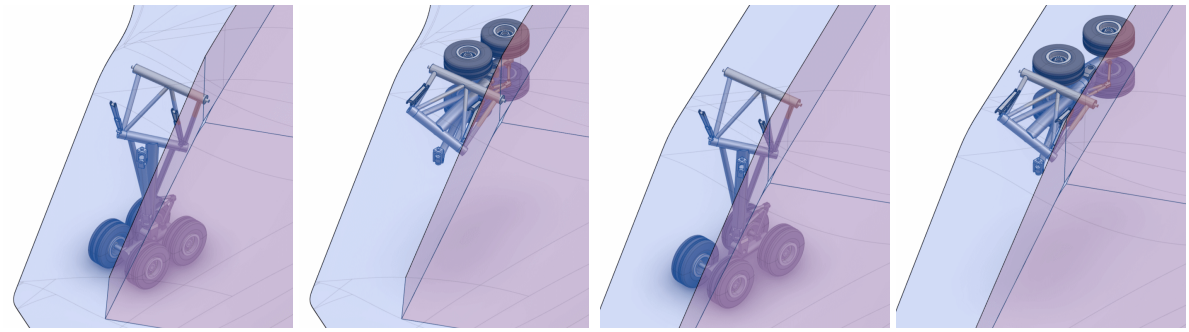

(a) FV-800 single optimisation gear concept. **(b)** FV-900 single optimisation gear concept

Figure 6.7: Overview of Flying-V family single optimisation right main landing gear concepts.

6.3.1. Quantitative Analysis

Table 6.9 presents structural mass results for the baseline gear, as well as for the gear designs specifically sized for the FV-800 and FV-900. The finite element mass estimations are adjusted using the mass correction factor f_c, calculated from Equation 4.2. Notably, the finite element mass estimates for the FV-800 and FV-900 are significantly higher compared to the baseline. The shorter landing gear of the FV-800 and FV-900 results in a higher correction factor, which marginally reduces the overall difference. Nonetheless, the single optimisation gear mass estimates, especially for the FV-800, remain considerably lighter.

Table 6.9: Flying-V family baseline (BL) and single optimisation (SO) landing gear, comparison of primary and total structure mass.

Aircraft	Estimated (kg)	$l_{mlg,ext}$ (m)	f_c (-)	Corrected (kg)	Total (kg)
BL	2463	6.22	1.17	2893	4317
FV-800 SO	1457	5.21	1.28	1869	2789
FV-900 SO	2056	5.80	1.22	2507	3742

Single optimisation landing gear group mass estimates are outlined in Table 6.10. The main gear rolling stock mass remains unchanged, as the baseline rolling stock was already sized for each specific aircraft. However, the reduction in structural mass and to a lesser extend nose gear mass (shorter strut), results in the single optimisation gear being significantly lighter than the baseline gear. Logically, the difference is most pronounced for the FV-800, as the baseline design poses the greatest degree of oversizing for this aircraft. The single optimisation gear for the FV-800 is approximately 3.5 tonnes lighter than the baseline, representing around 2% of the aircraft its maximum take-off mass (MTOM). For the FV-900, the difference is smaller, at around 1.4 tonnes, as its MTOM is closer to that of the FV-1000. Overall, the trend of decreasing gear mass contributions relative to the total aircraft mass, as aircraft mass decreases, aligns with observations by Chai and Mason [8] and Roskam [63].

Please note that single optimisation gear mass estimates are subject to limitations, similar to mass estimations presented in Section 6.2.

Table 6.10: Flying-V family baseline (BL) and single optimisation (SO) landing gear, comparison of group mass.

Item	FV-800 BL (kg)	FV-800 SO (kg)	FV-900 BL (kg)	FV-900 SO (kg)
Main gear (each)	5884	4223	6138	5513
Rolling stock	1096	1096	1330	1330
Structure	4317	2789	4317	3742
Controls	471	338	491	465
Nose gear	908	778	1042	955
Total (% MTOM)	12.7×10^3 (6.86)	9.22×10^3 (4.98)	13.3×10^3 (5.68)	11.9×10^3 (5.09)

Single optimisation gear stowage requirements are presented alongside baseline gear requirements in Table 6.11. The single optimisation concepts feature significantly smaller retracted gear volumes, which could be utilised to increase fuel tank capacity. Additionally, the concepts have reduced frontal cross-sections compared to the baseline, potentially offering improvements in aerodynamic performance.

Table 6.11: Flying-V family baseline (BL) and single optimisation (SO) landing gear, comparison of stowage requirements.

Item	BL	FV-800 SO	FV-900 SO
$l_{\text{retracted}}$ (m)	6.2	4.9	5.8
$w_{\text{retracted}}$ (m)	2.6	2.3	2.5
$h_{\text{retracted}}$ (m)	2.2	1.9	2.0
V_{box} (m^3)	35.5	21.4	29.0
$V_{\text{retracted}}$ (m^3)	30.5	18.7	25.4

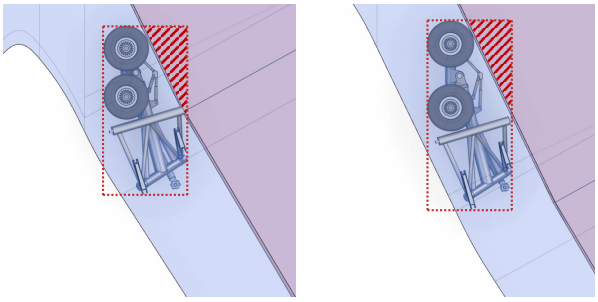

(a) FV-800. **(b)** FV-900.

Figure 6.8: Single optimisation gear, retracted gear volume definitions.

Cabin floor heights are presented in Table 6.12. Longitudinal locations X_{door} are estimated from Oosterom [10]. Vertical locations Z_{door} are measured from the ground. The Flying-V floor is considered to be 1.08 m below the aircraft centreline, obtained from the CATIA 3DX model. The shorter landing gears of the FV-800 and FV-900 have a direct impact on cabin floor heights. In particular, the cabin floor of the FV-800 is roughly 1 m lower than the baseline. The same trend is observed for the FV-900, though the effect is less pronounced due to its slightly longer gear.

Table 6.12: Flying-V family baseline (BL) and single optimisation (SO) concept landing gear, comparison of cabin floor height at door locations, aircraft at maximum ramp mass.

Item	FV-800 BL	FV-800 SO	FV-900 BL	FV-900 SO
$X_{\text{door,fwd}}$ (m)	5.8	5.8	5.8	5.8
$Z_{\text{door,fwd}}$ (m)	4.3	3.3	4.2	3.7
$X_{\text{door,aft}}$ (m)	26.6	26.6	32.2	32.2
$Z_{\text{door,aft}}$ (m)	5.4	4.4	5.6	5.1

6.3.2. Qualitative Analysis

The single optimisation landing gear designs do not introduce additional complexity and behave similar when it comes to emergency operation compared to the baseline design. From an integration perspective, the shorter bogie designs allow the engine to be mounted further forward, reducing the bending moments in the gear and engine attachment structure, potentially leading to a lower mass. FV-800 and FV-900 integration proposals are presented in Figure 6.9.

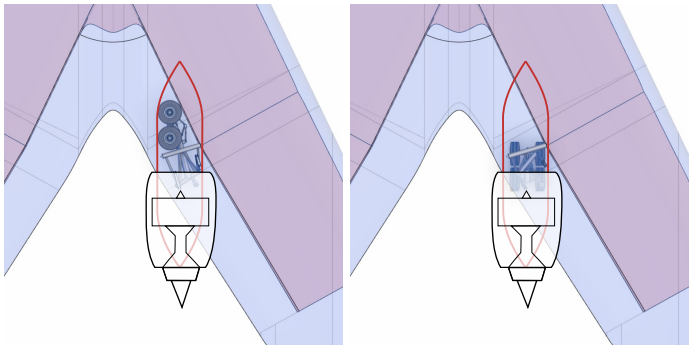

(a) FV-800 single optimisation.

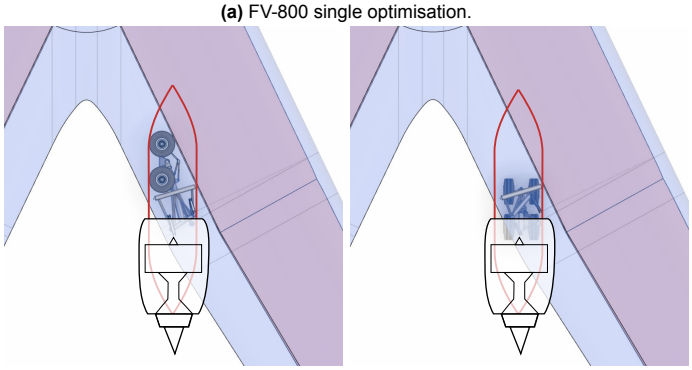

(b) FV-900 single optimisation.

Figure 6.9: Flying-V family single optimisation gear integration proposals.

Naturally, single aircraft gear optimisation results in reduced commonality across the Flying-V family. Variations in the lateral position of the trunnion and differences in brace locations lead to different mounting structures for the various landing gear concepts. Gear sizing differs, with variations in member length and wall thickness, leading to different structural mass. The bogie design is also unique to each model, offering mass and stowage benefits but further reducing commonality. Although the nose gear also differs, this variation was already present in the baseline design, and could be solved using a nose gear strut shortening mechanism, as discussed in Section 6.1.

However, certain elements of aircraft commonality can still be maintained even with different gear designs. The longitudinal attachment points relative to the centre of gravity are similar across all concepts, and due to the double folding strut, the stowed bogie position relative to the upper strut trunnion remains constant. In addition, the FV-800 and FV-900 single optimisation gears have less stringent stowage bay fairing requirements than the FV-1000 baseline. Together, this allows for using the same stowage bay fairing across the entire Flying-V family. While there are differences in the landing gear mounting structure, this shared fairing design opens up the possibility of a common family section, as discussed by Oosterom [10].

Commonality could be further enhanced by moving the landing gear attachment position to match that of the FV-1000, while retaining single optimisation (albeit less optimal) sizing to maintain the benefits of having lower mass for the smaller family members. Since gear folding axis orientations are already similar across all concepts, this adjustment would enable a more common gear mounting structure, facilitated by a shared upper strut trunnion location, with only a slight increase in gear length and mass. The brace attachment locations would still differ to accommodate the varying gear lengths.

6.4. Design Exploration Synthesis

In this section, the most suitable Flying-V landing gear is selected. A design with low complexity is preferred, as it reduces the number of components and potential points of failure. This results in increased reliability, easier maintenance, and reduced maintenance costs. Landing gear mass must be minimised to enhance payload capacity and fuel efficiency. The landing gear must have a compact design when retracted, minimising the frontal cross-section to reduce aerodynamic drag. Additionally, a small retracted volume allows for increased fuel tank capacity. Maximising commonality between family members is essential to limiting production and certification costs, which enhances the commercial viability of the Flying-V. Ultimately, for the Flying-V to be viable, the landing gear design must also be technically and operationally feasible.

Landing Gear Concept Comparison

The single folding strut (concept C1) offers the lowest complexity, but given the current set of requirements, it is not feasible for the FV-800, and compromises aerodynamic performance and commonality across the family. A 6-wheel bogie, an articulation mechanism, and a strut shortening mechanism increase complexity, but have all been successfully implemented in previous landing gear designs.

In terms of mass, implementing a 6-wheel bogie, reversing the stowage direction, and incorporating a strut shortening mechanism all result in a mass increase compared to the baseline. The implementation of the articulation mechanism, on the other hand, offers a reduction in landing gear mass. The benefits of adopting a single optimisation gear instead of a common (baseline) gear are significant, in particular for the FV-800, where the single optimisation gear is 3.5 tonnes lighter than the baseline, which roughly equates to 2% of the maximum take-off mass.

With respect to compactness, the benefits of the narrow 6-wheel bogie are negated as it requires a wider fairing, which increases the frontal cross-section compared to the baseline. Removing either the articulation mechanism or the strut shortening mechanism significantly increases the stowed gear volume. Using the single optimisation gear for smaller family members may lead to a considerable reduction in stowage volume. The same fairing can still be used due to the double folding strut, which allows for maintaining a constant bogie position relative to the trunnion across the family, irrespective of gear length.

Regarding feasibility, all concepts, with the exception of the single folding strut, exhibit feasible kinematics and integration. The potential for integrating the gear and engine mounting structure is similar across the designs, with the engines mounted aft of the landing gear for all concepts. The engine position varies slightly depending on the bogie length, but this has minimal impact on overall integration. It is found that removing the articulation mechanism increases the static height of the aircraft, leading to a cabin floor height being significantly higher than that of existing wide-body aircraft. This increased height may present challenges for compatibility with existing ground support equipment. For other gear concepts, the cabin floor height is comparable to those of existing wide-body aircraft.

The Best Landing Gear for the Flying-V Family

Overall, the baseline concept offers the optimal trade-off between the aforementioned criteria for both the FV-1000 and FV-900. The concept, which features a 4-wheel articulated bogie and a double folding strut that shortens upon retraction, provides the best compromise between complexity, mass, and stowage requirements. Additionally, the baseline concept features a favourable extension direction in the event of a primary extension method failure.

It must be noted that for the FV-900, using the baseline design results in performance penalties, including a reduced maximum pitch attitude for ground clearance (13.7° as opposed to the desired 14°) and a mass penalty (1.4 tonnes). Although the single optimisation concept provides greater ground clearance and a lower mass, commonality is prioritised. Optionally, commonality could be increased further by using the FV-1000 baseline concept for the FV-900 as well. The inclusion of the articulation mechanism provides additional ground clearance, albeit at the cost of a slight additional mass penalty.

For the FV-800, the baseline concept mass penalty is rather large (3.5 tonnes, roughly 2% of its maximum take-off mass). Given that it is already constrained by its available fuel tank volume, a heavier landing gear would further limit range and payload capacity. This justifies using the single optimisation

gear concept for the FV-800, at the expense of reduced commonality. In addition to being lighter, the single optimisation gear also offers better lateral stability, enhancing overall performance. The same fairing can still be used without modification. Optionally, the same trunnion attachment structure could be used as well, but this would slightly increase gear length and mass.

7

Conclusions and Recommendations

Research conclusions, design recommendations, and further research recommendations are discussed in this chapter.

7.1. Conclusions

The Flying-V landing gear is expected to significantly impact aircraft mass and design. Previous designs are based on outdated requirements and have shortcomings in feasibility, mass estimation reliability, integration, and family commonality. The objective of this research is to conduct a Flying-V landing gear design exploration to be able to answer the research question: *'What is the best landing gear for the Flying-V family?'*.

The optimal landing gear design for the Flying-V family is selected based on several key criteria, including feasibility, complexity, mass, structural integration, and family commonality. While these apply to any aircraft, they are more stringent for the Flying-V. Its high sweep angle wing requires a longer landing gear for sufficient ground clearance. This inherently results in higher landing gear mass, reducing the performance benefit of the Flying-V compared to conventional aircraft. Additionally, a longer gear raises the cabin floor height, which must remain compatible with ground support equipment, an important factor for the commercial viability of the aircraft. Without a central fuselage, compact gear stowage becomes more critical for aerodynamic performance. Also family commonality is not straightforward. Smaller family members have a shorter length and span, meaning they do not benefit from the longer gear required for the FV-1000, which undermines the advantage of using a common gear across all models. Additionally, unlike conventional aircraft, the positioning of the landing gear must facilitate integration of the engine mounting structure and engine, all connected to the same fuselage section to maintain family commonality.

Several key landing gear design considerations were explored, including single versus double folding struts, four-wheel versus six-wheel bogies, bogie articulation, strut shortening, and stowage direction. The benefits of dedicated FV-800 and FV-900 landing gear over a common FV-1000-sized gear were also assessed. All these features were incorporated into various landing gear concepts, which were then evaluated for their feasibility, performance, and integration within the Flying-V family. The single folding strut was found to be unfeasible. The six-wheel bogie resulted in a heavier gear compared to the four-wheel configuration. Although it offered reduced stowage bay height, the width increased, ultimately leading to a comparable cross-section and stowage volume. Bogie articulation effectively reduced mass and increased compactness, though at the cost of higher complexity. Strut shortening also improved compactness, though it slightly increased mass. Folding the gear in forward direction for stowage resulted in significantly lower gear mass compared to stowage in backward direction, and offers the additional advantage of being more favourable in the event of an extension mechanism failure. Finally, dedicated derivative designs for the FV-800 and FV-900 featured significant reductions in mass and stowage requirements, while still maintaining a high degree of commonality across the Flying-V family.

The best Flying-V landing gear concept features a double folding strut, a four-wheel bogie, strut shortening, and forward retraction. For the FV-1000, the gear weighs 13.6 tonnes, representing 5.1% of its

maximum take-off mass (MTOM), and includes bogie articulation for improved ground clearance. The same gear is used for the FV-900, with adjustments to the rolling stock sizing and without bogie articulation, resulting in a 13.3-tonne gear (5.7% of MTOM). Although a dedicated gear for the FV-900 could reduce the mass to 11.9 tonnes, and despite a slight reduction in maximum allowed pitch attitude for ground clearance, commonality with the FV-1000 is prioritised. Alternatively, bogie articulation could be implemented on the FV-900 as well, only marginally increasing mass and complexity, but improving ground clearance and commonality. Differently, for the FV-800, a gear with dedicated sizing is selected. Compared to the other family members, the FV-800 is much more constrained by fuel tank capacity, which justifies deviating from the commonality principle. The resulting FV-800-sized gear weighs 9.2 tonnes (5.0% of MTOM), significantly reducing mass compared to using the FV-1000-sized common gear, which would weigh 12.7 tonnes for the FV-800.

It is important to interpret the mass estimates with caution. Fundamentally, the structural sizing is based on simplified quasi-static load conditions, excluding dynamic and asymmetric loads, and assumes uniform loads in each member. Additionally, all members are modelled as tubes, each with a fixed diameter and uniform wall thickness. While this simplification provides consistency in the analysis and concept comparison, it inherently constrains the design. Internal gear loads are found to be sensitive to support brace positioning, which have not been fully optimised in this study. The structural mass estimation relies on a simplified 1D finite element model that does not account for components such as torque links and locking mechanisms. The correction equation used to adjust the primary structure mass estimate is derived from a small calibration sample, which may affect the precision of the results. Additionally, the assumption of constant relative contributions from miscellaneous structural components and controls tends to amplify minor differences in structural mass. Furthermore, the scope of this design exploration is inherently limited, as the range of potential design considerations and variations is vast, and not all could be evaluated within this research. Nevertheless, the results provide a robust foundation for concept comparison, trend exploration, and guiding future development of the Flying-V.

7.2. Recommendations

In this section, recommendations for the further development of the Flying-V landing gear are presented. These recommendations are grouped by topic, addressing key areas that require additional refinement or research.

Main Landing Gear

The main landing gear requires further design refinement in several key areas to improve the accuracy and extend the scope of the feasibility analysis and mass estimation. One significant area that has not been addressed in this research is the attachment structure, which is expected to add significant mass to the aircraft. Torque links, locking mechanisms, actuators and brake rods need to be included to reduce reliance on sensitive mass correction factors and enhance the feasibility evaluation.

Additionally, asymmetric and dynamic loading conditions should be incorporated, and multibody simulations should replace quasi-static assumptions for a more accurate representation of structural behaviour. The structure could be further optimised by exploring the use of different member profiles, which may provide better load distribution or weight savings compared to the tubular members used in this research. In areas where the wall thickness of members is constrained by machinability, reducing the diameter could decrease the overall mass. Conversely, in regions where the wall thickness is governed by stress or buckling considerations, increasing the diameter could allow for thinner walls and further mass reduction, though this would come at the expense of compactness. Ultimately, mass analysis should be integrated into the landing gear optimisation process, allowing the attachment structure and brace positioning to be optimised to minimise total landing gear mass.

To minimise the number of components, the torque links could potentially be integrated with the articulation mechanism. Unlike the FV-800 and FV-1000, the FV-900 requires a dedicated bogie folding mechanism, as it lacks an articulation system capable of performing this function. Additionally, composite materials present a promising alternative to 300M steel for various landing gear components, particularly those subjected to uniaxial loads, with the potential to reduce overall landing gear mass.

The main landing gear is relatively complex compared to conventional designs, which may affect cost,

maintenance, and reliability. In this research, complexity has only been evaluated from a qualitative perspective, based on engineering judgement and comparisons with existing landing gear designs. While this provides an initial understanding, a thorough, industry-guided assessment of structural complexity and retraction kinematics is required to ensure the design is both technically feasible and economically viable.

Finally, the dynamic behaviour of the landing gear requires further investigation, particularly its susceptibility to instability (e.g., shimmy), which could be more prominent due to its long length and may result in excessive wear or failure.

Nose Landing Gear

The design of the nose landing gear has not been explored in this research, with current nose gear mass estimates based on statistical methods. It is found, however, that the Flying-V nose gear load fractions are higher than those of conventional aircraft, making these methods potentially inaccurate. While nose gear mass typically has a small impact on the total landing gear group mass, this may be different for the Flying-V due to the higher loads, necessitating the use of physics-based approaches for a more accurate estimation.

The Flying-V has a ground pitch attitude of -3°. Due to varying wheelbase lengths across the family, the FV-800 requires a longer nose gear than the FV-900, which in turn requires a longer gear than the FV-1000. This variation complicates family commonality, as the longer nose gear must be positioned further aft to have sufficient room for stowage, which also increases the nose gear load fraction. A potential solution is to implement a strut shortening mechanism in the nose gear of the FV-800 and FV-900, similar to that of the main landing gear.

Rotation Ability

In this research, the position of the main landing gear is optimised for maximum rotation ability, which is common practice for landing gear design. However, the actual ability of the aircraft to rotate remains unverified, and should be evaluated in future research.

Bogie articulation may potentially be beneficial for rotation ability. For all landing gear concepts, the rotated tipover constraint was active, meaning that positioning the gear further forward would have caused the aircraft to become unstable as it reaches its maximum pitch attitude. This was, however, evaluated considering that the aircraft rotates about the centre bogie pivot point. In fact, when the bogie is articulated, the aircraft pivot point shifts towards the aft wheel axle. This allows the gear to be moved further forward, benefiting rotation ability (and nose gear loads). It must be noted that this results in a slightly longer gear, and that appropriate derotation after touchdown must be guaranteed, e.g., the pitch attitude of the aircraft must be decreased before the bogie is derotated to maintain sufficient ground clearance.

Airport Compatibility

The wing tips of both the FV-1000 and FV-900 exceed the minimum taxiway separation distance during sharp turns, which could lead to colliding with objects or other aircraft. Landing gear positioning has only a minor impact on this issue. Further investigation is required to assess the operational limitations this may impose. A potential, albeit suboptimal, solution would be the implementation of main gear steering, which would enable lateral manoeuvring during taxiing (crabbing), allowing the aircraft to move sideways during a turn. However, this approach should be viewed as a last resort, as it introduces substantial complexity to the landing gear system and aircraft ground handling.

Further research into the necessity of downforce generation for achieving appropriate braking performance is recommended. Previous studies proposed downforce generation to enhance braking performance, particularly given the extended derotation phase of the Flying-V, which necessitates rapid deceleration once in the braking phase to achieve an appropriate stopping distance [22, 23]. However, the use of split flaps has shown to reduce the required pitch attitude, thereby shortening the derotation phase, potentially mitigating the need for downforce generation. Downforce significantly increases the load on the landing gear, heavily influencing the sizing of nearly all components. While its effect on tire sizing was considered, its impact on flotation performance was not evaluated in this research and could introduce additional operational limitations.

Noise

During approach, airframe noise, a majority of which originating from the landing gear, is already the dominant factor for the current generation of aircraft [64]. The long and complex landing gear of the Flying-V is likely to produce more noise than conventional landing gear. This concern extends to take-off as well, where the complex kinematics and slow retraction speeds delay the aircraft from reaching a clean configuration, potentially making landing gear noise relevant for the flyover noise reference point as well. As a result, landing gear noise may become a primary concern for the Flying-V, which needs to be investigated in future research.

References

[1] M. Klöwer et al. “Quantifying aviation’s contribution to global warming”. In: *Environmental Research Letters* 16 (10 Oct. 2021). ISSN: 17489326. DOI: 10.1088/1748-9326/ac286e.

[2] Airbus. *Global Market Forecast*. Tech. rep. AIRBUS, 2023.

[3] F. Faggiano et al. “Aerodynamic design of a flying V aircraft”. In: American Institute of Aeronautics and Astronautics Inc, AIAA, 2017. ISBN: 9781624105081. DOI: 10.2514/6.2017-3589.

[4] J. Benad. “The Flying V-A new Aircraft Configuration for Commercial Passenger Transport”. In: 2015. DOI: 10.25967/370094. URL: https://www.researchgate.net/publication/324150114.

[5] M. B. P. Claeys. “Flying V and Reference Air-craft Structural Analysis and Mass Comparison”. MA thesis. Delft University of Technology, 2018. URL: http://resolver.tudelft.nl/uuid:ee7f2ecb-cdb6-46de-8b57-d55b89f8c7e6.

[6] J. Benad and R. R. Vos. “Design of a Flying V Subsonic Transport”. In: 2022. URL: https://www.icas.org/ICAS_ARCHIVE/ICAS2022/data/preview/ICAS2022_0358.htm.

[7] E. Wallet. *Flying V*. 2020. URL: https://sketchfab.com/3d-models/airbus-flying-v-klm-9253a477c4b746f2ae212d737fb83521 (visited on 02/14/2023).

[8] S. T. Chai and W. H. Mason. *Landing Gear Integration in Aircraft Conceptual Design*. Virginia Polytechnic Institute and State University, Sept. 1996. URL: http://www.aoe.vt.edu/aoe/faculty/Mason_f/M96SC.html*current.

[9] G. Bourget. “The effect of landing gear implementation on Flying V aerodynamics, stability and controllability”. MA thesis. Delft University of Technology, 2020. URL: http://resolver.tudelft.nl/uuid:599eca91-6200-4d29-8dd7-e4e7060703e1.

[10] W. J. Oosterom. “Flying-V Family Design”. MA thesis. Delft University of Technology, 2021. URL: http://resolver.tudelft.nl/uuid:9e8f9a41-8830-405d-8676-c46bf6b07891.

[11] M. Rehbein. “Flying V Landing Gear The Kinematic Design and Weight Estimation of a Flying V Main Landing Gear”. MA thesis. Delft University of Technology, 2023. URL: http://resolver.tudelft.nl/uuid:e59f8fc0-7c96-4e60-8e14-ce16068875d2.

[12] R. Schmidt. *The Design of Aircraft Landing Gear*. SAE International, Feb. 2021. ISBN: 978-0-7680-9942-3.

[13] R. Rajamani et al. “Developing IVHM Requirements for Aerospace Systems”. In: Aug. 2013. DOI: 10.4271/2013-01-2333.

[14] P. van Ginneken. “Development of an Optimization Framework for Landing Gear Design”. MA thesis. Delft University of Technology, 2016. URL: http://resolver.tudelft.nl/uuid:ebb54c53-3c79-4e67-9405-7451e2eca850.

[15] B. Cowan. *A7-ALA Qatar A350-900 landing at Edinburgh airport runway 24*. 2018. URL: https://commons.wikimedia.org/wiki/File:Qatar_A350_at_Edinburgh.jpg (visited on 11/23/2022).

[16] H. G. Conway. *Landing Gear Design*. Chapman & Hall Ltd., 1958.

[17] EASA. *Certification Specifications and Acceptable Means of Compliance for Large Aeroplanes CS-25, Amendment 27*. 2021.

[18] Airbus. *A320 - AIRCRAFT CHARACTERISTICS - AIRPORT AND MAINTENANCE PLANNING*. 2020. URL: https://www.airbus.com/en/airport-operations-and-technical-data/aircraft-characteristics (visited on 01/06/2023).

[19] M. Bryant et al. “Control system and method for a semi-levered landing gear for an aircraft”. 2002.

[20] N. S. Currey. *Aircraft Landing Gear Design: Principles and Practices*. AIAA, 1988.

[21] M. R. van der Toorn. “Flying-V Family Design for Stability & Control”. MA thesis. Delft University of Technology, 2022. URL: http://resolver.tudelft.nl/uuid:c9c1ded2-a0a0-4e95-9d81-5d93e9f54ad2.

[22] G. J. de Zoeten. “Comparative Flight Performance Evaluation of the Flying-V and a Reference Aircraft”. MA thesis. Delft University of Technology, 2022. URL: http://resolver.tudelft.nl/uuid:3a5999b2-1bd9-4b38-86be-fb65c5087880.

[23] O. Erdinçler. “Aerodynamic and performance analysis of ground spoilers on the Flying V”. MA thesis. Delft University of Technology, 2021. URL: http://resolver.tudelft.nl/uuid:d8176c14-f3e1-4a6a-99b0-55c7251f9762.

[24] S. Eftekhar. “High Lift Split Flaps for the Flying-V”. MA thesis. Delft University of Technology, 2024. URL: http://resolver.tudelft.nl/uuid:0ad3c088-b6a6-472b-b60b-4b424a08e15c.

[25] W. J. Oosterom and R. Vos. “Conceptual Design of a Flying-V Aircraft Family”. In: American Institute of Aeronautics and Astronautics Inc, AIAA, 2022. ISBN: 9781624106354. DOI: 10.2514/6.2022-3200.

[26] R. C. J. Voeten. “Flying-V A design methodology for un-conventional engine mounting structures”. MA thesis. Delft University of Technology, 2022. URL: http://resolver.tudelft.nl/uuid:8ae4ad77-43d6-44d4-ae34-bb3b118587dd.

[27] Y. A. Laar. “Aerodynamic Design of a Flying V Aircraft in Transonic Conditions”. MA thesis. Delft University of Technology, 2023. URL: http://resolver.tudelft.nl/uuid:591093b2-5cdc-41c5-b564-3786f43d51db.

[28] P. Wu. “A Physics-based Approach to Assess Critical Load Cases for Landing Gears within Aircraft Conceptual Design”. PhD thesis. Delft University of Technology, 2019. DOI: 10.4233/uuid:193f6664-0f19-488f-af6a-21b17ba75be0. URL: https://doi.org/10.4233/uuid:193f6664-0f19-488f-af6a-21b17ba75be0.

[29] U. Kling et al. “A framework for unconventional landing gear design”. In: 2018.

[30] S. Cumnuantip. “LANDING GEAR CONCEPTUAL DESIGN AND STRUCTURAL OPTIMIZATION OF A LARGE BLENDED WING BODY CIVIL TRANSPORT AIRCRAFT”. In: 2015.

[31] A. Tfaily et al. “Landing gear integration in an industrial multi-disciplinary optimization environment”. In: vol. 7. SAE International, 2013. DOI: 10.4271/2013-01-2319.

[32] N. C. Heerens. “Landing gear design in an automated design environment”. MA thesis. Delft University of Technology, 2014. URL: http://resolver.tudelft.nl/uuid:d3239c8e-a423-4aa1-8752-c977d03d58e1.

[33] N. van Oene. “Landing Gear Design Integration for the TU Delft Initiator”. MA thesis. Delft University of Technology, 2019. URL: http://resolver.tudelft.nl/uuid:e08c31c2-1371-465d-a5bc-666433945249.

[34] C. Douglas et al. “Multidisciplinary Design Optimization of Aircraft Landing Gear”. In: American Institute of Aeronautics and Astronautics Inc, AIAA, 2021. ISBN: 9781624106101. DOI: 10.2514/6.2021-3023.

[35] H. Xia et al. “Mixed Integer Optimization of Aircraft Rolling Stock and Bogie”. In: American Institute of Aeronautics and Astronautics Inc, AIAA, 2021. ISBN: 9781624106101. DOI: 10.2514/6.2021-3024.

[36] S. Joosten et al. “Simulator Assessment of the Lateral-Directional Handling Qualities of the Flying-V”. In: American Institute of Aeronautics and Astronautics (AIAA), Jan. 2023. DOI: 10.2514/6.2023-0906.

[37] R. Torelli et al. “Piloted Simulator Evaluation of Low-Speed Handling Qualities of the Flying-V”. In: American Institute of Aeronautics and Astronautics (AIAA), Jan. 2023. DOI: 10.2514/6.2023-0907.

[38] P. Kraus. “An Analytical Approach to Landing Gear Weight Estimation”. In: Society of Allied Weight Engineers, Inc., 1970.

[39] R. C. Hibbeler. *Mechanics of Materials*. 9th. Pearson, 2020.

[40] C. E. Larsen and I. S. Raju. *Moving Aerospace Structural Design Practice to a Load and Resistance Factor Approach*. Tech. rep. NASA Langley Research Center, 2024.

[41] E. Torenbeek. *Synthesis of Subsonic Airplane Design*. Delft University Press, 1982. ISBN: 9024727243.

[42] Airbus. *A330 - AIRCRAFT CHARACTERISTICS - AIRPORT AND MAINTENANCE PLANNING*. 2021. URL: https://www.airbus.com/en/airport-operations-and-technical-data/aircraft-characteristics (visited on 01/06/2023).

[43] Airbus. *A350 - AIRCRAFT CHARACTERISTICS - AIRPORT AND MAINTENANCE PLANNING*. 2021. URL: https://www.airbus.com/en/airport-operations-and-technical-data/aircraft-characteristics (visited on 01/06/2023).

[44] FAA. *AC 150/5300-13B, Airport Design*. Federal Aviation Administration, 2022. URL: https://www.faa.gov/airports/engineering/airport_design/..

[45] ICAO. *Annex 14 - Aerodromes - Volume 1 - Aerodrome Design and Operations*. International Civil Aviation Organization, 2018.

[46] Airbus. *A380 - AIRCRAFT CHARACTERISTICS - AIRPORT AND MAINTENANCE PLANNING*. 2020. URL: https://www.airbus.com/en/airport-operations-and-technical-data/aircraft-characteristics (visited on 01/06/2023).

[47] Federal Aviation Administration William J. Hughes Technical Center. *ICAO-ACR*. Version 1.3. 2020. URL: https://www.airporttech.tc.faa.gov/Products/Airport-Safety-Papers-Publications/Airport-Safety-Detail/icao-acr-13 (visited on 12/17/2022).

[48] A. Elham, G. La Rocca, and M. J. van Tooren. “An Advanced Quasi-Analytical Weight Estimation Method for Airplane Lifting Surfaces”. In: Society of Allied Weight Engineers, Inc., 2012. URL: https://www.researchgate.net/publication/259266720.

[49] J. Roskam. *AIRPLANE DESIGN PART IV : LAYOUT DESIGN OF LANDING GEAR AND SYSTEMS*. Roskam Aviation and Engineering Corporation, 1989.

[50] D. Raymer. *Aircraft design: a conceptual approach*. AIAA, 2012.

[51] F. Caputo et al. “Established numerical techniques for the structural analysis of a regional aircraft landing gear”. In: *Advances in Materials Science and Engineering* 2018 (2018). ISSN: 16878442. DOI: 10.1155/2018/8536581.

[52] T. M. Inc. *Choosing the Algorithm*. Natick, Massachusetts, United States, 2024. URL: https://mathworks.com/help/optim/ug/choosing-the-algorithm.html.

[53] Aerospace Standard. “Gland Design: Nominal 3/8 in Cross Section for Custom Compression Type Seals”. In: *AS4832, SAE International* (2012).

[54] I. Y. Kim and O. de Weck. “Adaptive weighted sum method for multiobjective optimization: A new method for Pareto front generation”. In: *Structural and Multidisciplinary Optimization* 31 (Feb. 2006), pp. 105–116. DOI: 10.1007/s00158-005-0557-6.

[55] Dassault Systèmes. *3DEXPERIENCE CATIA*. Version R2024x 3.20. July 18, 2024. URL: https://www.3ds.com/products/catia/3dexperience-catia.

[56] L. van der Schaft. “Development, Model Generation and Analysis of a Flying V Structure Concept”. MA thesis. Delft University of Technology, 2017. URL: http://resolver.tudelft.nl/uuid:d9c9c02f-d67a-4e3c-93a7-eb20ed67cd03.

[57] FedEx. *Airbus A300-600/A310-200 Airfame Systems, ATA 32 Landing Gear*. Tech. rep. 2001.

[58] Airbus. *A310 - AIRCRAFT CHARACTERISTICS - AIRPORT AND MAINTENANCE PLANNING*. 2009. URL: https://www.airbus.com/en/airport-operations-and-technical-data/aircraft-characteristics (visited on 01/05/2024).

[59] Boeing. *707 - AIRPLANE CHARACTERISTICS AIRPORT PLANNING*. 2011. URL: https://www.boeing.com/commercial/airports/plan-manuals (visited on 01/05/2024).

[60] Airbus. *Operational Liaison Meeting FBW Aircraft - Avoiding Tail Strike*. Airbus. URL: https://www.smartcockpit.com/docs/Avoiding_Tailstrikes_by_Airbus.pdf (visited on 03/01/2024).

[61] A. M. Jorge. “Quantifying Wind Tunnel Effects on the Flying-V”. MA thesis. Delft University of Technology, 2023. URL: http://resolver.tudelft.nl/uuid:b9076ade-2d6e-4faf-882c-1f6115a1317a.

[62] Boeing. *767 Airplane Characteristics for Airport Planning*. 2023. URL: https://www.boeing.com/commercial/airports/plan_manuals.page (visited on 08/26/2024).

[63] J. Roskam. *AIRPLANE DESIGN PART V : COMPONENT WEIGHT ESTIMATION*. Roskam Aviation and Engineering Corporation, 1985.

[64] W. Dobrzynski. “Almost 40 years of airframe noise research: What did we achieve?” In: *Journal of Aircraft* 47 (2 2010), pp. 353–367. ISSN: 15333868. DOI: 10.2514/1.44457.

[65] J. Roskam. *Airplane fligt dynamics and automatic flight controls*. Design, Analysis and Research Corporation, 2001.

[66] Airbus. *A300 - AIRCRAFT CHARACTERISTICS - AIRPORT AND MAINTENANCE PLANNING*. 2009. URL: https://www.airbus.com/en/airport-operations-and-technical-data/aircraft-characteristics (visited on 01/05/2024).

A

CS-25 Landing Gear Ground Load Cases

This appendix serves as an overview of ground load cases used for structural sizing of the landing gear evaluated in this research. Load conditions prescribed in CS25 oftentimes impose multiple load case variations, for example due to variations in touchdown speed and mass. Imposed post loads as a result of each load case variation are summarised in a table A.1. Please refer to Chapter 3 for derivations and assumptions. Supportive geometry definitions are shown in Figure A.1.

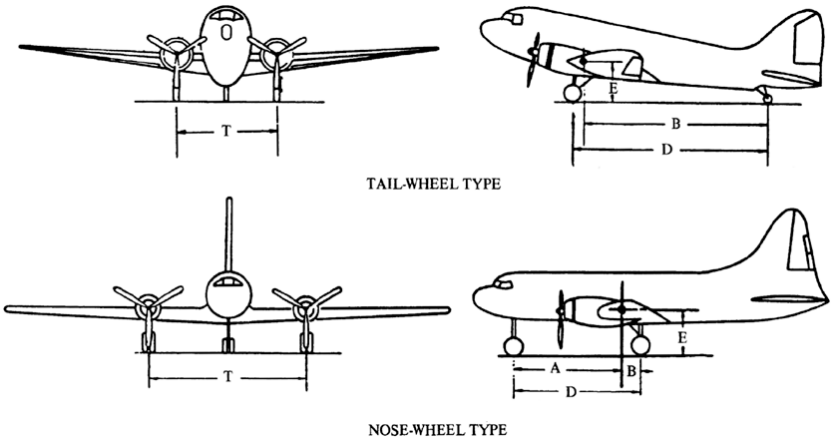

Figure A.1: Landing gear dimensions [17].

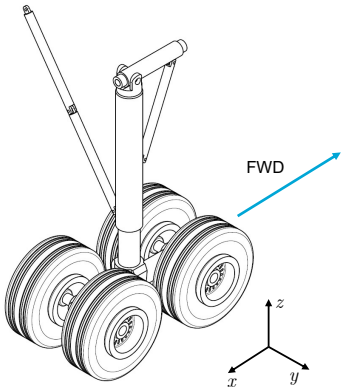

Figure A.2: Landing gear reference frame, showing right main landing gear.

A.1. Landing

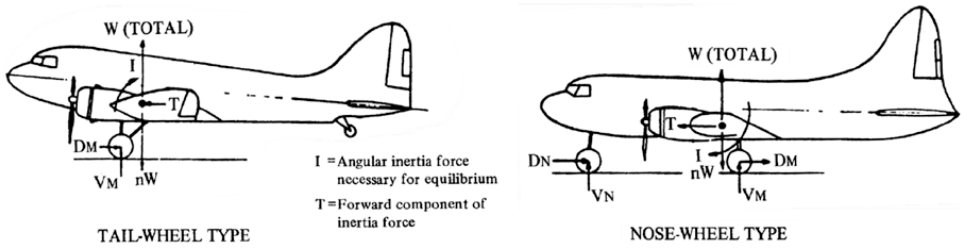

Figure A.3: CS 25.479 level landing conditions [17].

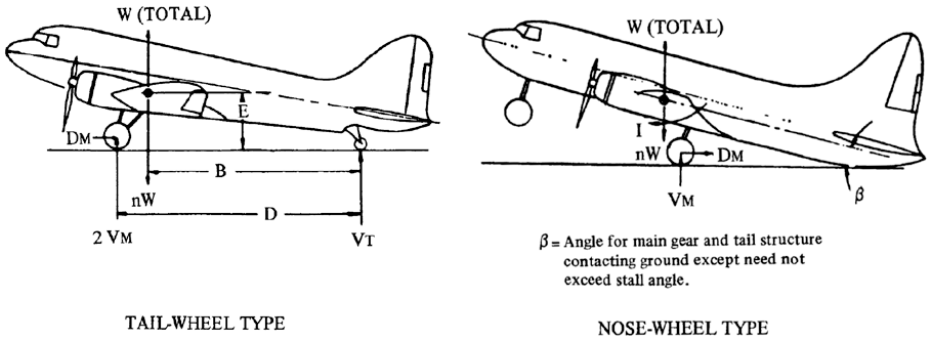

Figure A.4: CS 25.481 tail-down landing conditions [17].

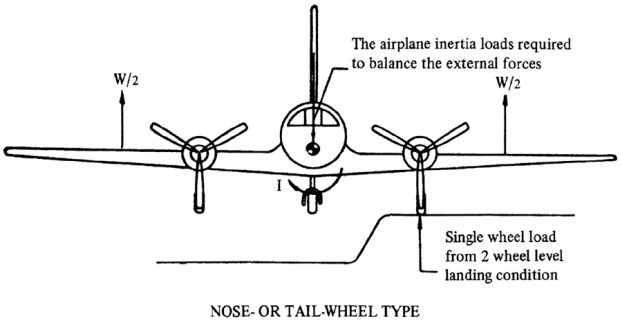

Figure A.5: CS 25.483 one-gear landing conditions [17].

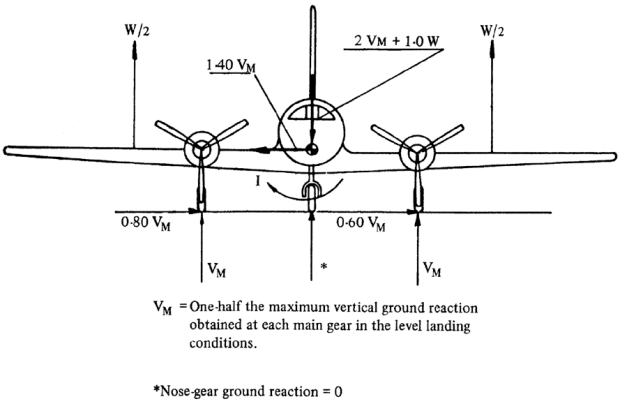

Figure A.6: CS 25.485 side load conditions [17].

A.2. Ground-handling

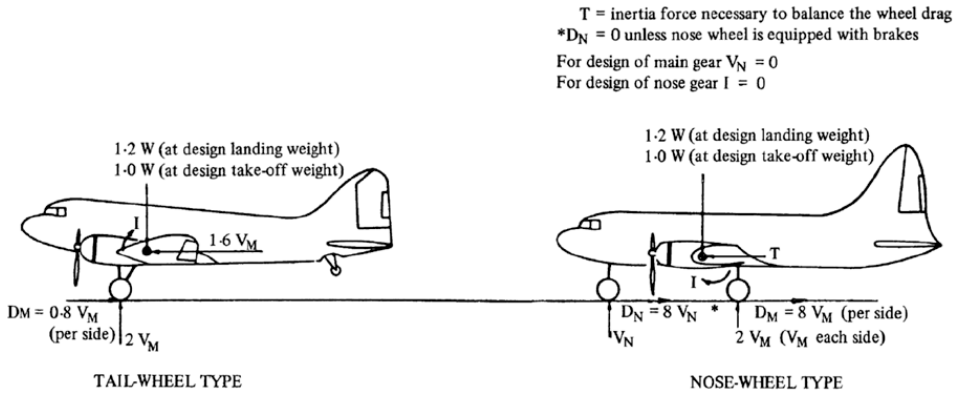

Figure A.7: CS 25.493 braked roll conditions [17].

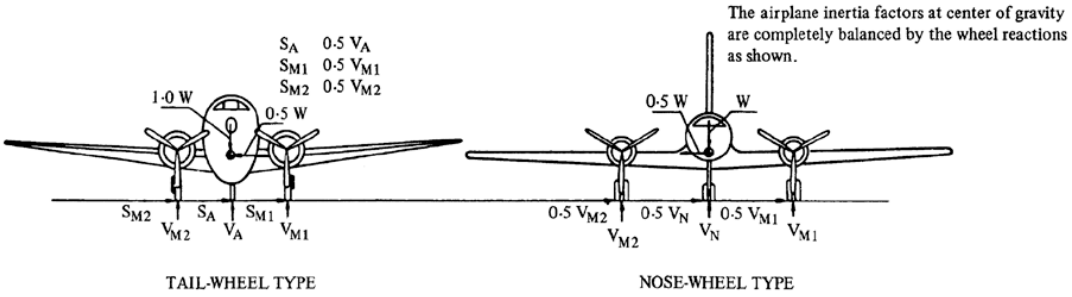

Figure A.8: CS 25.495 turning [17].

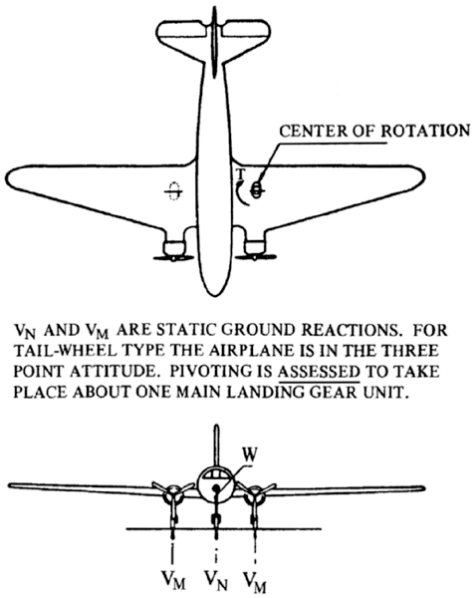

Figure A.9: CS 25.503 pivoting [17].

Table A.1: Overview of main gear loads used for structural sizing [17].

CS ID and Description	Type	LC ID	m (kg)	V_z (m/s)	θ (°)	L (N)	m_{mlg} (kg)	$F_{\text{mlg,x}}$ (N)[1]	$F_{\text{mlg,y}}$ (N)	$F_{\text{mlg,z}}$ (N)
CS 25.479 Level landing conditions	Landing	LVL 1	MLM	3.05	0	W	$\frac{1}{2}m$	$0.25F_{\text{mlg,z}}$	0	$\lambda_{\text{mlg}}gm_{\text{mlg}}$
	Landing	LVL 2	MLM	3.05	θ_{static}	W	$\frac{1}{2}\frac{A}{D}m$	$0.25F_{\text{mlg,z}}$	0	$\lambda_{\text{mlg}}gm_{\text{mlg}}$
	Landing	LVL 3	MTOM	1.83	0	W	$\frac{1}{2}m$	$0.25F_{\text{mlg,z}}$	0	$\lambda_{\text{mlg}}gm_{\text{mlg}}$
	Landing	LVL 4	MTOM	1.83	θ_{static}	W	$\frac{1}{2}\frac{A}{D}m$	$0.25F_{\text{mlg,z}}$	0	$\lambda_{\text{mlg}}gm_{\text{mlg}}$
	Landing	LAT 1	MLM	3.05	0	W	$\frac{1}{2}m$	$0.40F_{\text{mlg,z}}$	$\pm 0.25F_{\text{mlg,z}}$	$0.75\lambda_{\text{mlg}}gm_{\text{mlg}}$
	Landing	LAT 2	MLM	3.05	θ_{static}	W	$\frac{1}{2}\frac{A}{D}m$	$0.40F_{\text{mlg,z}}$	$\pm 0.25F_{\text{mlg,z}}$	$0.75\lambda_{\text{mlg}}gm_{\text{mlg}}$
CS 25.481 Tail-down landing conditions	Landing	TDL 1	MLM	3.05	θ_{max}	W	$\frac{1}{2}m$	0	0	$\lambda_{\text{mlg}}gm_{\text{mlg}}$
	Landing	TDL 2	MTOM	1.83	θ_{max}	W	$\frac{1}{2}m$	0	0	$\lambda_{\text{mlg}}gm_{\text{mlg}}$
CS 25.483 One-gear landing conditions	Landing	OGL 1	MLM	3.05	0	W	$\frac{1}{2}m$	$0.25F_{\text{mlg,z}}$	0	$\lambda_{\text{mlg}}gm_{\text{mlg}}$
	Landing	OGL 2	MTOM	1.83	0	W	$\frac{1}{2}m$	$0.25F_{\text{mlg,z}}$	0	$\lambda_{\text{mlg}}gm_{\text{mlg}}$
CS 25.485 Side-load conditions	Landing	SLL 1	MLM	3.05	0	W	$\frac{1}{2}m$	0	$-0.8F_{\text{mlg,z}}$[2]	$0.5\lambda_{\text{mlg}}gm_{\text{mlg}}$
	Landing	SLL 1	MLM	3.05	0	W	$\frac{1}{2}m$	0	$0.6F_{\text{mlg,z}}$[2]	$0.5\lambda_{\text{mlg}}gm_{\text{mlg}}$
	Landing	SLL 2	MTOM	1.83	0	W	$\frac{1}{2}m$	0	$-0.8F_{\text{mlg,z}}$[2]	$0.5\lambda_{\text{mlg}}gm_{\text{mlg}}$
	Landing	SLL 2	MTOM	1.83	0	W	$\frac{1}{2}m$	0	$0.6F_{\text{mlg,z}}$[2]	$0.5\lambda_{\text{mlg}}gm_{\text{mlg}}$
CS 25.491 Taxi, take-off and landing roll	Ground-handling	GRO 1	MTOM	0	θ_{static}	0	$\frac{1}{2}\frac{A}{D}m$	0	0	$1.7gm_{\text{mlg}}$[3]
	Ground-handling	GRO 2	MTOM	0	θ_{static}	0	$\frac{1}{2}\frac{A}{D}m$	$0.2F_{\text{mlg,z}}$	$\pm 0.2F_{\text{mlg,z}}$	$0.9\times 1.7gm_{\text{mlg}}$[3]
CS 25.493 Braked roll conditions	Ground-handling	BRR 1	MLM	0	0	0	$\frac{1}{2}m$	$0.8F_{\text{mlg,z}}$	0	$1.2gm_{\text{mlg}}$[3]
	Ground-handling	BRR 2	MLM	0	θ_{static}	0	$\frac{1}{2}\frac{A}{D}m$	$0.8F_{\text{mlg,z}}$	0	$1.2gm_{\text{mlg}}$[3]
	Ground-handling	BRR 3	MRM	0	0	0	$\frac{1}{2}m$	$0.8F_{\text{mlg,z}}$	0	$1.0gm_{\text{mlg}}$[3]
	Ground-handling	BRR 4	MRM	0	θ_{static}	0	$\frac{1}{2}\frac{A}{D}m$	$0.8F_{\text{mlg,z}}$	0	$1.0gm_{\text{mlg}}$[3]
CS 25.495 Turning	Ground-handling	TRN 1	MRM	0	θ_{static}	0	$\frac{1}{2}\frac{A}{D}m$	0	$\pm 0.5F_{\text{mlg,z}}$	$1.0gm_{\text{mlg}}$
CS 25.503 Pivoting	Ground-handling	PVT 1	MRM	0	θ_{static}	0	$\frac{1}{2}\frac{A}{D}m$	$0.8F_{\text{mlg,z}}$	0	$1.0gm_{\text{mlg}}$
CS 25.507 Reversed braking	Ground-handling	RBR 1	MRM	0	θ_{static}	0	$\frac{1}{2}\frac{A}{D}m$	$-0.55F_{\text{mlg,z}}$	0	$1.0gm_{\text{mlg}}$

[1] If case describes landing conditions, spin-up and spring back loads may be higher than prescribed drag loads. Please refer to Section 3.5 for more information.
[2] For right main landing gear.
[3] For taxi, take-off and landing roll and braked roll conditions, generated downforce must be added to the vertical reaction, if applicable.

B

Input Data Derivations

B.1. Aircraft specifications

B.1.1. Centre of gravity relative to mean aerodynamic chord

Commonly, longitudinal aircraft centre of gravity locations are expressed relative to the mean aerodynamic chord (MAC). The mean aerodynamic chord (MAC) length can be calculated using Equation B.1, where MAC_i and S_i are the mean aerodynamic chord and surface area of a wing planform panel, as illustrated in Figure B.1 [65]. The wing planform panels have a root chord $c_{\text{i},1}$, a tip chord $c_{\text{i},2}$, a taper ratio λ_i, and a span y. The x-position of the MAC leading edge x_MAC can be calculated using Equation B.2, where Λ is the leading edge sweep angle.

$$\text{MAC} = \frac{\sum_{\text{i}=1}^{\text{m}+1} \text{MAC}_\text{i} S_\text{i}}{\sum_{\text{i}=1}^{\text{m}+1} S_\text{i}}, \text{ where: } \text{MAC}_\text{i} = \frac{2}{3} c_{\text{i},1} \left(\frac{1 + \lambda_\text{i} + \lambda_\text{i}^2}{1 + \lambda_\text{i}} \right), \text{ and } S_\text{i} = \frac{y_{\text{i}+1} - y_\text{i}}{2} (c_{\text{i},1} + c_{\text{i},2}) \tag{B.1}$$

$$x_\text{MAC} = \frac{\sum_{\text{i}=1}^{\text{m}+1} x_{\text{MAC}_\text{i}} S_\text{i}}{\sum_{\text{i}=1}^{\text{m}+1} S_\text{i}}, \text{ where: } x_{\text{MAC}_\text{i}} = \frac{(y_{\text{i}+1} - y_\text{i})(1 + 2\lambda_\text{i})}{3(1 + \lambda_\text{i})} \tan \Lambda_{\text{LE,i}} \tag{B.2}$$

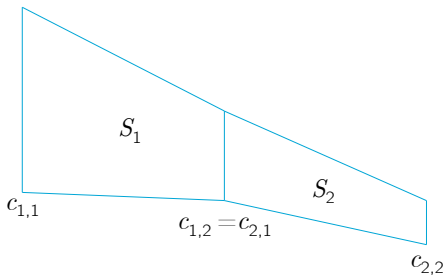

Figure B.1: Wing planform with two planform panels.

The centre of gravity CG_x can now be expressed relative to the mean aerodynamic chord using Equation B.3.

$$\text{CG}_{x,\%MAC} = \frac{\text{CG}_x - x_\text{MAC}}{\text{MAC}} \tag{B.3}$$

B.1.2. Vertical centre of gravity location

The vertical centre of gravity location, or centre of gravity height, is required to evaluate the vertical reaction load on the nose gear during braking, and to evaluate ground stability after push-back and when the aircraft is in the maximum pitch-up attitude.

Centre of gravity heights of aircraft considered in this research are assumed to be similar to that of the A300-B2, which is estimated using the group weight contributions specified by Roskam [63]. Each weight group is assumed to have a uniform distribution of mass, such that the mass can be represented by a point mass m_{i}. The point mass is acting at an assumed centroid location $\bar{z}_{\text{i}}$. Only weight groups contributing to the empty weight of the aircraft are considered, as payload and fuel are assumed to leave the vertical location of the centre of gravity unaffected. The relative weight group contributions to the total aircraft weight for the A300-B2 are shown in Table B.1 [63]. A300-B2 weight group centroid height is measured from the scaled drawings provided in the A300 Aircraft Characteristics for Airport Planning manuals [66], as illustrated in Figure B.2. Substituting the group weight contributions and heights into Equation B.4, a centre of gravity height of 4.12 m is obtained.

$$\bar{z}_{\text{cg}} = \frac{\sum_{\text{i}=1}^{\text{n}} \bar{z}_{\text{i}} m_{\text{i}}}{\sum_{\text{i}=1}^{\text{n}} m_{\text{i}}} \tag{B.4}$$

Table B.1: A300-B2 group weight contributions and heights.

Weight group	Contribution	Letter	Height
Nacelle group	0.023	A	2.26 m
Power plant	0.076	B	2.26 m
Landing gear group	0.045	C	2.26 m
Wing group	0.146	D	4.28 m
Fuselage group	0.119	E	4.86 m
Fixed equipment	0.116	F	4.86 m
Empennage group	0.020	G	7.71 m
Total	0.545	-	4.12 m

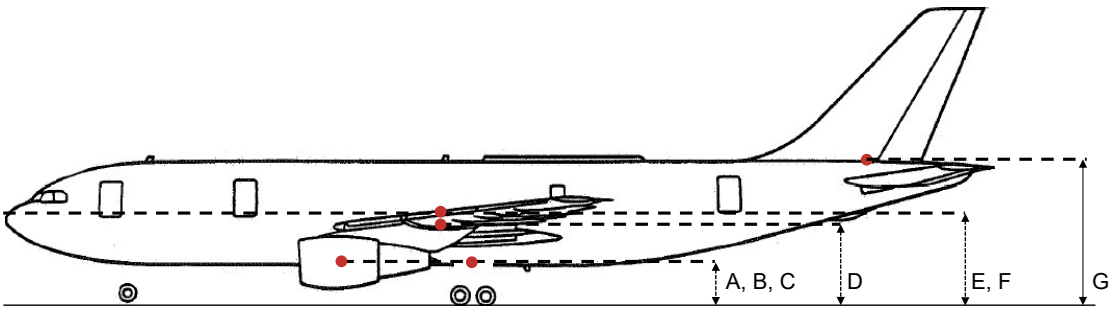

Figure B.2: A300-B2 weight group height definitions.

Taking the centre of gravity height (4.12 m) relative to the fuselage centreline height (4.86 m), and normalising it with the fuselage height or diameter (5.64 m) [66], we obtain:

$$\bar{z}_{\text{cg,cl}} = -0.13 H_{\text{fuselage}} \tag{B.5}$$

Please note that a positive $\bar{z}_{\text{cg,cl}}$ denotes a location above the fuselage centreline, following standard aircraft design reference frame convention.

B.1.3. Maximum aircraft pitch attitudes

The method for calculating the maximum pitch attitude of an aircraft when the shock absorber is in its static position is illustrated in Figure B.3. A first line is drawn that is tangent to the aircraft fuselage and intersects the aircraft pivot point, in this case the bogie joint. A second line is drawn perpendicular to the ground surface, intersecting the intersection of the first line and aircraft fuselage. Then, a third line is drawn, extending from the aircraft pivot point, intersecting the second line where it intersects the ground surface. The maximum aircraft pitch attitude with static shock absorber $\theta_{\text{max,statSA}}$ is then given by the circular arc between the two lines that have their origin at the aircraft pivot point, as illustrated in the figure.

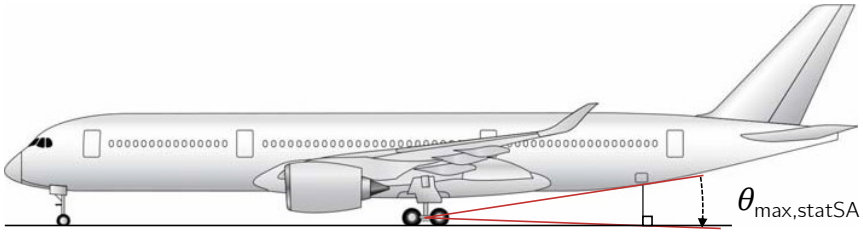

Figure B.3: Maximum aircraft pitch angle with fully compressed shock absorber. Image modified from [43].

The maximum aircraft pitch attitude with extended shock absorber $\theta_{\text{max,extSA}}$ is estimated using assumed equal differences between the static and extended shock absorber maximum pitch attitudes compared to other aircraft. Examples are provided in Table B.2.

Table B.2: Maximum aircraft pitch attitudes with static shock absorber ($\theta_{\text{max,statSA}}$) and extended shock absorber ($\theta_{\text{max,extSA}}$) [60].

Aircraft	$\theta_{\text{max,statSA}}$	$\theta_{\text{max,extSA}}$
A319	$13.9°$	$15.5°$
A320	$11.7°$	$13.5°$
A321	$9.7°$	$11.2°$
A340-300	$10.1°$	$14.2°$

C

Additional Verification and Validation Study Data

C.1. Reference aircraft gear design initialisation

Table C.1: Reference aircraft geometry specifications, based on Airport Planning Manuals as discussed in Section 4.2 [58, 59].

Item	Unit	Format	A310-200	B707-320
MDS_A	m	(x, y, z)	(19.9, 2.8, -1.2)	(22.9, 1.9, -1.7)
MDS_B	m	(x, y, z)	(23.8, 1.9, -1.2)	(23.8, 1.9, -1.7)
MDS_C	m	(x, y, z)	(21.9, 7.8, -0.3)	(23.8, 4.3, -1.1)
x_{mlg}	-	$x_{lb} \leq x_0 \leq x_{ub}$	$0.0 \leq 0.5 \leq 1.0$	$0.0 \leq 0.5 \leq 1.0$
y_{mlg}	-	$x_{lb} \leq x_0 \leq x_{ub}$	$0.0 \leq 0.5 \leq 1.0$	$0.0 \leq 0.5 \leq 1.0$
NDS_A	m	(x, y, z)	(1.4, 0.0, -1.4)	(1.4, 0.0, -1.2)
NDS_B	m	(x, y, z)	(8.4, 0.0, -2.5)	(6.4, 0.0, -2.2)
x_{nlg}	-	$x_{lb} \leq x_0 \leq x_{ub}$	$0.0 \leq 0.5 \leq 1.0$	$0.0 \leq 0.5 \leq 1.0$
$s_{rs,min}$	m	-	0.02	0.02
$s_{cl,min}$	m	-	0.27	0.22
$s_{fpb,min}$	m	-	0.02	0.02
l_{fpb}	m	-	1.4	1.4
CCP_1	m	(x, y, z)	(44.9, 0.0, 1.3)	(41.2, 0.0, -1.3)
CCP_2	m	(x, y, z)	(35.3, 0.0, -1.8)	(37.5, 0.0, -1.8)
CCP_3	m	(x, y, z)	(28.6, 22.0, 0.5)	(33.4, 22.2, 0.6)
CCP_4	m	(x, y, z)	(15.0, 7.8, -4.1)	(26.7, 15.5, -1.6)
$GMCP_1$	m	(x, y, z)	(28.6, -22.0, 0.5)	(33.4, -22.2. 0.6)
$GMCP_2$	m	(x, y, z)	(0.0, 0.0, -0.2)	(0.0, 0.0, -0.2)
$GMCP_3$	m	(x, y, z)	(46.7, -8.1, 2.2)	(46.6, -7.0, 1.8)

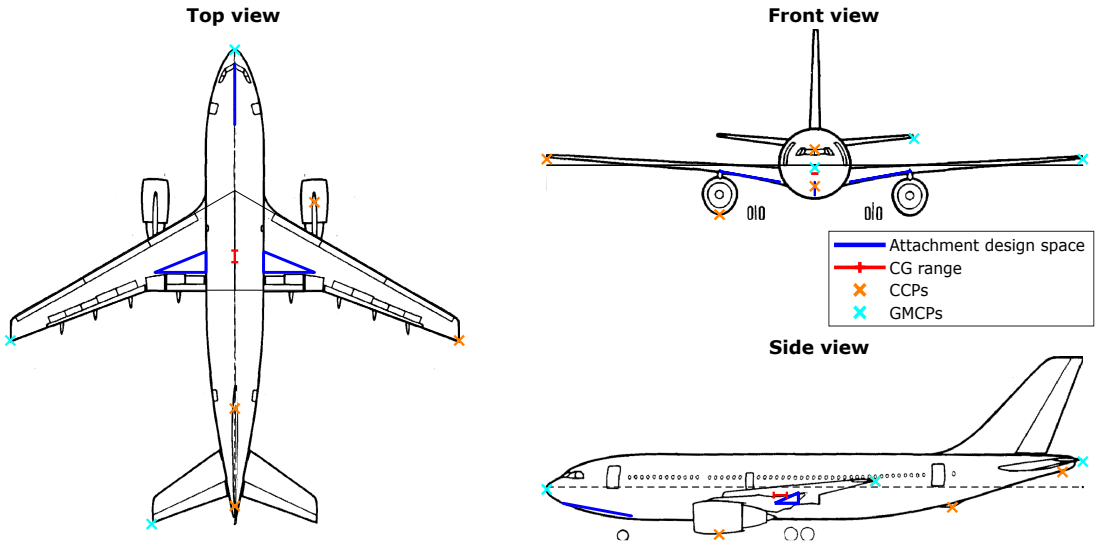

Figure C.1: A310-200 gear attachment design spaces, critical points, and centre of gravity range. Image modified from [43].

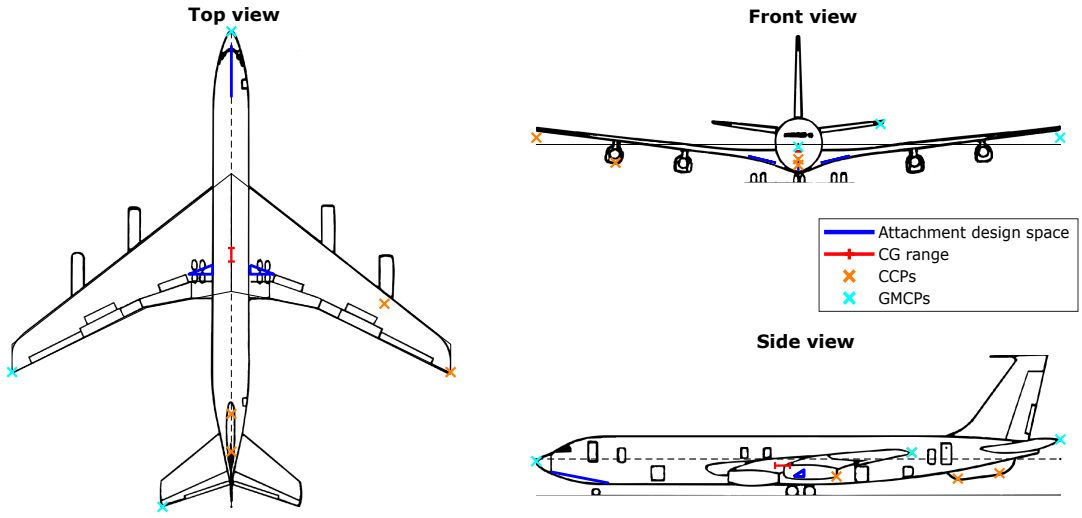

Figure C.2: Boeing 707-320 gear attachment design spaces, critical points, and centre of gravity range. Image modified from [43].

Table C.2: Reference aircraft mass specifications, based on Airport Planning Manuals as discussed in Section 4.2 [58, 59].

Item	Unit	Format	A310-200	B707-320
CG_{fwd}	m	(x, y, z)	(19.8, 0.0, -0.7)	(21.2, 0.0, -0.6)
$CG_{fwd,\%MAC}$	% MAC	-	16	8
CG_{aft}	m	(x, y, z)	(20.9, 0.0, -0.7)	(22.6, 0.0, -0.6)
$CG_{aft,\%MAC}$	% MAC	-	35	28
MRM	kg	-	1.43×10^5	1.44×10^5
MTOM	kg	-	1.42×10^5	1.42×10^5
MLM	kg	-	1.22×10^5	0.94×10^5
OEM	kg	-	0.78×10^5	0.65×10^5
MRM_{range}	-	(x_{fwd}, x_{aft})	(0.0, 1.0)	(0.0, 1.0)
$MTOM_{range}$	-	(x_{fwd}, x_{aft})	(0.0, 1.0)	(0.0, 1.0)
MLM_{range}	-	(x_{fwd}, x_{aft})	(0.0, 1.0)	(0.0, 1.0)

Table C.3: Reference aircraft operational requirements, based on landing gear background study (Section 2.4) and Airport Planning Manuals, as discussed in Section 4.2 [42, 43].

Item	Unit	Format	A310-200	B707-320
$\theta_{\text{tpb,min}}$	°	-	15.0	15.0
$\psi_{\text{tno,max}}$	°	-	63.0	63.0
ϕ_{max}	°	-	8.0	8.0
θ_{stat}	°	-	0.0	0.0
$\theta_{\text{max,statSA}}$	°	-	12.0	6.0
$\theta_{\text{max,extSA}}$	°	-	13.8	7.8
$\hat{\beta}_{\text{nlg,min}}$	-	$x_{\text{lb}} \leq x_0 \leq x_{\text{ub}}$	$0.065 \leq 0.10 \leq 0.15$	$0.04 \leq 0.10 \leq 0.15$
$\hat{\beta}_{\text{nlg,max}}$	-	$x_{\text{lb}} \leq x_0 \leq x_{\text{ub}}$	$0.065 \leq 0.10 \leq 0.15$	$0.04 \leq 0.10 \leq 0.15$
$\beta_{\text{mlg,max}}$	-	-	N.A.	N.A.
TDG	-	-	5	4
$\lambda_{\text{steering}}$	°	-	65	60
V_1	m/s	-	90.0	90.0

Table C.4: Reference aircraft strut and bogie concept specifications.

Item	Unit	Format	A310-200	B707-320
Strut	-	-	Concept A	Concept A
l_{ss}	m	$x_{\text{lb}} \leq x_0 \leq x_{\text{ub}}$	$1.0 \leq 2.0 \leq 6.0$	$1.0 \leq 2.0 \leq 6.0$
$\theta_{\text{ss,ext}}$	°	$x_{\text{lb}} \leq x_0 \leq x_{\text{ub}}$	$-9.0 \leq -5.0 \leq 0.0$	$-9.0 \leq -5.0 \leq 0.0$
$\theta_{\text{ss,ret}}$	°	-	0.0	0.0
$\phi_{\text{ss,ret}}$	°	-	-80.0	-86.0
$\psi_{\text{mlg,ret}}$	°	$x_{\text{lb}} \leq x_0 \leq x_{\text{ub}}$	$0.0 \leq 0.0 \leq 0.0$	$0.0 \leq 0.0 \leq 0.0$
l_{us}	m	-	N.A.	N.A.
$\theta_{\text{us,ext}}$	°	$x_{\text{lb}} \leq x_0 \leq x_{\text{ub}}$	N.A.	N.A.
$\phi_{\text{us,ext}}$	°	$x_{\text{lb}} \leq x_0 \leq x_{\text{ub}}$	N.A.	N.A.
$\theta_{\text{us,ret}}$	°	-	N.A.	N.A.
$\phi_{\text{us,ret}}$	°	-	N.A.	N.A.
l_{hs}	m	-	N.A.	N.A.
θ_{hs}	°	-	N.A.	N.A.
Bogie	-	-	Concept A	Concept A
l_{offset}	m	-	N.A.	N.A.
$l_{\text{ineffective}}$	m	-	0.45	0.45
$\theta_{\text{nlg,ret}}$	°	-	110	115

Table C.5: Reference aircraft bogie and tyre sizing specifications.

Item	Unit	Format	A310-200	B707-320
$N_{\text{mlg,w}}$	-	-	8	8
$N_{\text{mlg,ss}}$	-	-	2	2
l_{bogie}	m	-	1.40	1.42
w_{bogie}	m	-	0.93	0.88
Tyre_{mlg}	-	-	46x17.0R20	46x16
$N_{\text{nlg,w}}$	-	-	2	2
w_{nlg}	m	-	0.63	0.56
Tyre_{nlg}	-	-	40x14R16	39x13
$a_{x,\text{des}}$	m/s^2	-	3.5	3.5

Table C.6: Reference aircraft shock absorber sizing specifications.

Item	Unit	Format	A310-200	B707-320
λ_{mlg}	-	-	1.20	1.20
$P_{\text{mlg,static}}$	MPa	-	13.8	13.8
b_{mlg}	-	-	0.10	0.10
λ_{nlg}	-	-	1.30	1.30
$P_{\text{nlg,static}}$	MPa	-	13.8	13.8
b_{nlg}	-	-	0.10	0.10
s_{Fmax}	-	-	0.30	0.30

Table C.7: Reference aircraft special landing gear feature specifications.

Item	Unit	Format	A310-200	B707-320
Articulation	-	Boolean	False	False
$\lambda_{\text{mlg,art}}$	-	-	N.A.	N.A.
θ_{bogie}	$^\circ$	$x_{\text{lb}} \leq x_0 \leq x_{\text{ub}}$	N.A.	N.A.
$l_{\text{x,pivot}}$	m	-	N.A.	N.A.
$l_{\text{z,pivot}}$	m	-	N.A.	N.A.
$l_{\text{margin,art}}$	m	-	N.A.	N.A.
Shortening	-	Boolean	False	False
$l_{\text{shortening}}$	m	-	N.A.	N.A.

C.2. Reference aircraft stick model generation

Table C.8: Design vector before and after optimisation.

Variable	Unit	x_{lb}	x_0	x_{ub}	A310-200	B707-320
x_{mlg}	-	0.00	0.50	1.00	0.68	0.00
y_{mlg}	-	0.00	0.50	1.00	0.38	0.55
x_{nlg}	-	0.00	0.50	1.00	0.90	0.47
l_{ss}	m	1.50	2.00	8.00	3.23	1.72
$\theta_{ss,ext}$	°	-9.00	-5.00	0.00	-5.67	0.00
$\psi_{mlg,ret}$	°	0.00	0.00	0.00	0.00	0.00
$\theta_{us,ext}$	°	0.00	0.00	0.00	N.A.	N.A.
$\phi_{us,ext}$	°	0.00	0.00	0.00	N.A.	N.A.
θ_{bogie}	°	0.00	0.00	21.0	N.A.	N.A.
$\hat{\beta}_{nlg,min}$	-	0.04	0.10	0.15	0.065	0.043
$\hat{\beta}_{nlg,max}$	-	0.04	0.10	0.15	0.145	0.109

Table C.9: Stick model generation constraint activity.

Constraint	A310-200	B707-320
Longitudinal stability - minimum nlg load	Active	Inactive
Longitudinal stability - maximum nlg load	Inactive	Inactive
Longitudinal stability - rotated tipover	Active	Inactive
Longitudinal stability - push-back tipover	Active	Inactive
Lateral stability - lateral turnover	Inactive	Inactive
Ground clearance - static shock absorber	Active	Active
Ground clearance - extended shock absorber	Inactive	Inactive
Airframe integration - nlg stowage	Inactive	Active
Airframe integration - mlg stowage	Active	Active
Ground manoeuvring - taxiway design group	Inactive	Inactive
Ground manoeuvring - 180° turn	Inactive	Inactive

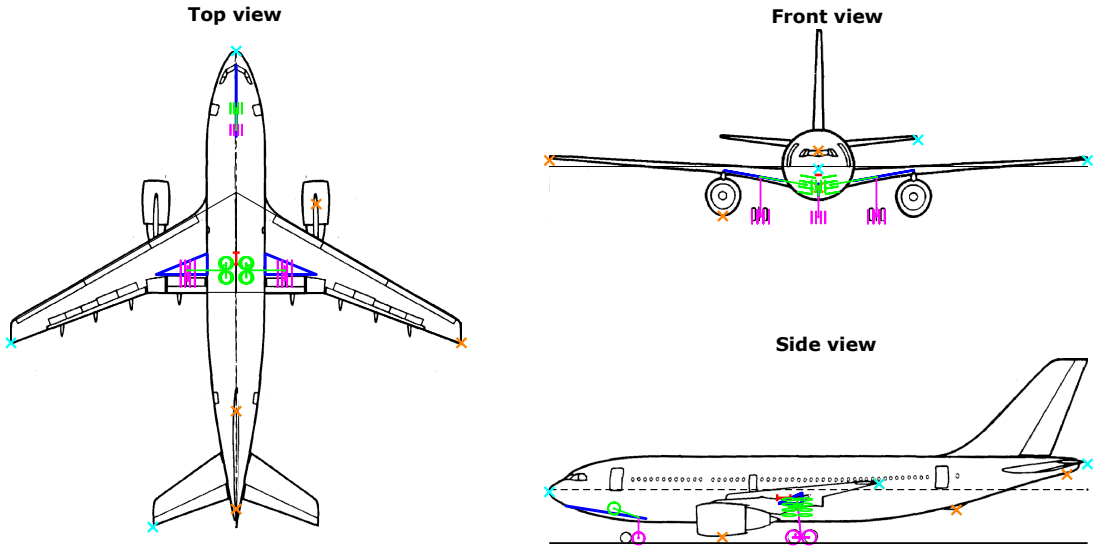

Figure C.3: A310-200 gear stick model results after optimisation.

Table C.10: A310-200 gear stick model validation

Item	Unit	Estimated	Actual	Est/Act
X_{mlg}	m	21.8	21.9	1.00
Y_{mlg}	m	4.72	4.80	0.98
$l_{\text{mlg,static}}$	m	3.28	-	-
$l_{\text{mlg,extended}}$	m	3.80	-	-
X_{nlg}	m	7.72	6.67	1.15
$l_{\text{nlg,static}}$	m	1.79	-	-
$l_{\text{nlg,extended}}$	m	2.25	-	-

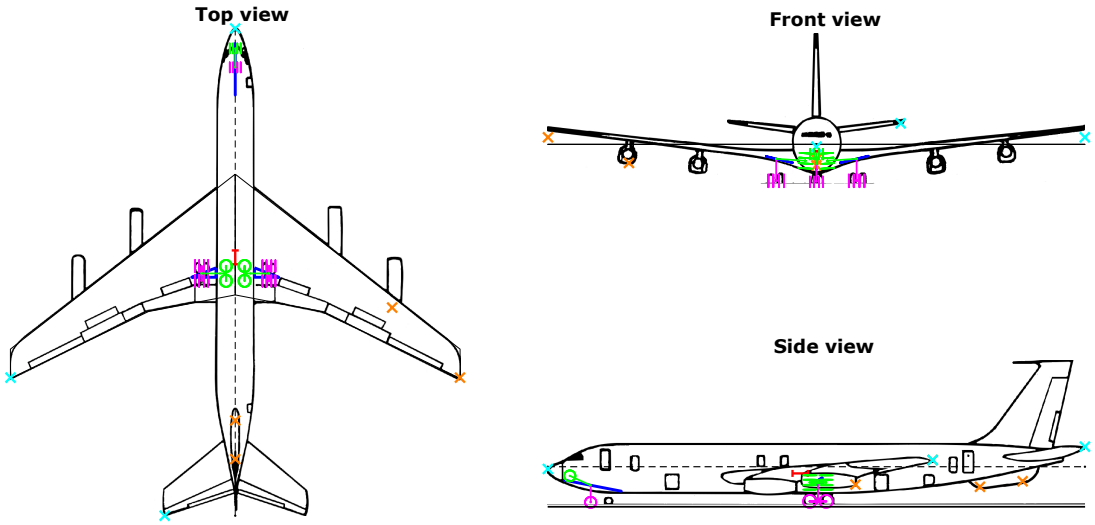

Figure C.4: Boeing 707-320 gear stick model results after optimisation.

Table C.11: Boeing 707-320 gear stick model validation

Item	Unit	Estimated	Actual	Est/Act
x_{mlg}	m	23.4	23.3	1.00
y_{mlg}	m	3.22	3.37	0.96
$l_{\text{mlg,static}}$	m	1.76	-	-
$l_{\text{mlg,extended}}$	m	2.31	-	-
x_{nlg}	m	3.73	5.30	0.70
$l_{\text{nlg,static}}$	m	1.54	-	-
$l_{\text{nlg,extended}}$	m	2.02	-	-

C.3. Finite element model verification

Table C.12: Generic gear model node specifications.

Node	x (m)	y (m)	z (m)	Type
O	0.00	0.00	0.00	Hinge
A	0.00	0.00	-1.40	Beam
B	0.00	0.00	-1.80	Beam
C	0.00	0.00	-2.35	Hinge
D	0.10	0.00	0.00	-
E	1.00	0.00	0.00	Beam
F	1.10	0.00	0.00	-
G	1.00	0.00	-0.12	Hinge
H	0.20	0.00	-1.40	Hinge
I	0.00	-0.20	-1.80	Hinge
J	0.00	-1.97	-0.03	-
K_L	0.71	-0.44	-2.35	Hinge
K_C	0.71	0	-2.35	Beam
K_R	0.71	0.44	-2.35	Hinge
L_L	-0.71	-0.44	-2.35	Hinge
L_C	-0.71	0	-2.35	Beam
L_R	-0.71	0.44	-2.35	Hinge
M_L	0.71	-0.44	-2.83	-
M_R	0.71	0.44	-2.83	-
N_L	-0.71	-0.44	-2.83	-
N_R	-0.71	0.44	-2.83	-

General

Shear loads V_x and V_y, axial load N_z, bending moments M_x and M_y and torsional load T_z are defined as illustrated in Figure C.5.

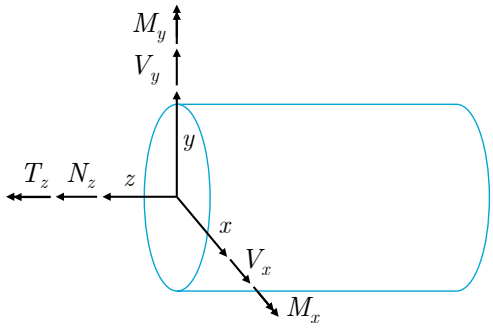

Figure C.5: Structural analysis load definitions.

Bogie beam

$$V_{x,\text{bogie}} = 0 \tag{C.1}$$

$$V_{y,\text{bogie}} = F_{z,\text{K}} = F_{z,\text{L}} \tag{C.2}$$

$$N_{z,\text{bogie}} = F_{x,\text{K}} \vee N_z = -F_{x,\text{L}} \tag{C.3}$$

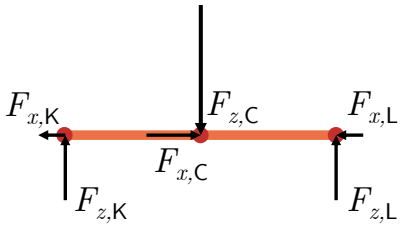

Figure C.6: Bogie beam free body diagram.

$$M_{x,\mathrm{bogie}} = F_{z,\mathrm{K}} l_{\mathrm{KC}} = F_{z,\mathrm{L}} l_{\mathrm{LC}} \tag{C.4}$$

$$M_{y,\mathrm{bogie}} = 0 \tag{C.5}$$

$$T_{z,\mathrm{bogie}} = 0 \tag{C.6}$$

Shock strut

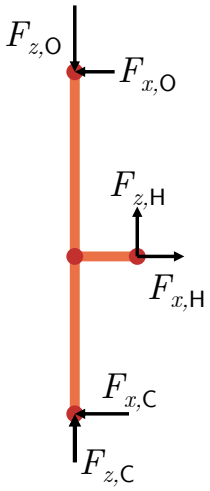

Figure C.7: Shock strut free body diagram.

$$V_{x,\mathrm{strut}} = F_{x,\mathrm{C}} \tag{C.7}$$

$$V_{y,\mathrm{strut}} = 0 \tag{C.8}$$

$$N_{z,\mathrm{strut}} = -(F_{z,\mathrm{C}} + F_{z,\mathrm{H}}) = -(F_{z,\mathrm{C}} + N_{z,\mathrm{dragbrace}} \cos(\theta_{\mathrm{dragbrace}})) \tag{C.9}$$

$$M_{x,\mathrm{strut}} = 0 \tag{C.10}$$

$$M_{y,\mathrm{strut}} = -F_{x,\mathrm{C}} l_{\mathrm{HC}} \tag{C.11}$$

$$T_{z,\mathrm{strut}} = 0 \tag{C.12}$$

Drag brace

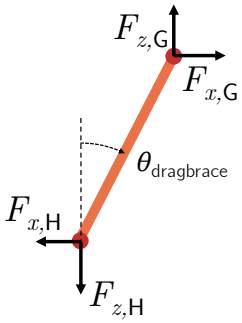

Figure C.8: Drag brace free body diagram.

$$V_{x,\mathrm{dragbrace}} = 0 \tag{C.13}$$

$$V_{y,\mathrm{dragbrace}} = 0 \tag{C.14}$$

$$T_{z,\mathrm{dragbrace}} = \frac{F_{x,\mathrm{H}}}{\sin\left(\theta_{\mathrm{dragbrace}}\right)} = \frac{F_{z,\mathrm{H}}}{\cos\left(\theta_{\mathrm{dragbrace}}\right)} = \frac{F_{x,\mathrm{C}} l_{\mathrm{OC}}}{l_{\mathrm{OH}} \sin\left(\theta_{\mathrm{dragbrace}}\right) + l_{\mathrm{AH}} \cos\left(\theta_{\mathrm{dragbrace}}\right)} \tag{C.15}$$

$$M_{x,\mathrm{dragbrace}} = 0 \tag{C.16}$$

$$M_{y,\mathrm{dragbrace}} = 0 \tag{C.17}$$

$$T_{z,\mathrm{dragbrace}} = 0 \tag{C.18}$$

C.4. Gear mass estimation validation

C.4.1. 3D model generation

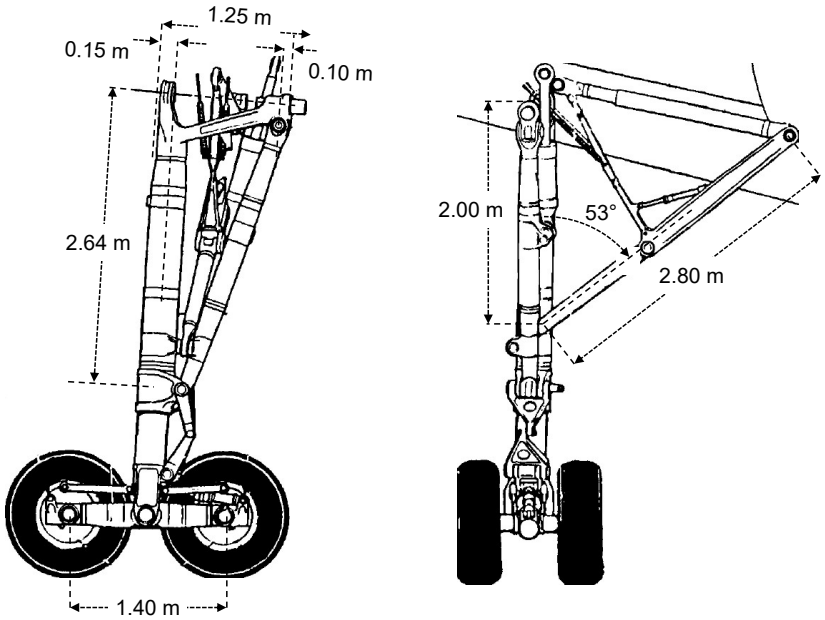

(a) Right main landing gear, right view. **(b)** Right main landing gear, front view.

Figure C.9: A310-200 main gear dimensions, modified from [20].

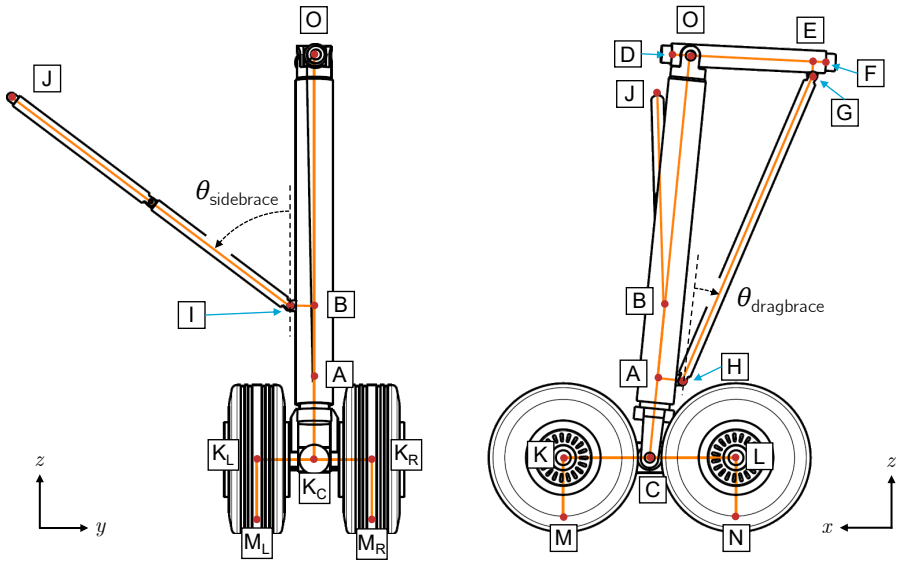

(a) Right main landing gear, back view. **(b)** Right main landing gear, right view.

Figure C.10: A310-200 main gear model node definitions.

Table C.13: A310-200 gear model node specifications (static shock absorber position).

Node	x (m)	y (m)	z (m)	Type
O	0.000	0.000	0.000	Hinge
A	0.260	0.000	-2.617	Beam
B	0.201	0.000	-2.020	Beam
C	0.324	0.000	-3.263	Hinge
D	0.150	0.009	0.007	-
E	-0.997	-0.058	-0.049	Beam
F	-1.097	-0.065	-0.054	-
G	-0.991	-0.059	-0.169	Hinge
H	0.061	-0.012	-2.637	Hinge
I	0.213	-0.204	-2.019	Hinge
J	0.261	-2.442	-0.336	-
K_L	1.023	-0.464	-3.263	Hinge
K_C	1.023	0.000	-3.263	Beam
K_R	1.023	0.464	-3.263	Hinge
L_L	-0.374	-0.464	-3.263	Hinge
L_C	-0.374	0.000	-3.263	Beam
L_R	-0.374	0.464	-3.263	Hinge
M_L	1.023	-0.464	-3.750	-
M_R	1.023	0.464	-3.750	-
N_L	-0.374	-0.464	-3.750	-
N_R	-0.374	0.464	-3.750	-

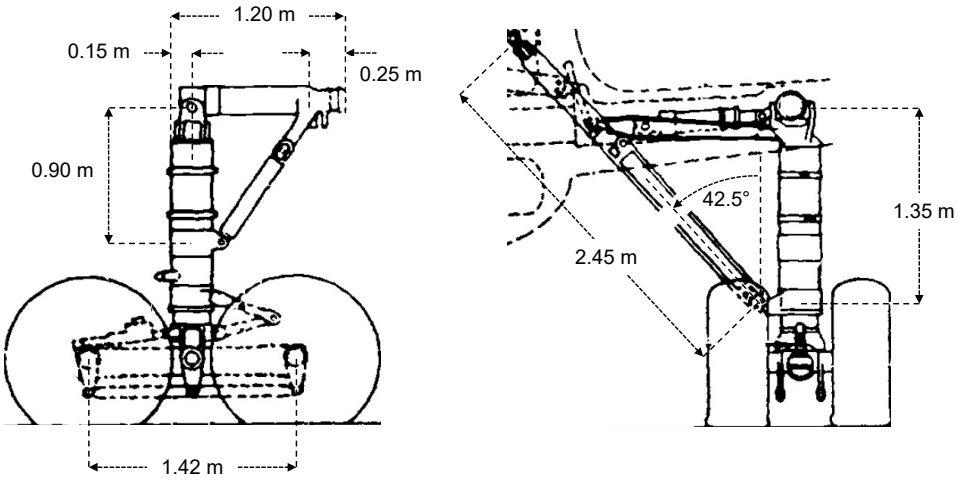

(a) Right main landing gear, right view. **(b)** Right main landing gear, back view.

Figure C.11: Boeing 707-320 main gear dimensions, modified from [20].

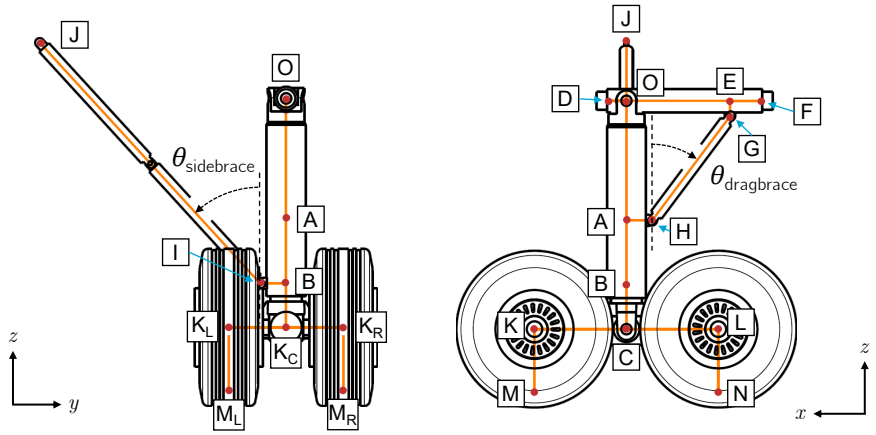

(a) Right main landing gear, back view. **(b)** Right main landing gear, right view.

Figure C.12: Boeing 707-320 main gear model node definitions.

Table C.14: Boeing 707-320 gear model node specifications (static shock absorber position).

Node	x (m)	y (m)	z (m)	Type
O	0.000	0.000	0.000	Hinge
A	0.000	0.000	-0.920	Beam
B	0.000	0.000	-1.420	Beam
C	0.000	0.000	-1.759	Hinge
D	0.150	0.000	0.000	-
E	-0.800	0.000	0.000	Beam
F	-1.050	0.000	0.000	-
G	-0.800	0.000	-0.120	Hinge
H	-0.200	0.000	-0.920	Hinge
I	0.000	-0.200	-1.420	Hinge
J	0.000	-1.890	0.424	-
K_L	0.710	-0.440	-1.759	Hinge
K_C	0.710	0.000	-1.759	Beam
K_R	0.710	0.440	-1.759	Hinge
L_L	-0.710	-0.440	-1.759	Hinge
L_C	-0.710	0.000	-1.759	Beam
L_R	-0.710	0.440	-1.759	Hinge
M_L	0.710	-0.440	-2.242	-
M_R	0.710	0.440	-2.242	-
N_L	-0.710	-0.440	-2.242	-
N_R	-0.710	0.440	-2.242	-

C.4.2. Structural sizing

Tables C.15 and C.17 describe the external loads on the main landing gear of the A310-200 and the Boeing 707-320, following from the load cases outlined in Table A.1. Tables C.16 and C.18 describe the internal loads corresponding to the most critical load case for each structural component. Load case id (LC ID) specifications SU, SB, IB and OB describe spin-up, spring-back, inboard and outboard load conditions respectively. Columns m_{mlg}, θ, x_{s} and r_{tyre} describe the mass on the gear, the aircraft pitch attitude, the shock absorber extension, and the loaded tyre radius. Loads in x and z-direction are applied to nodes K_L, K_R, L_L and L_R. Loads in y-direction are applied to nodes nodes M_L, M_R, N_L and N_R.

Table C.15: Overview of A310-200 external main gear loads.

LC ID	m_{mlg} (kg)	θ (°)	x_{s} (m)	r_{tyre} (in)	F_{x,K_L,K_R} (N)	F_{x,L_L,L_R} (N)	F_{y,M_L,M_R} (N)	F_{y,N_L,N_R} (N)	F_{z,K_L,K_R} (N)	F_{z,L_L,L_R} (N)
LVL 1 SU	6.08×10^4	0.0	0.383	20.2	1.14×10^5	1.14×10^5	0.00	0.00	1.79×10^5	1.79×10^5
LVL 1 SB	6.08×10^4	0.0	0.383	20.2	-1.14×10^5	-1.14×10^5	0.00	0.00	1.79×10^5	1.79×10^5
LVL 2 SU	5.66×10^4	0.0	0.383	20.4	1.07×10^5	1.07×10^5	0.00	0.00	1.67×10^5	1.67×10^5
LVL 2 SB	5.66×10^4	0.0	0.383	20.4	-1.07×10^5	-1.07×10^5	0.00	0.00	1.67×10^5	1.67×10^5
LVL 3 SU	7.10×10^4	0.0	0.383	19.6	1.34×10^5	1.34×10^5	0.00	0.00	2.09×10^5	2.09×10^5
LVL 3 SB	7.10×10^4	0.0	0.383	19.6	-1.34×10^5	-1.34×10^5	0.00	0.00	2.09×10^5	2.09×10^5
LVL 4 SU	6.62×10^4	0.0	0.383	19.9	1.25×10^5	1.25×10^5	0.00	0.00	1.95×10^5	1.95×10^5
LVL 4 SB	6.62×10^4	0.0	0.383	19.9	-1.25×10^5	-1.25×10^5	0.00	0.00	1.95×10^5	1.95×10^5
LAT 1 SU/IB	6.08×10^4	0.0	0.416	21.7	8.58×10^4	8.58×10^4	-3.35×10^4	-3.35×10^4	1.34×10^5	1.34×10^5
LAT 1 SU/OB	6.08×10^4	0.0	0.416	21.7	8.58×10^4	8.58×10^4	3.35×10^4	3.35×10^4	1.34×10^5	1.34×10^5
LAT 1 SB/IB	6.08×10^4	0.0	0.416	21.7	-8.58×10^4	-8.58×10^4	-3.35×10^4	-3.35×10^4	1.34×10^5	1.34×10^5
LAT 1 SB/OB	6.08×10^4	0.0	0.416	21.7	-8.58×10^4	-8.58×10^4	3.35×10^4	3.35×10^4	1.34×10^5	1.34×10^5
LAT 2 SU/IB	5.66×10^4	0.0	0.416	21.9	8.00×10^4	8.00×10^4	-3.13×10^4	-3.13×10^4	1.25×10^5	1.25×10^5
LAT 2 SU/OB	5.66×10^4	0.0	0.416	21.9	8.00×10^4	8.00×10^4	3.13×10^4	3.13×10^4	1.25×10^5	1.25×10^5
LAT 2 SB/IB	5.66×10^4	0.0	0.416	21.9	-8.00×10^4	-8.00×10^4	-3.13×10^4	-3.13×10^4	1.25×10^5	1.25×10^5
LAT 2 SB/OB	5.66×10^4	0.0	0.416	21.9	-8.00×10^4	-8.00×10^4	3.13×10^4	3.13×10^4	1.25×10^5	1.25×10^5
TDL 1 SU	6.08×10^4	13.8	0.383	20.2	1.14×10^5	1.14×10^5	0.00	0.00	1.79×10^5	1.79×10^5
TDL 1 SB	6.08×10^4	13.8	0.383	20.2	-1.14×10^5	-1.14×10^5	0.00	0.00	1.79×10^5	1.79×10^5
TDL 2 SU	7.10×10^4	13.8	0.383	19.6	1.34×10^5	1.34×10^5	0.00	0.00	2.09×10^5	2.09×10^5
TDL 2 SB	7.10×10^4	13.8	0.383	19.6	-1.34×10^5	-1.34×10^5	0.00	0.00	2.09×10^5	2.09×10^5
OGL 1 SU	6.08×10^4	0.0	0.383	20.2	1.14×10^5	1.14×10^5	0.00	0.00	1.79×10^5	1.79×10^5
OGL 1 SB	6.08×10^4	0.0	0.383	20.2	-1.14×10^5	-1.14×10^5	0.00	0.00	1.79×10^5	1.79×10^5
OGL 2 SU	7.10×10^4	0.0	0.383	19.6	1.34×10^5	1.34×10^5	0.00	0.00	2.09×10^5	2.09×10^5
OGL 2 SB	7.10×10^4	0.0	0.383	19.6	-1.34×10^5	-1.34×10^5	0.00	0.00	2.09×10^5	2.09×10^5
SLL 1 IB	6.08×10^4	0.0	0.383	22.0	0.00	0.00	-7.15×10^4	-7.15×10^4	8.94×10^4	8.94×10^4
SLL 1 OB	6.08×10^4	0.0	0.383	22.0	0.00	0.00	5.36×10^4	3.36×10^4	8.94×10^4	8.94×10^4
SLL 2 IB	7.10×10^4	0.0	0.383	21.7	0.00	0.00	-8.36×10^4	-8.36×10^4	1.04×10^5	1.04×10^5
SLL 2 OB	7.10×10^4	0.0	0.383	21.7	0.00	0.00	6.27×10^4	6.27×10^4	1.04×10^5	1.04×10^5
GRO 1	6.64×10^4	0.0	0.044	18.2	0.00	0.00	0.00	0.00	2.77×10^5	2.77×10^5
GRO 2 IB	6.64×10^4	0.0	0.044	18.8	4.98×10^4	4.98×10^4	-4.98×10^4	-4.98×10^4	2.49×10^5	2.49×10^5
GRO 2 OB	6.64×10^4	0.0	0.044	18.8	4.98×10^4	4.98×10^4	4.98×10^4	4.98×10^4	2.49×10^5	2.49×10^5
BRR 1	6.08×10^4	0.0	0.044	20.2	1.43×10^5	1.43×10^5	0.00	0.00	1.79×10^5	1.79×10^5
BRR 2	5.68×10^4	0.0	0.044	20.4	1.33×10^5	1.33×10^5	0.00	0.00	1.67×10^5	1.67×10^5
BRR 3	7.15×10^4	0.0	0.044	20.2	1.40×10^5	1.40×10^5	0.00	0.00	1.75×10^5	1.75×10^5
BRR 4	6.68×10^4	0.0	0.044	20.5	1.31×10^5	1.31×10^5	0.00	0.00	1.64×10^5	1.64×10^5
TRN 1 IB	6.68×10^4	0.0	0.044	20.5	0.00	0.00	-8.19×10^4	-8.19×10^4	1.75×10^5	1.75×10^5
TRN 1 OB	6.68×10^4	0.0	0.044	20.5	0.00	0.00	8.19×10^4	8.19×10^4	1.75×10^5	1.75×10^5
PVT 1	6.68×10^4	0.0	0.044	20.5	1.31×10^5	1.31×10^5	0.00	0.00	1.64×10^5	1.64×10^5
RBR 1	6.68×10^4	0.0	0.044	20.5	-9.01×10^4	-9.01×10^4	0.00	0.00	1.64×10^5	1.64×10^5

Table C.16: A310-200 right main landing gear structural loads for critical load case in each component.

Member	LC ID	V_x (N)	V_y (N)	N_z (N)	M_x (N)	M_y (N)	T_z (N)	Failure mode
Trunnion	LVL 3 SU	1.45×10^4	2.66×10^6	6.79×10^5	2.68×10^5	-8.13×10^3	3.30×10^2	Stress
Cylinder	LVL 3 SU	6.03×10^5	3.56×10^4	2.92×10^6	3.79×10^4	-6.51×10^5	-9.55×10^3	Stress
Piston	TDL 2 SB	-6.59×10^5	0.00	-7.42×10^6	0.00	5.80×10^5	0.00	Stress
Bogie beam	GRO 1	0.00	5.54×10^5	0.00	3.86×10^5	0.00	0.00	Stress
Wheel axle	GRO 2 IB	4.98×10^4	2.49×10^5	4.98×10^4	-1.39×10^5	2.30×10^4	0.00	Stress
Drag brace	TDL 2 SB	-1.84×10^3	0.00	-2.46×10^6	0.00	-5.00×10^3	4.13×10^1	Buckling
Side brace	LVL 3 SU	1.28×10^4	0.00	-8.20×10^5	0.00	2.50×10^3	-7.19×10^2	Machinability

Table C.17: Overview of Boeing 707-320 external main gear loads.

LC ID	m_{mlg} (kg)	θ (°)	x_{s} (m)	r_{tyre} (in)	$F_{x,\text{K}_\text{L},\text{K}_\text{R}}$ (N)	$F_{x,\text{L}_\text{L},\text{L}_\text{R}}$ (N)	$F_{y,\text{M}_\text{L},\text{M}_\text{R}}$ (N)	$F_{y,\text{N}_\text{L},\text{N}_\text{R}}$ (N)	$F_{z,\text{K}_\text{L},\text{K}_\text{R}}$ (N)	$F_{z,\text{L}_\text{L},\text{L}_\text{R}}$ (N)
LVL 1 SU	4.70×10^4	0.0	0.392	20.4	8.85×10^4	8.85×10^4	0.00	0.00	1.38×10^5	1.38×10^5
LVL 1 SB	4.70×10^4	0.0	0.392	20.4	-8.85×10^4	-8.85×10^4	0.00	0.00	1.38×10^5	1.38×10^5
LVL 2 SU	4.50×10^4	0.0	0.392	20.5	8.48×10^4	8.48×10^4	0.00	0.00	1.33×10^5	1.33×10^5
LVL 2 SB	4.50×10^4	0.0	0.392	20.5	-8.48×10^4	-8.48×10^4	0.00	0.00	1.33×10^5	1.33×10^5
LVL 3 SU	7.09×10^4	0.0	0.392	19.2	1.33×10^5	1.33×10^5	0.00	0.00	2.09×10^5	2.09×10^5
LVL 3 SB	7.09×10^4	0.0	0.392	19.2	-1.33×10^5	-1.33×10^5	0.00	0.00	2.09×10^5	2.09×10^5
LVL 4 SU	6.79×10^4	0.0	0.392	19.4	1.28×10^5	1.28×10^5	0.00	0.00	2.00×10^5	2.00×10^5
LVL 4 SB	6.79×10^4	0.0	0.392	19.4	-1.28×10^5	-1.28×10^5	0.00	0.00	2.00×10^5	2.00×10^5
LAT 1 SU/IB	4.70×10^4	0.0	0.427	21.4	6.64×10^4	6.64×10^4	-2.59×10^4	-2.59×10^4	1.04×10^5	1.04×10^5
LAT 1 SU/OB	4.70×10^4	0.0	0.427	21.4	6.64×10^4	6.64×10^4	2.59×10^4	2.59×10^4	1.04×10^5	1.04×10^5
LAT 1 SB/IB	4.70×10^4	0.0	0.427	21.4	-6.64×10^4	-6.64×10^4	-2.59×10^4	-2.59×10^4	1.04×10^5	1.04×10^5
LAT 1 SB/OB	4.70×10^4	0.0	0.427	21.4	-6.64×10^4	-6.64×10^4	2.59×10^4	2.59×10^4	1.04×10^5	1.04×10^5
LAT 2 SU/IB	4.50×10^4	0.0	0.427	21.4	6.36×10^4	6.36×10^4	-2.49×10^4	-2.49×10^4	9.94×10^4	9.94×10^4
LAT 2 SU/OB	4.50×10^4	0.0	0.427	21.4	6.36×10^4	6.36×10^4	2.49×10^4	2.49×10^4	9.94×10^4	9.94×10^4
LAT 2 SB/IB	4.50×10^4	0.0	0.427	21.4	-6.36×10^4	-6.36×10^4	-2.49×10^4	-2.49×10^4	9.94×10^4	9.94×10^4
LAT 2 SB/OB	4.50×10^4	0.0	0.427	21.4	-6.36×10^4	-6.36×10^4	2.49×10^4	2.49×10^4	9.94×10^4	9.94×10^4
TDL 1 SU	4.70×10^4	7.8	0.392	20.4	8.85×10^4	8.85×10^4	0.00	0.00	1.38×10^5	1.38×10^5
TDL 1 SB	4.70×10^4	7.8	0.392	20.4	-8.85×10^4	-8.85×10^4	0.00	0.00	1.38×10^5	1.38×10^5
TDL 2 SU	7.09×10^4	7.8	0.392	19.2	1.33×10^5	1.33×10^5	0.00	0.00	2.09×10^5	2.09×10^5
TDL 2 SB	7.09×10^4	7.8	0.392	19.2	-1.33×10^5	-1.33×10^5	0.00	0.00	2.09×10^5	2.09×10^5
OGL 1 SU	4.70×10^4	0.0	0.392	20.4	8.85×10^4	8.85×10^4	0.00	0.00	1.38×10^5	1.38×10^5
OGL 1 SB	4.70×10^4	0.0	0.392	20.4	-8.85×10^4	-8.85×10^4	0.00	0.00	1.38×10^5	1.38×10^5
OGL 2 SU	7.09×10^4	0.0	0.392	19.2	1.33×10^5	1.33×10^5	0.00	0.00	2.09×10^5	2.09×10^5
OGL 2 SB	7.09×10^4	0.0	0.392	19.2	-1.33×10^5	-1.33×10^5	0.00	0.00	2.09×10^5	2.09×10^5
SLL 1 IB	4.70×10^4	0.0	0.392	21.5	0.00	0.00	-5.53×10^4	-5.43×10^4	6.92×10^4	6.92×10^4
SLL 1 OB	4.70×10^4	0.0	0.392	21.5	0.00	0.00	4.15×10^4	4.15×10^4	6.92×10^4	6.92×10^4
SLL 2 IB	7.09×10^4	0.0	0.392	20.9	0.00	0.00	-8.34×10^4	-8.34×10^4	1.04×10^5	1.04×10^5
SLL 2 OB	7.09×10^4	0.0	0.392	20.9	0.00	0.00	6.26×10^4	6.26×10^4	1.04×10^5	1.04×10^5
GRO 1	6.79×10^4	0.0	0.035	18.0	0.00	0.00	0.00	0.00	2.83×10^5	2.83×10^5
GRO 2 IB	6.79×10^4	0.0	0.035	18.5	5.10×10^4	5.10×10^4	-5.10×10^4	-5.10×10^4	2.55×10^5	2.55×10^5
GRO 2 OB	6.79×10^4	0.0	0.035	18.5	5.10×10^4	5.10×10^4	5.10×10^4	5.10×10^4	2.55×10^5	2.55×10^5
BRR 1	4.70×10^4	0.0	0.035	20.2	1.43×10^5	1.43×10^5	0.00	0.00	1.79×10^5	1.79×10^5
BRR 2	4.50×10^4	0.0	0.035	20.4	1.34×10^5	1.34×10^5	0.00	0.00	1.67×10^5	1.67×10^5
BRR 3	7.18×10^4	0.0	0.035	20.2	1.40×10^5	1.40×10^5	0.00	0.00	1.75×10^5	1.75×10^5
BRR 4	6.88×10^4	0.0	0.035	20.5	1.31×10^5	1.31×10^5	0.00	0.00	1.64×10^5	1.64×10^5
TRN 1 IB	6.88×10^4	0.0	0.035	20.5	0.00	0.00	-8.19×10^4	-8.19×10^4	1.64×10^5	1.64×10^5
TRN 1 OB	6.88×10^4	0.0	0.035	20.5	0.00	0.00	8.19×10^4	8.19×10^4	1.64×10^5	1.64×10^5
PVT 1	6.88×10^4	0.0	0.035	20.5	1.31×10^5	1.31×10^5	0.00	0.00	1.64×10^5	1.64×10^5
RBR 1	6.88×10^4	0.0	0.035	20.5	-9.01×10^4	-9.01×10^4	0.00	0.00	1.64×10^5	1.64×10^5

Table C.18: Boeing 707-320 right main landing gear structural loads for critical load case in each component.

Member	LC ID	V_x (N)	V_y (N)	N_z (N)	M_x (N)	M_y (N)	T_z (N)	Failure mode
Trunnion	LVL 3 SU	8.91×10^3	1.89×10^6	7.17×10^5	1.90×10^5	8.23×10^3	-1.99×10^3	Stress
Cylinder	TDL 2 SU	-6.51×10^5	-2.55×10^3	8.32×10^5	1.20×10^3	8.12×10^5	-1.07×10^4	Stress
Piston	TDL 2 SB	-6.42×10^5	0.00	-7.54×10^5	0.00	4.44×10^5	0.00	Stress
Bogie beam	GRO 1	0.00	5.66×10^5	0.00	4.01×10^5	0.00	0.00	Stress
Wheel axle	GRO 1 IB	5.10×10^4	2.55×10^5	5.10×10^4	-1.36×10^5	2.23×10^4	0.00	Stress
Drag brace	TDL 2 SB	2.55×10^3	0.00	-1.98×10^6	0.00	1.81×10^3	4.16×10^2	Stress
Side brace	TRN 1 IB	1.84×10^2	0.00	-6.78×10^5	0.00	-2.59×10^2	-7.59×10^1	Buckling

D

Additional Flying-V Gear Implementation Data

D.1. Baseline Gear Design

D.1.1. Stick Model Generation

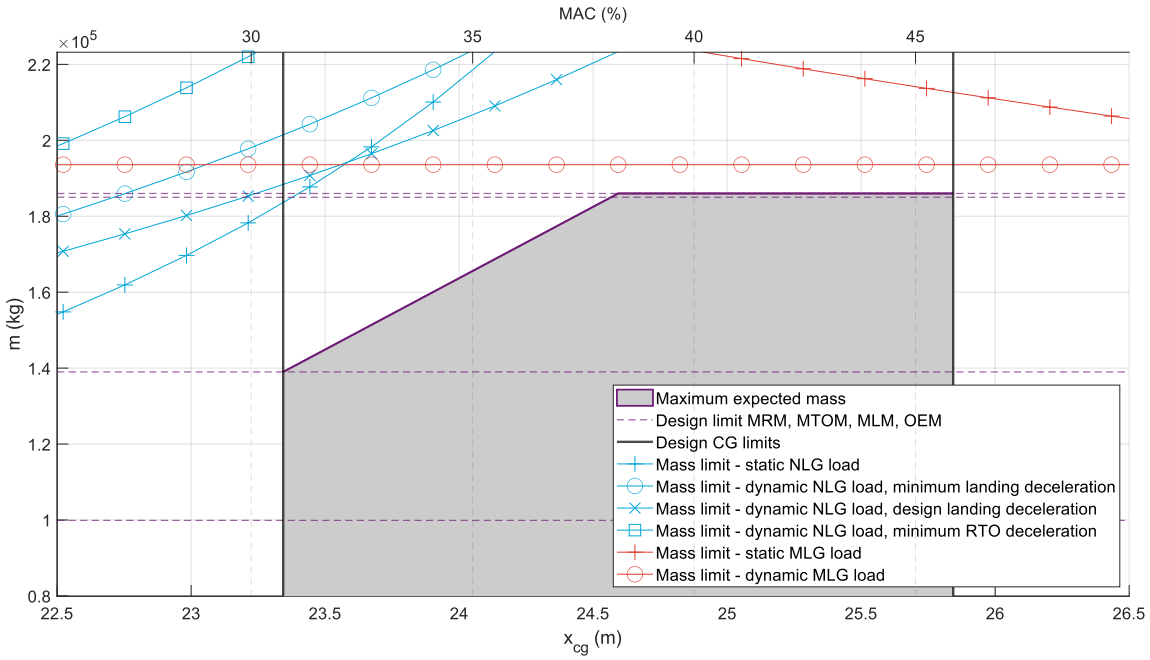

Figure D.1: FV-800 baseline gear loading diagram.

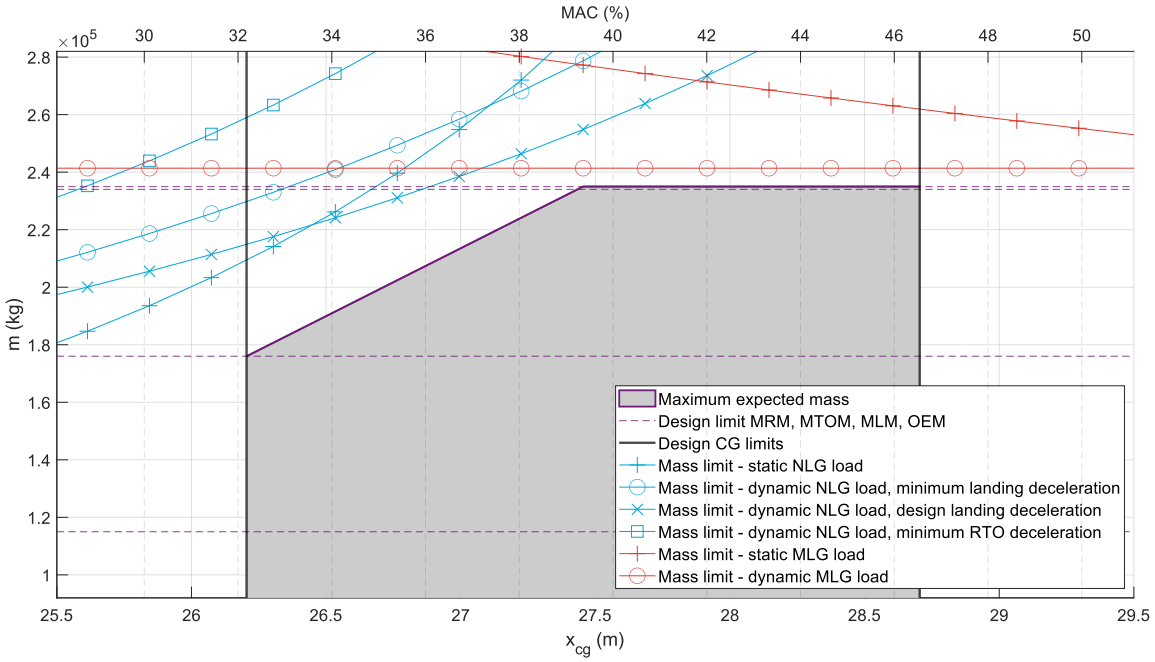

Figure D.2: FV-900 baseline gear loading diagram.

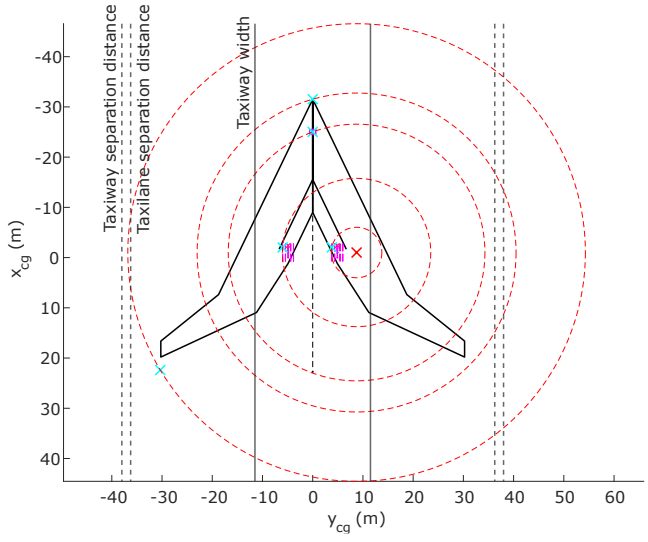

Figure D.3: FV-900 wing tip, nose, nose gear, left main gear and right main gear turning radii for a right turn with maximum nose gear steering angle.

D.1.2. 3D Model Generation

Table D.1: FV-1000 baseline gear model node specifications (static position). Nodes are defined as illustrated in Figure 5.14.

Node	x (m)	y (m)	z (m)	Type	Node	x (m)	y (m)	z (m)	Type
O1	0.000	0.000	0.000	Beam	S7	1.064	0.000	-4.914	Beam
D1	0.323	-1.092	0.161	-	S8	1.074	0.000	-5.064	Beam
D2	0.281	-0.949	0.140	Beam	A1	0.687	0.000	-4.540	Hinge
D3	-0.281	0.949	-0.140	Beam	A2	0.824	0.000	-4.931	Hinge
D4	-0.323	1.092	-0.161	-	A3	-0.008	0.000	-4.671	Hinge
D5	1.490	-0.541	-1.656	Hinge	A4	-0.064	0.000	-4.605	Beam
D6	0.219	0.541	-2.181	Hinge	A5	-0.108	0.000	-4.679	Hinge
C1	2.566	0.039	0.364	-	A6	0.316	0.000	-5.496	Hinge
C2	1.229	1.081	-0.301	-	B1	1.106	0.000	-5.517	Hinge
C3	1.570	-0.521	-1.436	Hinge	B2	1.091	0.000	-5.797	Beam
C4	0.299	0.561	-1.961	Hinge	B3	0.302	0.000	-5.756	Beam
C5	2.590	1.018	-1.350	-	K_L	2.100	-0.810	-5.850	Hinge
C6	1.305	0.282	-4.727	Universal	K_C	2.100	0.000	-5.850	Beam
C7	1.328	0.282	-5.046	Beam	K_R	2.100	0.810	-5.850	Hinge
O2	0.854	0.000	-1.918	Beam	L_L	0.083	-0.810	-5.744	Hinge
S1	1.327	-0.403	-1.723	Beam	L_C	0.083	0.000	-5.744	Beam
S2	0.404	0.383	-2.104	Beam	L_R	0.083	0.810	-5.744	Hinge
S3	1.129	-0.119	-3.796	Beam	M_L	2.070	-0.810	-6.417	-
S4	0.986	0.000	-3.806	Beam	M_R	2.070	0.810	-6.417	-
S5	0.843	0.119	-3.816	Beam	N_L	0.053	-0.810	-6.311	-
S6	1.036	0.000	-4.515	Beam	N_R	0.053	0.810	-6.311	-

D.1.3. Structural Sizing

Tables D.3 describes the external loads on the FV-1000 baseline concept right main landing gear, following from the load cases outlined in Table A.1. Table D.2 describes the internal loads corresponding to the most critical load case for each structural component. Load case id (LC ID) specifications SU, SB, IB and OB describe spin-up, spring-back, inboard and outboard load conditions respectively. For landing load cases, P1 indicates the initial (de-articulation) shock absorber compression phase, with only two wheels on the ground. P2 represents the second phase, with all wheels on the ground. Columns m_{mlg}, θ, x_{s} and r_{tyre} describe the mass on the gear, the aircraft pitch attitude, the shock absorber extension, and the loaded tyre radius. Loads in x and z-direction are applied to nodes K_L, K_R, L_L and L_R. Loads in y-direction are applied to nodes nodes M_L, M_R, N_L and N_R.

Table D.2: FV-1000 baseline concept right main landing gear structural loads for critical load case in each component.

Member	LC ID	V_x (N)	V_y (N)	N_z (N)	M_x (N)	M_y (N)	T_z (N)	Failure mode
Upper strut trunnion	BRR 3	1.09×10^{6}	-2.43×10^{6}	-3.86×10^{5}	-3.30×10^{5}	-1.26×10^{5}	-1.04×10^{4}	Stress
Drop link member 1	GRO 2 IB	1.75×10^{4}	4.12×10^{4}	-2.30×10^{6}	-6.17×10^{4}	2.12×10^{4}	3.95×10^{3}	Stress
Drop link member 2	GRO 2 IB	3.77×10^{3}	2.91×10^{4}	3.81×10^{5}	-3.85×10^{4}	9.28×10^{3}	3.94×10^{3}	Stress
Drop link member 3	None	-	-	-	-	-	-	Machinability
Drop link member 4	BRR 3	-2.34×10^{4}	3.51×10^{4}	2.62×10^{6}	2.92×10^{4}	-3.01×10^{4}	1.20×10^{3}	Stress
Drop link brace 1	None	-	-	-	-	-	-	Machinability
Drop link brace 2	GRO 2 IB	3.90×10^{4}	2.99×10^{3}	-2.07×10^{6}	-3.85×10^{2}	5.90×10^{4}	-4.79×10^{3}	Stress
Shock strut trunnion	GRO 2 IB	6.47×10^{4}	3.20×10^{6}	-1.03×10^{6}	-6.01×10^{5}	7.49×10^{4}	3.94×10^{3}	Stress
Shock strut cylinder	GRO 2 IB	-5.20×10^{5}	7.29×10^{5}	-2.23×10^{6}	-1.49×10^{6}	-1.40×10^{6}	-7.46×10^{4}	Stress
Shock strut piston	BRR 3	3.76×10^{3}	1.71×10^{6}	-1.85×10^{6}	-1.26×10^{6}	-3.95×10^{4}	-3.37×10^{4}	Stress
Shock strut brace 1	GRO 2 IB	1.93×10^{3}	-4.26×10^{2}	-1.08×10^{5}	0.00	0.00	0.00	Stress
Shock strut brace 2	BRR 4	-4.58×10^{4}	-7.94×10^{4}	-3.42×10^{6}	-9.14×10^{4}	2.48×10^{4}	9.07×10^{3}	Stress
Shock strut brace 3	BRR 3	4.05×10^{4}	2.59×10^{3}	-2.80×10^{6}	0.00	0.00	0.00	Buckling
Bogie beam	GRO 1	3.30×10^{2}	1.33×10^{6}	4.83×10^{1}	1.35×10^{6}	-5.89×10^{2}	-2.15×10^{2}	Stress
Aft wheel axle	GRO 2 IB/OB	-1.51×10^{5}	5.94×10^{5}	1.20×10^{5}	5.35×10^{5}	1.24×10^{5}	5.74×10^{3}	Stress
Front wheel axle	GRO 2 IB/OB	-1.51×10^{5}	5.94×10^{5}	1.20×10^{5}	5.35×10^{5}	1.24×10^{5}	5.74×10^{3}	Stress
AM member 1	LVL 3 P1 SU	9.35×10^{3}	-8.24×10^{4}	1.61×10^{6}	-3.34×10^{4}	1.32×10^{3}	8.27×10^{2}	Stress
AM member 2	LVL 3 P1 SU	1.65×10^{3}	-4.20×10^{4}	-1.63×10^{6}	-4.56	5.17×10^{2}	5.59×10^{1}	Stress
AM member 3	SSL 2 P1 IB	-3.20×10^{4}	2.02×10^{3}	3.17×10^{5}	-4.00×10^{2}	-3.04×10^{4}	-1.54×10^{3}	Stress
Shortening members	GRO 1	0.00	0.00	-2.65×10^{6}	0.00	0.00	0.00	Stress

Table D.3: Overview of FV-1000 baseline concept external main gear loads.

LC ID	m_{mlg} (kg)	θ (°)	x_{s} (m)	r_{tyre} (in)	$F_{x,\text{K}_\text{L},\text{K}_\text{R}}$ (N)	$F_{x,\text{L}_\text{L},\text{L}_\text{R}}$ (N)	$F_{y,\text{M}_\text{L},\text{M}_\text{R}}$ (N)	$F_{y,\text{N}_\text{L},\text{N}_\text{R}}$ (N)	$F_{z,\text{K}_\text{L},\text{K}_\text{R}}$ (N)	$F_{z,\text{L}_\text{L},\text{L}_\text{R}}$ (N)
LVL 1 P1 SU	1.00×10^5	0	0.602	27.1	1.10×10^5	0.00	0.00	0.00	1.72×10^5	0.00
LVL 1 P1 SB	1.00×10^5	0	0.602	27.1	-1.10×10^5	0.00	0.00	0.00	1.72×10^5	0.00
LVL 1 P2 SU	1.00×10^5	0	0.192	24.2	6.74×10^4	1.73×10^5	0.00	0.00	2.70×10^5	2.70×10^5
LVL 1 P2 SB	1.00×10^5	0	0.192	24.2	6.74×10^4	-1.73×10^5	0.00	0.00	2.70×10^5	2.70×10^5
LVL 2 P1 SU	8.99×10^4	-3	0.602	27.2	9.88×10^4	0.00	0.00	0.00	1.54×10^5	0.00
LVL 2 P1 SB	8.99×10^4	-3	0.602	27.2	-9.88×10^4	0.00	0.00	0.00	1.54×10^5	0.00
LVL 2 P2 SU	9.29×10^4	-3	0.192	24.5	6.27×10^4	1.60×10^5	0.00	0.00	2.51×10^5	2.51×10^5
LVL 2 P2 SB	9.29×10^4	-3	0.192	24.5	6.27×10^4	-1.60×10^5	0.00	0.00	2.51×10^5	2.51×10^5
LVL 3 P1 SU	1.33×10^5	0	0.602	26.7	1.46×10^5	0.00	0.00	0.00	2.28×10^5	0.00
LVL 3 P1 SB	1.33×10^5	0	0.602	26.7	-1.46×10^5	0.00	0.00	0.00	2.28×10^5	0.00
LVL 3 P2 SU	1.33×10^5	0	0.192	22.9	8.97×10^4	2.30×10^5	0.00	0.00	3.59×10^5	3.59×10^5
LVL 3 P2 SB	1.33×10^5	0	0.192	22.9	8.97×10^4	-2.30×10^5	0.00	0.00	3.59×10^5	3.59×10^5
LVL 4 P1 SU	1.20×10^5	-3	0.602	26.8	1.31×10^5	0.00	0.00	0.00	2.05×10^5	0.00
LVL 4 P1 SB	1.20×10^5	-3	0.602	26.8	-1.31×10^5	0.00	0.00	0.00	2.05×10^5	0.00
LVL 4 P2 SU	1.24×10^5	-3	0.192	23.3	8.34×10^4	2.13×10^5	0.00	0.00	3.33×10^5	3.33×10^5
LVL 4 P2 SB	1.24×10^5	-3	0.192	23.3	8.34×10^4	-2.13×10^5	0.00	0.00	3.33×10^5	3.33×10^5
LAT 1 P1 SU/IB	1.00×10^5	0	0.633	27.4	8.24×10^4	0.00	-3.22×10^4	0.00	1.29×10^5	0.00
LAT 1 P1 SU/OB	1.00×10^5	0	0.633	27.4	8.24×10^4	0.00	3.22×10^4	0.00	1.29×10^5	0.00
LAT 1 P1 SB/IB	1.00×10^5	0	0.633	27.4	-8.24×10^4	0.00	-3.22×10^4	0.00	1.29×10^5	0.00
LAT 1 P1 SB/OB	1.00×10^5	0	0.633	27.4	-8.24×10^4	0.00	3.22×10^4	0.00	1.29×10^5	0.00
LAT 1 P2 SU/IB	1.00×10^5	0	0.201	25.3	8.09×10^4	1.29×10^5	-5.06×10^4	-5.06×10^4	2.02×10^5	2.02×10^5
LAT 1 P2 SU/OB	1.00×10^5	0	0.201	25.3	8.09×10^4	1.29×10^5	5.06×10^4	5.06×10^4	2.02×10^5	2.02×10^5
LAT 1 P2 SB/IB	1.00×10^5	0	0.201	25.3	8.09×10^4	-1.29×10^5	-5.06×10^4	-5.06×10^4	2.02×10^5	2.02×10^5
LAT 1 P2 SB/OB	1.00×10^5	0	0.201	25.3	8.09×10^4	-1.29×10^5	5.06×10^4	5.06×10^4	2.02×10^5	2.02×10^5
LAT 2 P1 SU/IB	8.99×10^4	-3	0.633	27.5	7.41×10^4	0.00	-2.89×10^4	0.00	1.16×10^5	0.00
LAT 2 P1 SU/OB	8.99×10^4	-3	0.633	27.5	7.41×10^4	0.00	2.89×10^4	0.00	1.16×10^5	0.00
LAT 2 P1 SB/IB	8.99×10^4	-3	0.633	27.5	-7.41×10^4	0.00	-2.89×10^4	0.00	1.16×10^5	0.00
LAT 2 P1 SB/OB	8.99×10^4	-3	0.633	27.5	-7.41×10^4	0.00	2.89×10^4	0.00	1.16×10^5	0.00
LAT 2 P2 SU/IB	9.29×10^4	-3	0.201	25.5	7.52×10^4	1.20×10^5	-4.70×10^4	-4.70×10^4	1.88×10^5	1.88×10^5
LAT 2 P2 SU/OB	9.29×10^4	-3	0.201	25.5	7.52×10^4	1.20×10^5	4.70×10^4	4.70×10^4	1.88×10^5	1.88×10^5
LAT 2 P2 SB/IB	9.29×10^4	-3	0.201	25.5	7.52×10^4	-1.20×10^5	-4.70×10^4	-4.70×10^4	1.88×10^5	1.88×10^5
LAT 2 P2 SB/OB	9.29×10^4	-3	0.201	25.5	7.52×10^4	-1.20×10^5	4.70×10^4	4.70×10^4	1.88×10^5	1.88×10^5
TDL 1 P1 SU	1.00×10^5	14	0.602	27.1	1.10×10^5	0.00	0.00	0.00	1.72×10^5	0.00
TDL 1 P1 SB	1.00×10^5	14	0.602	27.1	-1.10×10^5	0.00	0.00	0.00	1.72×10^5	0.00
TDL 1 P2 SU	1.00×10^5	14	0.192	24.2	0.00	1.73×10^5	0.00	0.00	2.70×10^5	2.70×10^5
TDL 1 P2 SB	1.00×10^5	14	0.192	24.2	0.00	-1.73×10^5	0.00	0.00	2.70×10^5	2.70×10^5
TDL 2 P1 SU	1.33×10^5	14	0.602	26.7	1.46×10^5	0.00	0.00	0.00	2.28×10^5	0.00
TDL 2 P1 SB	1.33×10^5	14	0.602	26.7	-1.46×10^5	0.00	0.00	0.00	2.28×10^5	0.00
TDL 2 P2 SU	1.33×10^5	14	0.192	22.9	0.00	2.30×10^5	0.00	0.00	3.59×10^5	3.59×10^5
TDL 2 P2 SB	1.33×10^5	14	0.192	22.9	0.00	-2.30×10^5	0.00	0.00	3.59×10^5	3.59×10^5
OGL 1 P1 SU	1.00×10^5	0	0.602	27.1	1.10×10^5	0.00	0.00	0.00	1.72×10^5	0.00
OGL 1 P1 SB	1.00×10^5	0	0.602	27.1	-1.10×10^5	0.00	0.00	0.00	1.72×10^5	0.00
OGL 1 P2 SU	1.00×10^5	0	0.192	24.2	6.74×10^4	1.73×10^5	0.00	0.00	2.70×10^5	2.70×10^5
OGL 1 P2 SB	1.00×10^5	0	0.192	24.2	6.74×10^4	-1.73×10^5	0.00	0.00	2.70×10^5	2.70×10^5
OGL 2 P1 SU	1.33×10^5	0	0.602	26.7	1.46×10^5	0.00	0.00	0.00	2.28×10^5	0.00
OGL 2 P1 SB	1.33×10^5	0	0.602	26.7	-1.46×10^5	0.00	0.00	0.00	2.28×10^5	0.00
OGL 2 P2 SU	1.33×10^5	0	0.192	22.9	8.97×10^4	2.30×10^5	0.00	0.00	3.59×10^5	3.59×10^5
OGL 2 P2 SB	1.33×10^5	0	0.192	22.9	8.97×10^4	-2.30×10^5	0.00	0.00	3.59×10^5	3.59×10^5
SLL 1 P1 IB	1.00×10^5	0	0.602	27.8	0.00	0.00	-6.87×10^4	0.00	8.58×10^4	0.00
SLL 1 P1 OB	1.00×10^5	0	0.602	27.8	0.00	0.00	5.15×10^4	0.00	8.58×10^4	0.00
SLL 1 P2 IB	1.00×10^5	0	0.192	26.3	0.00	0.00	-2.16×10^5	-2.16×10^5	1.35×10^5	1.35×10^5
SLL 1 P2 OB	1.00×10^5	0	0.192	26.3	0.00	0.00	1.62×10^5	1.62×10^5	1.35×10^5	1.35×10^5
SLL 2 P1 IB	1.33×10^5	0	0.602	27.5	0.00	0.00	-9.13×10^4	0.00	1.14×10^5	0.00
SLL 2 P1 OB	1.33×10^5	0	0.602	27.5	0.00	0.00	6.85×10^4	0.00	1.14×10^5	0.00
SLL 2 P2 IB	1.33×10^5	0	0.192	25.6	0.00	0.00	-1.44×10^5	-1.44×10^5	1.79×10^5	1.79×10^5
SLL 2 P2 OB	1.33×10^5	0	0.192	25.6	0.00	0.00	1.08×10^5	1.08×10^5	1.79×10^5	1.79×10^5
GRO 1	1.24×10^5	-3	0.054	18.1	0.00	0.00	0.00	0.00	6.67×10^5	6.67×10^5
GRO 2 IB	1.24×10^5	-3	0.054	19.1	1.20×10^5	1.20×10^5	-1.20×10^5	-1.20×10^5	6.01×10^5	6.01×10^5
GRO 2 OB	1.24×10^5	-3	0.054	19.1	1.20×10^5	1.20×10^5	1.20×10^5	1.20×10^5	6.01×10^5	6.01×10^5
BRR 1	1.00×10^5	0	0.054	22.0	3.34×10^5	3.34×10^5	0.00	0.00	4.17×10^5	4.17×10^5
BRR 2	9.30×10^4	-3	0.054	22.4	3.10×10^5	3.10×10^5	0.00	0.00	3.88×10^5	3.88×10^5
BRR 3	1.34×10^5	0	0.054	20.8	3.93×10^5	3.93×10^5	0.00	0.00	4.91×10^5	4.91×10^5
BRR 4	1.24×10^5	-3	0.054	21.3	3.65×10^5	3.65×10^5	0.00	0.00	4.57×10^5	4.57×10^5
TRN 1 IB	1.24×10^5	-3	0.054	23.7	0.00	0.00	-1.52×10^5	-1.52×10^5	3.05×10^5	3.05×10^5
TRN 1 OB	1.24×10^5	-3	0.054	23.7	0.00	0.00	1.52×10^5	1.52×10^5	3.05×10^5	3.05×10^5
PIV 1	1.24×10^5	-3	0.054	21.3	3.65×10^5	3.65×10^5	0.00	0.00	4.57×10^5	4.57×10^5
RBR 1	1.24×10^5	-3	0.054	23.7	-1.67×10^5	-1.67×10^5	0.00	0.00	3.05×10^5	3.05×10^5

D.2. Gear Concept Variations

D.2.1. Gear Model Generation

6-Wheel Bogie Concept

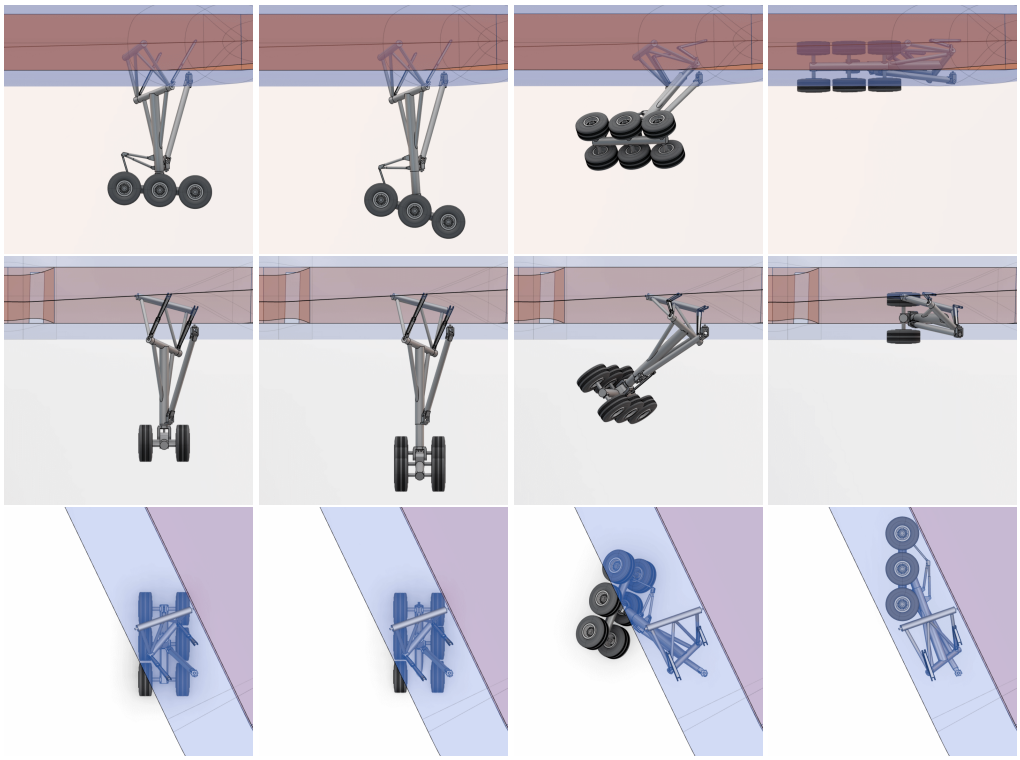

Figure D.4: FV-1000 main landing gear 6-wheel bogie concept (C2) retraction kinematics, left view, back view and top view.

Table D.4: FV-1000 6-wheel bogie concept (C2) gear model node specifications (static position). Nodes are defined as illustrated in Figure 5.14.

Node	x (m)	y (m)	z (m)	Type	Node	x (m)	y (m)	z (m)	Type
O1	0.000	0.000	0.000	Beam	A1	0.584	0.000	-4.248	Hinge
D1	0.366	-1.054	0.277	-	A2	0.722	0.000	-4.639	Hinge
D2	0.318	-0.917	0.241	Beam	A3	-0.394	0.000	-4.141	Hinge
D3	-0.318	0.917	-0.241	Beam	A4	-0.431	0.000	-4.063	Beam
D4	-0.366	1.054	-0.277	-	A5	-0.492	0.000	-4.123	Hinge
D5	1.394	-0.543	-1.447	Hinge	A6	-0.175	0.000	-5.197	Hinge
D6	0.119	0.543	-1.951	Hinge	B1	1.004	0.000	-5.339	Hinge
C1	2.395	0.217	0.373	-	B2	0.989	0.000	-5.518	Beam
C2	1.004	1.263	-0.131	-	B3	-0.189	0.000	-5.457	Beam
C3	1.474	-0.523	-1.227	Hinge	K_L	2.387	-0.735	-5.592	Hinge
C4	0.199	0.563	-1.731	Hinge	K_C	2.387	0.000	-5.592	Beam
C5	2.135	1.200	-1.200	-	K_R	2.387	0.735	-5.592	Hinge
C6	1.224	0.231	-4.434	Universal	L_L	-0.409	-0.735	-5.445	Hinge
C7	1.246	0.231	-4.753	Beam	L_C	-0.409	0.000	-5.445	Beam
O2	0.757	0.000	-1.699	Beam	L_R	-0.409	0.735	-5.445	Hinge
S1	1.265	-0.433	-1.498	Beam	M_L	2.360	-0.735	-6.120	-
S2	0.350	0.346	-1.860	Beam	M_R	2.360	0.735	-6.120	-
S3	1.028	-0.119	-3.533	Beam	N_L	-0.436	-0.735	-5.973	-
S4	0.885	0.000	-3.543	Beam	N_R	-0.436	0.735	-5.973	-
S5	0.743	0.119	-3.553	Beam	P_L[1]	0.989	-0.735	-5.518	Beam
S6	0.993	0.000	-4.224	Beam	P_R[1]	0.989	0.735	-5.518	Beam
S7	0.961	0.000	-4.623	Beam	Q_L[2]	0.962	-0.735	-6.047	-
S8	0.971	0.000	-4.772	Beam	Q_R[2]	0.962	0.735	-6.047	-

[1] Centre wheel axle.
[2] Centre tyres.

Bogie Articulation Exclusion Concept

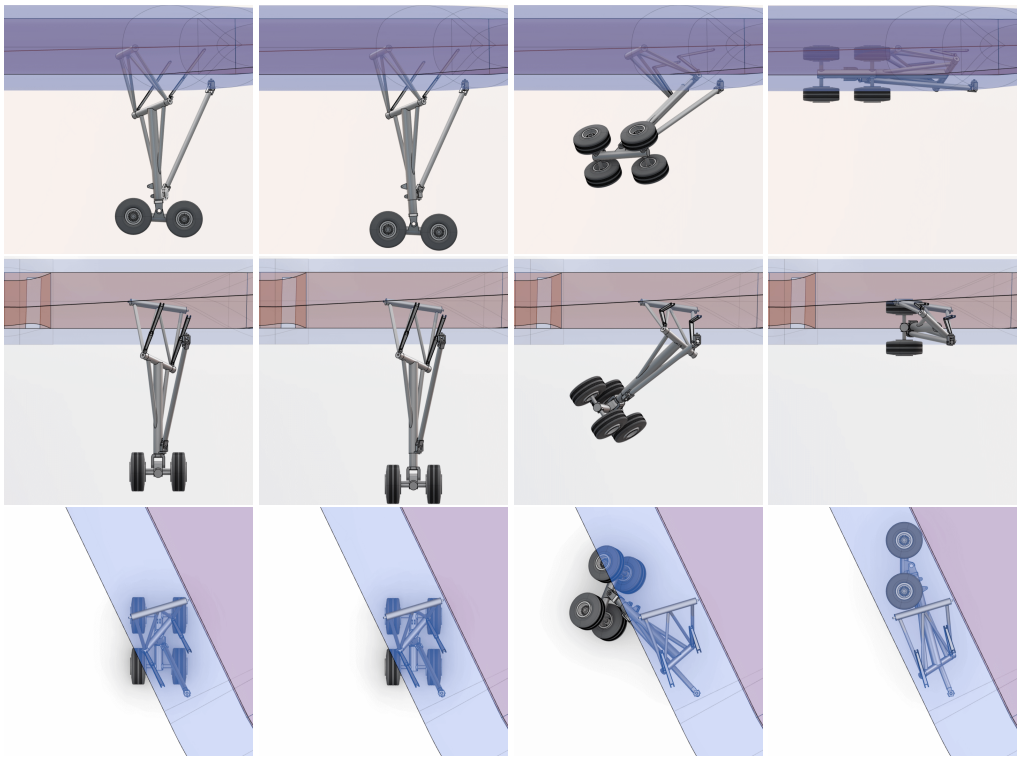

Figure D.5: FV-1000 main landing gear bogie articulation exclusion concept (C3) retraction kinematics, left view, back view and top view.

Table D.5: FV-1000 bogie articulation exclusion concept (C3) gear model node specifications (static position). Nodes are defined as illustrated in Figure 5.14.

Node	x (m)	y (m)	z (m)	Type	Node	x (m)	y (m)	z (m)	Type
O1	0.000	0.000	0.000	Beam	S3	1.287	-0.119	-4.390	Beam
D1	0.324	-1.091	0.164	-	S4	1.144	0.000	-4.400	Beam
D2	0.282	-0.949	0.143	Beam	S5	1.001	0.119	-4.410	Beam
D3	-0.282	0.949	-0.143	Beam	S8	1.245	0.000	-5.847	Beam
D4	-0.324	1.091	-0.164	-	B1	1.276	0.000	-6.287	Hinge
D5	1.628	-0.541	-1.967	Hinge	B2	1.262	0.000	-6.566	Beam
D6	0.357	0.541	-2.491	Hinge	K_L	2.270	-0.810	-6.619	Hinge
C1	3.064	0.158	0.093	-	K_C	2.270	0.000	-6.619	Beam
C2	1.706	1.221	-0.391	-	K_R	2.270	0.810	-6.619	Hinge
C3	1.708	-0.521	-1.747	Hinge	L_L	0.254	-0.810	-6.514	Hinge
C4	0.437	0.561	-2.271	Hinge	L_C	0.254	0.000	-6.514	Beam
C5	3.339	1.120	-1.420	-	L_R	0.254	0.810	-6.514	Hinge
C6	1.498	0.231	-5.508	Universal	M_L	2.240	-0.810	-7.186	-
C7	1.521	0.231	-5.828	Beam	M_R	2.240	0.810	-7.186	-
O2	0.992	0.000	-2.229	Beam	N_L	0.223	-0.810	-7.081	-
S1	1.465	-0.403	-2.034	Beam	N_R	0.223	0.810	-7.081	-
S2	0.542	0.383	-2.415	Beam					

Strut Shortening Exclusion Concept

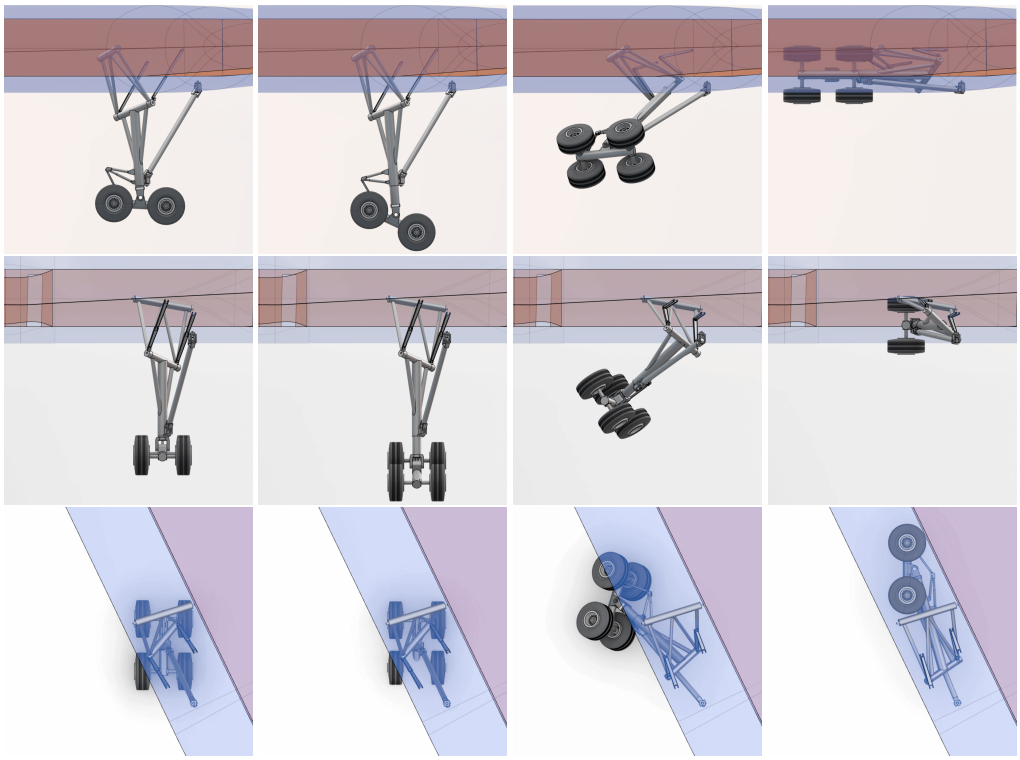

Figure D.6: FV-1000 main landing gear strut shortening exclusion concept (C4) retraction kinematics, left view, back view and top view.

Table D.6: FV-1000 strut shortening exclusion concept (C4) gear model node specifications (static position). Nodes are defined as illustrated in Figure 5.14.

Node	x (m)	y (m)	z (m)	Type	Node	x (m)	y (m)	z (m)	Type
O1	0.000	0.000	0.000	Beam	S7	1.170	0.000	-4.971	Beam
D1	0.335	-1.083	0.194	-	S8	1.181	0.000	-5.121	Beam
D2	0.292	-0.942	0.168	Beam	A1	0.793	0.000	-4.597	Hinge
D3	-0.292	0.942	-0.168	Beam	A2	0.931	0.000	-4.988	Hinge
D4	-0.335	1.083	-0.194	-	A3	-0.010	0.000	-4.522	Hinge
D5	1.612	-0.541	-1.930	Hinge	A4	-0.046	0.000	-4.444	Beam
D6	0.341	0.541	-2.455	Hinge	A5	-0.108	0.000	-4.504	Hinge
C1	2.825	0.159	0.130	-	A6	0.423	0.000	-5.552	Hinge
C2	1.466	1.221	-0.355	-	B1	1.213	0.000	-5.574	Hinge
C3	1.692	-0.521	-1.710	Hinge	B2	1.198	0.000	-5.853	Beam
C4	0.421	0.561	-2.235	Hinge	B3	0.409	0.000	-5.812	Beam
C5	3.429	1.160	-1.420	-	K_L	2.207	-0.810	-5.906	Hinge
C6	1.434	0.231	-4.783	Universal	K_C	2.207	0.000	-5.906	Beam
C7	1.456	0.231	-5.102	Beam	K_R	2.207	0.810	-5.906	Hinge
O2	0.976	0.000	-2.193	Beam	L_L	0.189	-0.810	-5.800	Hinge
S1	1.449	-0.403	-1.997	Beam	L_C	0.189	0.000	-5.800	Beam
S2	0.526	0.383	-2.378	Beam	L_R	0.189	0.810	-5.800	Hinge
S3	1.242	-0.119	-3.940	Beam	M_L	2.177	-0.810	-6.473	-
S4	1.099	0.000	-3.950	Beam	M_R	2.177	0.810	-6.473	-
S5	0.956	0.119	-3.960	Beam	N_L	0.160	-0.810	-6.367	-
S6	1.143	0.000	-4.572	Beam	N_R	0.160	0.810	-6.367	-

Reverse Stowage Concept

Table D.7: FV-1000 reverse stowage concept (C5) gear model node specifications (static position). Nodes are defined as illustrated in Figure 5.14.

Node	x (m)	y (m)	z (m)	Type	Node	x (m)	y (m)	z (m)	Type
O1	0.000	0.000	0.000	Beam	S7	-0.315	0.000	-4.813	Beam
D1	0.102	1.076	0.391	-	S8	-0.304	0.000	-4.963	Beam
D2	0.089	0.936	0.340	Beam	A1	-0.692	0.000	-4.439	Hinge
D3	-0.089	-0.936	-0.340	Beam	A2	-0.554	0.000	-4.830	Hinge
D4	-0.102	-1.076	-0.391	-	A3	-1.387	0.000	-4.570	Hinge
D5	0.162	0.517	-1.995	Hinge	A4	-1.443	0.000	-4.504	Beam
D6	-1.209	-0.517	-1.657	Hinge	A5	-1.486	0.000	-4.578	Hinge
C1	-1.397	0.017	0.085	-	A6	-1.063	0.000	-5.395	Hinge
C2	-2.425	-0.977	0.223	-	B1	-0.273	0.000	-5.416	Hinge
C3	0.242	0.537	-1.775	Hinge	B2	-0.287	0.000	-5.696	Beam
C4	-1.129	-0.497	-1.437	Hinge	B3	-1.076	0.000	-5.655	Beam
C5	-2.587	1.150	-1.450	-	K_L	0.721	-0.810	-5.749	Hinge
C6	-0.581	0.255	-4.662	Universal	K_C	0.721	0.000	-5.749	Beam
C7	-0.558	0.255	-4.981	Beam	K_R	0.721	0.810	-5.749	Hinge
O2	-0.524	0.000	-1.826	Beam	L_L	-1.296	-0.810	-5.643	Hinge
S1	-0.014	0.384	-1.952	Beam	L_C	-1.296	0.000	-5.643	Beam
S2	-1.009	-0.366	-1.707	Beam	L_R	-1.296	0.810	-5.643	Hinge
S3	-0.245	0.113	-3.698	Beam	M_L	0.692	-0.810	-6.316	-
S4	-0.392	0.000	-3.708	Beam	M_R	0.692	0.810	-6.316	-
S5	-0.539	-0.113	-3.719	Beam	N_L	-1.326	-0.810	-6.210	-
S6	-0.343	0.000	-4.414	Beam	N_R	-1.326	0.810	-6.210	-

D.2.2. Structural Sizing

6-Wheel Bogie Concept

Table D.8: FV-1000 6-wheel bogie concept (C2) right main landing gear structural loads for critical load case in each component.

Member	LC ID	V_x (N)	V_y (N)	N_z (N)	M_x (N)	M_y (N)	T_z (N)	Failure mode
Upper strut trunnion	BRR 3	1.38×10^{6}	-3.19×10^{6}	-4.72×10^{5}	-4.21×10^{5}	-1.51×10^{5}	-2.02×10^{1}	Stress
Drop link member 1	GRO 2 IB	3.35×10^{1}	4.50×10^{1}	-2.54×10^{6}	-6.23×10^{1}	4.03×10^{1}	3.48×10^{3}	Stress
Drop link member 2	GRO 2 IB	-2.10×10^{3}	8.57×10^{3}	6.05×10^{5}	1.17×10^{1}	5.49×10^{3}	1.04×10^{3}	Stress
Drop link member 3	None	-	-	-	-	-	-	Machinability
Drop link member 4	BRR 3	-4.75×10^{1}	7.50×10^{1}	3.41×10^{6}	-6.17×10^{1}	-4.39×10^{1}	2.60×10^{3}	Stress
Drop link brace 1	BRR 3	4.01×10^{1}	-1.07×10^{3}	-2.33×10^{5}	-3.76×10^{1}	4.36×10^{1}	-9.46×10^{2}	Stress
Drop link brace 2	GRO 2 IB	5.11×10^{1}	3.50×10^{3}	-1.88×10^{6}	-3.19×10^{2}	6.83×10^{1}	-4.01×10^{3}	Stress
Shock strut trunnion	BRR 3	6.34×10^{1}	3.13×10^{6}	8.25×10^{5}	8.52×10^{5}	3.24×10^{1}	-2.45×10^{3}	Stress
Shock strut cylinder	BRR 3	-8.17×10^{5}	8.30×10^{5}	7.01×10^{5}	-1.91×10^{6}	-1.38×10^{6}	-3.52×10^{1}	Stress
Shock strut piston	BRR 3	3.62×10^{2}	1.71×10^{6}	-1.85×10^{6}	-1.29×10^{6}	-4.09×10^{1}	-3.85×10^{1}	Stress
Shock strut brace 1	GRO 2 IB	-2.56×10^{1}	-1.23×10^{3}	4.01×10^{6}	6.62×10^{1}	1.59×10^{1}	5.44×10^{3}	Stress
Shock strut brace 2	BRR 3	-4.14×10^{1}	-1.45×10^{5}	-4.21×10^{6}	-1.45×10^{5}	2.65×10^{1}	1.06×10^{3}	Stress
Shock strut brace 3	BRR 3	5.46×10^{1}	-5.16×10^{2}	-2.82×10^{6}	0.00	0.00	0.00	Buckling
Bogie beam	GRO 1	2.33×10^{2}	8.92×10^{5}	7.93×10^{1}	1.25×10^{6}	4.26×10^{1}	-2.05×10^{3}	Stress
Aft wheel axle	GRO 2 IB/OB	-1.01×10^{5}	3.96×10^{5}	8.04×10^{1}	3.27×10^{5}	7.50×10^{1}	1.43×10^{3}	Stress
Centre wheel axle	GRO 2 IB/OB	-1.01×10^{5}	3.96×10^{5}	8.04×10^{1}	3.27×10^{5}	7.50×10^{1}	1.43×10^{3}	Stress
Front wheel axle	GRO 2 IB/OB	-1.01×10^{5}	3.96×10^{5}	8.04×10^{1}	3.27×10^{5}	7.50×10^{1}	1.43×10^{3}	Stress
AM member 1	TDL 2 P1 SU	1.31×10^{3}	-9.38×10^{1}	1.52×10^{6}	-5.37×10^{1}	-3.95×10^{2}	3.51×10^{2}	Stress
AM member 2	TDL 2 P1 SU	-2.54×10^{3}	-4.39×10^{1}	-1.57×10^{6}	0.00	9.84×10^{1}	-7.96×10^{1}	Buckling
AM member 3	SLL 2 P1 IB	-2.46×10^{1}	1.95×10^{3}	2.28×10^{5}	-4.80×10^{2}	-2.57×10^{1}	-1.15×10^{3}	Stress
Shortening members	GRO 1	0.00	0.00	-1.85×10^{6}	0.00	0.00	0.00	Stress

Table D.9: FV-1000 6-wheel bogie concept (C2) right main landing gear structural member sizing. Nodes are defined as illustrated in Figure 5.14, with P_L and P_R added to represent the centre wheel axle. Dimensions shown in bold are fixed, based on either the piston diameter or wheel rim diameter, as described in Section 3.5.

Member	Nodes	l (m)	r_i (m)	r_o (m)	t (m)	A (m^2)	m (kg)
Upper strut trunnion	D1-D2-O1-D3-D4	2.300	0.116	**0.134**	0.018	0.014	250.7
Drop link member 1	D2-D5	2.036	0.054	**0.067**	0.013	0.005	78.9
Drop link member 2	O1-D5	2.082	0.063	**0.067**	0.004	0.002	29.7
Drop link member 3	O1-D6	2.030	0.064	**0.067**	0.003	0.001	21.3
Drop link member 4	D3-D6	1.805	0.051	**0.067**	0.016	0.006	84.0
Drop link brace 1	C2-C4	1.923	0.063	**0.067**	0.004	0.001	23.0
Drop link brace 2	C1-C3	1.989	0.057	**0.067**	0.010	0.004	62.9
Shock strut trunnion	D5-S1-O2-S3-D6	1.750	0.110	**0.134**	0.024	0.018	250.4
Shock strut cylinder	O2-S4-S6-S7-S8	3.081	**0.168**	0.192	0.024	0.027	658.0
Shock strut piston	S8-B1	2.109[1,2]	0.149	**0.168**	0.019	0.019	313.8
Shock strut brace 1	S1-S3	2.073	0.073	**0.084**	0.011	0.005	90.1
Shock strut brace 2	S2-S5	1.753	0.067	**0.084**	0.017	0.008	110.6
Shock strut brace 3	C5-C6	3.497	0.102	**0.109**	0.007	0.005	128.9
Bogie beam	K-B2-L	2.800	0.152	**0.168**	0.016	0.016	344.7
Aft wheel axle	K_L-K_R	1.470	0.103	**0.112**	0.009	0.006	73.5
Centre wheel axle	P_L-P_R	1.470	0.103	**0.112**	0.009	0.006	73.5
Front wheel axle	L_L-L_R	1.470	0.103	**0.112**	0.009	0.006	73.5
AM member 1[3]	A1-A4	1.650[1]	0.035	**0.050**	0.016	0.004	54.0
AM member 2[3]	A2-A3	1.322[1]	0.044	**0.050**	0.006	0.002	19.2
AM member 3[3]	A5-A6	1.120	0.046	**0.050**	0.004	0.001	11.1
Shortening members	-	0.500	0.042	**0.050**	0.009	0.003	9.8
Total	-	-	-	-	-	-	2762

[1] Extended length plus a margin of 2.75 times the respective piston diameter (Section 3.4.2).
[2] Includes the bogie pivot offset distance l_{offset} is added here.
[3] Articulation mechanism.

Table D.10: Overview of FV-1000 6-wheel bogie concept (C2) external main gear loads.

LC ID	m_{mlg} (kg)	θ (°)	x_{s} (m)	r_{tyre} (in)	$F_{x,\text{K}_{\text{L}},\text{K}_{\text{R}}}$ (N)	$F_{x,\text{L}_{\text{L/R}},\text{P}_{\text{L/R}}}$ (N)	$F_{y,\text{M}_{\text{L}},\text{M}_{\text{R}}}$ (N)	$F_{y,\text{N}_{\text{L/R}},\text{Q}_{\text{L/R}}}$ (N)	$F_{z,\text{K}_{\text{L}},\text{K}_{\text{R}}}$ (N)	$F_{z,\text{L}_{\text{L/R}},\text{P}_{\text{L/R}}}$ (N)
LVL 1 P1 SU	1.00×10^5	0	0.743	25.1	8.79×10^4	0.00	0.00	0.00	1.37×10^5	0.00
LVL 1 P1 SB	1.00×10^5	0	0.743	25.1	-8.79×10^4	0.00	0.00	0.00	1.37×10^5	0.00
LVL 1 P2 SU	1.00×10^5	0	0.224	22.7	4.50×10^4	1.15×10^5	0.00	0.00	1.80×10^5	1.80×10^5
LVL 1 P2 SB	1.00×10^5	0	0.224	22.7	4.50×10^4	-1.15×10^5	0.00	0.00	1.80×10^5	1.80×10^5
LVL 2 P1 SU	8.86×10^4	-3	0.743	25.1	7.79×10^4	0.00	0.00	0.00	1.22×10^5	0.00
LVL 2 P1 SB	8.86×10^4	-3	0.743	25.1	-7.79×10^4	0.00	0.00	0.00	1.22×10^5	0.00
LVL 2 P2 SU	9.31×10^4	-3	0.224	22.9	4.19×10^4	1.07×10^5	0.00	0.00	1.67×10^5	1.67×10^5
LVL 2 P2 SB	9.31×10^4	-3	0.224	22.9	4.19×10^4	-1.07×10^5	0.00	0.00	1.67×10^5	1.67×10^5
LVL 3 P1 SU	1.33×10^5	0	0.743	24.8	1.17×10^5	0.00	0.00	0.00	1.83×10^5	0.00
LVL 3 P1 SB	1.33×10^5	0	0.743	24.8	-1.17×10^5	0.00	0.00	0.00	1.83×10^5	0.00
LVL 3 P2 SU	1.33×10^5	0	0.224	21.6	5.98×10^4	1.53×10^5	0.00	0.00	2.39×10^5	2.39×10^5
LVL 3 P2 SB	1.33×10^5	0	0.224	21.6	5.98×10^4	-1.53×10^5	0.00	0.00	2.39×10^5	2.39×10^5
LVL 4 P1 SU	1.18×10^5	-3	0.743	24.9	1.04×10^5	0.00	0.00	0.00	1.62×10^5	0.00
LVL 4 P1 SB	1.18×10^5	-3	0.743	24.9	-1.04×10^5	0.00	0.00	0.00	1.62×10^5	0.00
LVL 4 P2 SU	1.24×10^5	-3	0.224	21.9	5.57×10^4	1.43×10^5	0.00	0.00	2.23×10^5	2.23×10^5
LVL 4 P2 SB	1.24×10^5	-3	0.224	21.9	5.57×10^4	-1.43×10^5	0.00	0.00	2.23×10^5	2.23×10^5
LAT 1 P1 SU/IB	1.00×10^5	0	0.783	25.3	6.59×10^4	0.00	-2.58×10^4	0.00	1.03×10^5	0.00
LAT 1 P1 SU/OB	1.00×10^5	0	0.783	25.3	6.59×10^4	0.00	2.58×10^4	0.00	1.03×10^5	0.00
LAT 1 P1 SB/IB	1.00×10^5	0	0.783	25.3	-6.59×10^4	0.00	-2.58×10^4	0.00	1.03×10^5	0.00
LAT 1 P1 SB/OB	1.00×10^5	0	0.783	25.3	-6.59×10^4	0.00	2.58×10^4	0.00	1.03×10^5	0.00
LAT 1 P2 SU/IB	1.00×10^5	0	0.234	23.5	5.40×10^4	8.63×10^4	-3.37×10^4	-3.37×10^4	1.35×10^5	1.35×10^5
LAT 1 P2 SU/OB	1.00×10^5	0	0.234	23.5	5.40×10^4	8.63×10^4	3.37×10^4	3.37×10^4	1.35×10^5	1.35×10^5
LAT 1 P2 SB/IB	1.00×10^5	0	0.234	23.5	5.40×10^4	-8.63×10^4	-3.37×10^4	-3.37×10^4	1.35×10^5	1.35×10^5
LAT 1 P2 SB/OB	1.00×10^5	0	0.234	23.5	5.40×10^4	-8.63×10^4	3.37×10^4	3.37×10^4	1.35×10^5	1.35×10^5
LAT 2 P1 SU/IB	8.86×10^4	-3	0.783	25.3	5.84×10^4	0.00	-2.28×10^4	0.00	9.13×10^4	0.00
LAT 2 P1 SU/OB	8.86×10^4	-3	0.783	25.3	5.84×10^4	0.00	2.28×10^4	0.00	9.13×10^4	0.00
LAT 2 P1 SB/IB	8.86×10^4	-3	0.783	25.3	-5.84×10^4	0.00	-2.28×10^4	0.00	9.13×10^4	0.00
LAT 2 P1 SB/OB	8.86×10^4	-3	0.783	25.3	-5.84×10^4	0.00	2.28×10^4	0.00	9.13×10^4	0.00
LAT 2 P2 SU/IB	9.31×10^4	-3	0.234	23.6	5.02×10^4	8.04×10^4	-3.14×10^4	-3.14×10^4	1.26×10^5	1.26×10^5
LAT 2 P2 SU/OB	9.31×10^4	-3	0.234	23.6	5.02×10^4	8.04×10^4	3.14×10^4	3.14×10^4	1.26×10^5	1.26×10^5
LAT 2 P2 SB/IB	9.31×10^4	-3	0.234	23.6	5.02×10^4	-8.04×10^4	-3.14×10^4	-3.14×10^4	1.26×10^5	1.26×10^5
LAT 2 P2 SB/OB	9.31×10^4	-3	0.234	23.6	5.02×10^4	-8.04×10^4	3.14×10^4	3.14×10^4	1.26×10^5	1.26×10^5
TDL 1 P1 SU	1.00×10^5	14	0.743	25.1	8.79×10^4	0.00	0.00	0.00	1.37×10^5	0.00
TDL 1 P1 SB	1.00×10^5	14	0.743	25.1	-8.79×10^4	0.00	0.00	0.00	1.37×10^5	0.00
TDL 1 P2 SU	1.00×10^5	14	0.224	22.7	0.00	1.15×10^5	0.00	0.00	1.80×10^5	1.80×10^5
TDL 1 P2 SB	1.00×10^5	14	0.224	22.7	0.00	-1.15×10^5	0.00	0.00	1.80×10^5	1.80×10^5
TDL 2 P1 SU	1.33×10^5	14	0.743	24.8	1.17×10^5	0.00	0.00	0.00	1.83×10^5	0.00
TDL 2 P1 SB	1.33×10^5	14	0.743	24.8	-1.17×10^5	0.00	0.00	0.00	1.83×10^5	0.00
TDL 2 P2 SU	1.33×10^5	14	0.224	21.6	0.00	1.53×10^5	0.00	0.00	2.39×10^5	2.39×10^5
TDL 2 P2 SB	1.33×10^5	14	0.224	21.6	0.00	-1.53×10^5	0.00	0.00	2.39×10^5	2.39×10^5
OGL 1 P1 SU	1.00×10^5	0	0.743	25.1	8.79×10^4	0.00	0.00	0.00	1.37×10^5	0.00
OGL 1 P1 SB	1.00×10^5	0	0.743	25.1	-8.79×10^4	0.00	0.00	0.00	1.37×10^5	0.00
OGL 1 P2 SU	1.00×10^5	0	0.224	22.7	4.50×10^4	1.15×10^5	0.00	0.00	1.80×10^5	1.80×10^5
OGL 1 P2 SB	1.00×10^5	0	0.224	22.7	4.50×10^4	-1.15×10^5	0.00	0.00	1.80×10^5	1.80×10^5
OGL 2 P1 SU	1.33×10^5	0	0.743	24.8	1.17×10^5	0.00	0.00	0.00	1.83×10^5	0.00
OGL 2 P1 SB	1.33×10^5	0	0.743	24.8	-1.17×10^5	0.00	0.00	0.00	1.83×10^5	0.00
OGL 2 P2 SU	1.33×10^5	0	0.224	21.6	5.98×10^4	1.53×10^5	0.00	0.00	2.39×10^5	2.39×10^5
OGL 2 P2 SB	1.33×10^5	0	0.224	21.6	5.98×10^4	-1.53×10^5	0.00	0.00	2.39×10^5	2.39×10^5
SLL 1 P1 IB	1.00×10^5	0	0.743	25.5	0.00	0.00	-5.49×10^4	0.00	6.87×10^4	0.00
SLL 1 P1 OB	1.00×10^5	0	0.743	25.5	0.00	0.00	4.12×10^4	0.00	6.87×10^4	0.00
SLL 1 P2 IB	1.00×10^5	0	0.224	24.3	0.00	0.00	-7.19×10^4	-7.19×10^4	8.99×10^4	8.99×10^4
SLL 1 P2 OB	1.00×10^5	0	0.224	24.3	0.00	0.00	5.40×10^4	5.40×10^4	8.99×10^4	8.99×10^4
SLL 2 P1 IB	1.33×10^5	0	0.743	25.3	0.00	0.00	-7.31×10^4	0.00	9.13×10^4	0.00
SLL 2 P1 OB	1.33×10^5	0	0.743	25.3	0.00	0.00	5.48×10^4	0.00	9.13×10^4	0.00
SLL 2 P2 IB	1.33×10^5	0	0.224	23.7	0.00	0.00	-9.57×10^4	-9.57×10^4	1.20×10^5	1.20×10^5
SLL 2 P2 OB	1.33×10^5	0	0.224	23.7	0.00	0.00	7.18×10^4	7.18×10^4	1.20×10^5	1.20×10^5
GRO 1	1.24×10^5	-3	0.068	17.9	0.00	0.00	0.00	0.00	4.46×10^5	4.46×10^5
GRO 2 IB	1.24×10^5	-3	0.068	18.7	8.03×10^4	8.03×10^4	-8.03×10^4	-8.03×10^4	4.01×10^5	4.01×10^5
GRO 2 OB	1.24×10^5	-3	0.068	18.7	8.03×10^4	8.03×10^4	8.03×10^4	8.03×10^4	4.01×10^5	4.01×10^5
BRR 1	1.00×10^5	0	0.068	20.9	2.22×10^5	2.22×10^5	0.00	0.00	2.78×10^5	2.78×10^5
BRR 2	9.32×10^4	-3	0.068	21.2	2.07×10^5	2.07×10^5	0.00	0.00	2.59×10^5	2.59×10^5
BRR 3	1.34×10^5	0	0.068	20.0	2.62×10^5	2.62×10^5	0.00	0.00	3.27×10^5	3.27×10^5
BRR 4	1.24×10^5	-3	0.068	20.4	2.44×10^5	2.44×10^5	0.00	0.00	3.05×10^5	3.05×10^5
TRN 1 IB	1.24×10^5	-3	0.068	22.2	0.00	0.00	-1.02×10^5	-1.02×10^5	2.03×10^5	2.03×10^5
TRN 1 OB	1.24×10^5	-3	0.068	22.2	0.00	0.00	1.02×10^5	1.02×10^5	2.03×10^5	2.03×10^5
PIV 1	1.24×10^5	-3	0.068	20.4	2.44×10^5	2.44×10^5	0.00	0.00	3.05×10^5	3.05×10^5
RBR 1	1.24×10^5	-3	0.068	22.2	-1.12×10^5	-1.12×10^5	0.00	0.00	2.03×10^5	2.03×10^5

Bogie Articulation Exclusion Concept

Table D.11: FV-1000 bogie articulation exclusion concept (C3) right main landing gear structural loads for critical load case in each component.

Member	LC ID	V_x (N)	V_y (N)	N_z (N)	M_x (N)	M_y (N)	T_z (N)	Failure mode
Upper strut trunnion	GRO 2 IB	7.12×10^5	2.78×10^6	-5.07×10^5	-3.19×10^5	6.68×10^4	-2.45×10^4	Stress
Drop link member 1	GRO 2 IB	3.22×10^4	4.21×10^4	-2.77×10^6	-7.64×10^4	5.06×10^4	2.47×10^3	Stress
Drop link member 2	GRO 2 IB	1.34×10^4	3.52×10^4	3.37×10^5	-5.46×10^4	3.26×10^4	5.56×10^3	Stress
Drop link member 3	None	-	-	-	-	-	-	Machinability
Drop link member 4	TDL 2 SB	1.97×10^4	-9.95×10^3	-2.29×10^6	1.60×10^4	3.61×10^4	-6.02×10^2	Stress
Drop link brace 1	None	-	-	-	-	-	-	Machinability
Drop link brace 2	GRO 2 IB	3.58×10^4	6.37×10^3	-2.06×10^6	-1.14×10^3	6.51×10^4	-9.78×10^3	Buckling
Shock strut trunnion	GRO 2 IB	6.98×10^4	3.48×10^6	-1.05×10^6	-6.23×10^5	8.34×10^4	4.00×10^3	Stress
Shock strut cylinder	GRO 2 IB	-5.11×10^5	7.23×10^5	-2.23×10^6	-1.63×10^6	-1.53×10^6	-8.64×10^4	Stress
Shock strut piston	BRR 3	4.53×10^3	1.71×10^6	-1.85×10^6	-1.25×10^6	-4.73×10^4	-3.97×10^4	Stress
Shock strut brace 1	GRO 2 IB	-5.51×10^4	-3.08×10^4	4.42×10^6	7.21×10^4	2.34×10^4	6.33×10^3	Stress
Shock strut brace 2	TDL 2 SB	3.23×10^3	3.36×10^4	3.77×10^6	8.79×10^4	2.89×10^4	-5.78×10^3	Stress
Shock strut brace 3	BRR 3	4.15×10^4	8.69×10^2	-2.65×10^6	-9.96	2.13	0.00	Buckling
Bogie beam	GRO 1	5.57×10^2	1.32×10^6	1.14×10^2	1.33×10^6	-7.41×10^2	4.86×10^2	Stress
Aft wheel axle	GRO 2 IB/OB	-1.50×10^5	5.88×10^5	1.19×10^5	5.29×10^5	1.24×10^5	7.87×10^3	Stress
Front wheel axle	GRO 2 IB/OB	-1.50×10^5	5.88×10^5	1.19×10^5	5.29×10^5	1.24×10^5	7.87×10^3	Stress
Shortening members	GRO 1	0.00	0.00	-2.31×10^6	0.00	0.00	0.00	Stress

Table D.12: FV-1000 bogie articulation exclusion concept right main landing gear structural member sizing. Nodes are defined as illustrated in Figure 5.14. Dimensions shown in bold are fixed, based on either the piston diameter or wheel rim diameter, as described in Section 3.5.

Member	Nodes	l (m)	r_i (m)	r_o (m)	t (m)	A (m^2)	m (kg)
Upper strut trunnion	D1-D2-O1-D3-D4	2.300	0.120	**0.134**	0.014	0.011	201.8
Drop link member 1	D2-D5	2.535	0.051	**0.067**	0.016	0.006	117.0
Drop link member 2	O1-D5	2.610	0.061	**0.067**	0.006	0.002	46.8
Drop link member 3	O1-D6	2.574	0.064	**0.067**	0.003	0.001	27.1
Drop link member 4	D3-D6	2.468	0.058	**0.067**	0.009	0.003	66.4
Drop link brace 1	C2-C4	2.362	0.064	**0.067**	0.003	0.001	24.8
Drop link brace 2	C1-C3	2.385	0.054	**0.067**	0.013	0005	89.2
Shock strut trunnion	D5-S1-O2-S3-D6	1.750	0.113	**0.134**	0.021	0.016	220.4
Shock strut cylinder	O2-S4-S6-S7-S8	3.627	**0.168**	0.192	0.024	0.027	775.6
Shock strut piston	S8-B1	1.755[1,2]	0.149	**0.168**	0.019	0.018	254.0
Shock strut brace 1	S1-S3	2.379	0.071	**0.084**	0.013	0.006	115.0
Shock strut brace 2	S2-S5	2.064	0.072	**0.084**	0.012	0.006	96.6
Shock strut brace 3	C5-C6	4.571	0.097	**0.109**	0.012	0.008	283.6
Bogie beam	K-B2-L	2.020	0.151	**0.168**	0.017	0.017	270.9
Aft wheel axle	K_L-K_R	1.620	0.102	**0.117**	0.015	0.010	130.8
Front wheel axle	L_L-L_R	1.620	0.102	**0.117**	0.015	0.010	130.8
Shortening members	-	0.500	0.042	**0.050**	0.009	0.002	9.7
Total	-	-	-	-	-	-	2861

[1] Extended length plus a margin of 2.75 times the respective piston diameter (Section 3.4.2).
[2] Includes the bogie pivot offset distance l_offset is added here.

Table D.13: Overview of FV-1000 bogie articulation exclusion concept (C3) external main gear loads.

LC ID	m_{mlg} (kg)	θ (°)	x_{s} (m)	r_{tyre} (in)	$F_{x,\text{K}_\text{L},\text{K}_\text{R}}$ (N)	$F_{x,\text{L}_\text{L},\text{L}_\text{R}}$ (N)	$F_{y,\text{M}_\text{L},\text{M}_\text{R}}$ (N)	$F_{y,\text{N}_\text{L},\text{N}_\text{R}}$ (N)	$F_{z,\text{K}_\text{L},\text{K}_\text{R}}$ (N)	$F_{z,\text{L}_\text{L},\text{L}_\text{R}}$ (N)
LVL 1 SU	1.00×10^5	0	0.429	24.2	1.73×10^5	1.73×10^5	0.00	0.00	2.70×10^5	2.70×10^5
LVL 1 SB	1.00×10^5	0	0.429	24.2	-1.73×10^5	-1.73×10^5	0.00	0.00	2.70×10^5	2.70×10^5
LVL 2 SU	9.19×10^4	-3	0.429	24.6	1.59×10^5	1.59×10^5	0.00	0.00	2.48×10^5	2.48×10^5
LVL 2 SB	9.19×10^4	-3	0.429	24.6	-1.59×10^5	-1.59×10^5	0.00	0.00	2.48×10^5	2.48×10^5
LVL 3 SU	1.33×10^5	0	0.429	22.9	2.30×10^5	2.30×10^5	0.00	0.00	3.59×10^5	3.59×10^5
LVL 3 SB	1.33×10^5	0	0.429	22.9	-2.30×10^5	-2.30×10^5	0.00	0.00	3.59×10^5	3.59×10^5
LVL 4 SU	1.22×10^5	-3	0.429	23.3	2.11×10^5	2.11×10^5	0.00	0.00	3.30×10^5	3.30×10^5
LVL 4 SB	1.22×10^5	-3	0.429	23.3	-2.11×10^5	-2.11×10^5	0.00	0.00	3.30×10^5	3.30×10^5
LAT 1 SU/IB	1.00×10^5	0	0.459	26.1	1.29×10^5	1.29×10^5	-5.06×10^4	-5.06×10^4	2.02×10^5	2.02×10^5
LAT 1 SU/OB	1.00×10^5	0	0.459	26.1	1.29×10^5	1.29×10^5	5.06×10^4	5.06×10^4	2.02×10^5	2.02×10^5
LAT 1 SB/IB	1.00×10^5	0	0.459	26.1	-1.29×10^5	-1.29×10^5	-5.06×10^4	-5.06×10^4	2.02×10^5	2.02×10^5
LAT 1 SB/OB	1.00×10^5	0	0.459	26.1	-1.29×10^5	-1.29×10^5	5.06×10^4	5.06×10^4	2.02×10^5	2.02×10^5
LAT 2 SU/IB	9.19×10^4	-3	0.459	26.3	1.19×10^5	1.19×10^5	-4.65×10^4	-4.65×10^4	1.86×10^5	1.86×10^5
LAT 2 SU/OB	9.19×10^4	-3	0.459	26.3	1.19×10^5	1.19×10^5	4.65×10^4	4.65×10^4	1.86×10^5	1.86×10^5
LAT 2 SB/IB	9.19×10^4	-3	0.459	26.3	-1.19×10^5	-1.19×10^5	-4.65×10^4	-4.65×10^4	1.86×10^5	1.86×10^5
LAT 2 SB/OB	9.19×10^4	-3	0.459	26.3	-1.19×10^5	-1.19×10^5	4.65×10^4	4.65×10^4	1.86×10^5	1.86×10^5
TDL 1 SU	1.00×10^5	14	0.429	24.2	1.73×10^5	1.73×10^5	0.00	0.00	2.70×10^5	2.70×10^5
TDL 1 SB	1.00×10^5	14	0.429	24.2	-1.73×10^5	-1.73×10^5	0.00	0.00	2.70×10^5	2.70×10^5
TDL 2 SU	1.33×10^5	14	0.429	22.9	2.30×10^5	2.30×10^5	0.00	0.00	3.59×10^5	3.59×10^5
TDL 2 SB	1.33×10^5	14	0.429	22.9	-2.30×10^5	-2.30×10^5	0.00	0.00	3.59×10^5	3.59×10^5
OGL 1 SU	1.00×10^5	0	0.429	24.2	1.73×10^5	1.73×10^5	0.00	0.00	2.70×10^5	2.70×10^5
OGL 1 SB	1.00×10^5	0	0.429	24.2	-1.73×10^5	-1.73×10^5	0.00	0.00	2.70×10^5	2.70×10^5
OGL 2 SU	1.33×10^5	0	0.429	22.9	2.30×10^5	2.30×10^5	0.00	0.00	3.59×10^5	3.59×10^5
OGL 2 SB	1.33×10^5	0	0.429	22.9	-2.30×10^5	-2.30×10^5	0.00	0.00	3.59×10^5	3.59×10^5
SLL 1 IB	1.00×10^5	0	0.429	26.3	0.00	0.00	-1.08×10^5	-1.08×10^5	1.35×10^5	1.35×10^5
SLL 1 OB	1.00×10^5	0	0.429	26.3	0.00	0.00	8.09×10^4	8.09×10^4	1.35×10^5	1.35×10^5
SLL 2 IB	1.33×10^5	0	0.429	25.6	0.00	0.00	-1.44×10^5	-1.44×10^5	1.79×10^5	1.79×10^5
SLL 2 OB	1.33×10^5	0	0.429	25.6	0.00	0.00	1.08×10^5	1.08×10^5	1.79×10^5	1.79×10^5
GRO 1	1.23×10^5	-3	0.041	18.2	0.00	0.00	0.00	0.00	6.61×10^5	6.61×10^5
GRO 2 IB	1.23×10^5	-3	0.041	19.2	1.19×10^5	1.19×10^5	-1.19×10^5	-1.19×10^5	5.95×10^5	5.95×10^5
GRO 2 OB	1.23×10^5	-3	0.041	19.2	1.19×10^5	1.19×10^5	1.19×10^5	1.19×10^5	5.95×10^5	5.95×10^5
BRR 1	1.00×10^5	0	0.041	22.0	3.34×10^5	3.34×10^5	0.00	0.00	4.17×10^5	4.17×10^5
BRR 2	9.22×10^4	-3	0.041	22.5	3.07×10^5	3.07×10^5	0.00	0.00	3.84×10^5	3.84×10^5
BRR 3	1.34×10^5	0	0.041	20.8	3.93×10^5	3.93×10^5	0.00	0.00	4.91×10^5	4.91×10^5
BRR 4	1.23×10^5	-3	0.041	21.4	3.62×10^5	3.62×10^5	0.00	0.00	4.53×10^5	4.53×10^5
TRN 1 IB	1.23×10^5	-3	0.041	23.7	0.00	0.00	-1.51×10^5	-1.51×10^5	3.02×10^5	3.02×10^5
TRN 1 OB	1.23×10^5	-3	0.041	23.7	0.00	0.00	1.51×10^5	1.51×10^5	3.02×10^5	3.02×10^5
PIV 1	1.23×10^5	-3	0.041	21.4	3.62×10^5	3.62×10^5	0.00	0.00	4.53×10^5	4.53×10^5
RBR 1	1.23×10^5	-3	0.041	23.7	-1.66×10^5	-1.66×10^5	0.00	0.00	3.02×10^5	3.02×10^5

Strut Shortening Exclusion Concept

Table D.14: FV-1000 strut shortening exclusion concept (C4) right main landing gear structural loads for critical load case in each component.

Member	LC ID	V_x (N)	V_y (N)	N_z (N)	M_x (N)	M_y (N)	T_z (N)	Failure mode
Upper strut trunnion	GRO 2 IB	6.04×10^5	2.53×10^6	-5.69×10^5	-2.81×10^5	7.65×10^4	-1.37×10^4	Stress
Drop link member 1	GRO 2 IB	1.97×10^4	3.30×10^4	-2.55×10^6	-6.27×10^4	2.87×10^4	2.98×10^3	Stress
Drop link member 2	GRO 2 IB	6.91×10^3	3.11×10^4	5.69×10^5	-4.39×10^4	1.79×10^4	4.06×10^3	Stress
Drop link member 3	None	-	-	-	-	-	-	Machinability
Drop link member 4	TRN 1 OB	2.16×10^3	-1.06×10^4	-1.83×10^6	-1.90×10^4	6.75×10^3	-2.04×10^2	Stress
Drop link brace 1	None	-	-	-	-	-	-	Machinability
Drop link brace 2	GRO 2 IB	4.06×10^4	3.61×10^3	-1.87×10^6	-5.73×10^2	6.68×10^4	-5.83×10^3	Stress
Shock strut trunnion	GRO 2 IB	6.68×10^4	3.08×10^6	-9.83×10^5	-5.66×10^5	7.64×10^4	3.18×10^3	Stress
Shock strut cylinder	GRO 2 IB	-5.14×10^5	7.25×10^5	-2.26×10^6	-1.41×10^6	-1.32×10^6	-7.61×10^4	Stress
Shock strut piston	BRR 3	2.39×10^3	1.71×10^6	-1.85×10^6	-1.26×10^6	-3.07×10^4	-2.58×10^4	Stress
Shock strut brace 1	GRO 2 IB	-4.63×10^4	6.42×10^3	3.80×10^6	7.62×10^4	1.97×10^4	4.76×10^3	Stress
Shock strut brace 2	BRR 4	-4.84×10^4	-5.11×10^4	-2.59×10^6	-6.02×10^4	-3.07×10^4	1.03×10^4	Stress
Shock strut brace 3	BRR 3	2.62×10^4	-5.79×10^2	-2.39×10^6	0.00	0.00	0.00	Buckling
Bogie beam	GRO 1	3.01×10^2	1.33×10^6	3.44×10^1	1.35×10^6	-4.86×10^2	4.91×10^2	Stress
Aft wheel axle	GRO 2 OB	-1.51×10^5	5.94×10^5	1.20×10^5	5.31×10^5	1.25×10^5	7.67×10^3	Stress
Front wheel axle	GRO 2 OB	-1.51×10^5	5.94×10^5	1.20×10^5	5.31×10^5	1.25×10^5	4.91×10^3	Stress
AM member 1	LVL 3 P1 SU	6.29×10^3	-1.02×10^5	1.84×10^6	-4.48×10^4	7.99×10^2	5.74×10^2	Stress
AM member 2	LVL 3 P1 SU	7.05×10^2	-5.71×10^4	-2.16×10^6	-3.28	4.78×10^2	2.59×10^1	Buckling
AM member 3	SLL 2 P1 IB	-2.35×10^4	1.20×10^3	3.41×10^5	-2.87×10^2	-2.79×10^4	-2.06×10^3	Stress

Table D.15: FV-1000 strut shortening exclusion concept (C4) right main landing gear structural member sizing. Nodes are defined as illustrated in Figure 5.14. Dimensions shown in bold are fixed, based on either the piston diameter or wheel rim diameter, as described in Section 3.5.

Member	Nodes	l (m)	r_i (m)	r_o (m)	t (m)	A (m^2)	m (kg)
Upper strut trunnion	D1-D2-O1-D3-D4	2.300	0.121	**0.134**	0.013	0.010	181.0
Drop link member 1	D2-D5	2.511	0.055	**0.067**	0.012	0.005	93.6
Drop link member 2	O1-D5	2.572	0.062	**0.067**	0.005	0.002	40.1
Drop link member 3	O1-D6	2.537	0.064	**0.067**	0.003	0.001	26.7
Drop link member 4	D3-D6	2.406	0.061	**0.067**	0.006	0.002	44.3
Drop link brace 1	C2-C4	2.250	0.064	**0.067**	0.003	0.001	23.6
Drop link brace 2	C1-C3	2.266	0.057	**0.067**	0.010	0.004	70.5
Shock strut trunnion	D5-S1-O2-S3-D6	1.750	0.116	**0.134**	0.018	0.014	196.4
Shock strut cylinder	O2-S4-S6-S7-S8	2.936	**0.168**	0.189	0.021	0.024	551.9
Shock strut piston	S8-B1	1.924[1,2]	0.149	**0.168**	0.019	0.019	279.5
Shock strut brace 1	S1-S3	1.974	0.073	**0.084**	0.011	0.006	87.0
Shock strut brace 2	S2-S5	1.660	0.076	**0.084**	0.008	0.004	54.0
Shock strut brace 3	C5-C6	4.019	0.101	**0.109**	0.008	0.005	167.3
Bogie beam	K-B2-L	2.020	0.151	**0.168**	0.017	0.017	275.3
Aft wheel axle	K_L-K_R	1.620	0.102	**0.117**	0.015	0.010	131.4
Front wheel axle	L_L-L_R	1.620	0.102	**0.117**	0.015	0.010	131.3
AM member 1[3]	A1-A4	1.630[1]	0.036	**0.050**	0.015	0.004	51.1
AM member 2[3]	A2-A3	1.325[1]	0.041	**0.050**	0.010	0.003	28.4
AM member 3[3]	A5-A6	1.175	0.045	**0.050**	0.005	0.001	13.7
Total	-	-	-	-	-	-	2447

[1] Extended length plus a margin of 2.75 times the respective piston diameter (Section 3.4.2).
[2] Includes the bogie pivot offset distance l_offset is added here.
[3] Articulation mechanism.

Table D.16: Overview of FV-1000 strut shortening exclusion concept (C4) external main gear loads.

LC ID	m_{mlg} (kg)	θ (°)	x_{s} (m)	r_{tyre} (in)	$F_{x,\text{K}_\text{L},\text{K}_\text{R}}$ (N)	$F_{x,\text{L}_\text{L},\text{L}_\text{R}}$ (N)	$F_{y,\text{M}_\text{L},\text{M}_\text{R}}$ (N)	$F_{y,\text{N}_\text{L},\text{N}_\text{R}}$ (N)	$F_{z,\text{K}_\text{L},\text{K}_\text{R}}$ (N)	$F_{z,\text{L}_\text{L},\text{L}_\text{R}}$ (N)
LVL 1 P1 SU	1.00×10^5	0	0.596	27.1	1.10×10^5	0.00	0.00	0.00	1.72×10^5	0.00
LVL 1 P1 SB	1.00×10^5	0	0.596	27.1	-1.10×10^5	0.00	0.00	0.00	1.72×10^5	0.00
LVL 1 P2 SU	1.00×10^5	0	0.194	24.2	6.74×10^4	1.73×10^5	0.00	0.00	2.70×10^5	2.70×10^5
LVL 1 P2 SB	1.00×10^5	0	0.194	24.2	6.74×10^4	-1.73×10^5	0.00	0.00	2.70×10^5	2.70×10^5
LVL 2 P1 SU	8.99×10^4	-3	0.596	27.2	9.88×10^4	0.00	0.00	0.00	1.54×10^5	0.00
LVL 2 P1 SB	8.99×10^4	-3	0.596	27.2	-9.88×10^4	0.00	0.00	0.00	1.54×10^5	0.00
LVL 2 P2 SU	9.29×10^4	-3	0.194	24.5	6.27×10^4	1.60×10^5	0.00	0.00	2.51×10^5	2.51×10^5
LVL 2 P2 SB	9.29×10^4	-3	0.194	24.5	6.27×10^4	-1.60×10^5	0.00	0.00	2.51×10^5	2.51×10^5
LVL 3 P1 SU	1.33×10^5	0	0.596	26.7	1.46×10^5	0.00	0.00	0.00	2.28×10^5	0.00
LVL 3 P1 SB	1.33×10^5	0	0.596	26.7	-1.46×10^5	0.00	0.00	0.00	2.28×10^5	0.00
LVL 3 P2 SU	1.33×10^5	0	0.194	22.9	8.97×10^4	2.30×10^5	0.00	0.00	3.59×10^5	3.59×10^5
LVL 3 P2 SB	1.33×10^5	0	0.194	22.9	8.97×10^4	-2.30×10^5	0.00	0.00	3.59×10^5	3.59×10^5
LVL 4 P1 SU	1.20×10^5	-3	0.596	26.8	1.31×10^5	0.00	0.00	0.00	2.05×10^5	0.00
LVL 4 P1 SB	1.20×10^5	-3	0.596	26.8	-1.31×10^5	0.00	0.00	0.00	2.05×10^5	0.00
LVL 4 P2 SU	1.24×10^5	-3	0.194	23.3	8.34×10^4	2.13×10^5	0.00	0.00	3.33×10^5	3.33×10^5
LVL 4 P2 SB	1.24×10^5	-3	0.194	23.3	8.34×10^4	-2.13×10^5	0.00	0.00	3.33×10^5	3.33×10^5
LAT 1 P1 SU/IB	1.00×10^5	0	0.627	27.4	8.24×10^4	0.00	-3.22×10^4	0.00	1.29×10^5	0.00
LAT 1 P1 SU/OB	1.00×10^5	0	0.627	27.4	8.24×10^4	0.00	3.22×10^4	0.00	1.29×10^5	0.00
LAT 1 P1 SB/IB	1.00×10^5	0	0.627	27.4	-8.24×10^4	0.00	-3.22×10^4	0.00	1.29×10^5	0.00
LAT 1 P1 SB/OB	1.00×10^5	0	0.627	27.4	-8.24×10^4	0.00	3.22×10^4	0.00	1.29×10^5	0.00
LAT 1 P2 SU/IB	1.00×10^5	0	0.203	25.3	8.09×10^4	1.29×10^5	-5.06×10^4	-5.06×10^4	2.02×10^5	2.02×10^5
LAT 1 P2 SU/OB	1.00×10^5	0	0.203	25.3	8.09×10^4	1.29×10^5	5.06×10^4	5.06×10^4	2.02×10^5	2.02×10^5
LAT 1 P2 SB/IB	1.00×10^5	0	0.203	25.3	8.09×10^4	-1.29×10^5	-5.06×10^4	-5.06×10^4	2.02×10^5	2.02×10^5
LAT 1 P2 SB/OB	1.00×10^5	0	0.203	25.3	8.09×10^4	-1.29×10^5	5.06×10^4	5.06×10^4	2.02×10^5	2.02×10^5
LAT 2 P1 SU/IB	8.99×10^4	-3	0.627	27.5	7.41×10^4	0.00	-2.89×10^4	0.00	1.16×10^5	0.00
LAT 2 P1 SU/OB	8.99×10^4	-3	0.627	27.5	7.41×10^4	0.00	2.89×10^4	0.00	1.16×10^5	0.00
LAT 2 P1 SB/IB	8.99×10^4	-3	0.627	27.5	-7.41×10^4	0.00	-2.89×10^4	0.00	1.16×10^5	0.00
LAT 2 P1 SB/OB	8.99×10^4	-3	0.627	27.5	-7.41×10^4	0.00	2.89×10^4	0.00	1.16×10^5	0.00
LAT 2 P2 SU/IB	9.29×10^4	-3	0.203	25.5	7.52×10^4	1.20×10^5	-4.70×10^4	-4.70×10^4	1.88×10^5	1.88×10^5
LAT 2 P2 SU/OB	9.29×10^4	-3	0.203	25.5	7.52×10^4	1.20×10^5	4.70×10^4	4.70×10^4	1.88×10^5	1.88×10^5
LAT 2 P2 SB/IB	9.29×10^4	-3	0.203	25.5	7.52×10^4	-1.20×10^5	-4.70×10^4	-4.70×10^4	1.88×10^5	1.88×10^5
LAT 2 P2 SB/OB	9.29×10^4	-3	0.203	25.5	7.52×10^4	-1.20×10^5	4.70×10^4	4.70×10^4	1.88×10^5	1.88×10^5
TDL 1 P1 SU	1.00×10^5	14	0.596	27.1	1.10×10^5	0.00	0.00	0.00	1.72×10^5	0.00
TDL 1 P1 SB	1.00×10^5	14	0.596	27.1	-1.10×10^5	0.00	0.00	0.00	1.72×10^5	0.00
TDL 1 P2 SU	1.00×10^5	14	0.194	24.2	0.00	1.73×10^5	0.00	0.00	2.70×10^5	2.70×10^5
TDL 1 P2 SB	1.00×10^5	14	0.194	24.2	0.00	-1.73×10^5	0.00	0.00	2.70×10^5	2.70×10^5
TDL 2 P1 SU	1.33×10^5	14	0.596	26.7	1.46×10^5	0.00	0.00	0.00	2.28×10^5	0.00
TDL 2 P1 SB	1.33×10^5	14	0.596	26.7	-1.46×10^5	0.00	0.00	0.00	2.28×10^5	0.00
TDL 2 P2 SU	1.33×10^5	14	0.194	22.9	0.00	2.30×10^5	0.00	0.00	3.59×10^5	3.59×10^5
TDL 2 P2 SB	1.33×10^5	14	0.194	22.9	0.00	-2.30×10^5	0.00	0.00	3.59×10^5	3.59×10^5
OGL 1 P1 SU	1.00×10^5	0	0.596	27.1	1.10×10^5	0.00	0.00	0.00	1.72×10^5	0.00
OGL 1 P1 SB	1.00×10^5	0	0.596	27.1	-1.10×10^5	0.00	0.00	0.00	1.72×10^5	0.00
OGL 1 P2 SU	1.00×10^5	0	0.194	24.2	6.74×10^4	1.73×10^5	0.00	0.00	2.70×10^5	2.70×10^5
OGL 1 P2 SB	1.00×10^5	0	0.194	24.2	6.74×10^4	-1.73×10^5	0.00	0.00	2.70×10^5	2.70×10^5
OGL 2 P1 SU	1.33×10^5	0	0.596	26.7	1.46×10^5	0.00	0.00	0.00	2.28×10^5	0.00
OGL 2 P1 SB	1.33×10^5	0	0.596	26.7	-1.46×10^5	0.00	0.00	0.00	2.28×10^5	0.00
OGL 2 P2 SU	1.33×10^5	0	0.194	22.9	8.97×10^4	2.30×10^5	0.00	0.00	3.59×10^5	3.59×10^5
OGL 2 P2 SB	1.33×10^5	0	0.194	22.9	8.97×10^4	-2.30×10^5	0.00	0.00	3.59×10^5	3.59×10^5
SLL 1 P1 IB	1.00×10^5	0	0.596	27.8	0.00	0.00	-6.87×10^4	0.00	8.58×10^4	0.00
SLL 1 P1 OB	1.00×10^5	0	0.596	27.8	0.00	0.00	5.15×10^4	0.00	8.58×10^4	0.00
SLL 1 P2 IB	1.00×10^5	0	0.194	26.3	0.00	0.00	-1.08×10^5	-1.08×10^5	1.35×10^5	1.35×10^5
SLL 1 P2 OB	1.00×10^5	0	0.194	26.3	0.00	0.00	8.09×10^4	8.09×10^4	1.35×10^5	1.35×10^5
SLL 2 P1 IB	1.33×10^5	0	0.596	27.5	0.00	0.00	-9.13×10^4	0.00	1.14×10^5	0.00
SLL 2 P1 OB	1.33×10^5	0	0.596	27.5	0.00	0.00	6.85×10^4	0.00	1.14×10^5	0.00
SLL 2 P2 IB	1.33×10^5	0	0.194	25.6	0.00	0.00	-1.44×10^5	-1.44×10^5	1.79×10^5	1.79×10^5
SLL 2 P2 OB	1.33×10^5	0	0.194	25.6	0.00	0.00	1.08×10^5	1.08×10^5	1.79×10^5	1.79×10^5
GRO 1	1.24×10^5	-3	0.054	18.1	0.00	0.00	0.00	0.00	6.67×10^5	6.67×10^5
GRO 2 IB	1.24×10^5	-3	0.054	19.1	1.20×10^5	1.20×10^5	-1.20×10^5	-1.20×10^5	6.01×10^5	6.01×10^5
GRO 2 OB	1.24×10^5	-3	0.054	19.1	1.20×10^5	1.20×10^5	1.20×10^5	1.20×10^5	6.01×10^5	6.01×10^5
BRR 1	1.00×10^5	0	0.054	22.0	3.34×10^5	3.34×10^5	0.00	0.00	4.17×10^5	4.17×10^5
BRR 2	9.30×10^4	-3	0.054	22.4	3.10×10^5	3.10×10^5	0.00	0.00	3.88×10^5	3.88×10^5
BRR 3	1.34×10^5	0	0.054	20.8	3.93×10^5	3.93×10^5	0.00	0.00	4.91×10^5	4.91×10^5
BRR 4	1.24×10^5	-3	0.054	21.3	3.65×10^5	3.65×10^5	0.00	0.00	4.57×10^5	4.57×10^5
TRN 1 IB	1.24×10^5	-3	0.054	23.7	0.00	0.00	-1.52×10^5	-1.52×10^5	3.05×10^5	3.05×10^5
TRN 1 OB	1.24×10^5	-3	0.054	23.7	0.00	0.00	1.52×10^5	1.52×10^5	3.05×10^5	3.05×10^5
PIV 1	1.24×10^5	-3	0.054	21.3	3.65×10^5	3.65×10^5	0.00	0.00	4.57×10^5	4.57×10^5
RBR 1	1.24×10^5	-3	0.054	23.7	-1.67×10^5	-1.67×10^5	0.00	0.00	3.05×10^5	3.05×10^5

Backward Stowage Concept

Table D.17: FV-1000 backward stowage concept (C5) right main landing gear structural loads for critical load case in each component.

Member	LC ID	V_x (N)	V_y (N)	N_z (N)	M_x (N)	M_y (N)	T_z (N)	Failure mode
Upper strut trunnion	BRR 3	-4.12×10^{4}	3.62×10^{6}	-1.71×10^{6}	-6.79×10^{5}	1.74×10^{4}	-2.13×10^{4}	Stress
Drop link member 1	BRR 3	3.46×10^{3}	2.84×10^{4}	-3.60×10^{6}	-3.51×10^{4}	2.19×10^{4}	1.44×10^{3}	Stress
Drop link member 2	GRO 2 OB	-6.50×10^{3}	2.19×10^{4}	-1.61×10^{6}	-2.51×10^{4}	-1.07×10^{4}	8.48×10^{2}	Stress
Drop link member 3	TRN 1 IB	1.37×10^{4}	-3.26×10^{4}	1.36×10^{6}	3.80×10^{4}	1.42×10^{4}	8.08×10^{3}	Stress
Drop link member 4	TRN 1 IB	4.38×10^{4}	-7.07×10^{4}	-1.41×10^{5}	9.31×10^{4}	6.69×10^{4}	-8.87×10^{3}	Stress
Drop link brace 1	TRN 1 IB	-1.62×10^{4}	3.29×10^{3}	-2.55×10^{6}	-4.01×10^{2}	-1.76×10^{4}	1.56×10^{4}	Buckling
Drop link brace 2	GRO 2 OB	1.98×10^{4}	-5.06×10^{3}	8.27×10^{5}	-2.49×10^{2}	3.60×10^{4}	-5.22×10^{3}	Stress
Shock strut trunnion	BRR 3	1.40×10^{5}	4.27×10^{6}	3.83×10^{5}	-8.79×10^{5}	9.30×10^{4}	1.46×10^{4}	Stress
Shock strut cylinder	BRR 3	5.57×10^{5}	-5.54×10^{5}	-3.99×10^{6}	-1.89×10^{6}	1.18×10^{6}	-1.15×10^{5}	Stress
Shock strut piston	BRR 3	8.00×10^{2}	1.71×10^{6}	-1.85×10^{6}	-1.27×10^{6}	3.24×10^{4}	3.25×10^{4}	Stress
Shock strut brace 1	BRR 3	7.51×10^{3}	5.03×10^{4}	4.94×10^{6}	1.25×10^{5}	-2.29×10^{4}	6.91×10^{3}	Stress
Shock strut brace 2	TRN 1 IB	3.77×10^{4}	1.54×10^{4}	2.94×10^{6}	5.18×10^{4}	1.49×10^{4}	5.44×10^{3}	Stress
Shock strut brace 3	None	-	-	-	-	-	-	Machinability
Bogie beam	GRO 1	3.21×10^{2}	1.33×10^{6}	4.68×10^{1}	1.35×10^{6}	-4.14×10^{2}	-4.10×10^{3}	Stress
Aft wheel axle	GRO 2 IB	1.51×10^{5}	-5.94×10^{5}	1.20×10^{5}	5.33×10^{5}	1.23×10^{5}	-1.21×10^{3}	Stress
Front wheel axle	GRO 2 IB	1.51×10^{5}	-5.94×10^{5}	1.20×10^{5}	5.33×10^{5}	1.24×10^{5}	1.68×10^{3}	Stress
AM member 1	LVL 3 P1 SU	-2.14×10^{3}	-8.30×10^{4}	1.61×10^{6}	-3.34×10^{4}	-8.92×10^{1}	-5.22×10^{2}	Stress
AM member 2	LVL 3 P1 SU	4.04×10^{3}	-4.29×10^{4}	-1.63×10^{6}	2.13	3.59×10^{2}	1.84×10^{2}	Stress
AM member 3	SLL 2 P1 IB	-3.31×10^{4}	-1.29×10^{3}	3.15×10^{5}	-3.21×10^{2}	-3.02×10^{4}	-1.86×10^{3}	Stress
Shortening members	GRO 1	0.00	0.00	-5.22×10^{4}	0.00	0.00	0.00	Stress

Table D.18: FV-1000 backward stowage concept (C5) right main landing gear structural member sizing. Nodes are defined as illustrated in Figure 5.14. Dimensions shown in bold are fixed, based on either the piston diameter or wheel rim diameter, as described in Section 3.5.

Member	Nodes	l (m)	r_i (m)	r_o (m)	t (m)	A (m^2)	m (kg)
Upper strut trunnion	D1-D2-O1-D3-D4	2.300	0.111	**0.134**	0.023	0.018	319.8
Drop link member 1	D2-D5	2.374	0.054	**0.067**	0.013	0.005	89.5
Drop link member 2	O1-D5	2.068	0.061	**0.067**	0.006	0.002	38.3
Drop link member 3	O1-D6	2.118	0.061	**0.067**	0.006	0.003	42.6
Drop link member 4	D3-D6	1.779	0.057	**0.067**	0.010	0.004	54.7
Drop link brace 1	C2-C4	2.160	0.054	**0.067**	0.013	0.005	82.3
Drop link brace 2	C1-C3	2.533	0.062	**0.067**	0.005	0.002	37.3
Shock strut trunnion	D5-S1-O2-S3-D6	1.750	0.106	**0.134**	0.028	0.021	289.2
Shock strut cylinder	O2-S4-S6-S7-S8	3.144	**0.168**	0.193	0.025	0.029	710.2
Shock strut piston	S8-B1	1.932[1,2]	0.149	**0.168**	0.019	0.019	283.0
Shock strut brace 1	S1-S3	1.782	0.067	**0.084**	0.017	0.008	114.3
Shock strut brace 2	S2-S5	2.082	0.076	**0.084**	0.008	0.004	67.3
Shock strut brace 3	C5-C6	3.891	0.104	**0.109**	0.005	0.004	108.2
Bogie beam	K-B2-L	2.020	0.151	**0.168**	0.017	0.017	275.5
Aft wheel axle	K_L-K_R	1.620	0.102	**0.117**	0.015	0.010	131.5
Front wheel axle	L_L-L_R	1.620	0.102	**0.117**	0.015	0.010	131.6
AM member 1[3]	A1-A4	1.326[1]	0.039	**0.050**	0.011	0.003	32.1
AM member 2[3]	A2-A3	1.147[1]	0.045	**0.050**	0.005	0.002	14.0
AM member 3[3]	A5-A6	0.920	0.045	**0.050**	0.005	0.002	11.3
Shortening members	-	0.500	0.042	**0.050**	0.009	0.003	9.8
Total	-	-	-	-	-	-	2843

[1] Extended length plus a margin of 2.75 times the respective piston diameter (Section 3.4.2).
[2] Includes the bogie pivot offset distance l_{offset} is added here.
[3] Articulation mechanism.

Table D.19: Overview of FV-1000 backward stowage concept (C5) external main gear loads.

LC ID	m_{mlg} (kg)	θ (°)	x_{s} (m)	r_{tyre} (in)	$F_{x,\text{K}_\text{L},\text{K}_\text{R}}$ (N)	$F_{x,\text{L}_\text{L},\text{L}_\text{R}}$ (N)	$F_{y,\text{M}_\text{L},\text{M}_\text{R}}$ (N)	$F_{y,\text{N}_\text{L},\text{N}_\text{R}}$ (N)	$F_{z,\text{K}_\text{L},\text{K}_\text{R}}$ (N)	$F_{z,\text{L}_\text{L},\text{L}_\text{R}}$ (N)
LVL 1 P1 SU	1.00×10^5	0	0.602	27.1	1.10×10^5	0.00	0.00	0.00	1.72×10^5	0.00
LVL 1 P1 SB	1.00×10^5	0	0.602	27.1	-1.10×10^5	0.00	0.00	0.00	1.72×10^5	0.00
LVL 1 P2 SU	1.00×10^5	0	0.192	24.2	6.74×10^4	1.73×10^5	0.00	0.00	2.70×10^5	2.70×10^5
LVL 1 P2 SB	1.00×10^5	0	0.192	24.2	6.74×10^4	-1.73×10^5	0.00	0.00	2.70×10^5	2.70×10^5
LVL 2 P1 SU	8.99×10^4	-3	0.602	27.2	9.88×10^4	0.00	0.00	0.00	1.54×10^5	0.00
LVL 2 P1 SB	8.99×10^4	-3	0.602	27.2	-9.88×10^4	0.00	0.00	0.00	1.54×10^5	0.00
LVL 2 P2 SU	9.29×10^4	-3	0.192	24.5	6.27×10^4	1.60×10^5	0.00	0.00	2.51×10^5	2.51×10^5
LVL 2 P2 SB	9.29×10^4	-3	0.192	24.5	6.27×10^4	-1.60×10^5	0.00	0.00	2.51×10^5	2.51×10^5
LVL 3 P1 SU	1.33×10^5	0	0.602	26.7	1.46×10^5	0.00	0.00	0.00	2.28×10^5	0.00
LVL 3 P1 SB	1.33×10^5	0	0.602	26.7	-1.46×10^5	0.00	0.00	0.00	2.28×10^5	0.00
LVL 3 P2 SU	1.33×10^5	0	0.192	22.9	8.97×10^4	2.30×10^5	0.00	0.00	3.59×10^5	3.59×10^5
LVL 3 P2 SB	1.33×10^5	0	0.192	22.9	8.97×10^4	-2.30×10^5	0.00	0.00	3.59×10^5	3.59×10^5
LVL 4 P1 SU	1.20×10^5	-3	0.602	26.8	1.31×10^5	0.00	0.00	0.00	2.05×10^5	0.00
LVL 4 P1 SB	1.20×10^5	-3	0.602	26.8	-1.31×10^5	0.00	0.00	0.00	2.05×10^5	0.00
LVL 4 P2 SU	1.24×10^5	-3	0.192	23.3	8.34×10^4	2.13×10^5	0.00	0.00	3.33×10^5	3.33×10^5
LVL 4 P2 SB	1.24×10^5	-3	0.192	23.3	8.34×10^4	-2.13×10^5	0.00	0.00	3.33×10^5	3.33×10^5
LAT 1 P1 SU/IB	1.00×10^5	0	0.633	27.4	8.24×10^4	0.00	-3.22×10^4	0.00	1.29×10^5	0.00
LAT 1 P1 SU/OB	1.00×10^5	0	0.633	27.4	8.24×10^4	0.00	3.22×10^4	0.00	1.29×10^5	0.00
LAT 1 P1 SB/IB	1.00×10^5	0	0.633	27.4	-8.24×10^4	0.00	-3.22×10^4	0.00	1.29×10^5	0.00
LAT 1 P1 SB/OB	1.00×10^5	0	0.633	27.4	-8.24×10^4	0.00	3.22×10^4	0.00	1.29×10^5	0.00
LAT 1 P2 SU/IB	1.00×10^5	0	0.201	25.3	8.09×10^4	1.29×10^5	-5.06×10^4	-5.06×10^4	2.02×10^5	2.02×10^5
LAT 1 P2 SU/OB	1.00×10^5	0	0.201	25.3	8.09×10^4	1.29×10^5	5.06×10^4	5.06×10^4	2.02×10^5	2.02×10^5
LAT 1 P2 SB/IB	1.00×10^5	0	0.201	25.3	8.09×10^4	-1.29×10^5	-5.06×10^4	-5.06×10^4	2.02×10^5	2.02×10^5
LAT 1 P2 SB/OB	1.00×10^5	0	0.201	25.3	8.09×10^4	-1.29×10^5	5.06×10^4	5.06×10^4	2.02×10^5	2.02×10^5
LAT 2 P1 SU/IB	8.99×10^4	-3	0.633	27.5	7.41×10^4	0.00	-2.89×10^4	0.00	1.16×10^5	0.00
LAT 2 P1 SU/OB	8.99×10^4	-3	0.633	27.5	7.41×10^4	0.00	2.89×10^4	0.00	1.16×10^5	0.00
LAT 2 P1 SB/IB	8.99×10^4	-3	0.633	27.5	-7.41×10^4	0.00	-2.89×10^4	0.00	1.16×10^5	0.00
LAT 2 P1 SB/OB	8.99×10^4	-3	0.633	27.5	-7.41×10^4	0.00	2.89×10^4	0.00	1.16×10^5	0.00
LAT 2 P2 SU/IB	9.29×10^4	-3	0.201	25.5	7.52×10^4	1.20×10^5	-4.70×10^4	-4.70×10^4	1.88×10^5	1.88×10^5
LAT 2 P2 SU/OB	9.29×10^4	-3	0.201	25.5	7.52×10^4	1.20×10^5	4.70×10^4	4.70×10^4	1.88×10^5	1.88×10^5
LAT 2 P2 SB/IB	9.29×10^4	-3	0.201	25.5	7.52×10^4	-1.20×10^5	-4.70×10^4	-4.70×10^4	1.88×10^5	1.88×10^5
LAT 2 P2 SB/OB	9.29×10^4	-3	0.201	25.5	7.52×10^4	-1.20×10^5	4.70×10^4	4.70×10^4	1.88×10^5	1.88×10^5
TDL 1 P1 SU	1.00×10^5	14	0.602	27.1	1.10×10^5	0.00	0.00	0.00	1.72×10^5	0.00
TDL 1 P1 SB	1.00×10^5	14	0.602	27.1	-1.10×10^5	0.00	0.00	0.00	1.72×10^5	0.00
TDL 1 P2 SU	1.00×10^5	14	0.192	24.2	0.00	1.73×10^5	0.00	0.00	2.70×10^5	2.70×10^5
TDL 1 P2 SB	1.00×10^5	14	0.192	24.2	0.00	-1.73×10^5	0.00	0.00	2.70×10^5	2.70×10^5
TDL 2 P1 SU	1.33×10^5	14	0.602	26.7	1.46×10^5	0.00	0.00	0.00	2.28×10^5	0.00
TDL 2 P1 SB	1.33×10^5	14	0.602	26.7	-1.46×10^5	0.00	0.00	0.00	2.28×10^5	0.00
TDL 2 P2 SU	1.33×10^5	14	0.192	22.9	0.00	2.30×10^5	0.00	0.00	3.59×10^5	3.59×10^5
TDL 2 P2 SB	1.33×10^5	14	0.192	22.9	0.00	-2.30×10^5	0.00	0.00	3.59×10^5	3.59×10^5
OGL 1 P1 SU	1.00×10^5	0	0.602	27.1	1.10×10^5	0.00	0.00	0.00	1.72×10^5	0.00
OGL 1 P1 SB	1.00×10^5	0	0.602	27.1	-1.10×10^5	0.00	0.00	0.00	1.72×10^5	0.00
OGL 1 P2 SU	1.00×10^5	0	0.192	24.2	6.74×10^4	1.73×10^5	0.00	0.00	2.70×10^5	2.70×10^5
OGL 1 P2 SB	1.00×10^5	0	0.192	24.2	6.74×10^4	-1.73×10^5	0.00	0.00	2.70×10^5	2.70×10^5
OGL 2 P1 SU	1.33×10^5	0	0.602	26.7	1.46×10^5	0.00	0.00	0.00	2.28×10^5	0.00
OGL 2 P1 SB	1.33×10^5	0	0.602	26.7	-1.46×10^5	0.00	0.00	0.00	2.28×10^5	0.00
OGL 2 P2 SU	1.33×10^5	0	0.192	22.9	8.97×10^4	2.30×10^5	0.00	0.00	3.59×10^5	3.59×10^5
OGL 2 P2 SB	1.33×10^5	0	0.192	22.9	8.97×10^4	-2.30×10^5	0.00	0.00	3.59×10^5	3.59×10^5
SLL 1 P1 IB	1.00×10^5	0	0.602	27.8	0.00	0.00	-6.87×10^4	0.00	8.58×10^4	0.00
SLL 1 P1 OB	1.00×10^5	0	0.602	27.8	0.00	0.00	5.15×10^4	0.00	8.58×10^4	0.00
SLL 1 P2 IB	1.00×10^5	0	0.192	26.3	0.00	0.00	-1.08×10^5	-1.08×10^5	1.35×10^5	1.35×10^5
SLL 1 P2 OB	1.00×10^5	0	0.192	26.3	0.00	0.00	8.09×10^4	8.09×10^4	1.35×10^5	1.35×10^5
SLL 2 P1 IB	1.33×10^5	0	0.602	27.5	0.00	0.00	-9.13×10^4	0.00	1.14×10^5	0.00
SLL 2 P1 OB	1.33×10^5	0	0.602	27.5	0.00	0.00	6.85×10^4	0.00	1.14×10^5	0.00
SLL 2 P2 IB	1.33×10^5	0	0.192	25.6	0.00	0.00	-1.44×10^5	-1.44×10^5	1.79×10^5	1.79×10^5
SLL 2 P2 OB	1.33×10^5	0	0.192	25.6	0.00	0.00	1.08×10^5	1.08×10^5	1.79×10^5	1.79×10^5
GRO 1	1.24×10^5	-3	0.054	18.1	0.00	0.00	0.00	0.00	6.67×10^5	6.67×10^5
GRO 2 IB	1.24×10^5	-3	0.054	19.1	1.20×10^5	1.20×10^5	-1.20×10^5	-1.20×10^5	6.01×10^5	6.01×10^5
GRO 2 OB	1.24×10^5	-3	0.054	19.1	1.20×10^5	1.20×10^5	1.20×10^5	1.20×10^5	6.01×10^5	6.01×10^5
BRR 1	1.00×10^5	0	0.054	22.0	3.34×10^5	3.34×10^5	0.00	0.00	4.17×10^5	4.17×10^5
BRR 2	9.30×10^4	-3	0.054	22.4	3.10×10^5	3.10×10^5	0.00	0.00	3.88×10^5	3.88×10^5
BRR 3	1.34×10^5	0	0.054	20.8	3.93×10^5	3.93×10^5	0.00	0.00	4.91×10^5	4.91×10^5
BRR 4	1.24×10^5	-3	0.054	21.3	3.65×10^5	3.65×10^5	0.00	0.00	4.57×10^5	4.57×10^5
TRN 1 IB	1.24×10^5	-3	0.054	23.7	0.00	0.00	-1.52×10^5	-1.52×10^5	3.05×10^5	3.05×10^5
TRN 1 OB	1.24×10^5	-3	0.054	23.7	0.00	0.00	1.52×10^5	1.52×10^5	3.05×10^5	3.05×10^5
PIV 1	1.24×10^5	-3	0.054	21.3	3.65×10^5	3.65×10^5	0.00	0.00	4.57×10^5	4.57×10^5
RBR 1	1.24×10^5	-3	0.054	23.7	-1.67×10^5	-1.67×10^5	0.00	0.00	3.05×10^5	3.05×10^5

D.3. Family Design

D.3.1. Gear Model Generation

FV-800

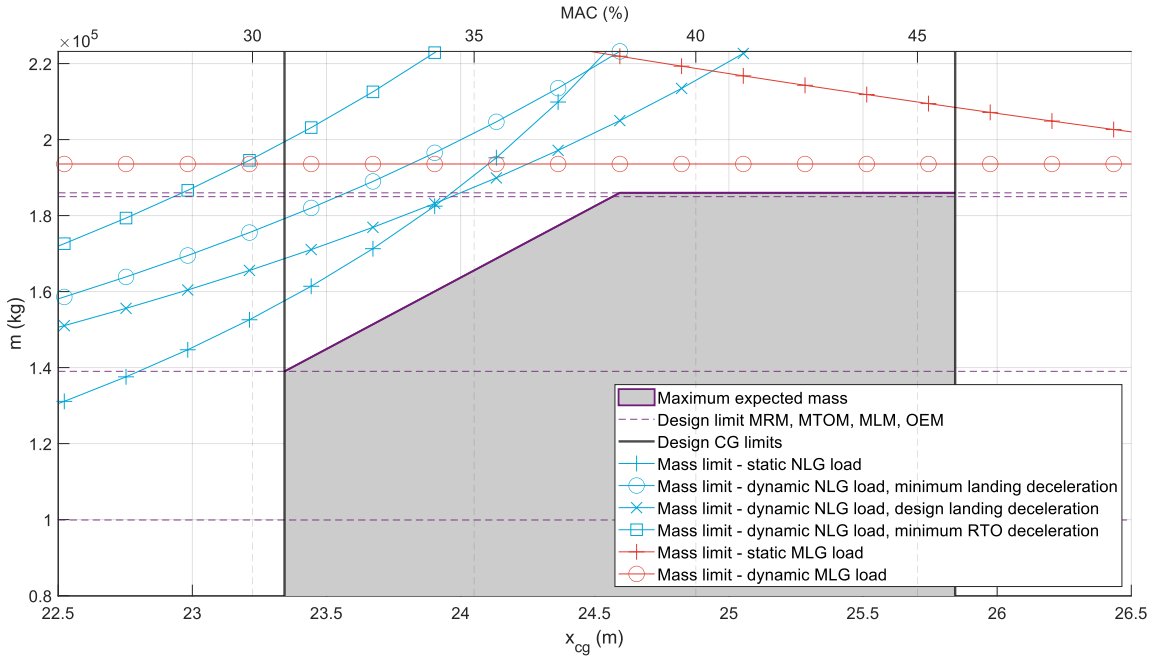

Figure D.7: FV-800 single optimisation gear - loading diagram.

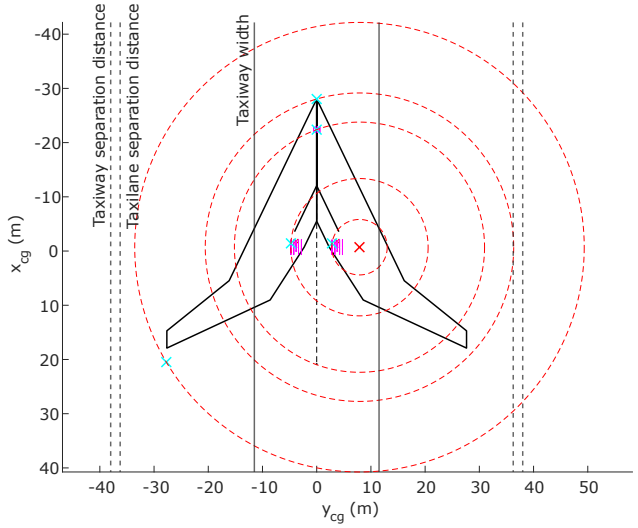

Figure D.8: FV-800 single optimisation gear - wing tip, nose, nose gear, left main gear and right main gear turning radii for a right turn with maximum nose gear steering angle.

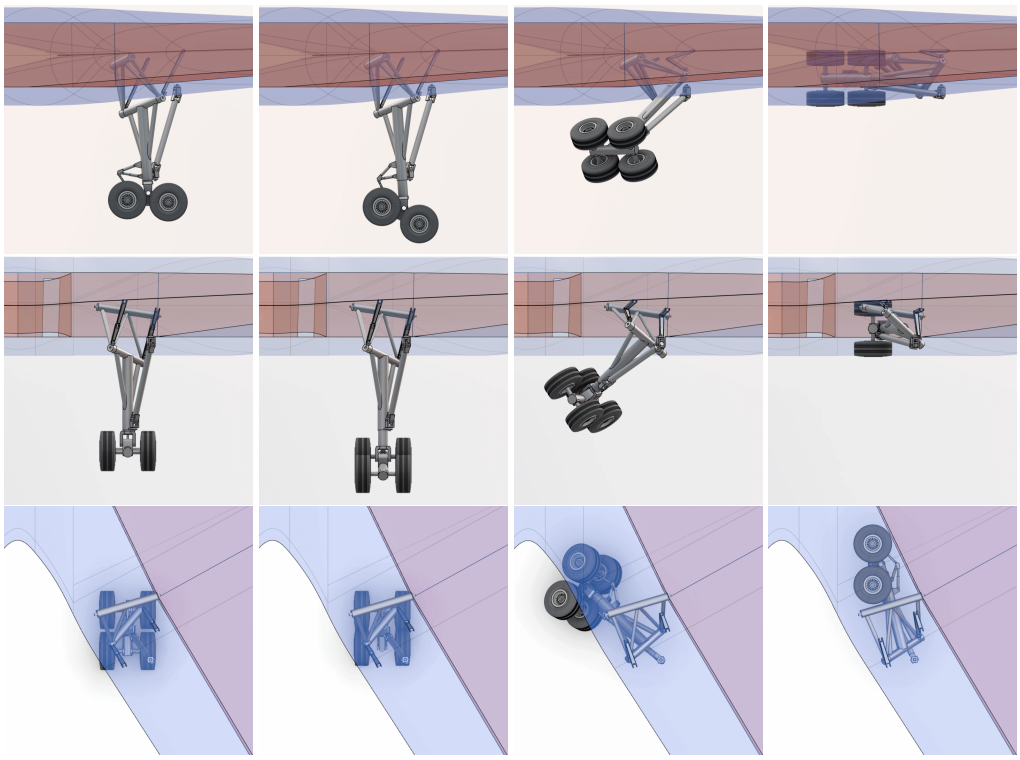

Figure D.9: FV-800 single optimisation main landing gear retraction kinematics, left view, back view and top view.

Table D.20: FV-800 single optimisation gear model node specifications (static position). Nodes are defined as illustrated in Figure 5.14.

Node	x (m)	y (m)	z (m)	Type	Node	x (m)	y (m)	z (m)	Type
O1	0.000	0.000	0.000	Beam	S7	0.852	0.000	-3.949	Beam
D1	0.309	-1.044	0.155	-	S8	0.863	0.000	-4.098	Beam
D2	0.267	-0.902	0.133	Beam	A1	0.475	0.000	-3.574	Hinge
D3	-0.267	0.902	-0.133	Beam	A2	0.613	0.000	-3.965	Hinge
D4	-0.309	1.044	-0.155	-	A3	-0.044	0.000	-3.849	Hinge
D5	1.319	-0.541	-1.273	Hinge	A4	0.116	0.000	-3.802	Beam
D6	0.048	0.541	-1.797	Hinge	A5	-0.138	0.000	-3.885	Hinge
C1	2.107	-0.101	0.367	-	A6	0.303	0.000	-4.528	Hinge
C2	0.885	1.031	0.083	-	B1	0.893	0.000	-4.539	Hinge
C3	1.399	-0.521	-1.053	Hinge	B2	0.879	0.000	-4.819	Beam
C4	0.128	0.561	-1.577	Hinge	B3	0.290	0.000	-4.788	Beam
C5	1.886	0.800	-1.150	-	K_L	1.588	-0.700	-4.856	Hinge
C6	1.115	0.231	-3.760	Universal	K_C	1.588	0.000	-4.856	Beam
C7	1.138	0.231	-4.079	Beam	K_R	1.588	0.700	-4.856	Hinge
O2	0.683	0.000	-1.535	Beam	L_L	0.170	-0.700	-4.782	Hinge
S1	1.156	-0.403	-1.340	Beam	L_C	0.170	0.000	-4.782	Beam
S2	0.233	0.383	-1.721	Beam	L_R	0.170	0.700	-4.782	Hinge
S3	0.934	-0.119	-3.063	Beam	M_L	1.560	-0.700	-5.384	-
S4	0.791	0.000	-3.073	Beam	M_R	1.560	0.700	-5.384	-
S5	0.648	0.119	-3.083	Beam	N_L	0.142	-0.700	-5.310	-
S6	0.824	0.000	-3.550	Beam	N_R	0.142	0.700	-5.310	-

FV-900

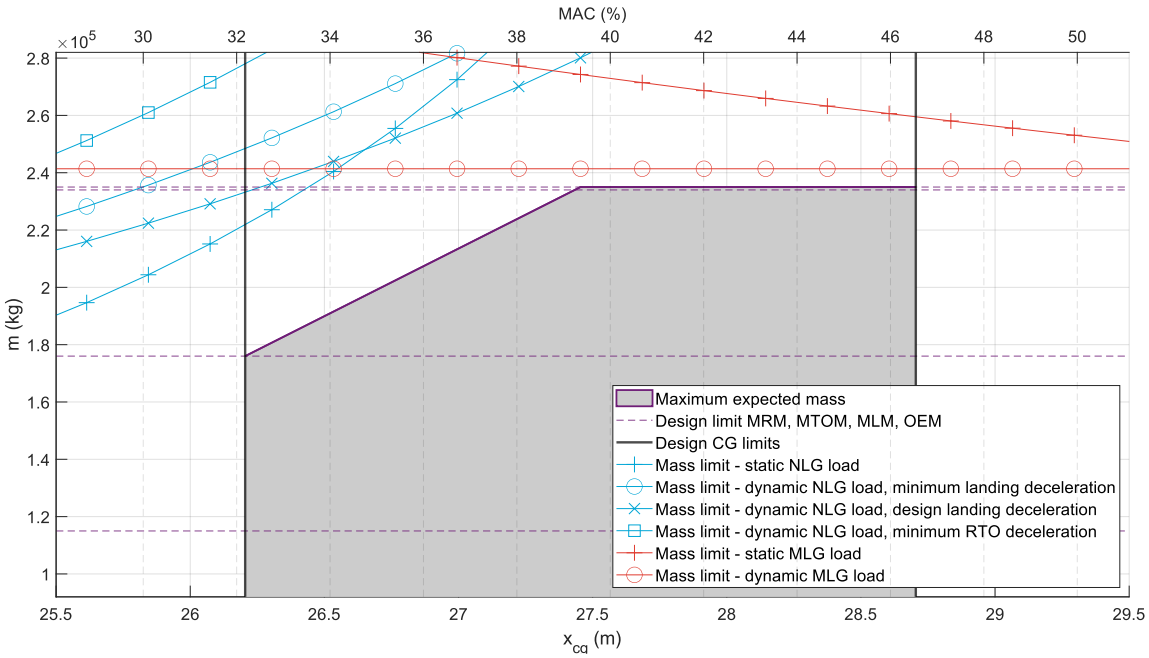

Figure D.10: FV-900 single optimisation gear - loading diagram.

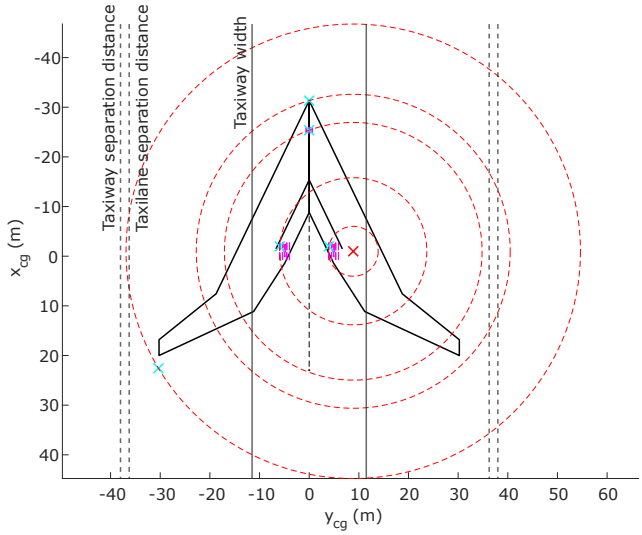

Figure D.11: FV-900 single optimisation gear - wing tip, nose, nose gear, left main gear and right main gear turning radii for a right turn with maximum nose gear steering angle.

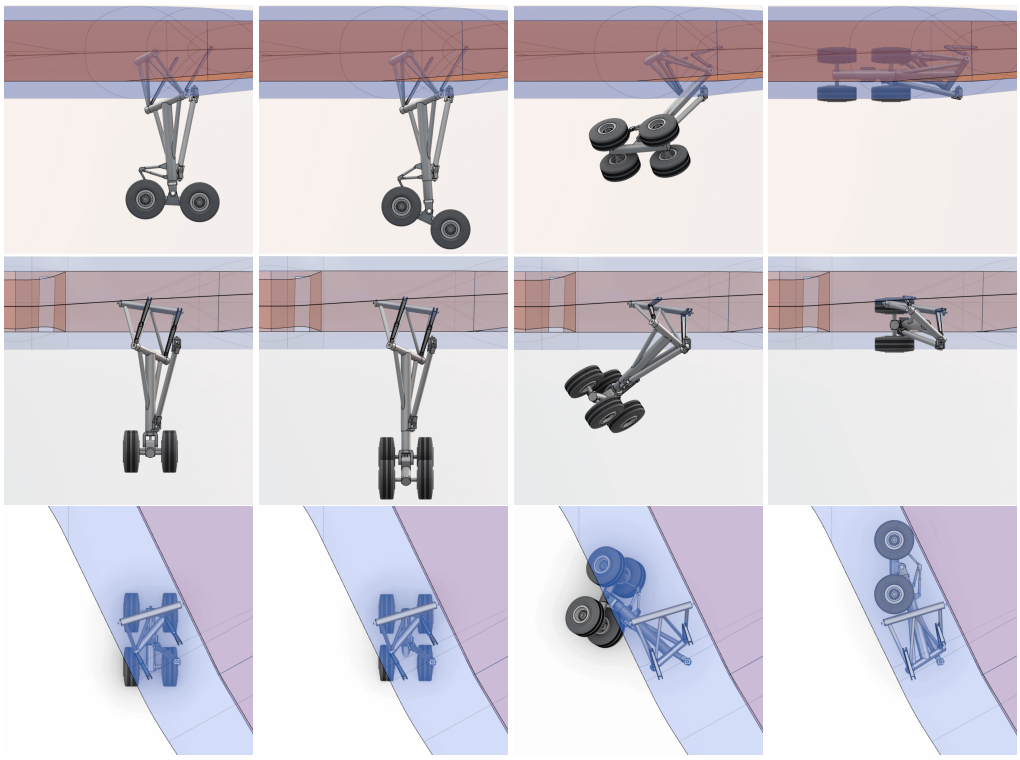

Figure D.12: FV-900 single optimisation main landing gear retraction kinematics, left view, back view and top view.

Table D.21: FV-900 single optimisation gear model node specifications (static position). Nodes are defined as illustrated in Figure 5.14.

Node	x (m)	y (m)	z (m)	Type	Node	x (m)	y (m)	z (m)	Type
O1	0.000	0.000	0.000	Beam	S7	0.930	0.000	-4.374	Beam
D1	0.323	-1.092	0.162	-	S8	0.940	0.000	-4.523	Beam
D2	0.281	-0.949	0.140	Beam	A1	0.553	0.000	-3.999	Hinge
D3	-0.281	0.949	-0.140	Beam	A2	0.690	0.000	-4.390	Hinge
D4	-0.323	1.092	-0.162	-	A3	-0.140	0.000	-4.138	Hinge
D5	1.376	-0.541	-1.400	Hinge	A4	-0.197	0.000	-4.073	Beam
D6	0.105	0.541	-1.925	Hinge	A5	-0.240	0.000	-4.148	Hinge
C1	2.375	-0.021	0.360	-	A6	0.202	0.000	-4.955	Hinge
C2	1.111	1.081	-0.045	-	B1	0.972	0.000	-4.975	Hinge
C3	1.456	-0.521	-1.180	Hinge	B2	0.957	0.000	-5.255	Beam
C4	0.185	0.561	-1.705	Hinge	B3	0.188	0.000	-5.215	Beam
C5	2.062	0.880	-1.260	-	K_L	1.946	-0.700	-5.307	Hinge
C6	1.193	0.231	-4.185	Universal	K_C	1.946	0.000	-5.307	Beam
C7	1.215	0.231	-4.504	Beam	K_R	1.946	0.700	-5.307	Hinge
O2	0.740	0.000	-1.663	Beam	L_L	-0.031	-0.700	-5.203	Hinge
S1	1.213	-0.403	-1.468	Beam	L_C	-0.031	0.000	-5.203	Beam
S2	0.290	0.383	-1.848	Beam	L_R	-0.031	0.700	-5.203	Hinge
S3	1.003	-0.119	-3.369	Beam	M_L	1.916	-0.700	-5.879	-
S4	0.860	0.000	-3.379	Beam	M_R	1.916	0.700	-5.879	-
S5	0.717	0.119	-3.389	Beam	N_L	-0.061	-0.700	-5.775	-
S6	0.902	0.000	-3.975	Beam	N_R	-0.061	0.700	-5.775	-

D.3.2. Structural Sizing

FV-800

Table D.22: FV-800 single optimisation right main landing gear structural loads for critical load case in each component.

Member	LC ID	V_x (N)	V_y (N)	N_z (N)	M_x (N)	M_y (N)	T_z (N)	Failure mode
Upper strut trunnion	BRR 4	9.59×10^{5}	-1.69×10^{6}	-2.69×10^{5}	-2.53×10^{5}	-1.21×10^{5}	-9.41×10^{3}	Stress
Drop link member 1	GRO 2 IB	5.62×10^{3}	3.52×10^{4}	-1.35×10^{6}	-3.86×10^{4}	5.37×10^{3}	3.85×10^{3}	Stress
Drop link member 2	GRO 2 IB	-1.77×10^{3}	1.93×10^{4}	3.06×10^{5}	-2.09×10^{4}	-2.04×10^{3}	2.26×10^{3}	Stress
Drop link member 3	None	-	-	-	-	-	-	Machinability
Drop link member 4	BRR 4	-2.23×10^{4}	3.01×10^{4}	1.85×10^{6}	-2.60×10^{4}	-2.16×10^{4}	2.02×10^{3}	Stress
Drop link brace 1	None	-	-	-	-	-	-	Machinability
Drop link brace 2	GRO 2 IB	4.66×10^{4}	8.35×10^{2}	-1.39×10^{6}	-8.13×10^{1}	4.70×10^{4}	-1.80×10^{3}	Stress
Shock strut trunnion	GRO 2 IB	4.07×10^{4}	1.95×10^{6}	-7.10×10^{5}	-3.57×10^{5}	4.52×10^{4}	1.96×10^{3}	Stress
Shock strut cylinder	BRR 3	-4.49×10^{5}	4.71×10^{5}	6.81×10^{5}	-1.03×10^{6}	-7.88×10^{5}	-5.94×10^{4}	Stress
Shock strut piston	BRR 3	2.97×10^{3}	1.19×10^{6}	-1.29×10^{6}	-8.52×10^{5}	-1.13×10^{4}	-8.89×10^{3}	Stress
Shock strut brace 1	GRO 2 IB	-2.12×10^{4}	2.77×10^{4}	2.42×10^{6}	5.68×10^{4}	1.28×10^{4}	2.61×10^{3}	Stress
Shock strut brace 2	BRR 4	-1.65×10^{4}	-6.73×10^{4}	-2.20×10^{6}	-6.60×10^{4}	1.35×10^{4}	3.19×10^{3}	Stress
Shock strut brace 3	BRR 3	1.77×10^{4}	6.26×10^{3}	-2.14×10^{6}	0.00	0.00	0.00	Buckling
Bogie beam	GRO 1	4.74×10^{2}	9.28×10^{5}	0.00	6.57×10^{5}	-3.95×10^{2}	-1.77×10^{2}	Stress
Aft wheel axle	GRO 2 OB	1.05×10^{5}	4.13×10^{5}	8.36×10^{4}	3.26×10^{5}	7.52×10^{4}	1.74×10^{3}	Stress
Front wheel axle	GRO 2 OB	1.05×10^{5}	4.13×10^{5}	8.36×10^{4}	3.26×10^{5}	7.54×10^{4}	1.18×10^{3}	Stress
AM member 1	LVL 3 P1 SU	7.52×10^{3}	-5.16×10^{4}	1.45×10^{6}	-1.86×10^{4}	1.67×10^{3}	7.67×10^{2}	Stress
AM member 2	LVL 3 P1 SU	-1.73×10^{3}	2.67×10^{4}	-1.36×10^{6}	2.08	-3.84×10^{2}	1.23×10^{2}	Stress
AM member 3	SLL 2 P1 IB	-3.40×10^{4}	6.60×10^{2}	3.18×10^{5}	-1.80×10^{2}	-2.72×10^{4}	-1.79×10^{3}	Stress
Shortening members	GRO 1	0.00	0.00	-6.67×10^{5}	0.00	0.00	0.00	Stress

Table D.23: FV-800 single optimisation right main landing gear structural member sizing. Nodes are defined as illustrated in Figure 5.14. Dimensions shown in bold are fixed, based on either the piston diameter or wheel rim diameter, as described in Section 3.5.

Member	Nodes	l (m)	r_i (m)	r_o (m)	t (m)	A (m^2)	m (kg)
Upper strut trunnion	D1-D2-O1-D3-D4	2.200	0.101	**0.114**	0.013	0.008	146.1
Drop link member 1	D2-D5	1.793	0.049	**0.057**	0.008	0.003	39.1
Drop link member 2	O1-D5	1.911	0.054	**0.057**	0.003	0.001	15.4
Drop link member 3	O1-D6	1.877	0.054	**0.057**	0.003	0.001	14.3
Drop link member 4	D3-D6	1.731	0.048	**0.057**	0.009	0.003	41.7
Drop link brace 1	C2-C4	1.884	0.054	**0.057**	0.003	0.001	14.3
Drop link brace 2	C1-C3	1.642	0.047	**0.057**	0.010	0.003	40.7
Shock strut trunnion	D5-S1-O2-S3-D6	1.750	0.099	**0.114**	0.015	0.010	134.7
Shock strut cylinder	O2-S4-S6-S7-S8	2.570	**0.143**	0.162	0.019	0.018	360.0
Shock strut piston	S8-B1	1.627[1,2]	0.126	**0.143**	0.017	0.014	184.6
Shock strut brace 1	S1-S3	1.761	0.062	**0.072**	0.010	0.004	55.7
Shock strut brace 2	S2-S5	1.449	0.062	**0.072**	0.010	0.004	46.7
Shock strut brace 3	C5-C6	2.780	0.088	**0.093**	0.005	0.003	67.1
Bogie beam	K-B2-L	1.420	0.132	**0.143**	0.011	0.010	110.0
Aft wheel axle	K_L-K_R	1.400	0.103	**0.112**	0.009	0.006	70.0
Front wheel axle	L_L-L_R	1.400	0.103	**0.112**	0.009	0.006	70.0
AM member 1[3]	A1-A4	1.070[1]	0.033	**0.043**	0.010	0.002	20.3
AM member 2[3]	A2-A3	0.903[1]	0.038	**0.043**	0.005	0.001	9.3
AM member 3[3]	A5-A6	0.780[1]	0.036	**0.043**	0.007	0.002	10.5
Shortening members	-	0.500	0.036	**0.043**	0.007	0.002	6.8
Total	-	-	-	-	-	-	

[1] Extended length plus a margin of 2.75 times the respective piston diameter (Section 3.4.2).
[2] Includes the bogie pivot offset distance l_offset is added here.
[3] Articulation mechanism.

Table D.24: Overview of FV-800 single optimisation external main gear loads.

LC ID	m_{mlg} (kg)	θ (°)	x_{s} (m)	r_{tyre} (in)	$F_{x,\text{K}_\text{L},\text{K}_\text{R}}$ (N)	$F_{x,\text{L}_\text{L},\text{L}_\text{R}}$ (N)	$F_{y,\text{M}_\text{L},\text{M}_\text{R}}$ (N)	$F_{y,\text{N}_\text{L},\text{N}_\text{R}}$ (N)	$F_{z,\text{K}_\text{L},\text{K}_\text{R}}$ (N)	$F_{z,\text{L}_\text{L},\text{L}_\text{R}}$ (N)
LVL 1 P1 SU	6.95×10^4	0	0.468	24.2	1.18×10^5	0.00	0.00	0.00	1.84×10^5	0.00
LVL 1 P1 SB	6.95×10^4	0	0.468	24.2	-1.18×10^5	0.00	0.00	0.00	1.84×10^5	0.00
LVL 1 P2 SU	6.95×10^4	0	0.159	22.5	4.69×10^4	1.20×10^5	0.00	0.00	1.87×10^5	1.87×10^5
LVL 1 P2 SB	6.95×10^4	0	0.159	22.5	4.69×10^4	-1.20×10^5	0.00	0.00	1.87×10^5	1.87×10^5
LVL 2 P1 SU	6.28×10^4	-3	0.468	24.4	1.07×10^5	0.00	0.00	0.00	1.66×10^5	0.00
LVL 2 P1 SB	6.28×10^4	-3	0.468	24.4	-1.07×10^5	0.00	0.00	0.00	1.66×10^5	0.00
LVL 2 P2 SU	6.46×10^4	-3	0.159	22.8	4.35×10^4	1.11×10^5	0.00	0.00	1.74×10^5	1.74×10^5
LVL 2 P2 SB	6.46×10^4	-3	0.159	22.8	4.35×10^4	-1.11×10^5	0.00	0.00	1.74×10^5	1.74×10^5
LVL 3 P1 SU	9.25×10^4	0	0.468	23.7	1.57×10^5	0.00	0.00	0.00	2.45×10^5	0.00
LVL 3 P1 SB	9.25×10^4	0	0.468	23.7	-1.57×10^5	0.00	0.00	0.00	2.45×10^5	0.00
LVL 3 P2 SU	9.25×10^4	0	0.159	21.4	6.24×10^4	1.60×10^5	0.00	0.00	2.50×10^5	2.50×10^5
LVL 3 P2 SB	9.25×10^4	0	0.159	21.4	6.24×10^4	-1.60×10^5	0.00	0.00	2.50×10^5	2.50×10^5
LVL 4 P1 SU	8.36×10^4	-3	0.468	23.9	1.42×10^5	0.00	0.00	0.00	2.22×10^5	0.00
LVL 4 P1 SB	8.36×10^4	-3	0.468	23.9	-1.42×10^5	0.00	0.00	0.00	2.22×10^5	0.00
LVL 4 P2 SU	8.59×10^4	-3	0.159	21.7	5.80×10^4	1.48×10^5	0.00	0.00	2.32×10^5	2.32×10^5
LVL 4 P2 SB	8.59×10^4	-3	0.159	21.7	5.80×10^4	-1.48×10^5	0.00	0.00	2.32×10^5	2.32×10^5
LAT 1 P1 SU/IB	6.95×10^4	0	0.492	24.6	8.84×10^4	0.00	-3.45×10^4	0.00	1.38×10^5	0.00
LAT 1 P1 SU/OB	6.95×10^4	0	0.492	24.6	8.84×10^4	0.00	3.45×10^4	0.00	1.38×10^5	0.00
LAT 1 P1 SB/IB	6.95×10^4	0	0.492	24.6	-8.84×10^4	0.00	-3.45×10^4	0.00	1.38×10^5	0.00
LAT 1 P1 SB/OB	6.95×10^4	0	0.492	24.6	-8.84×10^4	0.00	3.45×10^4	0.00	1.38×10^5	0.00
LAT 1 P2 SU/IB	6.95×10^4	0	0.167	23.4	5.62×10^4	9.00×10^4	-3.52×10^4	-3.52×10^4	1.41×10^5	1.41×10^5
LAT 1 P2 SU/OB	6.95×10^4	0	0.167	23.4	5.62×10^4	9.00×10^4	3.52×10^4	3.52×10^4	1.41×10^5	1.41×10^5
LAT 1 P2 SB/IB	6.95×10^4	0	0.167	23.4	5.62×10^4	-9.00×10^4	-3.52×10^4	-3.52×10^4	1.41×10^5	1.41×10^5
LAT 1 P2 SB/OB	6.95×10^4	0	0.167	23.4	5.62×10^4	-9.00×10^4	3.52×10^4	3.52×10^4	1.41×10^5	1.41×10^5
LAT 2 P1 SU/IB	6.28×10^4	-3	0.492	24.8	7.99×10^4	0.00	-3.12×10^4	0.00	1.25×10^5	0.00
LAT 2 P1 SU/OB	6.28×10^4	-3	0.492	24.8	7.99×10^4	0.00	3.12×10^4	0.00	1.25×10^5	0.00
LAT 2 P1 SB/IB	6.28×10^4	-3	0.492	24.8	-7.99×10^4	0.00	-3.12×10^4	0.00	1.25×10^5	0.00
LAT 2 P1 SB/OB	6.28×10^4	-3	0.492	24.8	-7.99×10^4	0.00	3.12×10^4	0.00	1.25×10^5	0.00
LAT 2 P2 SU/IB	6.46×10^4	-3	0.167	23.5	5.23×10^4	8.36×10^4	-3.27×10^4	-3.27×10^4	1.31×10^5	1.31×10^5
LAT 2 P2 SU/OB	6.46×10^4	-3	0.167	23.5	5.23×10^4	8.36×10^4	3.27×10^4	3.27×10^4	1.31×10^5	1.31×10^5
LAT 2 P2 SB/IB	6.46×10^4	-3	0.167	23.5	5.23×10^4	-8.36×10^4	-3.27×10^4	-3.27×10^4	1.31×10^5	1.31×10^5
LAT 2 P2 SB/OB	6.46×10^4	-3	0.167	23.5	5.23×10^4	-8.36×10^4	3.27×10^4	3.27×10^4	1.31×10^5	1.31×10^5
TDL 1 P1 SU	6.95×10^4	14	0.468	24.2	1.18×10^5	0.00	0.00	0.00	1.84×10^5	0.00
TDL 1 P1 SB	6.95×10^4	14	0.468	24.2	-1.18×10^5	0.00	0.00	0.00	1.84×10^5	0.00
TDL 1 P2 SU	6.95×10^4	14	0.159	22.5	0.00	1.20×10^5	0.00	0.00	1.87×10^5	1.87×10^5
TDL 1 P2 SB	6.95×10^4	14	0.159	22.5	0.00	-1.20×10^5	0.00	0.00	1.87×10^5	1.87×10^5
TDL 2 P1 SU	9.25×10^4	14	0.468	23.7	1.57×10^5	0.00	0.00	0.00	2.45×10^5	0.00
TDL 2 P1 SB	9.25×10^4	14	0.468	23.7	-1.57×10^5	0.00	0.00	0.00	2.45×10^5	0.00
TDL 2 P2 SU	9.25×10^4	14	0.159	21.4	0.00	1.60×10^5	0.00	0.00	2.50×10^5	2.50×10^5
TDL 2 P2 SB	9.25×10^4	14	0.159	21.4	0.00	-1.60×10^5	0.00	0.00	2.50×10^5	2.50×10^5
OGL 1 P1 SU	6.95×10^4	0	0.468	24.2	1.18×10^5	0.00	0.00	0.00	1.84×10^5	0.00
OGL 1 P1 SB	6.95×10^4	0	0.468	24.2	-1.18×10^5	0.00	0.00	0.00	1.84×10^5	0.00
OGL 1 P2 SU	6.95×10^4	0	0.159	22.5	4.69×10^4	1.20×10^5	0.00	0.00	1.87×10^5	1.87×10^5
OGL 1 P2 SB	6.95×10^4	0	0.159	22.5	4.69×10^4	-1.20×10^5	0.00	0.00	1.87×10^5	1.87×10^5
OGL 2 P1 SU	9.25×10^4	0	0.468	23.7	1.57×10^5	0.00	0.00	0.00	2.45×10^5	0.00
OGL 2 P1 SB	9.25×10^4	0	0.468	23.7	-1.57×10^5	0.00	0.00	0.00	2.45×10^5	0.00
OGL 2 P2 SU	9.25×10^4	0	0.159	21.4	6.24×10^4	1.60×10^5	0.00	0.00	2.50×10^5	2.50×10^5
OGL 2 P2 SB	9.25×10^4	0	0.159	21.4	6.24×10^4	-1.60×10^5	0.00	0.00	2.50×10^5	2.50×10^5
SLL 1 P1 IB	6.95×10^4	0	0.468	25.1	0.00	0.00	-7.36×10^4	0.00	9.20×10^4	0.00
SLL 1 P1 OB	6.95×10^4	0	0.468	25.1	0.00	0.00	5.52×10^4	0.00	9.20×10^4	0.00
SLL 1 P2 IB	6.95×10^4	0	0.159	24.2	0.00	0.00	-7.50×10^4	-7.50×10^4	9.37×10^4	9.37×10^4
SLL 1 P2 OB	6.95×10^4	0	0.159	24.2	0.00	0.00	5.62×10^4	5.62×10^4	9.37×10^4	9.37×10^4
SLL 2 P1 IB	9.25×10^4	0	0.468	24.8	0.00	0.00	-9.80×10^4	0.00	1.23×10^5	0.00
SLL 2 P1 OB	9.25×10^4	0	0.468	24.8	0.00	0.00	7.35×10^4	0.00	1.23×10^5	0.00
SLL 2 P2 IB	9.25×10^4	0	0.159	23.6	0.00	0.00	-9.98×10^4	-9.98×10^4	1.25×10^5	1.25×10^5
SLL 2 P2 OB	9.25×10^4	0	0.159	23.6	0.00	0.00	7.49×10^4	7.49×10^4	1.25×10^5	1.25×10^5
GRO 1	8.60×10^4	-3	0.042	17.6	0.00	0.00	0.00	0.00	4.64×10^5	4.64×10^5
GRO 2 IB	8.60×10^4	-3	0.042	18.4	8.35×10^4	8.35×10^4	-8.35×10^4	-8.35×10^4	4.18×10^5	4.18×10^5
GRO 2 OB	8.60×10^4	-3	0.042	18.4	8.35×10^4	8.35×10^4	8.35×10^4	8.35×10^4	4.18×10^5	4.18×10^5
BRR 1	6.95×10^4	0	0.042	20.7	2.32×10^5	2.32×10^5	0.00	0.00	2.90×10^5	2.90×10^5
BRR 2	6.46×10^4	-3	0.042	21.1	2.16×10^5	2.16×10^5	0.00	0.00	2.69×10^5	2.69×10^5
BRR 3	9.30×10^4	0	0.042	19.8	2.74×10^5	2.74×10^5	0.00	0.00	3.42×10^5	3.42×10^5
BRR 4	8.65×10^4	-3	0.042	20.2	2.54×10^5	2.54×10^5	0.00	0.00	3.18×10^5	3.18×10^5
TRN 1 IB	8.65×10^4	-3	0.042	22.1	0.00	0.00	-1.06×10^5	-1.06×10^5	2.12×10^5	2.12×10^5
TRN 1 OB	8.65×10^4	-3	0.042	22.1	0.00	0.00	1.06×10^5	1.06×10^5	2.12×10^5	2.12×10^5
PIV 1	8.65×10^4	-3	0.042	20.2	2.54×10^5	2.54×10^5	0.00	0.00	3.18×10^5	3.18×10^5
RBR 1	8.65×10^4	-3	0.042	22.1	-1.17×10^5	-1.17×10^5	0.00	0.00	2.12×10^5	2.12×10^5

FV-900

Table D.25: FV-900 single optimisation right main landing gear structural loads for critical load case in each component.

Member	LC ID	V_x (N)	V_y (N)	N_z (N)	M_x (N)	M_y (N)	T_z (N)	Failure mode
Upper strut trunnion	BRR 4	1.19E+06	-2.21E+06	-3.63E+05	-3.18E+05	-1.55E+05	-1.11E+04	Stress
Drop link member 1	GRO 2 IB	1.87E+04	4.75E+04	-1.88E+06	-5.84E+04	2.30E+04	4.11E+03	Stress
Drop link member 2	GRO 2 IB	3.33E+03	2.77E+04	2.55E+05	-3.38E+04	7.41E+03	4.13E+03	Stress
Drop link member 3	None	-	-	-	-	-	-	Machinability
Drop link member 4	BRR 3	-2.43E+04	3.71E+04	2.45E+06	-3.22E+04	-2.40E+04	1.55E+03	Stress
Drop link brace 1	None	-	-	-	-	-	-	Machinability
Drop link brace 2	GRO 2 IB	4.67E+04	2.62E+03	-1.79E+06	-3.01E+02	5.66E+04	-4.97E+03	Stress
Shock strut trunnion	BRR 4	7.46E+04	2.42E+06	-4.56E+05	5.35E+05	-3.72E+04	5.31E+03	Stress
Shock strut cylinder	BRR 3	-5.77E+05	6.08E+05	8.45E+05	-1.41E+06	-1.08E+06	-8.17E+04	Stress
Shock strut piston	BRR 3	2.40E+03	1.50E+06	-1.63E+06	-1.10E+06	-2.34E+04	-2.03E+04	Stress
Shock strut brace 1	GRO 2 IB	-3.09E+04	1.66E+04	3.28E+06	6.81E+04	1.72E+04	3.86E+03	Stress
Shock strut brace 2	BRR 4	-2.23E+04	-8.89E+04	-3.01E+06	-8.83E+04	1.87E+04	4.30E+03	Stress
Shock strut brace 3	BRR 3	3.26E+04	8.52E+03	-2.69E+06	2.49E-08	5.82E-09	-1.27E-06	Buckling
Bogie beam	GRO 1	2.68E+02	1.18E+06	6.21E+00	1.16E+06	-3.44E+02	-4.80E+02	Stress
Aft wheel axle	GRO 2 OB	-1.34E+05	5.23E+05	1.06E+05	4.16E+05	9.52E+04	3.19E+03	Stress
Front wheel axle	GRO 2 OB	-1.34E+05	5.23E+05	1.06E+05	4.16E+05	9.59E+04	1.44E+03	Stress
AM member 1	LVL 3 P1 SU	3.87E+03	-7.31E+04	1.52E+06	-3.06E+04	6.95E+02	6.70E+02	Stress
AM member 2	LVL 3 P1 SU	-1.84E+03	-3.67E+04	-1.56E+06	-1.28E-01	-2.39E+01	-5.63E+01	Stress
AM member 3	SLL 2 P1 IB	-3.09E+04	1.23E+03	3.00E+05	-2.64E+02	-2.77E+04	-1.72E+03	Stress
Shortening members	GRO 1	0.00E+00	0.00E+00	-9.42E+05	0.00E+00	0.00E+00	0.00E+00	Stress

Table D.26: FV-900 single optimisation right main landing gear structural member sizing. Nodes are defined as illustrated in Figure 5.14. Dimensions shown in bold are fixed, based on either the piston diameter or wheel rim diameter, as described in Section 3.5.

Member	Nodes	l (m)	r_i (m)	r_o (m)	t (m)	A (m^2)	m (kg)
Upper strut trunnion	D1-D2-O1-D3-D4	2.300	0.113	**0.127**	0.014	0.010	187.7
Drop link member 1	D2-D5	1.934	0.053	**0.064**	0.011	0.004	60.3
Drop link member 2	O1-D5	2.036	0.061	**0.064**	0.003	0.001	21.3
Drop link member 3	O1-D6	2.002	0.061	**0.064**	0.003	0.001	19.2
Drop link member 4	D3-D6	1.871	0.054	**0.064**	0.010	0.004	54.3
Drop link brace 1	C2-C4	1.971	0.061	**0.064**	0.003	0.001	18.9
Drop link brace 2	C1-C3	1.862	0.054	**0.064**	0.010	0.004	53.3
Shock strut trunnion	D5-S1-O2-S3-D6	1.750	0.110	**0.127**	0.017	0.012	170.4
Shock strut cylinder	O2-S4-S6-S7-S8	2.868	**0.159**	0.180	0.021	0.022	495.4
Shock strut piston	S8-B1	1.862[1,2]	0.141	**0.159**	0.018	0.017	247.8
Shock strut brace 1	S1-S3	1.934	0.069	**0.080**	0.011	0.005	75.8
Shock strut brace 2	S2-S5	1.621	0.069	**0.080**	0.011	0.005	67.5
Shock strut brace 3	C5-C6	3.183	0.096	**0.103**	0.007	0.004	103.8
Bogie beam	K-B2-L	1.980	0.142	**0.159**	0.017	0.016	245.0
Aft wheel axle	K_L-K_R	1.400	0.106	**0.117**	0.011	0.008	86.7
Front wheel axle	L_L-L_R	1.400	0.106	**0.117**	0.011	0.008	86.7
AM member 1[3]	A1-A4	1.272[1]	0.037	**0.048**	0.011	0.003	29.5
AM member 2[3]	A2-A3	1.103[1]	0.043	**0.048**	0.005	0.001	12.8
AM member 3[3]	A5-A6	0.920[1]	0.043	**0.048**	0.005	0.002	10.9
Shortening members	-	0.500	0.040	**0.048**	0.008	0.002	8.6
Total	-	-	-	-	-	-	2056

[1] Extended length plus a margin of 2.75 times the respective piston diameter (Section 3.4.2).
[2] Includes the bogie pivot offset distance l_offset is added here.
[3] Articulation mechanism.

Table D.27: Overview of FV-900 single optimisation external main gear loads.

LC ID	m_{mlg} (kg)	θ (°)	x_{s} (m)	r_{tyre} (in)	$F_{x,\text{K}_\text{L},\text{K}_\text{R}}$ (N)	$F_{x,\text{L}_\text{L},\text{L}_\text{R}}$ (N)	$F_{y,\text{M}_\text{L},\text{M}_\text{R}}$ (N)	$F_{y,\text{N}_\text{L},\text{N}_\text{R}}$ (N)	$F_{z,\text{K}_\text{L},\text{K}_\text{R}}$ (N)	$F_{z,\text{L}_\text{L},\text{L}_\text{R}}$ (N)
LVL 1 P1 SU	8.80×10^4	0	0.587	26.7	1.02×10^5	0.00	0.00	0.00	1.60×10^5	0.00
LVL 1 P1 SB	8.80×10^4	0	0.587	26.7	-1.02×10^5	0.00	0.00	0.00	1.60×10^5	0.00
LVL 1 P2 SU	8.80×10^4	0	0.188	24.3	5.94×10^4	1.52×10^5	0.00	0.00	2.37×10^5	2.37×10^5
LVL 1 P2 SB	8.80×10^4	0	0.188	24.3	5.94×10^4	-1.52×10^5	0.00	0.00	2.37×10^5	2.37×10^5
LVL 2 P1 SU	7.91×10^4	-3	0.587	26.8	9.18×10^4	0.00	0.00	0.00	1.43×10^5	0.00
LVL 2 P1 SB	7.91×10^4	-3	0.587	26.8	-9.18×10^4	0.00	0.00	0.00	1.43×10^5	0.00
LVL 2 P2 SU	8.19×10^4	-3	0.188	24.6	5.52×10^4	1.41×10^5	0.00	0.00	2.21×10^5	2.21×10^5
LVL 2 P2 SB	8.19×10^4	-3	0.188	24.6	5.52×10^4	-1.41×10^5	0.00	0.00	2.21×10^5	2.21×10^5
LVL 3 P1 SU	1.17×10^5	0	0.587	26.3	1.36×10^5	0.00	0.00	0.00	2.12×10^5	0.00
LVL 3 P1 SB	1.17×10^5	0	0.587	26.3	-1.36×10^5	0.00	0.00	0.00	2.12×10^5	0.00
LVL 3 P2 SU	1.17×10^5	0	0.188	23.1	7.89×10^4	2.02×10^5	0.00	0.00	3.16×10^5	3.16×10^5
LVL 3 P2 SB	1.17×10^5	0	0.188	23.1	7.89×10^4	-2.02×10^5	0.00	0.00	3.16×10^5	3.16×10^5
LVL 4 P1 SU	1.05×10^5	-3	0.587	26.5	1.22×10^5	0.00	0.00	0.00	1.91×10^5	0.00
LVL 4 P1 SB	1.05×10^5	-3	0.587	26.5	-1.22×10^5	0.00	0.00	0.00	1.91×10^5	0.00
LVL 4 P2 SU	1.09×10^5	-3	0.188	23.4	7.34×10^4	1.88×10^5	0.00	0.00	2.94×10^5	2.94×10^5
LVL 4 P2 SB	1.09×10^5	-3	0.188	23.4	7.34×10^4	-1.88×10^5	0.00	0.00	2.94×10^5	2.94×10^5
LAT 1 P1 SU/IB	8.80×10^4	0	0.618	27.0	7.67×10^4	0.00	-2.99×10^4	0.00	1.20×10^5	0.00
LAT 1 P1 SU/OB	8.80×10^4	0	0.618	27.0	7.67×10^4	0.00	2.99×10^4	0.00	1.20×10^5	0.00
LAT 1 P1 SB/IB	8.80×10^4	0	0.618	27.0	-7.67×10^4	0.00	-2.99×10^4	0.00	1.20×10^5	0.00
LAT 1 P1 SB/OB	8.80×10^4	0	0.618	27.0	-7.67×10^4	0.00	2.99×10^4	0.00	1.20×10^5	0.00
LAT 1 P2 SU/IB	8.80×10^4	0	0.197	25.2	7.12×10^4	1.14×10^5	-4.45×10^4	-4.45×10^4	1.78×10^5	1.78×10^5
LAT 1 P2 SU/OB	8.80×10^4	0	0.197	25.2	7.12×10^4	1.14×10^5	4.45×10^4	4.45×10^4	1.78×10^5	1.78×10^5
LAT 1 P2 SB/IB	8.80×10^4	0	0.197	25.2	7.12×10^4	-1.14×10^5	-4.45×10^4	-4.45×10^4	1.78×10^5	1.78×10^5
LAT 1 P2 SB/OB	8.80×10^4	0	0.197	25.2	7.12×10^4	-1.14×10^5	4.45×10^4	4.45×10^4	1.78×10^5	1.78×10^5
LAT 2 P1 SU/IB	7.91×10^4	-3	0.618	27.1	6.89×10^4	0.00	-2.69×10^4	0.00	1.08×10^5	0.00
LAT 2 P1 SU/OB	7.91×10^4	-3	0.618	27.1	6.89×10^4	0.00	2.69×10^4	0.00	1.08×10^5	0.00
LAT 2 P1 SB/IB	7.91×10^4	-3	0.618	27.1	-6.89×10^4	0.00	-2.69×10^4	0.00	1.08×10^5	0.00
LAT 2 P1 SB/OB	7.91×10^4	-3	0.618	27.1	-6.89×10^4	0.00	2.69×10^4	0.00	1.08×10^5	0.00
LAT 2 P2 SU/IB	8.19×10^4	-3	0.197	25.4	6.63×10^4	1.06×10^5	-4.14×10^4	-4.14×10^4	1.66×10^5	1.66×10^5
LAT 2 P2 SU/OB	8.19×10^4	-3	0.197	25.4	6.63×10^4	1.06×10^5	4.14×10^4	4.14×10^4	1.66×10^5	1.66×10^5
LAT 2 P2 SB/IB	8.19×10^4	-3	0.197	25.4	6.63×10^4	-1.06×10^5	-4.14×10^4	-4.14×10^4	1.66×10^5	1.66×10^5
LAT 2 P2 SB/OB	8.19×10^4	-3	0.197	25.4	6.63×10^4	-1.06×10^5	4.14×10^4	4.14×10^4	1.66×10^5	1.66×10^5
TDL 1 P1 SU	8.80×10^4	14	0.587	26.7	1.02×10^5	0.00	0.00	0.00	1.60×10^5	0.00
TDL 1 P1 SB	8.80×10^4	14	0.587	26.7	-1.02×10^5	0.00	0.00	0.00	1.60×10^5	0.00
TDL 1 P2 SU	8.80×10^4	14	0.188	24.3	0.00	1.52×10^5	0.00	0.00	2.37×10^5	2.37×10^5
TDL 1 P2 SB	8.80×10^4	14	0.188	24.3	0.00	-1.52×10^5	0.00	0.00	2.37×10^5	2.37×10^5
TDL 2 P1 SU	1.17×10^5	14	0.587	26.3	1.36×10^5	0.00	0.00	0.00	2.12×10^5	0.00
TDL 2 P1 SB	1.17×10^5	14	0.587	26.3	-1.36×10^5	0.00	0.00	0.00	2.12×10^5	0.00
TDL 2 P2 SU	1.17×10^5	14	0.188	23.1	0.00	2.02×10^5	0.00	0.00	3.16×10^5	3.16×10^5
TDL 2 P2 SB	1.17×10^5	14	0.188	23.1	0.00	-2.02×10^5	0.00	0.00	3.16×10^5	3.16×10^5
OGL 1 P1 SU	8.80×10^4	0	0.587	26.7	1.02×10^5	0.00	0.00	0.00	1.60×10^5	0.00
OGL 1 P1 SB	8.80×10^4	0	0.587	26.7	-1.02×10^5	0.00	0.00	0.00	1.60×10^5	0.00
OGL 1 P2 SU	8.80×10^4	0	0.188	24.3	5.94×10^4	1.52×10^5	0.00	0.00	2.37×10^5	2.37×10^5
OGL 1 P2 SB	8.80×10^4	0	0.188	24.3	5.94×10^4	-1.52×10^5	0.00	0.00	2.37×10^5	2.37×10^5
OGL 2 P1 SU	1.17×10^5	0	0.587	26.3	1.36×10^5	0.00	0.00	0.00	2.12×10^5	0.00
OGL 2 P1 SB	1.17×10^5	0	0.587	26.3	-1.36×10^5	0.00	0.00	0.00	2.12×10^5	0.00
OGL 2 P2 SU	1.17×10^5	0	0.188	23.1	7.89×10^4	2.02×10^5	0.00	0.00	3.16×10^5	3.16×10^5
OGL 2 P2 SB	1.17×10^5	0	0.188	23.1	7.89×10^4	-2.02×10^5	0.00	0.00	3.16×10^5	3.16×10^5
SLL 1 P1 IB	8.80×10^4	0	0.587	27.3	0.00	0.00	-6.39×10^4	0.00	7.99×10^4	0.00
SLL 1 P1 OB	8.80×10^4	0	0.587	27.3	0.00	0.00	4.79×10^4	0.00	7.99×10^4	0.00
SLL 1 P2 IB	8.80×10^4	0	0.188	26.1	0.00	0.00	-9.50×10^4	-9.50×10^4	1.19×10^5	1.19×10^5
SLL 1 P2 OB	8.80×10^4	0	0.188	26.1	0.00	0.00	7.12×10^4	7.12×10^4	1.19×10^5	1.19×10^5
SLL 2 P1 IB	1.17×10^5	0	0.587	27.1	0.00	0.00	-8.49×10^4	0.00	1.06×10^5	0.00
SLL 2 P1 OB	1.17×10^5	0	0.587	27.1	0.00	0.00	6.37×10^4	0.00	1.06×10^5	0.00
SLL 2 P2 IB	1.17×10^5	0	0.188	25.5	0.00	0.00	-1.26×10^5	-1.26×10^5	1.58×10^5	1.58×10^5
SLL 2 P2 OB	1.17×10^5	0	0.188	25.5	0.00	0.00	9.47×10^4	9.47×10^4	1.58×10^5	1.58×10^5
GRO 1	1.09×10^5	-3	0.053	18.9	0.00	0.00	0.00	0.00	5.88×10^5	5.88×10^5
GRO 2 IB	1.09×10^5	-3	0.053	19.8	1.06×10^5	1.06×10^5	-1.06×10^5	-1.06×10^5	5.29×10^5	5.29×10^5
GRO 2 OB	1.09×10^5	-3	0.053	19.8	1.06×10^5	1.06×10^5	1.06×10^5	1.06×10^5	5.29×10^5	5.29×10^5
BRR 1	8.80×10^4	0	0.053	22.3	2.94×10^5	2.94×10^5	0.00	0.00	3.67×10^5	3.67×10^5
BRR 2	8.19×10^4	-3	0.053	22.7	2.73×10^5	2.73×10^5	0.00	0.00	3.42×10^5	3.42×10^5
BRR 3	1.18×10^5	0	0.053	21.3	3.46×10^5	3.46×10^5	0.00	0.00	4.32×10^5	4.32×10^5
BRR 4	1.09×10^5	-3	0.053	21.8	3.22×10^5	3.22×10^5	0.00	0.00	4.03×10^5	4.03×10^5
TRN 1 IB	1.09×10^5	-3	0.053	23.8	0.00	0.00	-1.34×10^5	-1.34×10^5	2.68×10^5	2.68×10^5
TRN 1 OB	1.09×10^5	-3	0.053	23.8	0.00	0.00	1.34×10^5	1.34×10^5	2.68×10^5	2.68×10^5
PIV 1	1.09×10^5	-3	0.053	21.8	3.22×10^5	3.22×10^5	0.00	0.00	4.03×10^5	4.03×10^5
RBR 1	1.09×10^5	-3	0.053	23.8	-1.48×10^5	-1.48×10^5	0.00	0.00	2.68×10^5	2.68×10^5